**Theme Issue**

# Vacuum science, techniques and technologies
# Vakuumske znanosti, tehnike in tehnologije

Guest Editor:
**Alenka Vesel**

ISSN 1580-2949
UDK 669+666+678+53 MTAEC9, 46(1)1–91(2012)

| MATER. TEHNOL. | LETNIK VOLUME 46 | ŠTEV. NO. 1 | STR. P. 1–91 | LJUBLJANA SLOVENIJA | JAN.–FEB. 2012 |
|---|---|---|---|---|---|

## VSEBINA – CONTENTS

# PREDGOVOR

# FOREWORD

This issue of the Journal “Materiali in tehnologije” is devoted to vacuum techniques and technologies. Application of vacuum has spread enormously in the last decades and nowadays comprises topics ranging from traditional surface science to nanomaterials and biointerfaces. Many crucial technologies introduced in the last decades run under low pressure conditions. Among them, technologies based on application of non-equilibrium states of gases at reduced pressure are particularly popular since they allow modifications on the surface of materials that lead to unusual properties. Many papers published in this issue are related to application of low-pressure gaseous plasma for modification of advanced materials. Several aspects including plasma excitation and characterization are addressed. Other papers deal with yet poorly understood phenomena in characterization of materials by techniques that apply high or ultra - high vacuum. Some papers touch open problems in modification of materials by chemical methods as well as application of non-vacuum characterization techniques. The papers in this issue represent valuable reading matter highly recommended to researchers working in different fields of vacuum technique and technologies.

Guest Editor
A/Prof. Dr. Alenka Vesel

Ta izdaja revije »Materiali in Tehnologije« je posvečena tehnikam in tehnologijam, ki temeljijo na uporabi vakuuma. Njegova uporaba se je v zadnjih desetletjih izredno razmahnila, tako da danes vsebuje različna področja od klasične znanosti o površinah do nanoskopskih in bioloških materialov. Mnogi ključni tehnološki postopki, ki so bili razviti v zadnjem desetletju, potekajo pri znižanem tlaku. Med njimi so najpomembnejši tisti, ki za obdelavo materialov izkoriščajo neravnovesna stanja plinov. Tovrstne obdelave namreč vodijo k zanimivim lastnostim materialov, ki jih s standardnimi postopki ni mogoče doseči. Mnogi članki v pričujoči izdaji revije opisujejo prav uporabo nizkotlačne plinske plazme za modifikacijo površinskih lastnosti materialov, kakor tudi metode za ustvarjanje plazme in merjenje njenih značilnosti. Drugi prispevki opisujejo doslej še vedno slabo poznane specifičnosti analitskih tehnik, ki temeljijo na uporabi visokega in ultra visokega vakuuma. Nekateri znanstveni članki se dotaknejo tudi klasičnih kemijskih postopkov za modifikacijo materialov, kakor tudi nekaterih ne-vakuumskih tehnik za njihovo karakterizacijo. Prispevki v tej številki revije predstavljajo priporočljivo čtivo za raziskovalce, ki pri svojem delu uporabljajo različne vakuumske tehnike in tehnologije.

Gostujoča urednica
doc. dr. Alenka Vesel

UDK 533.9
Review article/Pregledni članek

ISSN 1580-2949
MTAEC9, 46(1)7(2012)

# HETEROGENEOUS SURFACE RECOMBINATION OF NEUTRAL NITROGEN ATOMS

## HETEROGENA POVRŠINSKA REKOMBINACIJA DUŠIKOVIH NEVTRALNIH ATOMOV

**Alenka Vesel**

Center of Excellence for Polymer Materials and Technologies, Tehnološki park 24, 1000 Ljubljana, Slovenia
alenka.vesel@ijs.si

*Prejem rokopisa – received: 2011-06-14; sprejem za objavo – accepted for publication: 2011-07-18*

An overview of data reported in literature on heterogeneous surface recombination of nitrogen atoms is presented. The data are often scattered for over an order of magnitude depending on experimental technique and perhaps also on surface finish. As a general rule the recombination coefficient is rather small for materials that do not chemisorb nitrogen atoms, and it is rather large for some metals that are known as catalysts. Values as low as $5\times10^{-8}$ have been reported for Pyrex glass, although a typical value of the recombination coefficient for glasses is rather $1\times10^{-5}$. The similar order of magnitude is found for very stable polymers such as polytetrafluoroethylene (teflon), although larger values are typical for some other polymers. The recombination coefficient for metals is typically $10^{-2}$ but can be as large as 0.3 for selected catalysts.

Keywords: nitrogen plasma, neutral nitrogen atoms, surface recombination, recombination probability

Podajamo pregled podatkov iz literature o heterogeni površinski rekombinaciji dušikovih atomov. Obstoječi podatki se pogosto razlikujejo za več kot velikostni red odvisno od eksperimentalne tehnike in verjetno tudi od predobdelave površine. V splošnem je rekombinacijski koeficient precej majhen za materiale, ki ne kemisorbirajo dušikovih atomov in precej velik za nekatere materiale, ki so znani kot katalizatorji. Zelo majhne vrednosti okoli $5\times10^{-8}$ so bile objavljene za steklo Pyrex, čeprav je bolj značilna vrednost rekombinacijskega koeficienta za steklo okoli $1\times10^{-5}$. Podoben velikostni red velja tudi za polimere kot je politetrafluoroetilen (teflon), medtem ko so za ostale polimere značilne precej višje vrednosti. Rekombinacijski koeficient za kovine je tipično okoli $10^{-2}$, vendar je lahko tudi precej višji okoli 0.3 za nekatere katalitične materiale.

Ključne besede: dušikova plazma, nevtralni atomi dušika, površinska rekombinacija, verjetnost za rekombinacijo

## 1 INTRODUCTION

Nitrogen plasma has attracted much attention in the past decades not only due to application for surface modifications of various materials[1–2] but also due to some specific characteristics of excited particles found in non-equilibrium nitrogen plasma.[3] Low pressure non-equilibrium gaseous plasma is always characterized by a rather high average energy of electrons and a rather low kinetic temperature of all other particles.[4–6] The simplest example of such plasma is created in a noble gas. Free electrons are accelerated in an appropriate electric field, typically next to the powered electrode and enter plasma volume with a kinetic energy often exceeding 100 eV. In plasma volume they suffer from elastic collisions with slow electrons. These collisions assure for a rapid thermalization of the fast electrons: they effectively loose their kinetic energy, while plasma electrons gain it. According to the basic roles of statistical mechanics such intensive energy exchange always leads to a Maxwellian distribution of particles over their kinetic energy.

Plasma is therefore rich with electrons with a Maxwellian energy distribution function. The high energy tail of the function is exponential so the electrons may gain practically any kinetic energy well above their average kinetic energy. Number of electrons with very high kinetic energy (in the high energy tail) are capable of ionizing any atom or molecule. In the case of noble gas such direct ionization may occur since there is a lack of low energy excited states of atoms. For instance, the first excited state of helium atom is at 20.2 eV[7] while the ionization energy is 24.6 eV.[8] Similar considerations apply for many other atomic plasmas, but fail completely in the case of nitrogen plasma. Namely, nitrogen plasma has some unique characteristics due to many different excited states that may or may not be metastable. The unique properties of these excited states make characterization and understanding of nitrogen plasma rather difficult, let alone interaction of such plasma with solid materials.

## 2 CHARACTERISTICS OF LOW-PRESSURE NON-EQUILIBRIUM NITROGEN PLASMA

Nitrogen molecules are characterized by a variety of different excited states. Most of these excited states are metastable with a typical radiative lifetime exceeding 1 ms. The dissociation energy of a nitrogen molecule is much higher than for many other molecules including oxygen, hydrogen and alike. The ionization energy is also rather high at about 14.5 eV.[9] Some excited states of nitrogen molecules are presented in Refs. 2 and 3. The richness of excited states causes many channels for electron energy loss at inelastic collisions with nitrogen

molecules. Unlike for the case of noble gases where the channels are limited, a collision with a fast electron from a high energy tail is likely to cause excitation of such a molecule rather than dissociation or even ionization. Electrons with a lower kinetic energy are likely to excite vibrationaly excited states. Nitrogen molecules are famous for many vibrational excited states. Unlike in many other gases where superelastic collisions between vibrationaly excited molecules and other particles cause substational cooling of the vibrational states, the coupling between vibrational and translational states for nitrogen molecules is extremely poor. A consequence of that is that nitrogen molecules are found in highly vibrationaly excited states even in a plasma created by a weak electrical discharge.[9,10] The high excitation energy of electronically excited states as well as rich population of vibrationaly excited states of nitrogen molecules in gaseous plasma allow for interesting inelastic collisions that may lead to either dissociation or even ionization of nitrogen molecules. Such multistep processes, that involve firstly excitations by electron impact and then redistribution of the potential energy finally causing dissociation or ionization, make any predictions about the behaviour of nitrogen plasma very difficult. Until recently, not many methods have appeared for determination of the basic plasma parameters such as dissociation fraction in nonequilibrium plasma. Application of optical absorption techniques i.e. TALIF,[11] NO titration,[12] and catalytic probes[13,14] definitely help understanding interaction between nitrogen plasma and solid materials.

Reactive particles of particular importance are neutral nitrogen atoms in the ground state. In nitrogen plasma they are usually found at the kinetic temperature close to the temperature of plasma facing components. In many technologically important nitrogen plasmas they actually represent the most important reactants. The interaction between neutral nitrogen atoms and solid materials can be either chemical or physical. Chemical interaction stands for a chemical reaction between a nitrogen atom and a solid material atom. Nitrogen atoms can either bond onto the surface forming a sort of a nitride, or pick an atom from the surface forming a radical that can leave the surface. A typical example of the latter mechanism is etching of organic materials or hydrogenated carbon by neutral nitrogen atoms.[15]

The consequence of the chemical reactions is a loss of neutral nitrogen atoms. The loss rate definitely depends on the intensity of the chemical reactions. In many practical cases however, chemical reactions are not predominant mechanism of neutral nitrogen atom loss. In many cases, the major mechanism is a physical reaction which is often called heterogeneous surface recombination. Nitrogen atoms are chemically rather reactive and can chemisorb on surfaces of different materials. If such chemisorption occurs, another atom from the gas phase may adsorb on the same site. The abundance of chemisorbed atoms can quickly cause formation of a molecule which does not fill strong chemisorption bonds but is rather desorbed from the surface immediately after being formed. This is so called Eley-Rideal mechanism of heterogeneous surface recombination. The other mechanism is the so called Langmuir-Hinshelwood which postpones surface migration of nitrogen atoms until they found a suitable site where they recombine and leave the surface of the solid material as a molecule. Whatever the mechanism is the recombination probability is often expressed in the terms of recombination coefficient which has been defined as the ratio between the number of atoms recombining on a surface area in a unit time and the total flux of atoms on the surface from the gas phase. Since the loss of atoms by a surface recombination is often the most important mechanism for draining atoms from plasma many authors attempted to measure it.

## 3 SELECTED RESULTS FOR NITROGEN ATOM RECOMBINATION COEFFICIENTS

The literature on recombination of neutral nitrogen atoms is scattered among different journals and also different periods. The techniques used for quantification of the recombination probabilities heavily depend on a sort of model predicting the behaviour of atoms near a surface. As mentioned earlier nitrogen atoms are usually not produced by direct impact dissociation of a molecule in a ground state but also at other collisions. In practice it means that the atoms can be also produced away from glowing discharge in the region called an afterglow. In fact, measurements in the discharge itself are usually too complicated and often not very reliable so the majority of recombination coefficients was measured under afterglow conditions.

The recombination coefficients for two types of glasses often used in construction of vacuum systems as well as plasma reactors are presented in **Table 1**. A quick look at the **Table 1** reveals that the recombination coefficient is very low. This means that nitrogen atoms practically do not interact with glasses. The explanation has been given implicitly in the upper text and will be only stressed again here. The luck of chemisorption states on chemically very inert glasses prevent substantional sticking of nitrogen atoms on the surface so the probability of recombination is extremely low. A detailed consideration of **Table 1** indicates a rather large scattering of the experimental results. The smallest value of $5\times10^{-8}$ was found by Brennenen[16] while on the other hand Gordiets[17] reported values of the order of $10^{-4}$ and even larger for a more complex experiment. The discrepancy of the results is therefore over four orders of magnitude and may be explained by particularities of the experimental set-ups, surface finish of the materials and possibly also the purity of materials used at particular experiment.

**Table 1:** Recombination coefficients for borosilicate glass (Pyrex) and quartz glass as obtained by different authors
**Tabela 1:** Rekombinacijski koeficienti za borosilikatno steklo (Pyrex) in kvarčno steklo

| Reference | Material | Recombination coefficient | Temperature (K) | Pressure (Pa) | Method |
|---|---|---|---|---|---|
| Brennen[16] | Pyrex | $5\times10^{-8}$ | 294 | 66.5–1330 Pa | afterglow intensity decay in a static system |
| Wentink[18] | Pyrex | $3\times10^{-5}$ | 300 | > 40 Pa | Pt heat resistance thermometer |
| Ricard[19] | Pyrex | $10^{-5}$ | 300 | 399 Pa | afterglow intensity measurements |
| Sancier[20] | Pyrex | $5\times10^{-5}$ | 300 | 2.4 Pa | difussion method + measurements of the luminescence and the heat of lumophors excited by N atoms |
| Marshall[21] | Pyrex | $3\times10^{-4}$ | 300 | 66.5–266 Pa | electron spin resonance measurements |
| Yamashita[22] | Pyrex | $3.2\times10^{-6}$ | 300 | 80–560 Pa | static system + mass spectrometer |
| Mavroyannis[23] | Pyrex | $7.5\times10^{-5}$ | / | 333 Pa | flow system + NO titration |
| Young[24] | Pyrex | $1.7\times10^{-5}$ | / | 133–1596 Pa | flow system+ afterglow intensity measurements |
| Gordiets[25] | Pyrex | $2\times10^{-4}$ | <400 | 266 Pa | kinetic model + actinometry + LIF[1] |
| Lefevre[26] | Pyrex | $2\times10^{-4}$ | | 1500 Pa | numerical procedure of hydrodynamic model and kinetic model + OES[2] and NO titration |
| Oinuma[27] | Pyrex | $6.8\times10^{-5}$ | 323 | atmospheric pressure | two-dimensional numerical model |
| Marshall[28] | Quartz | $8.3\times10^{-4}$ | 300 | 399–1729 Pa | flow system + ESR[3] measurements |
| Marshall[28] | Quartz | $6.9\times10^{-4}$ | 598 | 399–1729 Pa | flow system + ESR measurements |
| Marshall[28] | Quartz | $9.6\times10^{-4}$ | 779 | 399–1729 Pa | flow system + ESR measurements |
| Marshall[28] | Quartz | $1.51\times10^{-3}$ | 995 | 399–1729 Pa | flow system + ESR measurements |
| Marshall[28] | Quartz | $2{,}04\times10^{-3}$ | 1224 | 399–1729 Pa | flow system + ESR measurements |
| Evenson[29] | Quartz | $0.7\times10^{-5}$ | / | 400 Pa | flow system + ESR measurements |
| Evenson[29] | Quartz | $5.5\times10^{-4}$ | / | 400 Pa | flow system + ESR measurements |
| Belmonte[30] | Quartz | $9.3\times10^{-5}$ Exp(–3700/RT) | 300–823 | 1500 Pa $Ar/N_2$=1000/50 sccm | numerical procedure of hydrodynamic model + OES and NO titration |
| Kim[32] | silica | $\sim10^{-4}$ | | 27 Pa | smith diffusion method + thermocouple probe |
| Adams[31] | Si | $2.6\times10^{-3}$ | ~ 300 | 133 Pa | two-dimensional model (Chantry equation) + TALIF[1] calibrated by NO titration |
| Adams[31] | Si | $1.6\times10^{-3}$ | ~ 300 | 399 Pa | |
| Adams[31] | Si | $5\times10^{-5}$ | ~ 300 | 665 Pa | |
| Herron[33] | Pyrex contaminated with water | $1.6\times10^{-5}$ | 195–450 | 400 Pa | flow system + NO titration |

**Table 2:** Recombination coefficients for polymer PTFE, plastic foil (the authors give no information on the type of the foil) and ceramics BN
**Tabela 2:** Rekombinacijska koeficienta za polimer PTFE, plastično folijo (avtorji niso podali informacije o vrsti folije) in keramiko BN

| Reference | Material | Recombination coefficient | Temperature (K) | Pressure (Pa) | Method |
|---|---|---|---|---|---|
| Ricard[19] | Plastic foil | $3\times10^{-4}$ | 300 | 399 Pa | afterglow intensity measurements |
| Ricard[19] | Teflon | $10^{-5}$ | 300 | 399 Pa | afterglow intensity measurements |
| Young[24] | Teflon | $2.9\times10^{-5}$ | / | 133–1596 Pa | flow system+ afterglow intensity measurements |
| Evenson[29] | Teflon | $0.2\times10^{-6}$ | / | 40 Pa | resonant cavity, pure nitrogen plasma |
| Evenson[29] | Teflon | $2.5\times10^{-5}$ | / | 40 Pa | resonant cavity, nitrogen plasma with oxygen impurities |
| Oinuma[27] | BN | $4.8\times10^{-5}$ | 323 | atmospheric pressure | two-dimensional numerical model |
| Adams[31] | BN | $2\times10^{-4}$ | 300 | 665 Pa | two-dimensional model (Chantry equation) + TALIF calibrated by NO titration |

A similar behaviour as for glasses is found for some polymers. PTFE (teflon) has been known for decades as a very inert material. Not surprisingly, the recombination coefficient for nitrogen atoms has been found as low as for glasses. **Table 2** summarizes the recombination coefficients for two types of polymers. Again, a rather low recombination coefficient of $10^{-4}$ is due to a lack of adsorption sites for neutral nitrogen atoms on such materials. Similarly low coefficients were also found for some ceramics. The value for boron nitride is added to **Table 2**. The coefficient is somehow higher than for glasses or Teflon and this fact can be explained by existence of irregularities on the surface of otherwise well bounded material.

Moderately large recombination coefficients are found for many metals including silver (Ag), aluminium (Al), iron (Fe), and molybdenum (Mo). The recombination coefficients for these materials are presented in

[1] (TA)LIF – (Two Atom) Laser Induced Fluorescence
[2] OES – Optical Emission Spectroscopy
[3] ESR – Electron Spin Resonance

**Table 3:** The recombination coefficients for metals such as Ag, Al, Cu, Fe, Mo and for stainless steel. Data for Mo were estimated from the graph $\gamma(T)$ which was published in a relevant reference.
**Tabela 3:** Rekombinacijski koeficienti za kovine Ag, Al, Cu, Fe, Mo ter za nerjavno jeklo. Podatki za Mo so bili odčitani iz grafa $\gamma(T)$, ki je bil objavljen v ustrezni literaturi označeni v tabeli.

| Reference | Material | Recombination coefficient | Temperature (K) | Pressure (Pa) | Method |
|---|---|---|---|---|---|
| Hartunian[34] | Ag | $<10^{-2}$ | 300 | 13–133 Pa | catalytic probe + NO titration |
| Ricard[19] | Al | $6\times10^{-4}$ | 300 | 399 Pa | afterglow intensity measurements |
| Hartunian[34] | Al | $<10^{-2}$ | 300 | 13–133 Pa | catalytic probe + NO titration |
| Adams[31] | Al | $2.8\times10^{-3}$ | 300 | 133 Pa | two-dimensional model (Chantry equation) + TALIF calibrated by NO titration |
| Adams[31] | Al | $1.8\times10^{-3}$ | 300 | 399 Pa | |
| Adams[31] | Al | $1.0\times10^{-3}$ | 300 | 665 Pa | |
| Oinuma[27] | Al | $1.8\times10^{-4}$ | 323 | atmospheric pressure | two-dimensional numerical model |
| Ricard[19] | Cu | $2\times10^{-3}$ | 300 | 399 Pa | afterglow intensity measurements |
| Hartunian[34] | Cu | $7\times10^{-2}$ | 300 | 13–133 Pa | catalytic probe + NO titration |
| Lefevre[35] | Fe foil with $Fe_2O_3$ layer | $8.2\times10^{-2}$ Exp (–11400/RT) | 300–473 | 1500 Pa $Ar/N_2$=1000/50 sccm | numerical procedure of hydrodynamic model + OES + NO titration |
| Belmonte[36] | $Fe_2N_{1-x}$ | $1\times10^{-2}$ | 823 | 900 Pa $Ar/N_2$=60%/40% | numerical procedure of hydrodynamic model + OES + NO titration |
| Belmonte[30] | nitrided Fe foil | $6.7\times10^{-4}$ | 300 | 1500 Pa $Ar/N_2$=1000/50 sccm | numerical procedure of hydrodynamic model + OES + NO titration |
| Mozetic[13] | nitrided Fe foil | 0.21 | 400 | 100 Pa $N_2$=600 sccm Ar=200–3000 sccm | catalytic probe |
| Lefevre[37] | $Fe_2O_3$ | 58.1×Exp (–26940/RT) | 300–330 | 1500 Pa Ar with 4.7% $N_2$ | numerical procedure of hydrodynamic model + OES + NO titration |
| Hays[38] | Mo sputtered on Pyrex | $4.4\times10^{-3}$ | 283 | 665 Pa | intensity measurements during plasma decay (continuity equation) |
| Hays[38] | Mo sputtered on Pyrex | $4.8\times10^{-3}$ | 307 | 665 Pa | |
| Hays[38] | Mo sputtered on Pyrex | $4.9\times10^{-3}$ | 317 | 665 Pa | |
| Hays[38] | Mo sputtered on Pyrex | $5.7\times10^{-3}$ | 407 | 665 Pa | |
| Hays[38] | Mo sputtered on Pyrex | $7.4\times10^{-3}$ | 482 | 665 Pa | |
| Hays[38] | Mo sputtered on Pyrex | $8.4\times10^{-3}$ | 557 | 665 Pa | |
| Hays[38] | Mo sputtered on quartz | $6.11\times10^{-3}$ | 300 | 13.3 Pa | intensity measurements during plasma decay (continuity equation) |
| Hays[38] | Mo sputtered on quartz | $5.58\times10^{-3}$ | 300 | 27.9 Pa | |
| Hays[38] | Mo sputtered on quartz | $2.73\times10^{-3}$ | 300 | 105 Pa | |
| Hays[38] | Mo sputtered on quartz | $2.19\times10^{-3}$ | 300 | 154.3 Pa | |
| Hays[38] | Mo sputtered on quartz | $2.11\times10^{-3}$ | 300 | 240 Pa | |
| Hays[38] | Mo sputtered on quartz | $4.52\times10^{-3}$ | 300 | 45.2 Pa | |
| Hays[38] | Mo sputtered on quartz | $3.68\times10^{-3}$ | 300 | 67.8 Pa | |
| Adams[31] | Stainless steel | $7.5\times10^{-3}$ | ~ 300 | 133 Pa | two-dimensional model (Chantry equation) + TALIF calibrated by NO titration |
| Adams[31] | Stainless steel | $6.3\times10^{-3}$ | ~ 300 | 399 Pa | |
| Adams[31] | Stainless steel | $4.8\times10^{-3}$ | ~ 300 | 665 Pa | |
| Singh[39] | Stainless steel | $7\times10^{-2}$ | 330 | 173–532 Pa | steady state plasma model + NMS[4] and EEDF[5] measurements |
| Oinuma[27] | Stainless steel | $1.8\times10^{-3}$ | 323 | atmospheric pressure | Two-dimensional numerical model |

[4] NMS – Neutral Mass Spectrometry
[5] EEDF – Electron Energy Distribution Function

**Table 4:** The recombination coefficients for catalytic materials such as Co, Ir, Pd, Pt and W. The recombination coefficient is temperature independent for Pd and Pt. For other materials the recombination coefficient is temperature dependent and it was estimated from the graph $\gamma(T)$ which was published in a relevant reference.

**Tabela 4:** Rekombinacijski koeficienti za katalitične materiale kot so Co, Ir, Pd, Pt in W. Rekombinacijski koeficient ni odvisen od temperature za materiala Pd in Pt. Za ostale materiale je temperaturno odvisen in je bil odčitan iz grafa $\gamma(T)$, ki je bil objavljen v ustrezni literaturi označeni v tabeli.

| Reference | Material | Recombination coefficient | Temperature (K) | Pressure (Pa) | Method |
|---|---|---|---|---|---|
| Halpern[40] | Co | 0.43 | 418 | 133 Pa | flow system + NO titration |
| Halpern[40] | Co | 0.51 | 446 | 133 Pa | flow system + NO titration |
| Halpern[40] | Co | 0.55 | 556 | 133 Pa | flow system + NO titration |
| Halpern[40] | Co | 0.54 | 605 | 133 Pa | flow system + NO titration |
| Halpern[40] | Co | 0.54 | 656 | 133 Pa | flow system + NO titration |
| Halpern[40] | Co | 0.55 | 676 | 133 Pa | flow system + NO titration |
| Halpern[40] | Co | 0.54 | 791 | 133 Pa | flow system + NO titration |
| Halpern[40] | Co | 0.49 | 882 | 133 Pa | flow system + NO titration |
| Halpern[40] | Co | 0.43 | 938 | 133 Pa | flow system + NO titration |
| Halpern[40] | Co | 0.41 | 987 | 133 Pa | flow system + NO titration |
| Halpern[40] | Ir | 0.32 | 1115 | 133 Pa | flow system + NO titration |
| Halpern[40] | Ir | 0.26 | 1146 | 133 Pa | flow system + NO titration |
| Halpern[40] | Ir | 0.34 | 1202 | 133 Pa | flow system + NO titration |
| Halpern[40] | Ir | 0.27 | 1246 | 133 Pa | flow system + NO titration |
| Halpern[40] | Ir | 0.27 | 1302 | 133 Pa | flow system + NO titration |
| Halpern[40] | Ir | 0.37 | 1400 | 133 Pa | flow system + NO titration |
| Halpern[40] | Ir | 0.38 | 1490 | 133 Pa | flow system + NO titration |
| Halpern[40] | Ir | 0.37 | 1517 | 133 Pa | flow system + NO titration |
| Halpern[40] | Ir | 0.38 | 1591 | 133 Pa | flow system + NO titration |
| Halpern[40] | Ir | 0.40 | 1678 | 133 Pa | flow system + NO titration |
| Halpern[40] | Ir | 0.46 | 1729 | 133 Pa | flow system + NO titration |
| Halpern[40] | Ir | 0.45 | 1779 | 133 Pa | flow system + NO titration |
| Halpern[40] | Ir | 0.47 | 1828 | 133 Pa | flow system + NO titration |
| Halpern[40] | Ir | 0.41 | 1872 | 133 Pa | flow system + NO titration |
| Halpern[40] | Ir | 0.45 | 1921 | 133 Pa | flow system + NO titration |
| Halpern[40] | Ir | 0.44 | 1946 | 133 Pa | flow system + NO titration |
| Halpern[40] | Ir | 0.48 | 2020 | 133 Pa | flow system + NO titration |
| Halpern[40] | Pd | 0.3 | 500–1100 | 133 Pa | flow system + NO titration |
| Halpern[40] | Pt | 0.31 | 500–1600 | 133 Pa | flow system + NO titration |
| Halpern[40] | W | 0.21 | 1614 | 133 Pa | flow system + NO titration |
| Halpern[40] | W | 0.24 | 1684 | 133 Pa | flow system + NO titration |
| Halpern[40] | W | 0.29 | 1759 | 133 Pa | flow system + NO titration |
| Halpern[40] | W | 0.32 | 1821 | 133 Pa | flow system + NO titration |
| Halpern[40] | W | 0.36 | 1896 | 133 Pa | flow system + NO titration |
| Halpern[40] | W | 0.40 | 1960 | 133 Pa | flow system + NO titration |
| Halpern[40] | W | 0.43 | 2023 | 133 Pa | flow system + NO titration |
| Halpern[40] | W | 0.48 | 2091 | 133 Pa | flow system + NO titration |
| Halpern[40] | W | 0.53 | 2161 | 133 Pa | flow system + NO titration |
| Halpern[40] | W | 0.57 | 2235 | 133 Pa | flow system + NO titration |
| Halpern[40] | W | 0.58 | 2315 | 133 Pa | flow system + NO titration |
| Halpern[40] | W | 0.68 | 2402 | 133 Pa | flow system + NO titration |
| Halpern[40] | W | 0.74 | 2500 | 133 Pa | flow system + NO titration |

**Table 3**. One should read the results for these particular materials with some precaution. These materials are known to form native oxide films. The oxide films can be removed prior to experiments with neutral nitrogen atoms but it is rather difficult to keep oxygen free surface in plasma reactors due to the existence of residual atmosphere, especially water vapour. The dissociation energy of water vapour is much lower than for nitrogen molecule so any water that appears in a nitrogen plasma reactor is likely to be dissociated to highly oxidative radicals such as O and OH. These radicals may stick on surfaces even though a lot of precautions were taken in order to assure appropriate cleanliness of the material surfaces.

The highest recombination coefficients are found for catalytic materials. The results for these particular materials are summarized in **Table 4**. These materials are known for their good chemisorption abilities and transformation of a variety of radicals to stable molecules even at low temperatures. Not surprisingly they are also good catalysts for neutral nitrogen atoms. The recombination coefficient can be as high as 0.4 at room temperature.

## 4 CONCLUSIONS

An overview of recombination coefficients was presented. The data summarized in this paper are useful for understanding the interaction between nitrogen plasma and solid materials. The first consideration goes for the right choice of the materials used for plasma facing components. More than obvious, catalytic materials should be avoided if a high density of nitrogen atoms in plasma is required. The best material for construction of nitrogen plasma reactors is the one with the lowest recombination coefficient, i.e. Pyrex. Just next to Pyrex is quartz glass. Both materials are high vacuum materials and thus very useful for construction of even large reactors where the purity of processing gas is important. From the recombination point of view polymers are often suitable but in practice they are usually avoided because they are not vacuum materials. If, for any reason glass should be avoided and only metals can be used, the recommended material is aluminium covered by a thin film of alumina (oxide). The oxide film should be compact and rather smooth in order to assure for low recombination coefficient and high stability of surface properties even after prolonged application. Other materials except some ceramics are not suitable as plasma facing components in nitrogen reactors due to a rather high recombination coefficient or rather unpredictable behaviour.

### Acknowledgements

The authors acknowledge the financial support from the Ministry of Higher Education, Science and Technology of the Republic of Slovenia through the contract No. 3211-10-000057 (Centre of Excellence Polymer Materials and Technologies).

## 5 REFERENCES

[1] A. Vesel, M. Mozetic, A. Zalar, Surf. Interface Anal., 40 (**2008**) 3–4, 661–663
[2] A. Vesel, I. Junkar, U. Cvelbar, J. Kovac, M. Mozetic, Surf. Interface Anal., 40 (**2008**) 11, 1444–1453
[3] A. Ricard, Reactive plasmas, SFV, Paris, 1996
[4] Z. Lj. Petrovic, V. Stojanovic, Z. Nikitovic, Plasma Sources Sci. Technol., 18 (**2009**) 3, 034017
[5] L. M. Isola, B. J. Gómez, V. Guerra, J. Phys. D Appl. Phys., 43 (**2010**) 1, 015202
[6] V. D. Stojanovic, B. M. Jelenkovic, Z. Lj. Petrovic, J. Appl. Phys., 81 (**1997**) 3, 1601–1603
[7] http://demonstrations.wolfram.com/LowerExcitedStatesOfHeliumAtom/
[8] http://hyperphysics.phy-astr.gsu.edu/hbase/quantum/helium.html
[9] A. Vesel, U. Cvelbar, M. Mozetic, N. Krstulovic, I. Labazan, S. Milosevic, Mater. Tehnol., 38 (**2004**) 3/4, 177–180
[10] R. Zaplotnik, M. Kolar, A. Doliska, K. Stana-Kleinschek, Mater. Tehnol., 45 (**2011**) 3, 195–199
[11] F. Gaboriau, U. Cvelbar, M. Mozetic, A. Erradi, B. Rouffet, J. Phys. D Appl. Phys. 42 (**2009**) 5, 055204
[12] M. Mozetic, A. Ricard, D. Babic, I. Poberaj, J. Levaton, V. Monna, U. Cvelbar, J. Vac. Sci. Technol. A 21 (**2003**), 369–374
[13] M. Mozetic, U. Cvelbar, A. Vesel, A. Ricard, D. Babic, I. Poberaj, J. Appl. Phys., 97 (**2005**) 10, 103308-1–103308-7
[14] M. Mozetic, Surf. Coat. Technol., 201 (**2007**) 9–11, 4837–4842
[15] J. A. Ferreira, F. L. Tabares, D. Tafalla, J. Nucl. Mater. 363–365 (**2007**), 888–892
[16] W. Brennen, E. C. Shane, J. Phys. Chem., 75 (**1971**), 1552
[17] B. Gordiets, C. M. Ferreira, J. Nahorny, D. Pagnon, M. Touzeau, M. Vialle, J. Phys. D: Appl. Phys., 29 (**1996**), 1021–1031
[18] Wentink T., J. O. Sullivan, K.L. Wray, J. Chem. Phys., 29 (**1958**) 231
[19] A. Ricard, A. Popescu, A. Baltog, C.P. Lungu, Le VIDE, 280 (**1996**), 248–253
[20] K. M. Sancier, W. J. Fredericks, J. L. Hatchett, H. Wise, J. Chem. Phys., 37 (**1962**), 860–864
[21] T. C. Marshall, Phys. Fluid, 5 (**1962**), 742–753
[22] T. Yamashita, J. Chem. Phys., 70 (**1979**), 4248
[23] C. Mavroyannis, C.A. Winkler, Can. J. Chem., 39 (**1961**), 1601–1607
[24] R. A. Young, J. Chem. Phys., 34 (**1961**), 1292–1294
[25] B. Gordiets, C. M. Ferreira, J. Nahorny, D. Pagnon, M. Touzeau, M. Vialle, J. Phys. D: Appl. Phys., 29 (**1996**), 1021–1031
[26] L. Lefevre, T. Belmonte, H Michel, J. Appl. Phys., 87 (**2000**), 7497
[27] G. Oinuma, Y. Inanaga, Y. Tanimura, M. Kuzumoto, Y. Tabata, K. Watanabe, J. Phys. D Appl. Phys., 43 (**2010**) 25, 255202-1–255202-8
[28] T. Marshall, J. Chem. Phys., 37 (**1962**), 2501–2502
[29] K. M. Evenson, D. S. Burch, J. Chem. Phys., 45 (**1966**), 2450–2460
[30] T. Belmonte, L. Lefevre, T. Czerwiec, H. Michel, A. Ricard, Thin Solid Films, 341 (**1999**), 27–30
[31] S. F. Adams, T.A. Miller, Plasma Sorces Sci. Technol., 9 (**2000**), 248–255
[32] Y. C. Kim, M. Boudart, Langmuir, 7 (**1991**), 2999–3005
[33] J. T. Herron, J. L. Franklin, P. Bradt, V. H. Diebeler, J. Chem. Phys., 30 (**1959**), 879–885
[34] R. A. Hartunian, W. P. Thompson, S. Safron, J. Chem. Phys., 43 (**1965**), 4003–4006
[35] L. Lefevre, T. Belmonte, T. Czerwiec, A. Ricard, H Michel, Appl. Surf. Sci., 153 (**2000**), 85–95
[36] T. Belmonte, S. Bockel, C. Bordot, D. Ablitzer, H. Michel, Appl. Surf. Sci., 135 (**1998**), 259–268
[37] L. Lefevre, T. Belmonte, T. Czerwiec, A. Ricard, H Michel, Surf. Coat. Technol., 116–119 (**1999**), 1244–1248
[38] G. N. Hays, C. J. Tracy, H. J. Oskam, J. Chem. Phys., 60 (**1974**), 2027
[39] H. Singh, J. W. Coburn, D. B. Graves, J. Appl. Phys., 88 (**2000**), 3748–3755
[40] B. Halpern, D. E. Rosner, Trans. Farad. Soc., 74 (**1978**), 1883–1912

UDK 533.9:66.017
Review article/Pregledni članek

ISSN 1580-2949
MTAEC9, 46(1)13(2012)

# DUSTY PLASMA DEPOSITION OF NANOCOMPOSITE THIN FILMS

## NALAGANJE NANOKOMPOZITNIH TANKIH PLASTI S PRAŠNO PLAZMO

**Aleksander Drenik[1], Richard Clergereaux[2]**

[1]Center of Excellence for Polymer Materials and Technologies, Tehnološki park 24, 1000 Ljubljana, Slovenia
[2]UPS, INPT, LAPLACE (Laboratoire Plasma et Conversion d'Energie), Université de Toulouse, 118 route de Narbonne, F-31062 Toulouse cedex 9, France
aleksander.drenik@ijs.si

*Prejem rokopisa – received: 2011-07-15; sprejem za objavo – accepted for publication: 2011-08-03*

Dusty plasma has traditionally been considered as pollutant species in plasma processes. However, lately it is being regarded as an interesting way of producing nanocomposite thin films. In this paper, the basics of dusty plasma physics are presented. Discussed is the nucleation and growth, which can be either a consequence of homogeneous plasma reactions, heterogeneous reactions on the plasma-surface interface or they can be injected externally into the plasma. The particles are negatively charged, which strongly influences their movement. The most important interaction is the repelling force in the plasma sheath which confines the particles to the plasma volume. Also presented in this paper are the basic properties of nanocomposite thin films and their application in modern technological and industrial applications. Examples of dusty plasma produced nanocomposite thin films are given in the final chapter.

Keywords: dusty plasma, nanocomposite thin films

Navadno so pojav prašne plazme v plazemskih reaktorjih povezovali z nečistočami v plazmi, zadnja leta pa jih dojemajo tudi kot zanimivo orodje za nalaganje nanokompozitnih tankih plasti. V pričujočem prispevku predstavljamo osnove fizike prašnih plazem. Govora je o nukleaciji in rasti, ki je lahko posledica homogenih reakcij v prostornini plazme, posledica heterogenih reakcij na stični plasti med plazmo in trdno površino, ali pa so lahko vstavljeni v plazmo od zunaj. Delci imajo negativen električni naboj, kar močno vpliva na njihovo gibanje. Najpomembnejša interakcija je odbojna sila v plašču plazme, ki zadržuje delce v prostornini plazme. V prispevku so pravtako predstavljene osnovne lastnosti nanokompozitnih tankih plasti in njihove uporabe v sodobnih tehnoloških in industrijskih aplikacijah. V zadnjem poglavju so predstavljeni primeri nanokompozitnih tankih plasti, pripravljeni s pomočjo prašne plazme.

Ključne besede: prašna plazma, nanokompozitne tanke plasti

## 1 INTRODUCTION

The phenomenon of formation of dusty particles in plasmas has been known almost as long as the plasmas themselves [1], however the research of the "dusty plasma" has considerably lagged behind the general knowledge of plasmas. Since then, plasmas have proven to be indispensable tools in research, technological and industrial processes, where their use ranges from relatively benign and non-intrusive surface modification to thermonuclear fusion, encompassing technologies such as selective etching[2–8], cleaning of metallic surfaces[9–12], biomedical application such as improving bio-compatibility of prosthetics[13] and sterilization[14,15], thin-film deposition, etc[9,12,16–28]. Regardless of the application, one of the key requirements for the plasma was purity as too high a concentration of impurities would hinder the efficiency of the process, if not outright rendering it useless. In this context, the appearance of dusty particles in the plasma was a most undesired occurrence.

However, in the recent years, there has been a renewed interest in the field of dusty plasmas. The motivation for the research ranges from the intent to increase the efficiency of production of solid particles to avoid the formation of dust altogether. Regardless of the motivation, the importance, and the world-wide interest in the field is perhaps best illustrated by the fact that one of the physical experiments aboard the International Space Station has been dedicated to the study of dusty plasmas under microgravity conditions[29]. Moreover, the perception of dusty plasmas in technological processes is also changing as they are not regarded merely as an unwanted side-effect, but also as a very attractive tool for producing nanocomposite thin films.

## 2 DUSTY PLASMA

### *2.1 Appearance of dust particles*

By definition, dusty plasma is plasma containing solid particles, usually of micrometric or nanometric proportions, however the source of the particles can differ greatly from case to case. The particles can be introduced externally, or they can be a consequence of reactions in the reactor, be it homogeneous reactions in the plasma volume or heterogeneous reactions on the solid surfaces within the reactor.

Particles of virtually any material and in sizes ranging from a couple of 10 nm to several μm can be injected into plasmas[29–32]. This kind of particle introduction is especially suited to basic research of dusty plasma properties, since it allows for a high degree of

control over the chemical composition and the size distribution of the solid particles.

In a way, external introduction of solid particles may also be a consequence of surface reactions in the plasma reactor, in which material from plasma-facing surfaces is ejected into the plasma. Such cases can include sputtering[33–36], evaporation, arching, etc[37]. Naturally, the control over the size distribution of the particles introduced into the plasma is, in this case, inherently much lower.

In contrast to externally injected particles, which are generally composed of different elements and compounds that make up the plasma, particles can also grow from precursors which are at the same time plasma species. Well documented examples of such particle growth are the appearance of solid particles in silane containing plasmas, and in plasmas containing hydrocarbon species such as methane, acetylene, etc.

In silane containing plasmas, the nucleation starts with the reaction[38]:

$$SiH_3^- + SiH_4 \rightarrow Si_2H_5^- + H_2 \qquad (1.1)$$

in which a negative silane ion $SiH_3^-$ reacts with a silane molecule, creating a heavier negative ion $SiH_3^-$ and a hydrogen molecule. The resulting heavier ion reacts with another silane molecule, forming an even heavier ion, and thus the reaction continues for larger and larger clusters:

$$Si_nH_{2n-1}^- + SiH_4 \rightarrow Si_{n+1} + H_{2n+3}^- + H_2 \qquad (1.2)$$

Such clusters grow to the size of approximately 2 nm. After that, the attachment of negative ions becomes more likely than the chain formation reaction, and agglomeration of clusters begins. This way, particles can grow up to several 100 nm in size[39]. An example of such particles is presented in **Figure 1**.

A similar reaction takes place in acetylene plasmas, where a negative ion, $C_2H^-$ reacts with an acetylene molecule[40]:

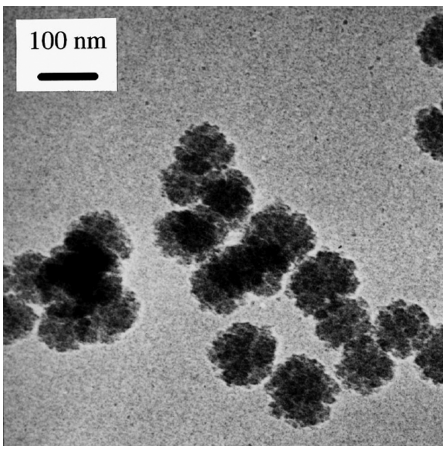


**Figure 1:** TEM image of Si – based particles, deposited in a dusty RF discharge, created in a mixture of argon and silane, **Figure 6** in[39]
**Slika 1:** TEM slika silicijevih delcev, ki so nastali v prašni RF razelektritvi mešanice argona in silana, **Slika 6** v[39]

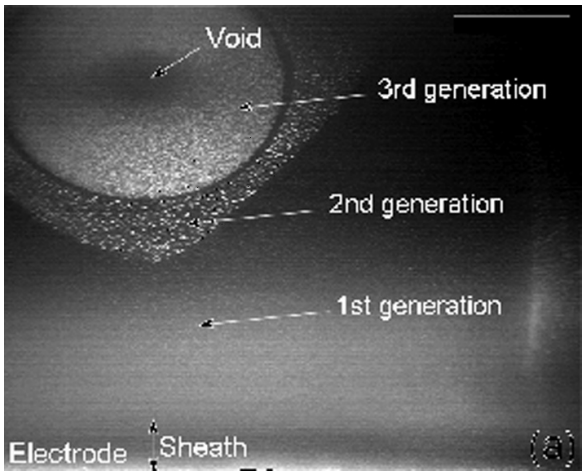


**Figure 2:** Generations of particles grown in the same discharge, **Figure 4a** in[29]
**Slika 2:** Generacije delcev, ki nastanejo v isti razelektritvi, **Slika 4a** v[29]

$$C_2H^- + C_2H_2 \rightarrow C_4H^- + H_2 \qquad (1.3)$$

The resulting heavier negative ion again engages in growth reactions:

$$C_{2n}H^- + C_2H_2 \rightarrow C_{2n+2}H^- + H_2 \qquad (1.4)$$

Dust particles composed from plasma species can also be formed in heterogeneous, surface reactions. In this case, plasma species are deposited on solid surfaces within the reactor, forming a thin film. Subsequently, this thin film is degraded in a way that it begins to crack or flake. The flakes peel off the surface and re-enter the plasma. This process generally produces the most random size and shape distribution of the dusty particles.

However, in a realistic case, the growth of particles can rarely be defined as only one of the described processes, rather than a combination of various processes. Erosion of material from solid surfaces does not necessarily result directly in a population of solid particles in the plasma – the material is not only eroded in the form of solid particles, but also in the form of precursors, from which particles grow in the gas phase.

Moreover, the choice of solid surfaces needs not to be limited only on walls of the plasma containing vessel, electrodes, target plates, etc. Indeed, the dust particles themselves can be eroded by the surrounding plasma, thus ejecting precursor species for a new generation of particles to be formed in the plasma[29,41]. The subsequently formed generations of particles are of course subject to the same erosion mechanism and so further generations are formed, resulting in a periodical growth of particle generations, as seen in **Figure 2** [29].

Most interestingly, combination of various growth mechanisms can result in a heterogeneous structure of the dusty particles. Particles, ejected from the solid plasma facing surfaces can act as nucleation centers for growth of layers deposited by the plasma. This results in particles with a core composed of material ejected from

the surface, and a shell composed of material grown from plasma species.[37]

### *2.2 Behavior of dust particles in the plasma*

The behavior of the dusty particles inside a plasma is governed most strongly by their electric charge. The most important feature of this interaction is that a negatively charged particle will be repelled away from the plasma sheath, thus being confined to the plasma volume. This significantly increases the residence time of the particles, allowing them to grow by several orders of magnitude before the electrostatic force is finally overcome by other forces acting on the particles. Most commonly, the chief force which counteracts the electrostatic repulsion is gravity, though experiments have also been performed in microgravity conditions.[29] Another important force is the drag force of the gas in flow-through experimental set-ups.

In magnetized plasmas, the magnetic field has also a prominent effect on the behavior of particles, provided they are moving around the plasma volume, rather than being stationary. The effect of the magnetic field is manifested in the curved trajectories of the particles[37,42]. It also contributes to the confinement of the particles to the plasma volume.

As any non-biased solid surface accumulates electrons from the plasma, we can expect the dusty particles to be negatively charged as well. However, this may not always be the case.

When we consider the particles grown in homogeneous gas-phase reactions in the plasma volume, we should keep in mind that particles acquire electric charge differently in different stages of their growth. The particle growth begins with the formation of negative clusters, that although increasing in size, they never appear to have more than one excess electron. Moreover, the negatively charged clusters are likely to transfer the electron to a positive ion (such as $Ar^+$), becoming neutral particles in the process. The electric charge of the clusters then depends on the electron affinity of the samples and the probability of the charge-transfer reaction. By losing an electron, and thus becoming electrically neutral, the growth of the cluster is terminated, as only negative ions engage in growth reactions. Moreover, the neutral particle is not confined by the potential drop and faces the danger of being carried away from the discharge region by the gas drift velocity. By electron attachment, the cluster becomes negative again, and both growth reactions and entrapment by electric field are resumed. Once the clusters reach a certain critical size, the attachment of negative ions becomes more likely than the growth of the original chain of the cluster. Thus, the electric charge can accumulate to greater quantities.

Conversely, when considering bigger particles, the situation is much different. We can consider the surface of the particle as any other plasma facing surface. This means that it will accumulate as much charge as necessary until the surface achieves the floating potential. This quantity of charge can be calculated if we consider the particle as a spherical capacitor with the capacity $C$:

$$C = \frac{4\pi\varepsilon_0}{\frac{1}{r} - \frac{1}{r+d_s}} \tag{1.5}$$

where $r$ is the particle diameter, $d_s$ is the sheath thickness and $\varepsilon_0$ is the vacuum permittivity constant. Of course, this equation is only valid when the particles are spherically shaped, which may not always be the case. The amount of charge, $q$, accumulated on the particle surface is:

$$q = CU_{\mathrm{fl}} \tag{1.6}$$

where $U_{fl}$ is the floating potential of the plasma. Again, this evaluation is valid only when the density of the particles in the plasma is low enough for the particles to be considered as independent.

However, when the density of the dusty particles increases so much that the average distance between particles becomes of the order of the Debye length, it is no longer possible to neglect the effect of the high density of the particles. An immediate effect of the high particle density is that the plasma is unable to provide the particles with enough electrons as required by to sustain the floating potential. Then, the average amount of charge carried by a single particle is:

$$q \approx \frac{n_i}{n_e} q_0 \tag{1.7}$$

where $n_i$ is the density of ions, $n_e$ is the density of electrons in the plasma and $q_0$ is the elementary charge. In such cases, the majority of the negative charge in the plasma is represented by the solid particles, rather than electrons. Obviously, the plasma can not remain unaffected by the dust particles.

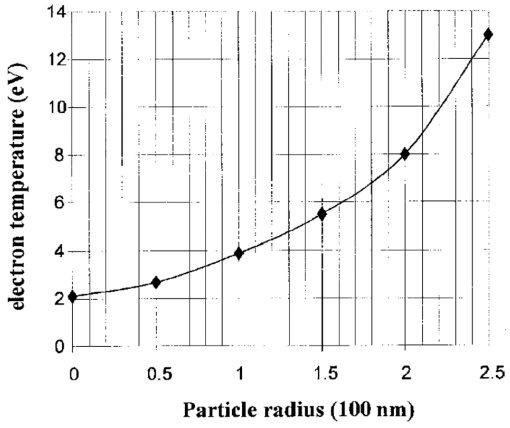


**Figure 3:** Theoretical prediction of the electron temperature as a function of the dust-particle size, **Figure 8** in[43]

**Slika 3:** Teoretična napoved temperature elektronov v odvisnosti od velikosti prašnih delcev, **Slika 8** v[43]

The most noticeable consequence of the increase of dust population is a significant decrease of the electron population. It has been shown that once the dust particles grow over a certain critical value, the electron density drops for a factor of about 5 [43].

At the same time, in order to sustain the same rate of ionization, the electron temperature drastically increases, up to 6 – 8 eV [43], illustrated in **Figure 3**. This in turn enhances the dissociation of source gas molecules by almost an order of magnitude. This phenomenon can be utilized in plasma processes, where a high degree of dissociation is required, such as PECVD. Particles are introduced into the discharge and effectively extracted (by electric or thermophoretic forces) in order to increase the efficiency of the plasma process. Dust can also cause instabilities in the plasma, which are reflected on the self-bias voltage, emitted light and plasma current[44,45].

The dusty particles do not influence only the discharge, but also each other. Once their density increases enough that they can not be considered independent, the interparticle interaction become increasingly important. Independent particles experience a confinement force only in the sheath region, whereas in the plasma volume, they are subject to other forces which govern their movement – gravity, drag forces of the gas flow, thermophoretic forces, etc. Thus independent particles would concentrate around the sheath region – the only place where the electrostatic interaction would counteract other forces, acting on the particles. In dusty dense plasmas, however, the particles fill out a fraction of the plasma volume which is considerably larger that the narrow sheath region, forming a cloud of particles[46]. The cloud is pressed against the sheath, however interparticle interactions are preventing it from collapsing. Particle clouds have been also observed to show collective movement[47] or even form crystalline structures[30–32].

### *2.3 Deposition of nanocomposite thin films by dusty plasma*

Although certain forms of nanocomposite materials have been in use for a long time, the current level of interest appeared – and the term "nanocomposite" was coined – with the advent of diagnostic techniques which allow for analyses of materials on the nanometric scale. Composite materials with nanometric components are particularly interesting because the nano-size of filler particles brings novel properties in practically any aspect, be it mechanical, electric, thermal, optical, electrochemical, catalytic, etc.

Nanocomposite thin films are no exception as they, too, feature very interesting properties and can be used as hard, nonflammable[48,49] or biocompatible coatings[33], field emitting materials[50–52], etc. Such nanocomposite thin films have thus many potential application in the field of aerospace, biotechnology or microelectronics, where they could be used to produce non-volatile memory devices[53], light emitting diodes[54], chemical sensors[55], absorbent layers for solar cells[56], quantum dots[57], etc.

An example of a biomedical application of such nanocomposite thin films are organosilicon thin films with embedded silver nanoclusters[33]. Silver ions and compounds have been long known to exhibit antimicrobial properties[58], however the price of silver is rather prohibitive for construction of massively used food containers, and due to its mechanical properties, it is also perhaps not the ideal material for medical devices such as orthopedic prosthesis, dental implants, etc. However, by embedding nanometric grains of silver into a matrix of polymer or organosilicon materials, it is possible to have the antimicrobic activities of silver for the price of plastics.

Silver nanograined organosilicon films were prepared in a capacitively coupled radiofrequency plasma reactor by a dual action of a simultaneous PE-CVD in an argon-hexamethyldisiloxane plasma and sputtering of a silver target on the powered electrode, which were applied alternately.[33] During the PE-CVD stage, $SiC_xO_yH_z$ complexes were deposited on the substrate surface and were polymerized. During the sputtering phase, a beam of energetic argon ions was used to sputter atoms of silver from the target. The silver atoms formed silver clusters which were embedded in the matrix. Thusly produced thin films exhibited an improved antifungal activity, which could be put to good use in various bio-medical and other applications.

Another interesting field of plasma deposited nanocomposite thin films are thin films with an amorphous hydrogenated carbon (a-C:H) matrix in which are embedded graphite-like nanograins. The a-C:H was extensively studied as it exhibits low-k and insulating properties, which makes it suitable a material as dielectric in ULSI chips, passivation or optical layer[59–61]. As a result, the methods of plasma deposition of a-C:H are now at the stage of high control of film quality, high efficiency and reproducibility[62]. Unfortunately, the thermal stability of a-C:H thin films leaves much to be desired – at the temperature of 200 °C, the structure is already degraded, which in turn leads to a degradation of the dielectric properties. Addition of graphite-like nanograins into an a-C:H matrix results in a semi-insulating material with a considerably higher thermal stability. Moreover, such nanocomposite thin films also exhibit photoconductive properties. The carbon-grained, a-C:H nanocomposites can be also used in biomedical applications[63]. Carbon-based materials are attractive as coatings of prostheses due to their biocompatibility, chemical inertness[64,65] and non-corrosiveness.

The conventional way of producing such nanocomposites is based on chemical synthesis[66]. It requires several steps involving different procedures, from synthesis of nanoparticles, mixing them with the matrix to the thin film deposition. This leads to a low level of control of the nanocomposite structure and the process

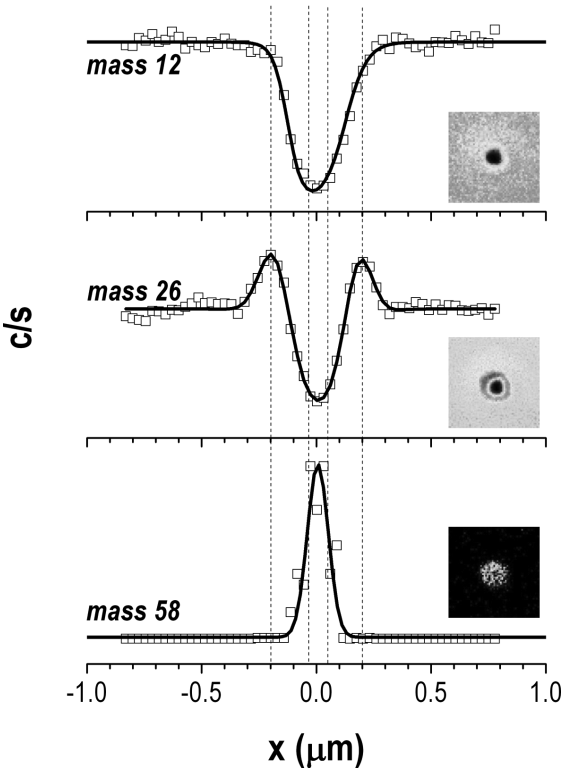


**Figure 4:** SIMS analysis of particles with a carbon-based shell around a metallic core, **Figure 8c** in[37]
**Slika 4:** SIMS analiza delcev z lupino iz ogljika okrog kovinskega jedra, **Slika 8c** v[37]

reproducibility. In contrast, using a dusty plasma as a deposition tool, the whole process is completed in a single step.

Graphite-like – a-C:H nanocomposites were deposited in a multipolar electron cyclotron resonance (ECR) microwave plasma, created in hydrocarbon containing gases such as methane and acetylene[37,42]. The key to the growth of powder particles in these cases was the magnetic field of the ECR reactor, which was used to confine the negatively charged particles to the plasma volume. The films were produced at relatively low pressures (0.1 Pa), where heterogeneous, surface-based reactions are much more probable than homogeneous reactions in the plasma volume, however, the magnetic confinement of negative ions facilitated the nucleation and growth of particles in the plasma volume. This procedure resulted in films with an a-C:H matrix and several 100 nm thick graphite-like grains[37]. However, in certain cases, the grains embedded in the film were found to have a heterogeneous structure. They were composed of an approximately 100 nm thick graphite-like shell around an approximately 20 nm thick metallic core, as seen in **Figure 4**. The metallic core originates in the erosion of the wall materials. Metallic particles enter the plasma where they act as nucleation center for growth of the graphite-like carbon layers.

## 3 CONCLUSION

Dusty plasma is, by definition, plasma which contains solid particles, usually of micrometric or nanometric dimensions. The particles can enter the plasma either by external injection, erosion of plasma-facing surfaces, heterogeneous surface reactions of plasma species or homogeneous reactions in the plasma volume, or a combination of various methods.

The particles acquire a negative electric charge, which strongly influences their behavior in the plasma volume. The most striking feature is that the electrostatic forces in the sheath region repel them from the walls of the plasma-containing vessel and confine them to the plasma volume. The particles have been observed also to interact with one-another, showing collective movement or forming crystalline structures. Moreover, the population of dust changes the properties of the discharge, where a significant drop in the electron density and a significant increase of the electron temperature are most notable.

The dusty plasmas are presented as an attractive tool for depositing nanocomposite thin films. Contrary to conventional methods where the deposition process involves several steps, in plasma deposition all phases of the process are completed in a single step. Such deposition techniques could be gainfully applied in many industrial and technological applications, ranging from microelectronic industry to aerospace industry and biomedical applications.

## Acknowledgement

The author acknowledges the financial support from the Ministry of Higher Education, Science and Technology of the Republic of Slovenia through the contract No. 3211-10-000057 (Center of Excellence Polymer Materials and Technologies).

## 4 REFERENCES

[1] I. Langmuir, C. G. Found, A. F. Dittmer, Science 60 (**1924**), 392
[2] M. K. Gunde, M. Kunaver, M. Mozetic, P. Pelicon, J. Simcic, M. Budnar, M. Bele, Surface Coatings International Part B-Coatings Transactions 85 (**2002**), 115–121
[3] M. Kunaver, M. Klanjsek-Gunde, M. Mozetic, A. Hrovat, Surface Coatings International, Part B-Coatings Transactions 86 (**2003**), 175–179
[4] M. Mozetic, Vacuum 71 (**2003**), 237–240
[5] M. K. Gunde, M. Kunaver, M. Mozetic, A. Hrovat, Powder Technology 148 (**2004**), 64–66
[6] M. Kunaver, M. Mozetic, M. Klanjsek-Gunde, Thin Solid Films 459 (**2004**), 115–117
[7] U. Cvelbar, M. Mozetic, M. Klanjsek-Gunde, Ieee Transactions on Plasma Science 33 (**2005**), 236–237
[8] A. Drenik, A. Vesel, M. Mozetic, Journal of Nuclear Materials 386 (**2009**), 893–895
[9] M. Mozetic, A. Zalar, M. Drobnic, Thin Solid Films 343 (**1999**), 101–104

[10] M. Mozetic, Informacije Midem-Journal of Microelectronics Electronic Components and Materials 33 (**2003**), 222–227
[11] M. Mozetic, A. Zalar, Vacuum 71 (**2003**), 233–236
[12] A. Vesel, M. Mozetic, A. Drenik, S. Milosevic, N. Krstulovic, M. Balat-Pichelin, I. Poberaj, D. Babic, Plasma Chemistry and Plasma Processing 26 (**2006**), 577–584
[13] I. Junkar, A. Vesel, U. Cvelbar, M. Mozetic, S. Strnad, Vacuum 84 (**2009**), 83–85
[14] Z. Vratnica, D. Vujosevic, U. Cvelbar, M. Mozetic, Ieee Transactions on Plasma Science 36 (**2008**), 1300–1301
[15] U. Cvelbar, M. Mozetic, N. Hauptman, M. Klanjsek-Gunde, Journal of Applied Physics 106 (**2009**)
[16] A. Vesel, M. Mozetic, A. Zalar, Applied Surface Science 200 (**2002**), 94–103
[17] C. Canal, F. Gaboriau, A. Ricard, M. Mozetic, U. Cvelbar, A. Drenik, Plasma Chemistry and Plasma Processing 27 (**2007**), 404–413
[18] U. Cvelbar, M. Mozetic, I. Junkar, A. Vesel, J. Kovac, A. Drenik, T. Vrlinic, N. Hauptman, M. Klanjsek-Gunde, B. Markoli, N. Krstulovic, S. Milosevic, F. Gaboriau, T. Belmonte, Applied Surface Science 253 (**2007**), 8669–8673
[19] A. Vesel, A. Drenik, M. Mozetic, A. Zalar, M. Balat-Pichelin, M. Bele, Vacuum 82 (**2007**), 228–231
[20] A. Vesel, M. Mozetic, A. Hladnik, J. Dolenc, J. Zule, S. Milosevic, N. Krstulovic, M. Klanjsek-Gunde, N. Hauptmann, Journal of Physics D-Applied Physics 40 (**2007**), 3689–3696
[21] A. Vesel, M. Mozetic, A. Zalar, Vacuum 82 (**2007**), 248–251
[22] T. Vrlinic, A. Vesel, U. Cvelbar, M. Krajnc, M. Mozetic, Surface and Interface Analysis 39 (**2007**), 476–481
[23] M. Mozetic, U. Cvelbar, A. Vesel, N. Krstulovic, S. Milosevic, Ieee Transactions on Plasma Science 36 (**2008**), 868–869
[24] A. Vesel, I. Junkar, U. Cvelbar, J. Kovac, M. Mozetic, Surface and Interface Analysis 40 (**2008**), 1444–1453
[25] A. Vesel, M. Mozetic, A. Drenik, N. Hauptman, M. Balat-Pichelin, Applied Surface Science 255 (**2008**), 1759–1765
[26] A. Vesel, M. Mozetic, A. Zalar, Surface and Interface Analysis 40 (**2008**), 661–663
[27] A. Vesel, M. Mozetic, Second International Workshop on Non-Equilibrium Processes in Plasmas and Environmental Science 162 (**2009**), 12015
[28] A. Vesel, M. Mozetic, S. Strnad, Z. Persin, K. Stana-Kleinschek, N. Hauptman, Vacuum 84 (**2009**), 79–82
[29] M. Mikikian, L. Boufendi, A. Bouchoule, H. M. Thomas, G. E. Morfill, A. P. Nefedov, V. E. Fortov, New Journal of Physics 5 (**2003**), 19.1–19.2
[30] L. Couedel, V. Nosenko, S. K. Zhdanov, A. V. Ivlev, H. M. Thomas, G. E. Morfill, Physical Review Letters 103 (**2009**), 215001
[31] V. Nosenko, S. Zhdanov, G. Morfill, Philosophical Magazine 88 (**2008**), 3747–3755
[32] V. Nosenko, S. K. Zhdanov, Contributions to Plasma Physics 49 (**2009**), 191–198
[33] C. Saulou, B. Despax, P. Raynaud, S. Zanna, P. Marcus, M. Mercier-Bonin, Applied Surface Science 256 (**2009**), S35–S39
[34] C. Arnas, C. Dominique, P. Roubin, C. Martin, C. Laffon, P. Parent, C. Brosset, B. Pegourie, Journal of Nuclear Materials 337 (**2005**), 69–73
[35] C. Arnas, C. Dorninique, P. Roubin, C. Martin, C. Brosset, B. Pegourie, Journal of Nuclear Materials 353 (**2006**), 80–88
[36] C. Arnas, A. Mouberi, K. Hassouni, A. Michau, G. Lombardi, X. Bonnin, F. Benedic, B. Pegourie, Journal of Nuclear Materials 390–91 (**2009**), 140–143
[37] M. Calafat, P. Yuryev, A. Drenik, A. Slim, R. Clergereaux, Plasma Processes and Polymers 8 (**2011**), 401–408
[38] A. A. Fridman, L. Boufendi, T. Hbid, B. V. Potapkin, A. Bouchoule, Journal of Applied Physics 79 (**1996**), 1303–1314
[39] F. Vivet, A. Bouchoule, L. Boufendi, Journal of Applied Physics 83 (**1998**), 7474–7481
[40] J. Berndt, E. Kovacevic, I. Stefanovic, L. Boufendi, Journal of Applied Physics 106 (**2009**), 063309-1–063309-8
[41] S. I. Krasheninnikov, R. D. Smirnov, Physics of Plasmas 16 (**2009**), 114501-1–114501-3
[42] M. Calafat, D. Escaich, R. Clergereaux, P. Raynaud, Y. Segui, Applied Physics Letters 91 (**2007**), 181502-1–181501-4
[43] L. Boufendi, A. Bouchoule, Plasma Sources Science & Technology 11 (**2002**), A211–A218
[44] M. Cavarroc, M. C. Jouanny, K. Radouane, M. Mikikian, L. Boufendi, Journal of Applied Physics 99 (**2006**), 064301-1–064301-7
[45] L. Boufendi, A. Bouchoule, T. Hbid, Journal of Vacuum Science & Technology a-Vacuum Surfaces and Films 14 (**1996**), 572–576
[46] L. Boufendi, A. Bouchoule, R. K. Porteous, J. P. Blondeau, A. Plain, C. Laure, Journal of Applied Physics 73 (**1993**), 2160–2162
[47] M. Schulze, A. von Keudell, P. Awakowicz, Plasma Sources Science & Technology 15 (**2006**), 556–563
[48] F. Belva, S. Bourbigot, S. Duquesne, C. Jama, M. Le Bras, C. Pelegris, M. Rivenet, Polymers for Advanced Technologies 17 (**2006**), 304–311
[49] S. Bourbigot, S. Duquesne, C. Jama, Macromolecular Symposia 233 (**2006**), 180–190
[50] A. V. Karabutov, S. K. Gordeev, V. G. Ralchenko, S. B. Korchagina, S. V. Lavrischev, S. V. Terekhov, K. I. Maslakov, A. P. Dementjev, Diamond and Related Materials 12 (**2003**), 1710–1716
[51] A. V. Karabutov, S. K. Gordeev, V. G. Ralchenko, S. B. Korchagina, S. V. Lavrischev, Vlasov, II, Diamond and Related Materials 12 (**2003**), 1698–1704
[52] A. V. Karabutov, S. K. Gordeev, V. G. Ralchenko, S. B. Korchagina, K. I. Maslakov, A. P. Dementjev, Surface and Interface Analysis 36 (**2004**), 455–460
[53] M. Bedjaoui, B. Despax, M. Caumont, C. Bonafos, Materials Science and Engineering B-Solid State Materials for Advanced Technology 124 (**2005**), 508–512
[54] H. Vach, Q. Brulin, Physical Review Letters 95 (**2005**), 4
[55] D. M. Bubb, R. A. McGill, J. S. Horwitz, J. M. Fitz-Gerald, E. J. Houser, R. M. Stroud, P. W. Wu, B. R. Ringeisen, A. Pique, D. B. Chrisey, Journal of Applied Physics 89 (**2001**), 5739–5746
[56] P. Oelhafen, A. Schuler, Solar Energy 79 (**2005**), 110–121
[57] H. Wang, S. P. Wong, W. Y. Cheung, N. Ke, M. F. Chiah, H. Liu, X. X. Zhang, Journal of Applied Physics 88 (**2000**), 2063–2067
[58] I. Chopra, Journal of Antimicrobial Chemotherapy 60 (**2007**), 447–448
[59] A. Grill, Thin Solid Films 398 (**2001**), 527–532
[60] A. Grill, Diamond and Related Materials 10 (**2001**), 234–239
[61] A. Grill, V. Patel, Applied Physics Letters 79 (**2001**), 803–805
[62] M. Kihel, R. Clergereaux, D. Escaich, M. Calafat, P. Raynaud, S. Sahli, Y. Segui, Diamond and Related Materials 17 (**2008**), 1710–1715
[63] P. Jolinat, R. Clergereaux, J. Farenc, P. Destruel, Journal of Physics D-Applied Physics 31 (**1998**), 1257–1262
[64] R. Clergereaux, D. Escaich, S. Martin, F. Gaillard, P. Raynaud, Thin Solid Films 482 (**2005**), 216–220
[65] R. Clergereaux, M. Calafat, F. Benitez, D. Escaich, I. S. de Larclause, P. Raynaud, J. Esteve, Thin Solid Films 515 (**2007**), 3452–3460
[66] J. Patscheider, Mrs Bulletin 28 (**2003**), 180–183

UDK 66
Original scientific article/Izvirni znanstveni članek

ISSN 1580-2949
MTAEC9, 46(1)19(2012)

# STABILIZATION OF RUTILE $TiO_2$ NANOPARTICLES WITH GLYMO IN POLYACRYLIC CLEAR COATING

## STABILIZACIJA RUTIL $TiO_2$ NANODELCEV Z GLYMO V POLIAKRILNEM TRANSPARENTNEM PREMAZU

**Jerneja Godnjavec[1], Bogdan Znoj[1,2], Jelica Vince[2], Miha Steinbucher[2], Andrej Žnidaršič[3], Peter Venturini[1,2]**

[1]Center of Excellence for Polymer Materials and Technologies, Tehnološki park 24, 1000 Ljubljana, Slovenia
[2]Helios Group, Količevo 2, 1230 Domžale, Slovenia
[3]Kolektor Nanotesla Institut Ljubljana, Stegne 29, 1521 Ljubljana, Slovenia
jerneja.godnjavec@polimat.si

*Prejem rokopisa – received: 2011-02-15; sprejem za objavo – accepted for publication: 2011-07-06*

Titanium dioxide ($TiO_2$), in the crystal form of rutile with high refractive index, 2.7, is one of the most important inorganic pigments. In the recent years nano $TiO_2$ has attracted interest as an inorganic material for nanocomposites. It is used for the development of photocatalysts[1,2], semiconductors in solar cells[3,4] and for the protection of materials from UV damage[5–8].
To achieve high UV absorbing efficiency of $TiO_2$ nanoparticles into polymer matrix and to yield a better compatibility with polymeric materials surface treatment of $TiO_2$ nanoparticles with 3-glycidyloxypropyltrimethoxysilane (GLYMO) in a polyacrylic clear coating was investigated. The grafting of GLYMO on the $TiO_2$ nanoparticles surface was characterized with TGA and FTIR techniques. The stability of $TiO_2$ nanoparticles in a acrylic clear coating was evaluated by zeta potential measurement. Microstructural analysis of nanoparticles was done by SEM and the influence of surface treatment on stability of nanoparticles in dispersion and acrylic coating was analysed. Finally the UV absorption effectivness of acrylic clear coating with treated nanoparticles of rutile $TiO_2$ was measured to determine the effect of improved dispersion. The performance of nanocomposite coatings was demonstrated trough accelerated weathering by gloss measurement. The results showed that surface treatment of $TiO_2$ nanoparticles with GLYMO improves nanoparticles dispersion and preserves UV protection of the acrylic clear coating.

Keywords: titanium dioxide, nanoparticles, polyacrylic clear coating, surface treatment, GLYMO, UV protection

Titanov dioksid ($TiO_2$), v rutilni kristalni obliki z visokim lomnim količnikom, 2.7, je eden najbolj pomembnih anorganskih pigmentov. V zadnjih letih je nano $TiO_2$ pritegnil pozornost kot anorganski material za nanokompozite. Uporablja se za razvoj fotokatalizatorjev[1,2], polprevodnikov in soalrnih celic[3,4] in za UV zaščito materialov[5–8].
Da bi dosegli ustrezno dispergiranje $TiO_2$ nanodelcev v polimerni matrici in boljšo kompatibilnost s polimernimi materiali smo preiskovali površinsko obdelavo $TiO_2$ nanodelcev v poliakrilnem transparentnem premazu. Za optimizacijo dispergiranja je bila površina nanodelcev obdelana z 3-glicidiloksipropiltrimetoksisilanom (GLYMO). Pripenjanje GLYMO na površino $TiO_2$ nanodelcev smo ovrednotili z termogravimetrično analizo (TGA) in s FTIR spektroskopsko analizo. Stabilnosti $TiO_2$ nanodelcev v akrilnem transparentnem premazu smo analizirali z meritvijo zeta potenciala. Mikrostrukturno analizo nanodelcev izvedli s SEM. Na koncu smo analizirali učinkovitost UV absorpcije akrilnega transparentnega premaza z površinsko obdelanimi rutil $TiO_2$ nanodelci, da bi določili efekt izboljšane disperzibilnosti. Z izpostavo pospešenega staranja smo določili funkcionalnost nanokompozitnih premazov na osnovi meritve sijaja. Rezultati so pokazali da površinska obdelava $TiO_2$ nanodelcev z GLYMO izboljša disperziblnost nanodelcev in ohrani UV zaščito akrilnega transparentnega premaza.

Ključne besede: titanov dioksid, nanodelci, poliakrilni transparentni premaz, površinska obdelava, GLYMO, UV zaščita

## 1 INTRODUCTION

Architectural coatings are usually used to enhance the durability of wood in exterior environment. Inorganic UV absorbers are often used in coatings formulations, since they increase polymer stability. $TiO_2$ possesses a lot of attracting advantages, like thermal stability and long-term life time, compared to traditional organic UV absorbers[9,10].

There are two limitations of using $TiO_2$ as UV absorber. First, $TiO_2$ particularly in anatase crystale form and less in rutile form exhibits strong photocatalytic behavior when absorbing UV-rays, which is harmful for the photostability of polymer materials[5]. As a result, $TiO_2$ nanoparticles as catalyst can create , which can produce highly reactive free radicals and exert strong oxidizing power.

Second, for producing suitable nanocomposites, it is necessary to disperse the nano-particles without agglomeration in organic binders[11,12]. Due to their extremly large surface-area/particle-size ratio, nano-particles have high tendency of agglomeration[13]. Many efforts have been taken in order to overcome the problem of agglomeration. Polymeric dispersants containing different functional groups are usuallly used in order to prevent the high tendency of nanoparticles to form aggregates in the wet state of coating and in the dry paint film. Polyacrylic acid, polyacrylamide and their copolymers are widely used to disperse inorganic particles in aqueous film[14]. Recently, to suppress the photocatalytic property of $TiO_2$, usually silica[15–17] or silane[18–20] were coated onto $TiO_2$ cores. Kang et al. suppressed the photocatalytic property of a $TiO_2$ by coating them with the $SiO_2$ shell in chloroform[17]. Toni et. al. coated dense

$SiO_2$ shells onto $TiO_2$ particles by seeded sol–gel process of tetraethyl silicate (TEOS) in ethanol[16]. The use of different coupling agents such as trialkoxy silanes for surface modification of nanoparticles is recommended. For example, Ukaji et. al. coated thin aminoethylaminopropyltrimethoxysilane layers onto $TiO_2$ particles in ethanol by adding silane during ball-milling dispersing procedure[8]. Shafi et. al. coated octadecyltrihydrosilane layers on $TiO_2$ surfaces in heptane by ultrasonic irradiation[21]. M. Sabzi et. al. showed that surface treatment of $TiO_2$ with aminopropyl trimethoxysilane improves nanoparticles dispersion and UV protection of the urethane clear coating[22].

The purpose of this study was to investigate the influence of $TiO_2$ nanoparticles surface modifiction by different wt. % of 3-glycidyloxypropyltrimethoxysilane on transparency and UV absorbing efficiency of polyacrylic coating.

## 2 EXPERIMENTAL WORK

### *2.1 Synthesis of $TiO_2$ nano crystalline particles in rutile crystal structure and preparation of a dispersion*

$TiO_2$ nanoparticles with rutile crystal structure were prepared by co-precipitation method which is described elsewhere[23]. Deagglomerated rutile nanoparticles were prepared as dispersion in water and propilenglycol in high-energy horizontal attrition mill.

### *2.2 Surface modification of $TiO_2$ nanoparticles in dispersion with silane coupling agent*

As silane coupling agent we used 3-glycidyloxypropyltrimethoxysilane (GLYMO) with chemical formula

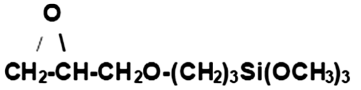

which is a bifunctional organosilane, possessing reactive organic epoxide and hydrolyzable inorganic metoxysilyl groups. It bounds chemically to both inorganic material and organic polymers. According to the producer in the presence of water the methoxy groups hydrolyze to form reactive silanol groups which bound to inorganic substance[24].

We prepared dispersions of $TiO_2$ nanoparticles grafted with GLYMO according to the following procedure. First, $TiO_2$ nanopowder in dispersion with wetting and defoaming agent was milled for 1,5 hour at 25 °C with organic surface active agent with zirconia balls 1 mm diameter. Than silane coupling agent of different concentrations was added as shown in **Table 1** and the dispersion was milled additionally for 1 hour at the same conditions.

**Table 1:** Weight ratio of GLYMO and nano $TiO_2$, dispersed in water
**Tabela 1:** Utežno razmerje GLYMO in nano $TiO_2$, dispergiranih v vodi

| Sample name | GLYMO/$TiO_2$ (/) |
|---|---|
| A | 0/1 |
| B | 0.1/1 |
| C | 1/1 |
| D | 2/1 |

### *2.3 Preparation of clearcoat with integrated rutile crystalline nanoparticles of $TiO_2$*

We prepared clearcoat in the laboratory as described elsewhere[23]. Water based dispersions of $TiO_2$ nanoparticles were than added to clearcoat of 0,6 wt. %, stirred at approximatly 1000 rpm for 20 minutes and prepared for the testing.

### *2.4 Characterization of the samples*

Surface morphology of coated sample was studied by scanning electron microscopy (SEM, ZEISS Gemini Supra 35 VP), with a maximum resolution up to 5 nm. Nanoparticles were dried on brass holders by adhesive carbon band with thin layer of gold. The samples were placed in the vacuum chamber of the instrument and then were examined at various magnifications. Grafting of GLYMO on $TiO_2$ nanoparticles was analysed by FT-IR. The infrared spectra of original and modified $TiO_2$ were conducted using a FT-IR spectrometer (PERKIN ELMER Spectrum 100) and thermogravimetrical analysis by TGA/DSC 1, METTLER TOLEDO.

Zeta potential was obtained to investigate the surface character of original $TiO_2$ and $TiO_2$ modified with GLYMO. The electro-phoretic mobility data, measured also by Zetasizer Nano series HT by of the dispersions were transformed into ζ-potential according to[25] (eq. 1):

$$\zeta = \left[ \frac{4\pi\eta\mu}{\varepsilon} \right] \quad (1)$$

where $\varepsilon$ is a dielectric constant of the dispersing medium and $\eta$ the solvent viscosity. pH was measured by pH meter (Mettler Toledo).

UV–VIS transmittance of modified samples was measured for estimating UV-shielding ability and transparency. 0.6 wt. % of surface treated $TiO_2$ nanoparticles was integrated into acrylic clear coating and 200 μm films were prepared. The different free film systems (coating-UV absorber) were analysed by UV-VIS spectrophotometer Varian Cary 100. The film transmittance was measured in the wavelength range 280 to 720 nm.

At the end, wood blocks measuring 15 × 7 $cm^2$ (longitudinal × tangential) × 0,5 cm width were cut from air dried boards from the specie pine. Two layers of clear coat of thickness of 200 μm were applied on pine blocks. Coated wood plates were used to assess weathering exposure degradation (QUV accelerated weathering tester, Q – PANEL LAB PRODUCTS). Simulation of exterior use was done by six weeks weathering by an

optimised cycle defined: 4h at (60 ± 3) °C and 4h water shower at (50 ± 3) °C. Only light of the solar type was activated on the QUV with sources type UVA-340 nm[26]. Gloss at 60° was measured by Micro-TRI-gloss (Byk Gardner).

## 3 RESULTS AND DISCUSSION

### *3.1 SEM characterization*

The size of the nanoparticles, grafted with GLYMO was analysed by scanning electron microsope (SEM). SEM images at two different magnifiations of sample C are shown on **Figure 1**. Agglomeration tendency of $TiO_2$ nanoparticles in the dispersion cannot be determined because of the preparation of the sample, however we assume, that some agglomerates are probably present as seen on SEM image. Individual particles can be identified, which appears to be polydisperse in size but below 100 nm.

### *3.2 TGA analysis*

To estimate the amount of GLYMO grafted on nanoparticles, the various percentage of GLYMO – grafted nano-$TiO_2$ particles were analyzed by TGA technique. **Figure 2** shows the TGA curves of untreated $TiO_2$ nanoparticle, GLYMO alone and treated $TiO_2$ nanoparticles with different percentages of GLYMO. For untreated nanoparticles (sample A), the weight loss from 120 till 600 °C is almost negligible and is probably due to desorption of physisorbed water [27]. For GLYMO alone the weight loss begins at 120 °C and ends at 200 °C. As can be seen for sample B, C and D, the various weight percentages of GLYMO grafted nanoparticles show sharp weight loss, beginning near 220 °C, continues till 620 °C, which is a consequence of oxidative thermal decomposition of grafted GLYMO as quantitatively shown in **Table 2**. The largest amount of grafted GLYMO was in the case of sample C.

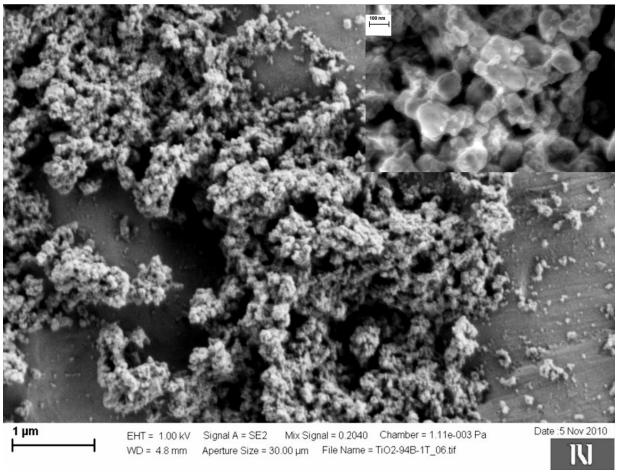


**Figure 1:** SEM image of sample C with inserted image at higher magnification

**Slika 1:** SEM posnetek vzorca C z vstavljenim posnetkom pri višji povečavi

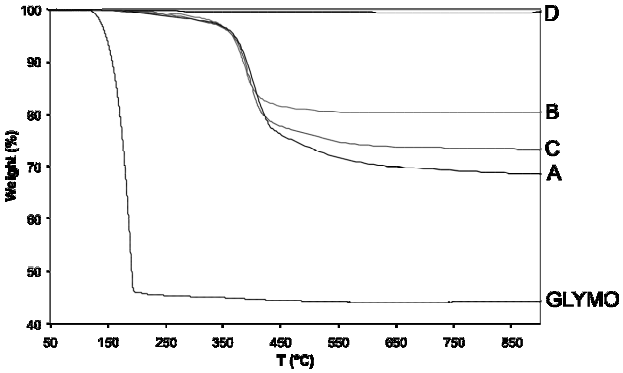


**Figure 2:** TGA curves of untreated $TiO_2$ nano-particle (sample A) and treated $TiO_2$ nano-particle (sample B–D). The composition of all samples is described in **Table 1**.

**Slika 2:** TGA krivulje površinsko neobdelanih (vzorec A) ter površinsko obdealnih (vzorci B–D) nanodelcev $TiO_2$. Sestava vseh vzorcev je podana v **Tabeli 1**.

**Table 2:** TGA-based weight losses caused by grafting of GLYMO and the amount grafted/added GLYMO of various GLYMO – grafted nanoparticles $TiO_2$. The composition of all samples is described in **Table 1**.

**Tabela 2:** Izguba mase vzorcev nanodelcev $TiO_2$ ter razmerje vezan/dodan GLYMO površinsko obdelanih in neobdelanih z GLYMO glede na TGA analizo. Sestava vseh vzorcev je podana v **Tabeli 1**.

| Sample | GLYMO:$TiO_2$ (/) | Weight loss caused by grafting of GLYMO | The amount grafted/added GLYMO (%) |
|---|---|---|---|
| A | 0 | / | / |
| B | 0,1 | 1,00 | 67 |
| C | 1 | 11,40 | 76 |
| D | 2 | 20,20 | 67 |
| GLYMO | / | / | / |

### *3.3 FTIR spectroscopy*

The hydroxyl groups on the surface of the $TiO_2$ nanoparticles (TiOH) are reactive sites for the reaction with alkoxy groups of silane compounds, however corresponding bands are not present in spectrum of unmodified $TiO_2$, since it was dried at 130 °C for 24h. The efficiency of silane grafting on $TiO_2$ nano-particles was determined by Fourier transform infrared spectroscopy (FTIR). **Figure 3** shows normalised FTIR spectra of unmodified $TiO_2$ nanoparticles (sample A), grafted $TiO_2$ nanoparticles with GLYMO (sample B – D), GLYMO alone and GLYMO with addition of water. In the spectra of all $TiO_2$ nano-particles the broad band between 400 and 800 $cm^{-1}$ correspond to Ti–O–Ti network. GLYMO posseses two functional groups: epoxi and metoxysilyl, which both hydrolize and condensate. Epoxy band in FTIR spectra is preserved, while the intensity of Si-O-Me band is decreased. Also two bands of hydroxyl groups appear at ~3300 and ~1640 $cm^{-1}$ because of hydrolysis of Si-O-Me groups. In spectra of

GLYMO with addition of water peak at 1050 $cm^{-1}$ appears, which we can assign to formation of Si-O-Si groups. Compared with the spectrum of non-modified $TiO_2$, FTIR spectrum of GLYMO modified sample exhibits some new characteristic absorption peaks. Peak at ~1200 and 1093 $cm^{-1}$ which belongs to Si-O-Me groups[28,29], was observed in the spectra of samples C and D, however not in the spectruum of sample B, which indicates that only in the case of sample B complete hydrolysis and condensation of GLYMO takes place. In contrast to GLYMO spectruum, we cannot observe in GLYMO modified $TiO_2$ spectra peak at 914 and 1254 $cm^{-1}$ which corresponds to epoxi group[30–34]. We presume that the epoxi group opens and reacts with -OH groups which were formed by the hydrolysis of metoxysilyl groups. The broad bend at ~1050 $cm^{-1}$ represent the Si-O-Si bond is observed which indicates the formation of Si-matrix[35]. The small peak in spectra of samples B – D at around 930 $cm^{-1}$ reconfirms condensation reaction between methoxysilyl groups of GLYMO and the $TiO_2$ surface hydroxyl groups[36,8].

To sum up, Si-O-Me groups of GLYMO have reacted completley only in the case of sample B, in samples C and D are still present. Epoxi groups of GLYMO have reacted completely in all GLYMO modified $TiO_2$ nanoparticles samples. The results of FTIR analysis confirm that Si-O-Si network has been formed probably around the $TiO_2$ nanoparticles and in small amount Si-atoms of GLYMO are bound to $TiO_2$ surface. Similarly, F. Bauer and coauthors reported about a polymerization-active siloxane shell formed around the nanoparticles $Al_2O_3$, when surface treated by GLYMO[37]. The reaction of GLYMO with $TiO_2$ nanoparticles leads to different kind of stabilization of nanoparticles in the dispersion as suggested by the producers of GLYMO, since they claim that in the presence of water the methoxysilyl groups hydrolyze to form reactive silanol groups which bound to inorganic substance[24].

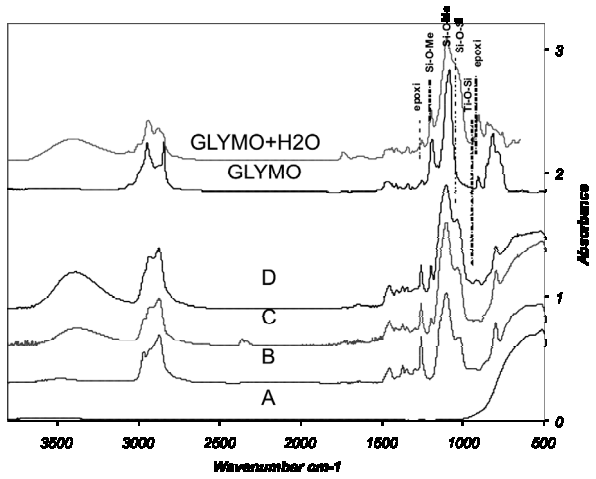


**Figure 3:** FTIR spectra of untreated nano-$TiO_2$ (sample A), grafted $TiO_2$ nano-particles with GLYMO (sample B–D), pure GLYMO and GLYMO with addition of water. The composition of all samples is described in **Table 1**.

**Slika 3:** FTIR spektri neobdelanega nano-$TiO_2$ (vzorec A), površinsko obdelanih nanodelcev $TiO_2$ z GLYMO (vzorec B–D), samo GLYMO, GLYMO z dodatkom vode. Sestava vseh vzorcev je podana v **Tabeli 1**.

### *3.4 pH and ζ-potencial measurement*

pH and ζ-potential measurement were used to quantify the conditions leading to the stability of $TiO_2$ dispersions. Relevant values of the pH – measurements and ζ-potential of unmodified and modified $TiO_2$ with GLYMO are collected in **Table 3** and in **Figure 4**. The pH variation from 4,6 to 5,9 upon adsorption of GLYMO was detected. An increase of the pH from 5,6 up to 5,94 when increasing GLYMO/$TiO_2$ from 0 to 1 (sample A, B and C) was accompanied with an increase of ζ-potential from ~-33 to around ~-39 mV, with subsequent increase in colloid stability. We assume that $TiO_2$ surface is probably mostly covered with modifier in monolayer. As ratio GLYMO/$TiO_2$ increases to 2, the pH decreases to 5,43, resulting in decrease in zeta potential to -35,5 mV. We predict that the reason for decrease in pH and ζ-potential is the excess amount of GLYMO or formatation of multilayer on $TiO_2$ surface as observed by E. Ukaji et. al.[8]. It is supposed that thicker layer could be formed due to subsequent growth of layer to dimers, oligomers, and polymers.

**Table 3:** pH values for $TiO_2$ dispersions, in the presence of different amounts of GLYMO (sample A–D). The composition of all samples is described in **Table 1**.

**Tabela 3:** pH vrednosti disperzij $TiO_2$ v prisotnosti različnih deležev GLYMO (vzorec A–D). Sestava vseh vzorcev je podana v **Tabeli 1**.

| Sample name | pH |
|---|---|
| A | 5,60 |
| B | 5,78 |
| C | 5,94 |
| D | 5,43 |

### *3.5 Ageing behaviour*

Artificial weathering results in surface degradation of the coatings, which affect the appearance of the coating,

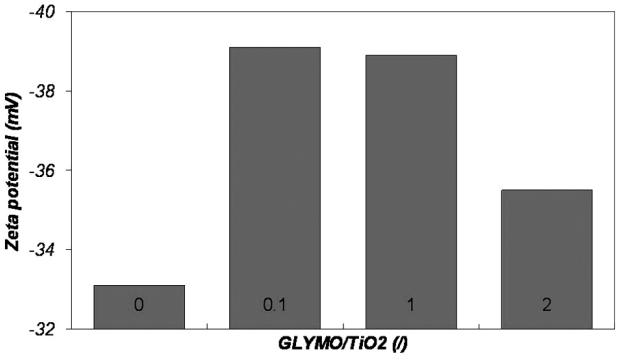


**Figure 4:** Zeta potential measurement vs. ratio GLYMO/$TiO_2$

**Slika 4:** Diagram meritev zeta potenciala v odvisnosti od razmerja GLYMO/$TiO_2$

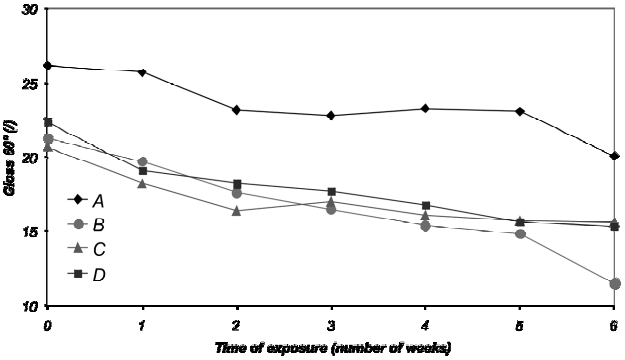


**Figure 5:** Gloss measurement vs. irradiation time in a QUV apparatus for the exterior use clearcotings with different UV absorbers, samples A–D, with their composition described in **Table 1**

**Slika 5:** Meritve sijaja v odvisnosti od časa izpostave v UV komori za premaz za zunanjo uporabo z različnimi UV absorberji, vzorci A–D, njhova sestava je podana v **Tabeli 1**

is the information on photostabilisation performances of UV absorbers[8,38,39]. M. Beyer and C. Jobos investigated the use of nano-scale light absorbers in water based glaze for outdoor applications. They showed that $TiO_2$ proved to be effective additives[6] in concentration 0,25 – 4 wt. % $TiO_2$ [9].

For outdoor weathering simulation of clearcoating gloss measurement during the exposure in QUV chambre for six weeks are displayed in **Figure 5**. **Figure 5** shows gloss 60° vs. time of exposure in QUV chambre for clearcoating with modified $TiO_2$ nanoparticles of different wt. ratios of GLYMO/$TiO_2$. The results illustrated that addition of GLYMO decreases the gloss 60°. During accelerated weathering the gloss changes are strongly correlated with the degradation level of the surface coating. In some composite materials the polymer around the filler particles will degrade due to the particle catalytic effect[40]. The accelerated weathering with water spray induced the washing out of degradation products on the coatings surface and consequently a fresh surface was further exposed. During the accelerated weathering a pronounced loss of gloss was observed for coatings formulated with nanoparticle UV absorber[41]. We can conclude that the surface treatemtnof $TiO_2$ nanoparticles with GLYMO reduces the gloss 60° of acrylic coating before exposure to accelerated weathering. The gloss change after six week exposure to accelerated weathering is the smalest in the case of sample C, which shows that the UV efficiency was improved the most, when ratio GLYMO/$TiO_2$ was 1.

## 4 CONCLUSIONS

Surface modification and characterization of $TiO_2$ nano-particles with GLYMO at different wt. percentages as an additive in a polyacrylic clear coating were investigated. TGA and FTIR analysis show that grafting of GLYMO on the nano-particles has occurred successfully. According to ζ-potential measurements the most stable $TiO_2$ nanoparticle dispersions are with ratio GLYMO:$TiO_2$ 0,1 and 1. At the end, artificial weathering results confirm that surface treatment of $TiO_2$ nanoparticles with GLYMO with ratio GLYMO:$TiO_2$ = 1 improves nanoparticles dispersion and consequently its transparency the most and improves UV protection of acrylic clear coating.

## Acknowledgement

The authors acknowledge the financial support from the Ministry of Higher Education, Science and Technology of the Republic of Slovenia through the contract No. 3211-10-000057 (Center of Excellence Polymer Materials and Technologies).

## 5 REFERENCES

[1] A. L. Linsebigler, G. Lu, J. T. Yates, Photocatalysis on $TiO_2$ surfaces: principles, mechanisms, and selected results, Chem. Rev. 95 (**1995**), 735–758

[2] H. Choi, Y.J. Kim, R.S. Varma, D.D. Dionysiou, Thermally stable nanocrystalline TiO2 photocatalysts synthesized via sol–gel methods modified with ionic liquid and surfactant molecules, Chem. Mater. 18 (**2006**), 5377–5384

[3] U Bach, D. Lupo, P. Comte, J. E. Moser, F. Weissortel, J. Salbeck, H. Spreitzer, M. Gratzel, Solid-state dye-sensitized mesoporous $TiO_2$ solar cells with high photon-to-electron conversion efficiencies, Nature 395 (**1998**), 583–585

[4] M. Anpo, M. Takeuchi, The design and development of highly reactive titanium oxide photocatalysts operating under visible light irradiation, J. Catal. 216 (**2003**), 505–516

[5] H. Y. Yang, S. K. Zhu, N. Pan, Studying the mechanisms of titanium dioxide as ultraviolet blocking additive for films and fabrics by an improved scheme, J. Appl. Polym. Sci. 92 (**2004**), 3201–3210

[6] F. Aloui, A. Ahajji, Y. Irmouli, B. George, B. Charrier, A. Merlin, Inorganic UV absorbers for the photostabilisation of wood-clear-coating systems: comparison with organic UV absorbers, Appl. Surf. Sci. 253 (**2007**), 3737–3745

[7] B. Mahltig, H. Bottcher, K. Rauch, U. Dieckmann, R. Nitsche, T. Fritz, Optimized UV protecting coatings by combination of organic and inorganic UV absorbers, Thin Solid Films 485 (**2005**), 108–114

[8] E. Ukaji, T. Furusawa, M. Sato, N. Suzuki, The effect of surface modification with silane coupling agent on suppressing the photo-catalytic activity of fine $TiO_2$ particles as inorganic UV filter, Appl. Surf. Sci. 254 (**2007**), 563–569

[9] N. S. Allen, M. Edgea, A. Ortega, G. Sandovla, C. M. Liauwa, J. Verrana, Degradation and stabilisation of polymers and coatings: nano versus pigmentary titania particles, Polym. Degrad. Stab. 85 (**2004**), 927–946

[10] M. Sangermano, E. Borlatto, F. D. D' Herin Bytner, A. Priola, G. Rizza, Photostabilization of cationic UV-cured coatings in the presence of nano $TiO_2$, Prog. Org. Coat. 59 (**2007**), 122–125

[11] C. Lu, Z. Cui, J. Guan, B. Yang, J. Shen, Research on Preparation, Structure and Properties of $TiO_2$/Polythiourethane Hybrid Optical Films with High Refractive Index Macromol. Mater. Eng. 288 (**2003**), 717–723

[12] C. Lu, Z. Cui, B. Yang., J. Shen, High refractive index thin films of ZnS/polythiourethane nanocomposites, J. Mater. Chem. 13 (**2003**), 526–530

[13] J. Jordan, K. I. Jacob, R. Tannenbaum, M.A. Sharaf, I. Jasiuk, Experimental trends in polymer nanocomposites—a review, Mater. Sci. Eng. A 393 (1e2) (**2005**), 1

[14] S. Farrokhpay, A review of polymeric dispersant stabilisation of titania pigment, Advances in Colloid and Interface Science, 151 (**2009**), 24–32

[15] O. K. Park, Y. S. Kang, B. G. Jo, Synthesis of $TiO_2$ nanoparticles coated with SiO2 for suppression of photocatalytic activity and increased dispersion stability, J. Ind. Eng. Chem. 10 (**2004**), 733–738

[16] A. M. El-Toni, S. Yin, T. Sato, Control of silica shell thickness and microporosity of titania–silica core–shell type nanoparticles to depress the photocatalytic activity of titania, J. Colloid Interface Sci. 300 (**2006**), 123–130

[17] O. K. Park, Y. S. Kang, Preparation and characterization of silica-coated $TiO_2$ nanoparticle, Colloids Surf. A 257–258 (**2005**), 261–265

[18] P. Katangur, P. K. Patra, S. B. Warner, Nanostructured ultraviolet resistant polymer coatings, Polym. Degrad. Stab. 91 (**2006**), 2437–2442

[19] A. M. Djerdjev, J. K. Beattie, R. W. O'Brien, Coating of silica on titania pigment particles examined by electroacoustics and dielectric response, Chem. Mater. 17 (**2005**), 3844–3849

[20] J. N. Ryan, M. Elimelech, J. L. Baeseman, R. D. Magelky, Silica-coated titania and zirconia colloids for subsurface transport field experiments, Environ. Sci. Technol 34 (**2000**), 2000–2005

[21] K. V. P. M. Shafi, A. Ulman, X. Yan, N. L. Yang, M. Himmelhaus, M. Grunze, Sonochemical preparation of silane-coated titania particles, Langmuir 17 (**2001**), 1726–1730

[22] M. Sabzi, S.M. Mirabedini, J. Zohuriaan-Mehr, M. Atai, Surface modification of $TiO_2$ nano-particles with silane coupling agent and investigation of its effect on the properties of polyurethane composite coating, Progress in Organic Coatings 65 (**2009**), 222–228

[23] J. Godnjavec, B. Znoj, P. Venturini, A. Žnidaršič. The application of rutile nano-crystalline titanium dioxide as UV absorber. Inf. MIDEM, 40 (**2010**) 1, 6–9

[24] http://svn.assembla.com/svn/camsi-x/src/fe/LITERATURA/Degussa-GLYMO.pdf

[25] Adamson AW Physical Chemistry of Surfaces, 5th edn. Wiley, New York, 1991, 218

[26] SIST EN ISO 11507:2002

[27] L. Jun, J.A. Siddiqui, R. M. Ottenbrite, Surface modification of inorganic oxide particles with silane coupling agent and organic dyes, Polym. Adv. Technol. 12 (**2001**), 285–292

[28] I. C. McNeill, M. H. Mohammed, Thermal analysis of blends of low density polyethylene, poly(ethyl acrylate) and ethylene ethyl acrylate copolymer with polydimethylsiloxane, Polymer Degradation and Stability, 50 (**1995**) 3, 285–295

[29] Wenxui Que, Y. Zhou, Y. L. Lam, Y. C. Chan, C. H. Kam, Optiocal and microstructural properties of sol-gel derived titania/organically modified silane thin films, Thin Solid Films, 358 (**2000**) 1–2, 16–21

[30] J. Macan, H. Ivanković, Influence of hydrolysis conditions on curing and properties of an epoxy-silane based hybrid material, 11. Conference on Materials, Processes, Friction and Wear MATRIB 06, Vela Luka, 22–24. 6. 2006, 99–104

[31] N. Eidelman, D. Raghavan, A. M. Forster, E. J. Amis, A. Karim, Combinatorial Approach to characterizing epoxy curing, Macromol. Rapid Commun., 25 (**2004**), 259–263

[32] http://www.shimadzu.com.br/analitica/aplicacoes/espectrofotometros/ftir/2_22-1.pdf

[33] G. Nikolić, S. Zlatković, M. Cakić, S. Cakić, C. Lacnjevac, Z. Rajic, Fast Fourier transform IR characterization of epoxy GY systems crosslinked with aliphatic and cycloapliphatic EH polyamine adducts, Sensors, 10 (**2010**), 684–696

[34] http://www.thefreelibrary.com/Insitu+monitoring+of+the+curing+of+epoxy+resins+by+DSC,+FTIR+and...-a0216041185

[35] N. Grošelj, M Gaberšček, U. Opara Krašovec, B. Orel, G. Dražič, P. Judeinstein, Electrical and IR spectroscopic studies of peroxopolytungstic acid/organic–inorganic hybrid gels, Solid State Ionics, 125 (**1999**) 1–4, 125–133

[36] Q. Cheng, C. Li, V. Pavlinked, P. Saha, H. Wang, Appl. Surf. Sci. 252 (**2006**), 4154–4160

[37] F. Bauer, U. Decker, H. Ernst, M. Findeisen, H. Langguth, R. Mehnert, V. Sauerland and R. Hinterwaldner, Functionalized inorganic/organic nanocomposites as new basic raw materials for adhesives and sealants International, Journal of Adhesion and Adhesives, 26 (**2006**) 7, 567–570

[38] M. Sakamoto, H. Okuda, J. Jpn. Soc. Colour. Mater. 68 (**1995**) 4, 203–210

[39] Y. Q. Li, S. Y. Fu, Y. Yang, Y. W. Mai, Facile synthesis of highly transparent polymer nanocomposites by introduction of core–shell structured nanoparticles, Chem. Mater. 20 (**2008**), 2637–2643

[40] A. C. Dodd, A. J. McKinley, M. Saunders, T. Tsuzuki, J. Nanopart. Res. 8 (**2006**), 43–51

[41] M. V. Cristeaa, B. Riedla, P. Blancheta, Enhancing the performance of exterior waterborne coatings for wood by inorganic nanosized UV absorbers, Progress in Organic Coatings, 69 (**2010**), 432–441

UDK 678.7:543.42
Original scientific article/Izvirni znanstveni članek

ISSN 1580-2949
MTAEC9, 46(1)25(2012)

# OPTICAL EMISSION CHARACTERIZATION OF EXTREMELY REACTIVE OXYGEN PLASMA DURING TREATMENT OF GRAPHITE SAMPLES

## KARAKTERIZACIJA EKSTREMNO REAKTIVNE KISIKOVE PLAZME Z OPTIČNO EMISIJSKO SPEKTROSKOPIJO MED OBDELAVO KOMPOZITA POLIMER – GRAFIT

**Zlatko Kregar[1], Marijan Bišćan[1], Slobodan Milošević[1], Kristina Eleršič[2], Rok Zaplotnik[2], Gregor Primc[2], Uroš Cvelbar[3]**

[1]Institut za fiziku, Bijenička 46, 10000 Zagreb, Croatia
[2]Institut "Jožef Stefan", Jamova cesta 39, 1000 Ljubljana, Slovenia
[3]Center of Excellence for Polymer Materials and Technologies, Tehnološki park 24, 1000 Ljubljana, Slovenia
zkregar@ifs.hr

*Prejem rokopisa – received: 2011-06-01; sprejem za objavo – accepted for publication: 2011-07-19*

Characteristics of oxygen plasma during treatment of polymer graphite composite were monitored by optical emission spectroscopy. Plasma was created in a rather small volume of about $3\times10^{-5}$ m$^{-3}$ within a quartz glass tube by an electrode-less radiofrequency discharge in the H mode. The discharge was established using an RF generator with the frequency of 13.56 MHz and the output power of 550 W. The composite samples were discs with a diameter of 25 mm and the thickness of 8 mm. Plasma was created in pure oxygen and characterized by an optical spectrometer through an optical fiber. A low-resolution spectrometer Avantes AvaSpec 3648 was adjusted to the lowest acquisition time due to intensive radiation. The optical spectra revealed several atomic lines originating from radiative transitions from highly excited states, CO bands from 3$^{rd}$ positive as well as Angstrom transitions, and a broad continuum between 400 and 700 nm. Weak carbon atomic lines in the UV and infra-red part of spectrum were detected as well. The intensity of major spectral features was measured versus treatment time for 30 s. The results showed continuous decrease of oxygen lines and simultaneous increase of a CO line at 266 nm and C line at 911 nm. Spectral features were explained by intensive oxidation of the graphite sample. The unusually high intensity of CO bands were explained by interaction of highly excited oxygen atoms with graphite samples, while the appearance of the broad continuum was explained by partial overlapping of radiative transitions within CO molecule.

Keywords: optical emission spectroscopy, oxygen plasma, surface modification, functional groups, graphite

Z optično emisijsko spektroskopijo smo spremljali lastnosti kisikove plazme med obdelavo kompozita polimer-grafit. Plazmo smo ustvarili v razmeroma majhni prostornini približno $3\times10^{-5}$ m$^{-3}$ znotraj kvarčne cevi. Za vzbujanje plazme smo uporabili brez-elektrodno visokofrekvenčno plinsko razelektritev v H načinu. Uporabili smo radiofrekvenčni generator, ki je deloval pri frekvenci 13,56 MHz in izhodni moči 550 W. Kompozitni vzorci so imeli valjasto obliko s premerom 25 mm in višino 8 mm. Plazmo smo vzbujali v čistem kisiku, njene karakteristike pa merili z optičnim spektrometrom. Uporabili smo spektrometer Avantes AvaSpec 3648, ki ima nizko ločljivost v širokem območju med okoli 180 nm in 1100 nm. Zaradi izredne svetilnosti plazme smo uporabili najmanjši integracijski čas. Optični spektri so pokazali značilne črte, ki izvirajo iz atomskih prehodov, molekularne pasove, ki izvirajo iz prehodov v CO radikalih (3. pozitivni in Angstromov sistem), kakor tudi širok kontinuum v območju med 400 in 700 nm. Opazili smo tudi šibke črte, ki izvirajo iz prehodov v C atomih. Intenziteto najpomembnejših spektralnih vrhov smo spremljali med obdelavo vzorcev, ki je trajala 30 s. Rezultati so pokazali stalno padanje intenzitete kisikovih črt, obenem pa rast CO črte pri 266 nm in C črte pri 911 nm. Rezultate smo pojasnili z intenzivno oksidacijo kompozitnih vzorcev. Nenavadno visok CO vrh smo pojasnili z močno kemijsko interakcijo, ki je posledica prisotnosti visoko vzbujenih kisikovih atomov, medtem ko smo pojav kontinuuma pripisali prekrivanju spektralnih pasov, ki izvirajo iz različnih prehodov znotraj molekule CO.

Ključne besede: optična emisijska spektroskopija, kisikova plazma, modifikacija površine, funkcionalne skupine, grafit

## 1 INTRODUCTION

Oxygen plasma is a popular medium for modification of different materials.[1–10] Unlike normal oxygen in thermal equilibrium, non-equilibrium state of oxygen gas reacts with materials already at room temperature.[11] Such high chemical reactivity is often attributed to high dissociation fraction of oxygen molecules even at relatively low power density.[12–17] Oxygen plasma is particularly suitable for treatment of carbon – containing materials.[18–23] The reaction channels include oxygen incorporation onto the surface of carbon containing materials as well as slow etching by formation of CO molecules and $CO_2$ molecules which quickly desorb from the sample surface under low pressure conditions and are pumped away.[24] If a sample contains a substantial amount of hydrogen (like polymers or hydrogenated carbon deposits) the reaction products are also OH radicals and $H_2O$ molecules.[25–26] In many cases the incorporation of oxygen onto the sample surface is sufficient in order to obtain desired modification of carbon containing materials.[27] In such cases, weakly ionized highly non-equilibrium plasma is applied. The technology based on application of weakly ionized oxygen plasma for modification of carbon-containing materials is often called surface functionalization.[28–31] In other cases, however, at

least a part of material should be removed in order to achieve appropriate results. Weakly ionized plasma is not reactive enough to allow for rapid removal of thick carbon films, so more aggressive plasma should be used. Typical examples of aggressive plasma include those created in relatively small volumes by rather powerful discharges, such as arc,[32] microwave[33] and radiofrequency discharges in the H mode.[34] Plasma created in such discharges is spatially limited by the existence of high electromagnetic fields and the power density may exceed $10^8$ W $m^{-3}$. Such plasma is never cold – the neutral gas kinetic temperature is usually over 1000 K. Still, plasma is highly non-equilibrium since the dissociation and ionization fractions are much higher than in thermal equilibrium at several 1000 K. Such plasma often allows for intensive chemical reactions taking place on the sample surface and is suitable for development of technologies for rapid removal of carbon containing materials from samples.[35–37]

## 2 EXPERIMENTAL

Experiments were performed in a plasma reactor pumped with a two stage rotary pump with the nominal pumping speed of 80 $m^3$ $h^{-1}$. Suitable pressure is adjusted in the reactor by leaking oxygen into the system during continuous pumping (the pressure was set to 75 Pa of oxygen). This allows for rapid removal of any reaction compounds from gaseous plasma. Plasma is created within small volume inside a quartz glass tube with the inner diameter of 36 mm. The length of plasma column is effectively limited to about 8 cm using a short water cooled copper coil connected to a radiofrequency generator operating at the standard frequency of 13.56 MHz and the maximal power of 1200 W. The generator is matched to the coil via a matching network consisting of two variable vacuum capacitors. The network is adjusted in order to allow efficiency of about 80 %. The forward power of 550 W was used at current experiments. Plasma was characterized by optical emission spectroscopy. We used a low-resolution spectrometer Avantes AvaSpec 3648 with the following characteristics: spectral resolution of 0.8 nm in the spectral range from 180 to 1100 nm. The radiation emitted from plasma was conducted to spectrometer via a fiber optical FC-IR waveguide. The waveguide tip was mounted approximately 5 mm above the sample as shown in **Figure 1**. Samples were commercially available pure graphite samples. The samples were in form of disc of a diameter of 25 mm and a thickness of 8 mm. They were immersed into the centre of plasma as shown in **Figure 1**.

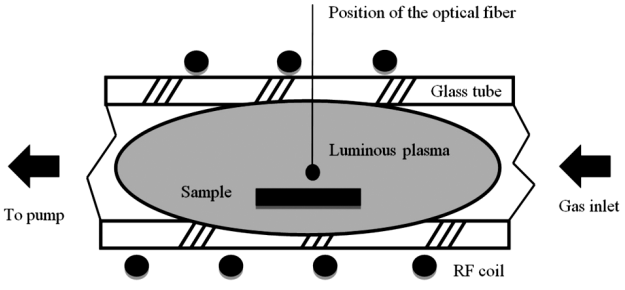


**Figure 1:** Schematic of the plasma reactor
**Slika 1:** Shema plazemskega reaktorja

## 3 RESULTS

A typical optical spectrum of oxygen plasma during treatment of a sample is shown in **Figure 2**. The spectrum presented has been corrected for spectral sensitivity of the spectrometer by means of a combined deuterium tungsten reference light source which allows for spectral calibration in the range from 240 nm to 940 nm (outside this range the calibration is unreliable due to low intensity of calibration lamp).[38] The spectrum is pretty rich. Apart from atomic oxygen and carbon emission lines very strong emission originating from excited states of CO molecules is observed. Also, a continuum is observed in the wide range from about 300 to 800 nm beneath the CO molecular emission. Insets show details of the UV part of the spectrum with resolved 3rd positive band of CO and IR part with a group of resolved C atomic lines. In UV region C atomic line at 248 nm is visible and a weak OH radical emission superimposed on (0,2) CO band.

The optical spectra were measured with an integration time of 7 ms (averaged 10 times) – effectively

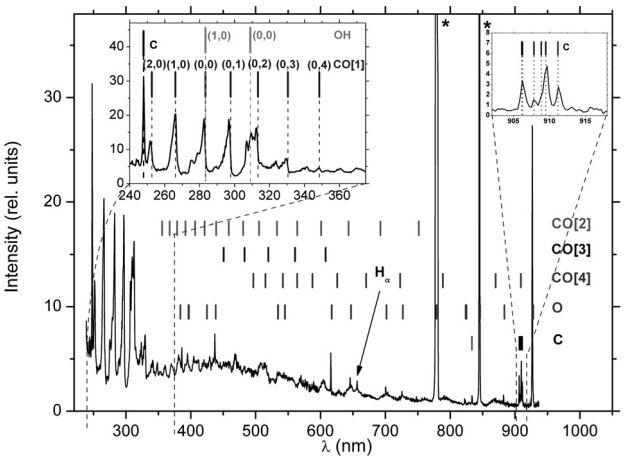


**Figure 2:** A typical spectrum of oxygen plasma during treatment of a composite sample. The spectrum was taken 30 s after initiation of plasma treatment. Stars denote spectral lines in saturation. Insets show details of the UV part of the spectrum with resolved 3rd positive band of CO and IR part with resolved C atomic lines. Abbreviations used: CO[1] = 3rd positive band, CO[2] = Triplet band, CO[3] = Angstrom band, CO[4] = Asundi band.

**Slika 2:** Značilni spekter kisikove plazme med obdelavo kompozitnega vzorca. Spekter smo zajeli po 30 s plazemski obdelavi. Z zvezdicami so označene emisijske črte, ki so bile v saturaciji. Vstavljeni sliki prikazujeta povečani del UV spektra z označenimi emisijskimi črtami 3. pozitivnega pasu CO molekule in povečani del IR spektra z označenimi atomskimi emisijskimi črtami C. Uporabljene kratice so: CO[1] = 3. pozitivni pas, CO[2] = pas tripleta, CO[3] = Angstromov pas, CO[4] = Asundijev pas.

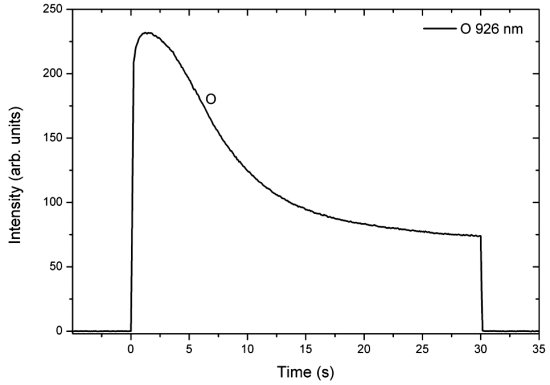


**Figure 3:** Spectral intensity time dependence of an atomic oxygen line at 926 nm
**Slika 3:** Časovna odvisnost kisikove črte na 926 nm

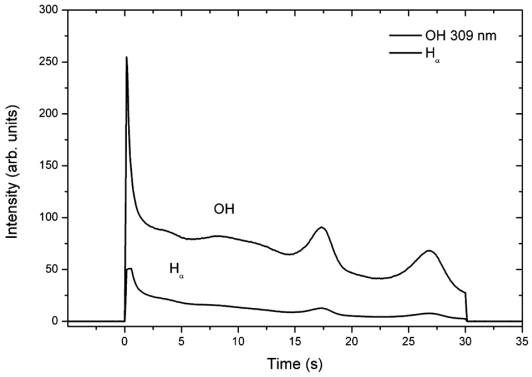


**Figure 5:** Spectral intensity time dependance of $H_\alpha$ line at 656 nm and OH band at 309 nm
**Slika 5:** Časovna odvisnost $H_\alpha$ črte pri 656 nm in OH črte pri 309 nm

measuring about 13 spectra per second. Appropriate home made software developed within LabVIEW allows for tracking of selected spectral features versus time. The behavior of an oxygen line at 926 nm is presented in **Figure 3**. **Figure 4** reveals the behavior of CO band (1,0) at 266 nm, C atomic line at 911 nm and continuum contribution at 464 nm. Wavelength representing continuum emission was chosen such to avoid any known atomic or molecular spectral features. **Figure 5** is a plot of $H_\alpha$ and OH lines at 656 and 309 nm, respectively. Since both H and OH spectral features overlap with continuum contribution, latter was subtracted.

## 4 DISCUSSION

The optical spectrum presented in **Figure 2** reveals some interesting features that are worth discussing. As expected, the neutral oxygen atom lines prevail. The most intensive are the lines at 777 and 844 nm that correspond to transitions $3p\ ^5P - 3s\ ^5S$ and $3p\ ^3P - 3s\ ^5S$, respectively. Both excited states are characterized by a pretty high excitation energy which is 10.99 eV and 10.74 eV, respectively. The appearance of these lines has been observed by numerous authors[39–42] and is explained by multi-stage excitation of oxygen atoms. Namely, as the excitation energy is pretty high, the states are unlikely to be reached by electron impact excitation from the ground state. There are several metastable states of oxygen atoms that allow for such step-like excitation.

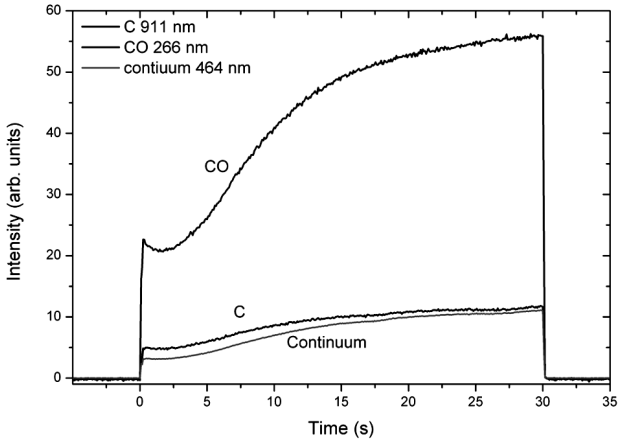


**Figure 4:** Spectral intensity time dependance of CO band at 266 nm, C atomic line at 911 nm and continuum at 464 nm
**Slika 4:** Časovna odvisnost CO črte pri 266 nm, C črte pri 911 nm in kontinuuma pri 464 nm

The appearance of CO bands in the spectrum presented in **Figure 2** is explained by intensive oxidation of the samples. The third positive band belongs to transitions between b $^3\Sigma^+$ and a $^3\Pi$ states. The intensity of this band is much stronger than at experiments with less aggressive plasma.[43] The 3rd positive band dominates the UV part of the spectrum, while on other hand the central part of spectrum (300 – 800 nm) presented in **Figure 2** is dominated by a broad continuum. It is well known that this part of spectrum is dominated by overlapped bands of the Angstrom band – B $^1\Sigma$ – A $^1\Pi$, the Asundi a' $^3\Sigma^+$ – a $^3\Pi$ and Triplet (d $^3\Delta$ –a $^3\Pi$).[24] In the present case, they are definitely present but their characteristic spectral structure is only partially visible, and can only partially contribute to the continuum.

The appearance of a continuum in emission spectra can be due to the presence of a body with a high temperature, or the presence of excited multi-atom molecules. The continuum peaks at about 450 nm so the temperature of a body that would radiate this continuum should be about 7000 K. The sample is not that hot – if it were, it would glow so intensively that it would be visible with a naked eye, and would produce significant infrared part of the continuum. Also, as mentioned earlier, the optical fiber was mounted in such a way that the focus was about 5 mm above the samples. The hot body, if present at all, should be of microscopic dimensions, not visible by a naked eye. Such very small particles should be pretty dense in plasma to be capable of emitting the continuum observed in **Figure 2**. Since the system is pumped with a rather powerful pump the existence of such particles is not probable.

Three-atom molecules that might be present in plasma are $CO_2$ and $H_2O$ and some more exotic ones.

The atoms may be formed at chemical reactions between oxygen reactive particles and the sample. The reactions definitely occur, but the molecules entering plasma are quickly dissociated in the rather powerful discharge. Namely, even the density of oxygen molecules in our plasma is pretty low. The discharge is just energetic enough to allow for rapid dissociation of molecules with moderate binding energy.

The continuum observed in **Figure 2** can be partially attributed to the specific properties of the spectrometer. As mentioned earlier, the resolution of our spectrometer is only about 0.8 nm. Any superposition of spectral features with a shift of less than 0.8 nm would appear as a broad line. A combination of such features would lead effectively to a continuum. The rather well defined lines in UV part of the spectrum continuum presented in **Figure 2** belong to the 3rd positive band. This band is frequently observed at plasma modification of organic materials, but is not the only one CO molecules can emit in the visible part of spectrum.[44] The Angstrom band is predominant in plasma with a rather low power density (or at least comparable to the 3rd positive band). In more powerful plasma, however, other transitions may become equally intensive, such as Asundi and Triplet band. If the spectral resolution of our spectrometer were better we would distinguish between spectral features arising from different bands. Low resolution of the spectrometer also prevents detailed characterization of spectral features that should allow for estimation of vibrational and rotational temperature of CO molecules. Nevertheless, the structure of ro-vibrational bands within the 3rd positive electronic transition in comparison to previous work[24] suggests existence of high rotational and vibrational temperatures which could partially contribute to the smeared out appearance of ro-vibrational structure. We note that time dependence of CO, C, and continuum emission is very similar pointing to the conclusion that continuum emission is of similar origin.

In the spectrum we clearly observe several neutral atomic carbon lines at 248 nm, 833 nm and around 910 nm. The right inset of **Figure 2** shows details of IR part indicating position of six carbon lines. Other C lines are not visible because they cannot be distinguished from the continuum in the visible part of the spectrum. The origin of C atoms can be sputtering of the sample by energetic ions from plasma. In our discharge configuration, however, no high DC voltages are present so ions are only accelerated in the sheath between unperturbed plasma and the sample which is kept at floating potential. The voltage drop across the sheath is only about 10 V so sputtering is practically absent in our plasma. Another possible explanation of the presence of C atoms in plasma is dissociation of CO molecules by electron impact. Since plasma is pretty energetic the density of electrons is high and they may even cause dissociation of the CO molecule although its binding energy is pretty high.

**Figure 3** represents time evolution of the oxygen atomic line at 926 nm (most prominent oxygen lines are in saturation). The line appears as soon as the discharge is turned on. In the first second it increases a little and then starts decreasing. The decreasing of the line intensity is due to loss of neutral oxygen atoms on the surface of the sample. The loss mechanisms include heterogeneous surface recombination and chemical reactions. The surface recombination often prevails[45], but not in our case. Namely, comparison of the oxygen line presented in **Figure 3** and CO line presented in **Figure 4** reveals complementarity. As oxygen line decreases, the CO and C lines increase. This complementarity indicates that the loss of O atoms as presented in **Figure 3** is due to formation of CO molecules rather than $O_2$ molecules. The increase of the CO and C lines intensity with increasing time is explained by increasing temperature of the sample. As mentioned earlier, the plasma is powerful and the neutral gas kinetic temperature is well above room temperature so the samples are heated by thermal accommodation of impinging gaseous particles. Other heating mechanisms include surface neutralization of charged particles, relaxation of metastables, surface recombination of radicals, and exothermic chemical reactions. The sample is therefore heated during plasma treatment. Since the probability for chemical reaction usually increases with increasing temperature, the production of CO molecules increases with treatment time as observed in **Figure 4**.

Another effect worth discussing is a pretty intensive CO emission just after turning on the discharge. Such an intensive line is rather unexpected since it is well known that the reaction probability for chemical interaction between oxygen plasma and organic materials is low at room temperature. The experimental system is, of course, at room temperature at ignition of the discharge. Surprisingly enough, the CO line is intensive even at the first spectra acquisition. Obviously, there should be a mechanism that allows for intensive oxidation at room temperature. Usually, temperature almost independent oxidation is explained by interaction of energetic ions with a sample. In our case, however, the ions have a low kinetic energy as discussed above. There should be other particles in plasma that allow for intensive oxidation even when the sample is at room temperature. The suitable candidates can be excited oxygen atoms in metastable states. They are definitely much more reactive than the atoms in the ground state and their density should be large in energetic plasmas. Unfortunately, very few experimental results on determination of the density of such particles are available, and they vary depending on the experimental setup. Wickramanayaka, found over 50 % of atoms in the first excited state in plasma very similar to ours[46]. Takeda, on the other hand, found orders of magnitude lower values[47].

Finally let us discuss the behavior of H and OH radicals as plotted in **Figure 5**. Both lines have an extreme at ignition of the discharge. This very short effect is often attributed to desorption of water molecules from the walls of the discharge chamber as well as from the sample. Namely, plasma radicals impinging the

surface supply quite a lot of potential and/or kinetic energy and cause desorption of water molecules. Since the supply is limited, the H and OH peaks drop in few seconds. They do not vanish, however, since the vacuum system contains adsorbed water molecules that slowly desorb from surfaces under vacuum conditions during plasma treatment. As mentioned earlier, water molecules quickly dissociate in plasma and this is the most probable explanation of rather high atomic H line observed in **Figure 5**.

## 5 CONCLUSION

Aggressive oxygen plasma was characterized during treatment of carbon containing samples. The systematic measurements revealed some interesting details. First, a broad continuum appeared in the range of visible light. Three different hypotheses that might explain the effect were presented and discussed. Consideration of physical and chemical effects as well as properties of our optical spectroscopy brought to a suggestion that the appearance of the continuum is partially due to relatively poor spectral resolution which prevents distinguishing between spectral features originating from different radiative transitions of CO molecules. Time evolution of the continuum radiation connects its origin with the origin of CO and C spectral emission. Second, the CO radiation was extremely high even just after igniting the discharge, when the samples are still at room temperature. This effect was explained by the presence of a substantial amount of neutral oxygen atoms in excited states. Metastable atoms interact with carbon at high probability even at room temperature and this explanation was suggested in the paper. The appearance of intense H atomic lines and OH band in the first second of plasma treatment was explained by desorption of water molecules from surfaces just after ignition of the discharge, while the decreasing of the oxygen atom line was explained by the loss due to chemical reactions.

## Acknowledgement

The authors acknowledge the financial support from the Slovenian Research Agency (project No. P2 – 0082), the Ministry of Higher Education, Science and Technology of the Republic of Slovenia through the contract No. 3211-10-000057 (Center of Excellence Polymer Materials and Technologies) as well as Croatian Ministry of Science, Education and Sports project 035-0352851-2856 and Slovenian-Croatian bilateral project BI-SLO-HR-01(2009-2010).

## 6 REFERENCES

[1] U. Cvelbar, M. Mozetic, I. Junkar, A. Vesel, J. Kovac, A. Drenik, T. Vrlinic, N. Hauptman, M. Klanjsek-Gunde, B. Markoli, N. Krstulovic, S. Milosevic, F. Gaboriau, T. Belmonte, Appl. Surf. Sci., 253 (**2007**) 21, 8669–8673

[2] A. Vesel, M. Mozetic, A. Drenik, N. Hauptman, M. Balat-Pichelin, Appl. Surf. Sci., 255 (**2008**) 5, 1759–1765

[3] A. Asadinezhad, I. Novak I, M. Lehocky, V. Sedlarik, A. Vesel, I. Junkar, P. Saha, I. Chodak, Plasma Processes Polym., 7 (**2010**) 6, 504–514

[4] M. Lehocky, A. Mracek, Czechoslovak J. Phys., 56 (**2006**) 7, B1277–B1282

[5] A. Vesel, A. Drenik, M. Mozetic, A. Zalar, M. Balat-Pichelin, M. Bele, Vacuum, 82 (**2007**) 2, 228–231

[6] N. Puac, Z. Lj. Petrovic, M. Radetic, A. Djordjevic, Mat. Sci. Forum, 494 (**2005**), 291–296

[7] M. Mozetic, J. Phys. D Appl. Phys., 44 (**2011**) 17, 174028-1–174028-9

[8] N. Médard, J-C. Soutif, F. Poncin-Epaillard, Langmuir 18 (**2002**), 2246–2253

[9] A. Vesel, M. Mozetic, A. Drenik, S. Milosevic, N. Krstulovic, M. Balat-Pichelin, I. Poberaj, D. Babic, Plasma Chem. Plasma P., 26 (**2006**), 577–584

[10] R. Kulcar, M. Friskovec, N. Hauptman, A. Vesel, M. Klanjsek-Gunde, Dyes Pigm., 86 (**2010**) 3, 271–277

[11] A. Vesel, M. Mozetic, A. Zalar, Appl. Surf. Sci., 200 (**2002**), 94–103

[12] G. Primc, R. Zaplotnik, A. Vesel, M. Mozetic, AIP Advances, 1 (**2011**) 2, 022129-1-022129-11

[13] K. Kutasi, V. Guerra, P. A Sa, Plasma Sources Sci. Technol., 20 (**2011**), 035006

[14] A. Drenik, U. Cvelbar, A. Vesel, M. Mozetic, Inf. MIDEM, 35 (**2005**), 85–91

[15] M. Tadokoro, A. Itoh, N. Nakano, Z. L. Petrovic, T. Makabe, IEEE Trans. Plasma Sci. 26 (**1998**), 1724–1732

[16] A. Vesel, M. Mozetic, M. Balat-Pichelin, Vacuum, 81 (**2007**) 9, 1088–1093

[17] M. Balat-Pichelin, A. Vesel, Chem. Phys., 327 (**2006**) 1, 112–118

[18] K. Elersic, I. Junkar, M. Modic, R. Zaplotnik, A. Vesel, U. Cvelbar, Mater. Tehnol., 45 (**2011**) 3, 232–239

[19] A. Vesel, Activation of polymer polyethylene terephthalate by exposure to $CO_2$ and $O_2$ plasma, Mater. Tehnol. 45 (**2011**) 2, 121–124

[20] M. Gorjanc, V. Bukosek, M. Gorensek, A. Vesel, Tex. Res. J., 80 (**2010**) 6, 557–567

[21] A. Vesel, K. Elersic, I. Junkar, B. Malic, Mater. Tehnol., 43 (**2009**) 6, 323–326

[22] I. Junkar, U. Cvelbar, A. Vesel, N. Hauptman, M. Mozetic, Plasma Processes Polym., 6 (**2009**) 10, 667–675

[23] M. Sowe, I. Novak, A. Vesel, I. Junkar, M. Lehocky, P. Saha, I. Chodak, Int. J. Polym. Anal. Ch., 14 (**2009**) 7, 641–651

[24] M. Biscan, Z. Kregar, N. Krstulovic, S. Milosevic, Plasma Chem. Plasma Process., 30 (**2010**) 3, 401–412

[25] N. Krstulovic, I. Labazan, S. Milosevic, U. Cvelbar, A. Vesel, M. Mozetic, J. Phys. D: Appl. Phys. 39 (**2006**), 3799–3804

[26] H. Kumagai, D. Hiroki, N. Fujii, T. Kobayashi, J. Vac. Sci. Technol. A, 22 (**2004**) 1, 1–7

[27] T. Vrlinic, A. Vesel, U. Cvelbar, M. Krajnc, M. Mozetic, Surf. Interface Anal., 39 (**2007**) 6, 476–481

[28] G. Kuhn, S. Weidner, R. Decker, A. Ghode, J. Friedrich, Surf. Coat. Technol., 116 (**1999**), 796–801

[29] A. Vesel, I. Junkar, U. Cvelbar, J. Kovac, M. Mozetic, Surf. Interface Anal., 40 (**2008**) 11, 1444–1453

[30] A. Vesel, Inf. MIDEM, 38 (**2009**), 257–265

[31] U. Cvelbar, B. Markoli, I. Poberaj, A. Zalar, L. Kosec, S. Spaic, Appl. Surf. Sci., 253 (**2006**) 4, 1861–1865

[32] J. Peters, B. Bartlett, J. Lindsay, J. Heberlein, Plasma Chem. Plasma Process., 28 (**2008**) 3, 331–352

[33] M. Mozetic, A. Vesel, U. Cvelbar, A. Ricard, Plasma Chem. Plasma Process., 26 (**2006**) 2, 103–117

[34] S. Xu, K. N. Ostrikov, Y. Li, E. L. Tsakadze, I.R. Jones, Physics of Plasmas, 8 (**2001**) 5, 2549–2557
[35] A. Vesel, M. Mozetic, P. Panjan, N. Hauptman, M. Klanjsek-Gunde, M. Balat-Pichelin, Surf. Coat. Technol., 204 (**2010**) 9–10, 1503–1508
[36] T. Belmonte, C. D. Pintassilgo, T. Czerwiec, G. Henrion, V. Hody, J. M. Thiebaut, J. Loureiro, Surf. Coat. Technol., 200 (**2005**) 1–4, 26–30
[37] A. Drenik, A. Vesel, M. Mozetic, J. Nucl. Mater., 386–388 (**2009**), 893–895
[38] Z. Kregar, N. Krstulovic, N. Glavan Vukelic, S. Milosevic, J. Phys. D, Appl. Phys, 42 (**2009**) 14, 145201
[39] U. Cvelbar, N. Krstulovic, S. Milosevic and M. Mozetic, Vacuum 82 (**2007**) 2, 224–227
[40] N. C. M. Fuller, M. V. Malyshev, V. M. Donnelly, I. P. Herman, Plasma Sources Sci. Technol., 9 (**2000**) 2, 116–127
[41] T. Tadokoro, H. Hirata, N. Nakano, Z. Lj. Petrovic, T. Makabe, Phys. Rev. E 57 (**1998**), R43–R46
[42] Z. Kregar, N. Krstulovic, S. Milosevic, K. Kenda, U. Cvelbar, and M. Mozetic, IEEE Trans. Plasma Sci., 36 (**2008**) 4, 1368–1369
[43] A. Vesel, M. Mozetic, A. Hladnik, J. Dolenc, J. Zule, S. Milosevic, N. Krstulovic, M. Klanjsek-Gunde, N. Hauptmann, J. Phys. D: Appl. Phys., 40 (**2007**) 12, 3689–3696
[44] C. Rond, A. Bultel, P. Boubert, B. G. Cheron, Chem. Phys., 354 (**2008**) 1–3, 16–26
[45] M. Mozetic, A. Vesel, A. Drenik, I. Poberaj, D. Babic, J. Nucl. Mater., 363–365 (**2007**), 1457–1460
[46] S. Wickramanayaka, N. Hosokawa, Y. Hatanaka, Jap. J. Appl. Phys. 30 (**1991**), 2897–2900
[47] K. Takeda, S. Takashima, M. Ito, M. Hori, Appl. Phys. Lett., 93 (**2008**) 2, 021501

UDK 533.9
Original scientific article/Izvirni znanstveni članek

ISSN 1580-2949
MTAEC9, 46(1)31(2012)

# METHOD FOR DYNAMIC CONTROL OF NEUTRAL ATOM DENSITY IN A PLASMA CHAMBER

## METODA ZA DINAMIČNO NADZOROVANJE GOSTOTE NEVTRALNIH ATOMOV V PLAZEMSKI KOMORI

**Gregor Primc**

Jožef Stefan Institute, Department F4, Jamova 39, 1000 Ljubljana, Slovenia
gregor.primc@ijs.si

*Prejem rokopisa – received: 2011-05-24; sprejem za objavo – accepted for publication: 2011-07-19*

Systematic measurements of neutral oxygen atoms under various conditions and with the presence of a special active element (recombinator) were performed. Measurements of oxygen atoms will be used for future work on the regulation and dynamic control of neutral oxygen atoms. The experiment was performed in an experimental plasma reactor with a main and a side tube made from borosilicate glass. The neutral atom density was measured by a nickel-fiber-optic catalytic probe at a fixed position in the side tube. It has been found out that the density of neutral oxygen atoms depended both on the pressure of the oxygen gas and excitation power, but mostly on the presence and the position of the recombinator. The measured densities were of the order of $10^{21}$ $m^{-3}$, which is a characteristic value in glass discharge chambers. Such orders of density suffice for the processing of organic materials. The problem with organic materials is that interaction with oxygen atoms heats the material. Therefore, it is often necessary to decrease the atom density as soon as possible. As it is described in this paper we achieved the decrease in the atom density by using a movable recombinator. The recombinator has enabled us to select the appropriate atom density without having to change the discharge parameters.

Keywords: weak ionized plasma, oxygen plasma, fiber-optic catalytic probe, active control, neutral atom, atom source

Ob spreminjanju različnih parametrov in ob priostnosti aktivnega elementa (rekombinatorja) smo opravili sistematične meritve. Meritve bodo osnova za prihodnje delo na regulaciji in dinamičnem nadzoru nevtralnih kisikovih atomov. Za eksperiment smo uporabili eksperimentalni plazemski reaktor z glavno in stransko cevjo iz borosilikatnega stekla. Z nikljevo optično katalitično sondo na fiksnem položaju v stranski cevi, smo merili gostoto nevtralnih atomov. Ugotovili smo, da je gostota kisikovih atomov odvisna tako od tlaka, kot od vzbujevalne moči RF generatorja, predvsem pa od prisotnosti in položaja samega rekombinatorja. Gostote dosežene v eksperimentalnem reaktorju so bile reda velikosti $10^{21}$ $m^{-3}$, kar je značilna vrednost pri razelektritvi v stekleni cevi. Izmerjene gostote atomov so primerne za obdelavo organskih materialov. Obdelavo v plazmi spremljata dva procesa. Koristno prestrukturiranje površine vzorca, ki je bil izpostavljen plazmi, in nezaželeno segrevanje vzorca. Ravno zaradi segrevanja je pomembno poznavanje gostote kisikovih atomov, saj lahko previsoke koncentracije povzročijo uničenje vzorca. Kot je opisano v tem delu, nam je zmanjšanje gostote atomov uspelo doseči z uporabo rekombinatorja. Izkazalo se je, da lahko z rekombinatorji izberemo primerno gostoto atomov neodvisno od razelektritvenih parametrov, kar je še posebej pomembno pri obdelavi materialov v plazmi.

Ključne besede: šibko ionizirana plazma, kisikova plazma, optična katalitična sonda, dinamični nadzor, nevtralni atomi, vir atomov

## 1 INTRODUCTION

Nowadays weakly ionized highly dissociated gaseous plasma is widely used for treatment of different materials.[1–4] Namely, plasma treatment of materials features excellent quality, stability and above all ecological integrity. Different technologies often use oxygen, nitrogen or hydrogen plasma, especially as an alternative to environmentally unfriendly wet chemical treatment. Plasma is mainly used for surface cleaning,[5–9] activation of organic materials,[10–22] selective etching of polymers and polymer composites,[23–28] cold ashing of biological samples, and in modern medicine applications for sterilization of sensitive materials[29–31] and lately also for nanomaterial synthesis.[32,33]

As already mentioned, material treatment may not always be environmentally friendly. It often requires a sufficiently reactive medium to induce chemical changes on the surface of a material. Wet chemical treatment presents a great burden to the environment, as it uses acids, lye, solvents or liquid hydrogenated hydrocarbons, which cause problems, such as health hazards during transports, increased consumption of energy and other resources tied to the production and the purification of such chemicals, storage and the industrial process itself and waste disposal after the process has been completed. Therefore, alternative methods, such as plasma treatment, are needed to minimize the impact of harmful chemicals on the environment.[34]

When treating different materials it is very important to know the density of plasma particles in the vicinity of a treated sample.[35] Method and treatment intensity are highly dependent on particle flux density on the surface of the sample. Furthermore, diverse gradients of concentration may appear in the processing chamber, so position of the sample is very important. Frequently a treated sample represents a strong sink for plasma particles, so that particle flux density on the surface of the sample is dependent on dimensional and material properties of the sample.[36] Therefore, it is important to know the exact

neutral atom density and being able to actively regulate it during treatment, independently of discharge parameters.

## 2 EXPERIMENT

The neutral atom density was measured in an oxygen plasma powered by RF generator. We used five different RF generator output powers from 200 W to 600 W (in 100 W steps) and four different pressures (50 Pa, 70 Pa, 90 Pa and 120 Pa). A special movable recombinator was used to control the neutral atom density in plasma reactor. At a given pressure we varied the position of recombinator relatively to the tip of the probe. Seven different recombinator positions were used: -7.5 cm, -2.6 cm, -1.3 cm, 0 cm, 1.3 cm, 2.6 cm and 4 cm (distance measured from the probe tip). And finally, at a fixed pressure and recombinator position we varied the RF generator power. Due to the hysteresis between E- and H-modes, we could not increase the power at exact 100 W steps, but rather adapted them during measurements.[37–39]

The experimental system, which was constructed to serve as a source of neutral oxygen atoms in the ground state at room kinetic temperature, is shown schematically in **Figure 1**. The vacuum system was pumped using a two stage rotary pump with a nominal pumping speed of 80 $m^3 h^{-1}$. The pump was connected to a 4-cm-wide glass tube via a high-vacuum-compatible angle valve. The vacuum elements were equipped with KF40 flanges. The conductivity near 100 Pa was much larger than the nominal pumping speed. Therefore, the effective pumping speed at the entrance to the glass tube was almost the same as the pumping speed of the pump. An absolute vacuum gauge was mounted perpendicular to the 4-cm-wide glass tube (**Figure 1a**). The glass tube was made from borosilicate glass (Schott 8250, Mainz, Germany), which has a low coefficient for the heterogeneous

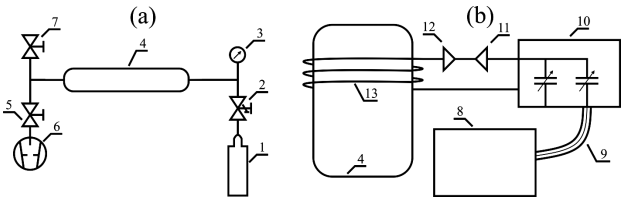


**Figure 1:** Part (a) represents a schematic of the experimental vacuum setup and part (b) represents a schematic of the electrical system. 1 – oxygen flask, 2 – precise needle valve used as an oxygen inlet, 3 – vacuum gauge, 4 – discharge tube, 5 – high vacuum valve, 6 – two stage rotary vacuum pump, 7 – air inlet valve, 8 – high frequency (13.56 MHz) RF power generator, 9 – coaxial cable, 10 – matching network, 11 – input power meter, 12 – output (reflected) power meter, 13 – RF coil.

**Slika 1:** Shema eksperimentalnega vakuumskega sistema (a) in shema električnega dela sistema (b). 1 – jeklenka s kisikom, 2 – precizni dozirni ventil za vpust plina, 3 – merilnik tlaka, 4 – razelektritvena cev, 5 – ventil, 6 – dvostopenjska rotacijska črpalka, 7 – ventil za vpust zraka, 8 – visoko frekvenčni (13.56 MHz) RF močnostni generator, 9 – koaksialni kabel, 10 – sklopitveni člen, 11 – usmerjevalni člen vstopne moči, 12 – usmerjevalni člen izhodne (odbite) moči, 13 – RF tuljava.

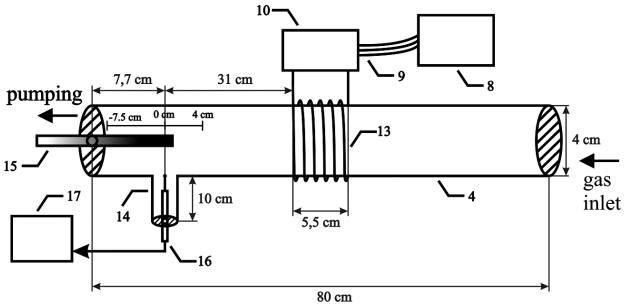


**Figure 2:** Technical drawing of plasma system. 4 – discharge tube, 8 – high frequency (13.56 MHz) RF power generator, 9 – coaxial cable, 10 – matching network, 14 – side tube, 15 – recombinator, 16 – nickel-fiber-optic catalytic probe, 17 – computer. The figure is not to scale.

**Slika 2:** Tehnična shema plazemskega sistema. 4 – razelektritvena cev, 8 – visoko frekvenčni (13.56 MHz) RF močnostni generator, 9 – koaksialni kabel, 10 – sklopitveni člen, 14 – stranska cev, 15 – rekombinator, 16 – nikljeva optična katalitična sonda, 17 – računalnik. Slika ni v merilu.

surface recombination of neutral oxygen atoms (less than $2\times10^{-3}$). The thickness of the glass tube was 2 mm; therefore, the inner diameter was 36 mm. The wide discharge tube also had a perpendicular side tube with the length of 10 cm and diameter of 1.5 cm (**Figure 2**). A manually movable copper rod with a high coefficient for heterogeneous surface recombination of oxygen atoms was used as a recombinator (**Figure 2**). The recombination coefficient of copper varies from $2.5\times10^{-2}$ to 0.17.[40] The recombinator was placed into the main glass tube in the afterglow region. The position of recombinator was varied by moving it along the axis of the main discharge tube. On the other side of the discharge tube plasma was excited by an RF coil wound around the tube. The coil was water cooled, and the segment of the tube with the wounded coil was cooled by forced air. This cooling prevented a substantial amount of heating of the tube in the discharge region. The coil was connected to a RF power generator via a matching network and a coaxial cable (**Figure 1b**). The two power meters measured the input and reflected power into and from the coil. Usually some of the power applied to the system is reflected back to the generator causing coaxial cable and the generator itself to heat up. The matching network consisted of two high-voltage high-frequency variable vacuum capacitors that were used for adapting the impedance of "plasma-coil" system to the impedance of the remaining circuit, which is 50 Ω.

A precise needle valve that served as an oxygen inlet was placed on the chamber and was connected to an oxygen flask via a standard copper tube, which had a diameter of 4 mm. Commercially-available oxygen that had a purity of 99.99% was used.

The density of neutral atoms was measured using a nickel-fiber-optic catalytic probe, which is described in detail in literature.[41–47] The probe was mounted 31 cm from the end of the coil in the side tube perpendicular to the main discharge tube. The absolute accuracy of the

probe is about 30%, but the relative sensitivity is extremely high, because it allows for the observation of even a small decrease in the oxygen atom density. The probe was coated by a nickel catalyst material, which (among some other materials) exhibits a constant recombination coefficient. It is important that the surface of the probe is properly prepared. To ensure stable surface recombination, the probe was exposed to a high flux of oxygen atoms, and consequently heated to a high temperature prior to systematic measurements. A thin oxide film was formed on the tip of the probe. Such thin film ensures for a repeatable and accurate measurements.

## 3 RESULTS

Measurements of oxygen atom density with nickel-fiber-optic catalytic probe were performed at various conditions (different pressure, power, and presence of recombinator). Even though the kinetic temperature of the gas is that of the surrounding gas (i.e. room temperature), the probe temperature quickly increased by several hundred Kelvin after the discharge was turned on. An example of such probe characteristic is shown in **Figure 3**. **Figure 3** shows the temperature of the fiber-optic catalytic probe as a function of time for five different excitation powers at a fixed pressure of 120 Pa and a fixed recombinator position at -2.6 cm. The maximum temperature was achieved after a few seconds to tens of seconds, depending on the discharge power. Such an increase in temperature is because of the very high probability of heterogeneous surface recombination for the oxygen atoms which cause heating of the probe. This probability was determined to be 0.27.[48]

The plot of the maximum probe temperature as a function of the recombinator position is shown in **Figure 4** for the case of the minimum pressure (50 Pa) used and in **Figure 5** for the case of maximum pressure (120 Pa) used at our experiments. The parameter is real power. Real power is the power that ignites the discharge

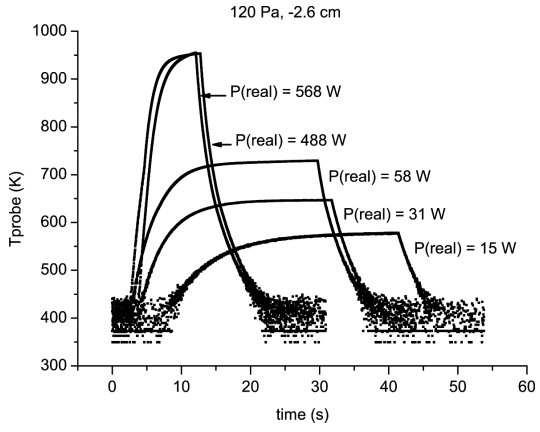


**Figure 3:** Temperature of the fiber-optic catalytic probe as a function of time at the pressure of 120 Pa and a fixed recombinator position

**Slika 3:** Temperatura optične katalitične sonde v odvisnosti od časa pri tlaku 120 Pa in fiksiranem položaju rekombinatorja

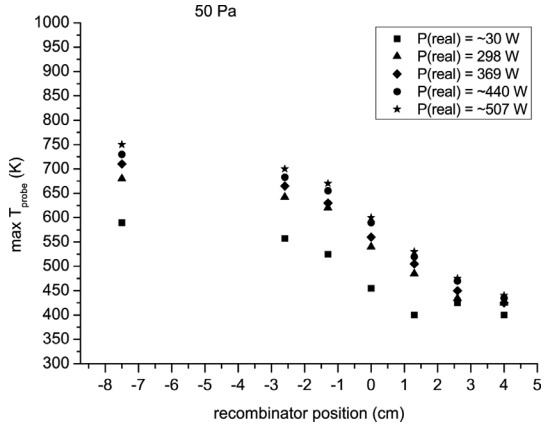


**Figure 4:** Maximum temperature of the probe as a function of recombinator position and the discharge power as a changing parameter. The pressure is 50 Pa.

**Slika 4:** Maksimalna temperatura sonde v odvisnosti od položaja rekombinatorja in razelektritvene moči. Tlak je bil 50 Pa.

and can be explained as a difference between the nominal or forward power and the reflected power ($P_{real} = P_{forward} - P_{reflected}$).

In **Figures 4 to 9** the recombinator position at –7.5 cm corresponds to a case when the recombinator is far away from the glow region i.e. far away from the source of oxygen atoms. While position at 4 cm corresponds to a case when the recombinator is placed very deep into the main glass tube and is therefore close to the glow region. We can see that the maximum probe temperature decreases when the recombinator is moved deeply into the glass tube. This decrease of maximum temperature is because of a lower flux of neutral oxygen atoms to the surface of the probe. The recombinator acts as a strong sink of oxygen atoms and, consequently, decreases the concentration of oxygen atoms in the discharge tube. Measuring of maximum probe temperature gives clear indication that we can control the density of oxygen atoms in plasma by changing the recom-

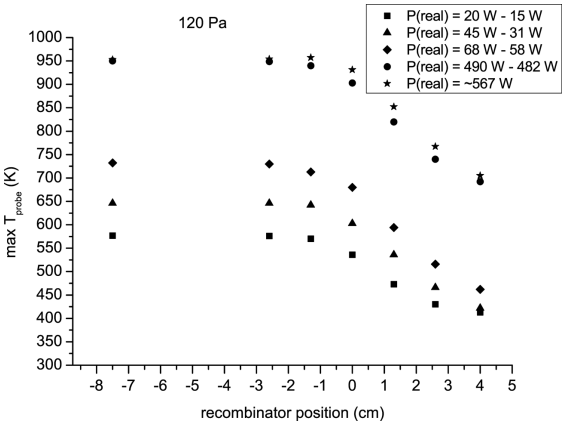


**Figure 5:** Maximum temperature of the probe as a function of recombinator position and the discharge power as a changing parameter. The pressure is 120 Pa.

**Slika 5:** Maksimalna temperatura sonde v odvisnosti od položaja rekombinatorja in razelektritvene moči. Tlak je bil 120 Pa.

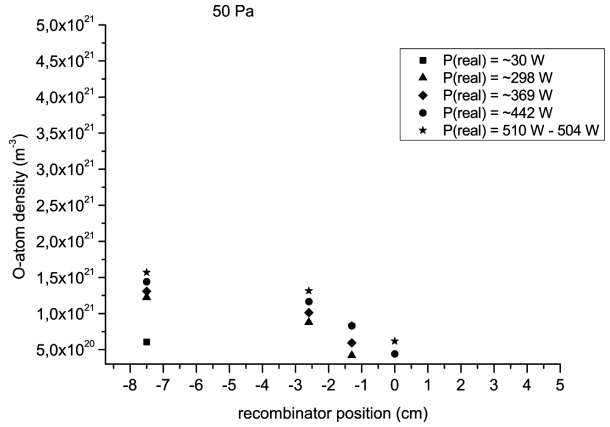


**Figure 6:** Density of neutral oxygen atoms at the probe position as a function of recombinator position and the discharge power as a changing parameter. The pressure is 50 Pa.

**Slika 6:** Gostota nevtralnih kisikovih atomov na področju sonde v odvisnoti od položaja rekombinatorja in razelektritvene moči. Tlak je bil 50 Pa.

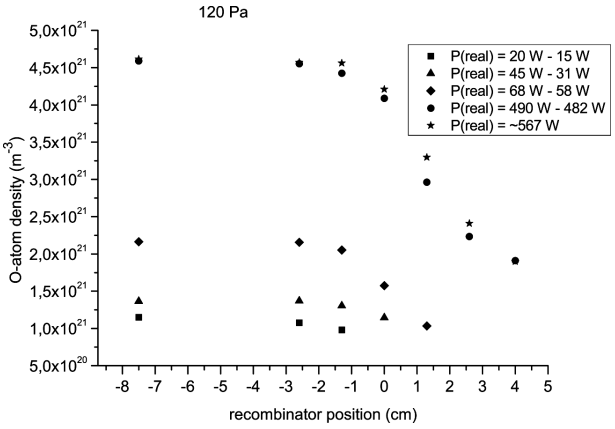


**Figure 7:** Density of neutral oxygen atoms at the probe position as a function of recombinator position and the discharge power as a changing parameter. The pressure is 120 Pa.

**Slika 7:** Gostota nevtralnih kisikovih atomov na področju sonde v odvisnoti od položaja rekombinatorja in razelektritvene moči. Tlak je bil 120 Pa.

binator position. In order to get absolute values for the density of oxygen atoms in the vicinity of the probe we have measured the temperature decay just after turning off the discharge. The neutral oxygen atom density was calculated from the time derivatives of the catalytic probe according to the following equation:[48]

$$n_0 = \frac{8mc_p}{vW_D\gamma A}\left(\frac{dT}{dt}\right) \quad (1)$$

where $m$ is the mass of the probe tip; $c_p$ is its specific heat capacity; $v$ is the average thermal velocity of oxygen atoms; $W_D$ is the dissociation energy of an oxygen molecule; $\gamma$ is the recombination coefficient of the oxygen atoms on the oxidized Ni surface; $A$ is the area of the catalyst and $dT/dt$ is the time derivative of the probe temperature just after turning off the discharge.

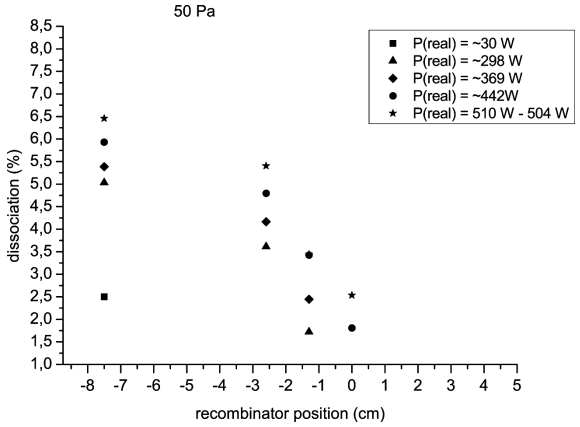


**Figure 8:** Dissociation fraction of the oxygen molecules at the probe position. The pressure is 50 Pa.

**Slika 8:** Disociacija kisikovih molekul na področju sonde. Tlak je bil 50 Pa.

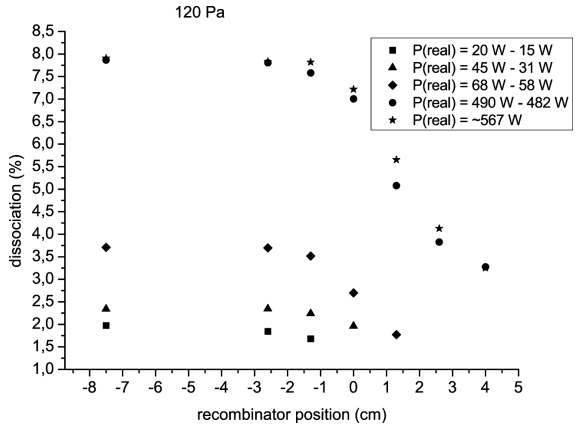


**Figure 9:** Dissociation fraction of the oxygen molecules at the probe position. The pressure is 120 Pa.

**Slika 9:** Disociacija kisikovih molekul na področju sonde. Tlak je bil 120 Pa.

**Figures 6 and 7** show the oxygen atom density at the probe position using different discharge powers. Again, only results for the minimum pressure of 50 Pa (**Figure 6**) and the maximum pressure of 120 Pa (**Figure 7**) are shown. Corresponding dissociation fractions of the oxygen molecules are shown in **Figures 8 and 9**. The dissociation fraction was calculated from the known pressure before turning on the discharge and the oxygen atom density using the following equation:

$$\eta = \frac{n_0 k_B T_g}{2p_{O_2}} \quad (2)$$

where $n_0$ is the oxygen atom density; $k_B$ is the Boltzmann constant; $T_g$ is the gas temperature; and $p_{O_2}$ is the oxygen pressure.

Note that some values are missing at graphs displaying the density of neutral oxygen atoms and dissociation fraction. At certain pressures, these values could not be measured because the probe signal was in the noise range.

## 4 DISCUSSION

Results displayed on **Figures 4 and 5** show a high temperature which at 600 W (in the case of 120 Pa) exceeds 900 K. At first glance such temperatures seem rather excessive because gas inside the chamber is at room temperature. Elevated probe temperature is interpreted by intensive recombination of neutral oxygen atoms on the surface of the probe. Oxygen plasma is rich in oxygen atoms. As we have already mentioned, the recombination coefficient of a glass discharge tube is low, therefore atoms recombine poorly on its surface. The excess of recombination is present on the surface of the probe and causes additional heating because of the nickel-catalyst coating on the tip of the probe. Because of this phenomenon the temperature of the probe is well above the temperature of the surrounding gas, which is approximately at room temperature.

The equilibrium temperature of the probe depends on the discharge power and oxygen pressure. In addition, the temperature of the probe largely depends on the recombinator position. Recombinator serves as a surface where extensive recombination of oxygen atoms takes place. As long as the position of the recombinator is far from the probe in the direction of the gas flow, it practically does not have any effect on the temperature of the probe. The directed gas velocity resulting in continuous pumping of the discharge tube is high enough to compensate the atom loss because of recombination reactions present on the surface of the copper recombinator. Moving recombinator closer to the probe noticeably influences on the oxygen atom recombination. In these circumstances the diffusion of the gas molecules and atoms is comparable to the directed velocity of the gas. The phenomenon is more distinctive when recombinator is pushed further inside the discharge tube passing the position of the probe. In this case, the recombinator causes a large decrease in the density of oxygen atoms in the vicinity of the probe. Therefore, the measured oxygen atom density is strongly dependent on the position of the recombinator. **Figures 4 and 5** show that the temperature of the probe decreases for approximately 50 K when we move the recombinator only for a centimetre. The recombinator therefore perfectly does its function, namely to decrease the neutral atom density independently of the discharge parameters. That was also the goal of the experiment; to quantitatively demonstrate that we may change the neutral atom density in any part of the discharge tube by moving the recombinator. When the recombinator is mounted deep inside the discharge tube (far right of the position of the probe) the temperature of the probe decreases rapidly and is, consequently, undetectable because of the noise picked up by the probe.

The temperature of the probe offers qualitative data about the neutral oxygen atom density. However, via measuring the time derivative of the temperature of the probe, quantitative data can be determined. The time derivatives allow us to calculate oxygen atom density in the vicinity of the probe. The calculated densities are of the order of $10^{21}$ $m^{-3}$, which is a characteristic value in glass discharge chambers. Such high order of neutral atom density suffices for treatment of organic materials. The problem with organic materials is that the interaction with oxygen atoms heats the material. Therefore, it is often necessary to decrease the atom density as soon as possible. As it is described in this paper, we achieved the decrease in the atom density by using a movable recombinator. The recombinator has enabled us to select the appropriate atom density without having to change the discharge parameters.

As it is illustrated on **Figures 8 and 9**, the dissociation fraction of oxygen molecules is few percent. Such dissociation degree ensures the right processing of materials.

## 5 CONCLUSIONS

Systematic measurements of neutral oxygen atom density in cold weakly ionized oxygen plasma were performed. A movable copper recombinator was used in order to influence the density of neutral atoms. The densities at various pressures, high frequency RF generator powers and recombinator positions were measured by a nickel-fiber-optic catalytic probe at a fixed position. The measurements were carefully processed and displayed in several graphs, indicating maximum probe temperature, neutral oxygen atom densities and oxygen dissociation fractions, all as a function of recombinator position. Even though manually moving a recombinator seems somewhat an old-fashioned method, it proved to be extremely useful at manipulating neutral oxygen atom density independently of the discharge parameters. This is particularly important in material processing, especially when we are dealing with very sensitive organic materials. In order to avoid substantial heating and degradation of material it is significant to know the density of neutral oxygen atoms in the vicinity of the treated sample as excessive concentrations may harm or even destroy it. As shown in this contribution it is very easy to control the density of neutral oxygen atoms by moving recombinator deeply towards (or away from) the discharge.

### Acknowledgement

The author acknowledges the financial support from the Slovenian Research Agency through project no. P2-0082.

## 6 REFERENCES

[1] M. Mozetic, Mater. Tehnol., 44 (**2010**) 4, 165–171
[2] B. Kasemo, Surface Science 500 (**2002**), 656–677
[3] H. J. Liu, D. Xie, L. M. Qian, XR. Deng, Y. X. Leng, N. Huang, Surf. Coat. Tech., 205 (**2011**) 8–9, 2697–2701

[4] D. Klee, H. Höcker, Adv. Polym. Sci. 149 (**2000**), 1–57
[5] M. Mozetic, A. Zalar, M. Drobnič, Thin Solid Films, 343–344 (**1999**), 101–104
[6] A. Vesel, M. Mozetic, P. Panjan, N. Hauptman, M. Klanjsek-Gunde, M. Balat-Pichelin, Surf. Coat. Technol., 204 (**2010**) 9/10, 1503–1508
[7] A. Drenik, A. Vesel, M. Mozetic, J. Nucl. Mater., 386–388 (**2009**), 893–895
[8] A. Vesel, M. Mozetic, A. Drenik, S. Milosevic, N. Krstulovic, M. Balat-Pichelin, I. Poberaj, D. Babic, Plasma Chem. Plasma P., 26 (**2006**), 577–584
[9] M. Mozetic, B. Praček, Inf. Midem, 28 (**1998**) 3, 171–174
[10] T. Vrlinic, A. Vesel, U. Cvelbar, M. Krajnc, M. Mozetic, Surf. Interface Anal., 39 (**2007**) 6, 476–481
[11] M. Mozetic, Vacuum, 71 (**2003**), 237–240
[12] T. Vrlinic, A. Vesel, U. Cvelbar, M. Krajnc, M. Mozetic, Surf. Interface Anal., 39 (**2007**) 6, 476–481
[13] C.-M. Chan, T.-M. Ko, H. Hiraoka. Surf. Sci. Rep., 24 (**1996**), 1–54
[14] A. Vesel, Mater. Tehnol., 45 (**2011**) 2, 121–124
[15] L.-A. O'Hare, S. Leadley, B. Parbhoo, Surf. Interface Anal., 33 (**2002**), 335–342
[16] I. Junkar, U. Cvelbar, A. Vesel, N. Hauptman, M. Mozetic, Plasma Processes Polym., 6 (**2009**) 10, 667–675
[17] N. Inagaki, K. Narushim, N. Tuchida, K. Miyazaki, J. Polym. Sci. Pol. Phys., 42 (**2004**), 3727–3740
[18] M. Gorjanc, V. Bukosek, M. Gorensek, A. Vesel, Tex. Res. J., 80 (**2010**) 6, 557–567
[19] R. Morent, N. De Geyter, L. Gengembre, C. Leys, E. Payen, S. Van Vlierberghe, E. Schacht, Eur. Phys. J. Appl. Phys. 43 (**2008**), 289–294
[20] A. Vesel, K. Elersic, I. Junkar, B. Malic, Mater. Tehnol., 43 (**2009**) 6, 323–326
[21] Z. Kregar, M. Biscan, S. Milosevic, A. Vesel, IEEE Trans. Plasma Sci. 39 (**2011**) 5, 1239–1246
[22] A. Vesel, Mater. Tehnol., 45 (**2011**) 3, 217–220
[23] M. Klanjsek Gunde, M. Kunaver, M. Mozetic, P. Pelicon, J. Simcic, M. Budnar, M. Bele, Surf. Coat. Int. B, 85 (**2002**), 115
[24] M. Kunaver, M. Klanjsek Gunde, M. Mozetic, A. Hrovat, Dyes Pigm., 57 (**2003**), 235–243
[25] M. Klanjsek Gunde, M. Kunaver, M. Mozetic, A. Hrovat, Powder Technol., 148 (**2001**), 64–66
[26] N. Vourdas, D. Kontziampasis, G. Kokkoris, V. Constantoudis, A. Goodyear, A. Tserepi, M. Cooke, E. Gogolides, Nanotehnology, 21 (**2010**), 08530
[27] M. Kunaver, M. Klanjsek Gunde, M. Mozetic, M. Kunaver, A. Hrovat, Surf. Coat. Int. B, 86 (**2003**), 175–179
[28] M. Kunaver, M. Mozetic, M. Klanjsek Gunde, Thin Solid Films, 459 (**2004**), 115–117
[29] D. Vujosevic, Z. Vratnica, A. Vesel, U. Cvelbar, M. Mozetic, A. Drenik, T. Mozetic, M. Klanjsek-Gunde, N. Hauptman, Mater. Tehnol., 40 (**2006**) 6, 227–232
[30] K. Elersic, I. Junkar, A. Spes, N. Hauptman, M. Klanjsek Gunde, A. Vesel, Mater. Tehnol., 44 (**2010**) 3, 153–156
[31] U. Cvelbar, M. Mozetic, N. Hauptman, M. Klanjsek-Gunde, J. Appl. Phys., 106 (**2009**) 10, 103303-1-103303-5
[32] M. Mozetic, J. Phys. D: Appl. Phys., 44 (**2011**) 17, 174028-1–174028-9
[33] M. Mozetic, U. Cvelbar, Adv. Mater., 17 (**2005**), 2138–2142
[34] A. Drenik, M. Mozetic, A. Vesel, U. Cvelbar, Journal of Physics: Conference Series, 207 (**2010**), 012009
[35] G. Primc, R. Zaplotnik, A. Vesel, M. Mozetic, AIP Advances 1 (**2011**) 2, 022129-1-022129-11
[36] N. Krstulovic, I. Labazan, S. Milosevic, U. Cvelbar, A. Vesel, M. Mozetic, J. Phys. D: Appl. Phys., 39 (**2006**) 17, 3799–3804
[37] R. Zaplotnik, A. Vesel, M. Mozetic, Europhys. Lett. 95 (**2011**), 55001-1 – 55001-5
[38] Y. W. Lee, H. L. Lee, T. H. Chung, J. Appl. Phys., 109 (**2011**) 11, 113302
[39] R. Zaplotnik, A. Vesel, Mater. Tehnol., 45 (**2011**) 3, 227–231
[40] A. Drenik, Dissertation, The probability of heterogeneous recombination of hydrogen and oxygen atoms on the surfaces of fusion-relevant materials, Jožef Stefan International Postgraduate School, Ljubljana 2009, 43
[41] M. Balat-Pichelin, A. Vesel, Chem. Phys., 327 (**2006**) 1, 112–118
[42] A. Vesel, A. Drenik, M. Mozetic, M. Balat-Pichelin, Vacuum, 84 (**2010**) 7, 969–974
[43] A. Drenik, A. Tomeljak, M. Mozetic, A. Vesel, D. Babic, M. Balat-Pichelin, Vacuum, 84 (**2010**) 1, 90–93
[44] M. Mozetic, A. Vesel, U. Cvelbar, A. Ricard, Plasma Chem. Plasma Process., 26 (**2006**) 2, 103–117
[45] A. Drenik, U. Cvelbar, A. Vesel, M. Mozetic, Inf. MIDEM, 35 (**2005**), 85–91
[46] M. Mozetic, A. Vesel, A. Drenik, I. Poberaj, D. Babic, J. Nucl. Mater., 363–365 (**2007**), 1457–1460
[47] A. Drenik, U. Cvelbar, A. Vesel, M. Mozetic, Strojarstvo, 48 (**2006**) 1/2, 17–22
[48] I. Sorli, R. Rocak, J. Vac. Sci. Technol. A, 18 (**2000**), 338

UDK 678.7
Original scientific article/Izvirni znanstveni članek

ISSN 1580-2949
MTAEC9, 46(1)37(2012)

# ENHANCEMENT OF MOLECULAR WEIGHT OF L-LACTIC ACID POLYCONDENSATES UNDER VACUUM IN SOLID STATE

## POVEČANJE MOLEKULARNE TEŽE POLIKONDENZATOV L-LAKTIČNE KISLINE V TRDNEM STANJU Z VAKUUMOM

**Pavel Kucharczyk[1], Vladimír Sedlařík[1], Ita Junkar[2], Darij Kreuh[3], Petr Sáha[1]**

[1]Centre of Polymer Systems, Polymer Centre, Tomas Bata University in Zlin, nam. T. G. Masaryka 5555, 760 01 Zlin, Czech Republic
[2]Jozef Stefan Institute, Jamova cesta 39, 1000 Ljubljana, Slovenia
[3]Ekliptik d.o.o., Teslova 30, 1000 Ljubljana, Slovenia
sedlarik@ft.utb.cz

*Prejem rokopisa – received: 2011-06-05; sprejem za objavo – accepted for publication: 2011-07-18*

Enhancement of L-lactic acid polycondensates by involving of postpolycondensation reactions in solid state under vacuum and catalyzed by stannous 2-ethylhexanoate were studied in the presented work. The catalyst was used only in postpolycondensation step. An effect of the catalyst concentration and postpolycondensation reaction time on resulting properties of poly(lactic acid) was studied by gel permeation chromatography, Fourier transform infrared spectroscopy and differential scanning calorimetry. Results show significant enhancement of molecular weight in case of the systems containing 2 wt. % of the catalyst due to the postpolycondensation procedure ($M_w$~91.0 kg/mol; i.e. 1655 % after 24 hours). However, further progress can be assumed with increasing reaction time. This enhancement of poly(lactic acid) molecular weight had a response corresponding to changes of both physico-chemical and thermal properties of the solid state postpolycondensation products.

Keywords: poly(lactic acid), solid state postpolycondensation, molecular weight enhancement

V tem delu smo za izboljšanje lastnosti polikondenzata L-laktične kisline raziskali vpliv postpolikondenzacijskih reakcij v trdnem stanju z vakuumom. Za katalizo smo v post polikondenzacijskem koraku uporabili katalizator kositrov 2-etilheksanoat. Vpliv koncentracije katalizatorja in časa postpolikondenzacijskih reakcij na lastnosti poli(laktične kisline) smo raziskovali z gel prepustno kromatografijo, fourierjevo transformacijsko infrardečo spektroskopijo in z diferenčno dinamično kalorimetrijo. Zaradi postpolikondenzacijskega postopka smo opazili bistveno povečanje molekulske mase v sistemu, kje smo uporabili 2 ut.% katalizatorja ($M_w$~91.0 kg/mol; 1655 % po 24 urah). Še dodatno povečanje bi najverjetneje lahko dosegli tudi s podaljšanjem časa reakcije. Izkazalo se je, da ima povečanje molekulske mase poli(laktične kisline) vpliv na fizikalno-kemijske, kot tudi na termične lastnosti trdnih postpolikondenzacijskih produktov.

Ključne besede: poli(laktična kislina), postpolikondenzacija trdnega stanja, izboljšanje molekulske teže

## 1 INTRODUCTION

Poly(lactic acid) (PLA) is one of the biodegradable polymers with promising applicability in the field of environmentally friendly materials production (e.g. packaging, disposable items) as well as in medicine (medical devices, drug carriers).[1–7] Generally, PLA can be synthesized by three basic ways; (i) ring opening polymerization; (ii) azeotropic distillation in solution; (iii) polycondensation in molten state.[8,9] First two methods are known to be experimentally difficult due to sensitivity to presence of impurities. The lastly mentioned method allows relatively low-demanding PLA preparation.[10,11] However, it is redeemed by low molecular weight of the polycondensation products, which is not acceptable for most of the engineering applications.[12]

The disadvantage of the low molecular weight polycondensation product can be offset by introduction of subsequent techniques – postpolycondensation reactions, which can yield a product with high molecular weight. Basically, two approaches have been known. The first one represents coupling reactions between functional groups intentionally introduced at the end of PLA chains (e.g. hydroxyl) and bifunctional compound (e.g. diisocyanate).[13] The second method involves reaction between ends of the PLA chains and/or residual monomer, which is usually carried out in solid state under specific conditions.[8] This postpolycondensation reaction is analogy to the method developed for molecular weight increasing of poly(ethylene terephthalate)[14], which has been also studied for an usage in medical applications.[15–17] The advantage of this method is fact that an addition of external chemical agents is not required.

There are several works describing solid state postpolycondensation of PLA. For instance, Zhang et al. reported two step (melt/solid) preparation of high molecular weight PLA.[18] Effect of crystallization on the solid state polycondensation of PLA was investigated by Xu et al.[19] These both works apply $SnCl_2$ as a catalyst for PLA prepolymer preparation and additional catalyst for postpolycondensation reaction. The resulting products had molecular weight in the range 20-150 kg/mol. Polydispersity index was mostly tightly below 2. However, to the best of our knowledge, solid state postpolycondensation of low molecular weight PLA prepared by

direct polycondensation of L-lactic acid without using of a catalyst has not been studied.

This work is dedicated to investigation of solid state postpolycondensation of low molecular weight L-lactic acid polycondensates prepared by non-catalyzed reaction. Various concentration of an organotin based compound was used for catalysis of the postpolycondensation step subsequently. Resulting products were characterized by gel permeation chromatography; differential scanning calorimetry and Fourier transform infrared spectroscopy.

## 2 EXPERIMENTAL PART

### *2.1 Materials*

L-lactic acid (LA) $C_3H_6O_3$, 80 % water solution, optical rotation $\alpha$ = 10.6° (measured by the polarimeter Optech P1000 at 22 °C, concentration of 10 %) was purchased from Lachner Neratovice, Czech Republic. Stannous 2-ethylhexanoate ($Sn(Oct)_2$) (~95 %) was supplied by Sigma Aldrich, Steinheim Germany. The solvents acetone $C_3H_6O$, chloroform $CHCl_3$ and methanol $CH_4O$ (all analytical grade) were bought from IPL Lukes, Uhersky Brod, Czech Republic.

### *2.2 Sample preparation*

The procedure as samples preparation is summarized in **Figure 1**. Generally, PLA prepolymer was prepared by direct melt polycondensation of L-lactic acid. A typical procedure was as follows: 50 ml lactic acid solution was added into a double necked flask (250 ml) equipped with a Teflon stirrer. The flask was then placed in an oil bath heated by magnetic stirrer with heating and connected to a laboratory apparatus for distillation under reduced pressure. The dehydration step followed at 160 °C, reduced pressure 15 kPa for 4 hours. The flask with dehydrated mixture was connected to the source of vacuum (100 Pa) and the reaction continued for 24 hours at the temperature 180°C. The resulting product was allowed to cool down at room temperature and then dissolved in acetone. The polymer solution was precipitated in a mixture of chilled methanol/distilled water 1:1 (v/v). The obtained product was filtrated, twice washed with hot distilled water (80 °C) and dried in at 55 °C for 48 hours under the pressure 15 kPa.

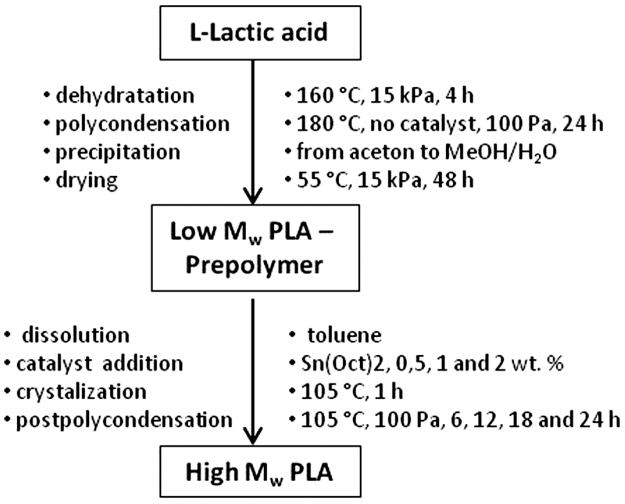


**Figure 1:** Scheme of two step preparation of high $M_w$ PLA through the postpolycondensation reaction in solid state

**Slika 1:** Shema dvostopenjske priprave visoko $M_w$ PLA z uporabo postpolikondezacijskih reakcij v trdnem stanju

Solid state postpolycondensation was proceeded as follows: 6 g of the prepolymer was dissolved in 20 ml of toluene and the catalyst was added to the polymer solution (0.5, 1 and 2 wt. %). The solvent was evaporated at elevated temperature (80 °C) and the residuals were dried for 6 hours at 50 °C and 3 kPa. After that the prepolymer containing the catalyst was placed into a test tube and crystallized at 105 °C for 1 hour. Finally, the test tubes were connected to the vacuum source (100 Pa). The sampling was done after 6, 12, 18 and 24 hours.

### *2.3 Characterization of samples*

#### *2.3.1 Determination of molecular weight by gel permeation chromatography (GPC)*

GPC analyses were performed using a chromatographic system Breeze (Waters) equipped with a PLgel Mixed-D column ((300 × 7.8) mm, 5 μm) (Polymer Laboratories Ltd). For detection, a Waters 2487 Dual absorbance detector at 254 nm was employed. Analyses were carried out at room temperature with a flow rate of 1.0 mL/min in chloroform. The column was calibrated using narrow molecular weight polystyrene standards with molar mass ranging from 580 g/mol to 480 000 g/mol (Polymer Laboratories Ltd). A 100 μL injection loop was used for all measurements. The sample concentration ranged from 1.6 mg/mL to 2.2 mg/mL. Data processing was carried out using the Waters Breeze GPC Software (Waters). The weight average molar mass $M_w$, number average molar mass $M_n$ and Polydispersity ($PDI=M_w/M_n$) of the tested samples were determined. Relative enhancement of $M_w$ ($EM_w$) was calculated according as follows:

$$EM_w(\%) = \frac{M_{wS}}{M_{w0}} \times 100 \quad (1)$$

where $M_{wS}$ represents $M_w$ of the sample and $M_{w0}$ is $M_w$ of the prepolymer.

#### *2.3.2 Fourier transform infrared spectroscopy (FTIR)*

Functional groups in LA polycondensation products were identified using FTIR analysis. The investigation was conducted on Nicolet 320 FTIR, equipped with attenuated total reflectance accessory (ATR) utilizing Zn-Se crystal and the software package "Omnic" over the range of 4000-650 $cm^{-1}$ at room temperature. The uniform resolution of 2 $cm^{-1}$ was maintained in all cases.

*2.3.3 Differential scanning calorimetry (DSC)*

For the determination of glass transition temperature $T_g$, melting point $T_m$ the differential scanning calorimetry was used. Approximately 8 mg of the sample were placed in an aluminium pan, sealed and analyzed on Mettler Toledo DSC1 STAR System under nitrogen flow (20 $cm^3$/min). The analysis was carried out according to the following programme: (i) first heating scan 0 – 195 °C (10 °C/min); (ii) annealing at 195 °C for 1 minute; (iii) cooling scan 195 – 0 °C (10 °C/min); (iv) annealing at 0 °C for 1 minute; (v) second heating scan 0 – 195 °C (10 °C/min). Melting point temperature ($T_m$) was obtained from the first heating cycle. The value of glass-transition temperature ($T_g$) was determined in the second heating scan at the midpoint stepwise increase of the specific heat associated with glass transition. The DSC results for prepolymer and the sample after 24 hours of postpolycondensation reaction are presented in this work.

## 3 RESULTS AND DISCUSSION

The results obtained from GPC analysis are summarized in **Table 1**. The prepolymer (see the scheme in **Figure 1**) had $M_w$ = 5.5 kg/mol and low *PDI*. It shows relatively narrow distribution of molecule chain lengths. Subsequently proceeded postpolycondensation reactions led to enhancement of $M_w$. However, significant increase in $M_w$ was observed mostly after 18 hours of the reaction. Further prolongation of the reaction time (24 hours) had positive effect on $M_w$ enhancement as well as addition of the catalyst ($Sn(Oct)_2$). It can be noticed in **Figure 2** where dependence of relative enhancement of $M_w$, $EM_w$, (Equation 1) is depicted as a function of postpolycondensation reaction time for various concentration of the catalyst. The lowest investigated concentration of the catalyst seemed to be not suitable for high $M_w$ PLA preparation. Maximal $EM_w$ was only 167 % in this case (9.2 kg/mol). Better results were noticed for the systems containing 1 wt. % of the catalyst. $EM_w$ was 502 % after 24 hours of the postpolycondensation reaction. However, it represents $M_w$ = 27.6 kg/mol, which is still not considerable as high $M_w$ product. Significantly different results were observed when the concentration of the catalyst was risen to 2 wt. %. As can be seen in **Figure 2**, $EM_w$ for this system was higher already after 12 hours of postpolycondensation reaction that those described above (0.5 and 1 wt. %, 24 hours). In addition, its $EM_w$ steeply increases with the reaction time. The sample after 24 hours of the reaction showed $EM_w$ = 1655 %. It corresponds to 91.0 kg/mol. *PDI* was 1.6. It reveals narrow distribution of the chain lengths.

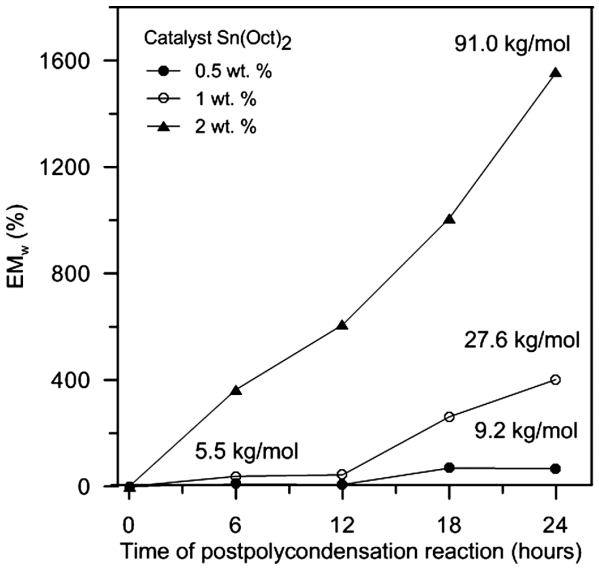


**Figure 2:** Relative enhancement of $M_w$ versus time of postpolycondensation reaction in presence of various catalyst concentrations

**Slika 2:** Relativno povečanje $M_w$ glede na čas polikondenzacijskih reakcij in v prisotnosti katalizatorja pri različnih koncentracijah

**Table 1:** GPC characteristics of the prepolymer and the samples after various times of postpolycondensation reaction

**Tabela 1:** GPC karakteristika predpolimera in vzorcev z različnimi časi postpolikondenzacijskih reakcij

| Catalyst concentration (wt. %) | Time of postpolycondensation reaction (hours) | | | | |
|---|---|---|---|---|---|
| | 0* | 6 | 12 | 18 | 24 |
| | $M_w$/PDI** | $M_w$/PDI | $M_w$/PDI | $M_w$/PDI | $M_w$/PDI |
| 0.5 | 5.5/1,68 | 6.0/2.6 | 5.4/1.7 | 9.3/1.8 | 9.2/2.3 |
| 1 | | 7.6/1.6 | 7.9/2.1 | 19.9/2.2 | 27.6/1.7 |
| 2 | | 25.5/2.6 | 38.9/2.6 | 60.9/2.9 | 91.0/1.6 |

* prepolymer

** $M_w$ – weight average molecular weight (kg/mol), PDI – polydispersity

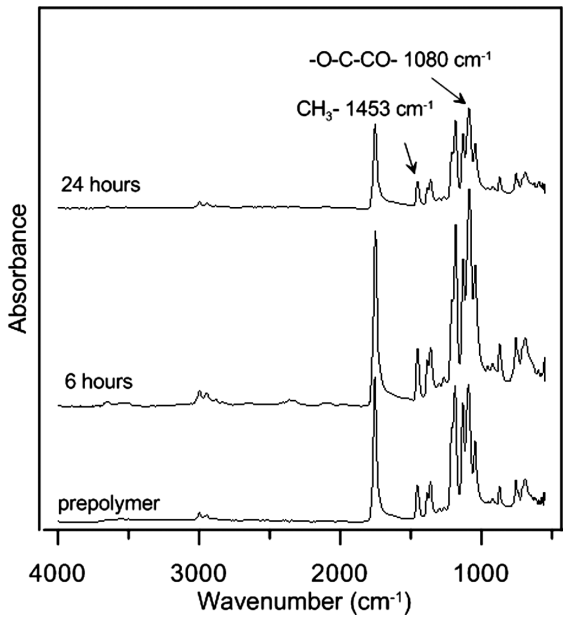


**Figure 3:** FTIR-ATR spectra of PLA prepolymer and products after 6 and 24 hours of postpolycondensation reaction (catalyzed by $Sn(Oct)_2$, 2 wt. %)

**Slika 3:** FTIR-ATR spekter PLA predpolimera in produktov po 6 in 24 urah postpolikondenzacijskih reakcij (katalizirano z 2 ut. % $Sn(Oct)_2$)

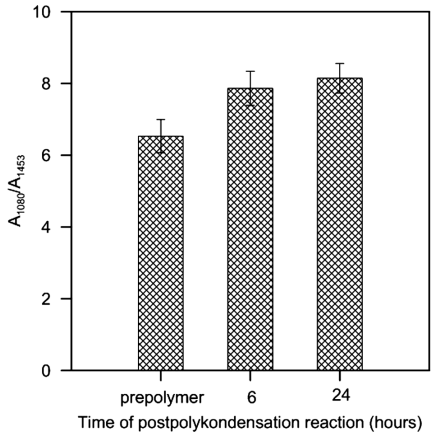


**Figure 4:** Normalized areas of the FTIR-ATR absorption peaks at 1080 $cm^{-1}$ of PLA prepolymer and products after 6 and 24 hours of postpolycondensation reaction (catalyzed by $Sn(Oct)_2$, 2 wt. %)

**Slika 4:** Normalizirana površina FTIR-ATR adsorpcijskih vrhov pri 1080 $cm^{-1}$ PLA predpolimera in produktov po 6 in 24 urah postpolikondenzacijskih reakcij (katalizirano z 2 ut. % $Sn(Oct)_2$)

The process of postpolycondensation of PLA was also investigated by FTIR-ATR analysis. **Figure 3** shows FTIR-ATR spectra of PLA precursor and the samples after 6 and 24 hours of postpolycondensation reaction in presence of 2 wt. % of the catalyst. A detailed description of PLA FTIR spectra can be found, for example, in our previous works.[11,12] From the observation of the postpolycondensation reaction point of view, it is interesting to focus on formation of new ester bonds, reduction of carboxylic and hydroxyl groups. Due to complexity of the PLA FTIR spectra, the most convenient could be the firstly mentioned ester bonds formation, which could be characterized by absorption at 1080 $cm^{-1}$.[20] Areas of this absorption peak, $A_{1080}$, were normalized on the peak area representing absorption of methyl groups at 1453 $cm^{-1}$ ($A_{1453}$). Dependence of $A_{1080}/A_{1453}$ versus time of the postpolycondensation reaction is depicted in **Figure 4**. It can be seen that concentration of ester bonds increases with rising time of the reaction. It is in agreement with the GPC results.

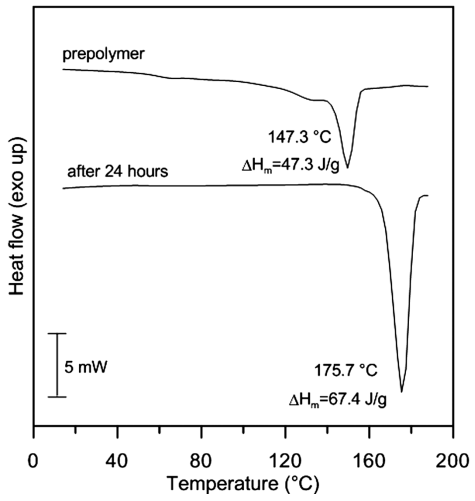


**Figure 5:** DSC curve (first heating scan) of PLA prepolymer and products after 24 hours of postpolycondensation reaction (catalyzed by $Sn(Oct)_2$, 2 wt. %)

**Slika 5:** DSC krivulja (prvo gretje) PLA predpolimera in produktov po 24 urah postpolikondenzacijskih reakcij (katalizirano z 2 ut. % $Sn(Oct)_2$)

The significant enhancement of $M_w$ described above affects properties of the resulting PLA including thermal behavior of the polymer. **Figure 5** shows DSC spectra (first heating scan) of the prepolymer and PLA postpolycondensation product obtained after 24 hours in presence of 2 wt. % of the catalyst. It can be noticed that increasing $M_w$ of the PLA samples (see **Table 1**) led to significant shift of the $T_m$ towards higher values (from 147.3 to 175.7 °C). Enthalpy of melting, $\Delta H_m$, was 47.3 and 67.4 J/g, respectively (**Figure 5**). It means that a content of crystalline phase in the treated samples increased noticeably (from 50.5 to 71.9 %, $\Delta H_{m0}$ = 93.7 J/g)[21] due to postpolycondensation reaction connected with rising of $M_w$. In addition, glass transition temperature, $T_g$, (taken from the second heating scan – not shown here) was also increased from 45.2 °C (PLA precursor) to 53.6 °C (after 24 hours of the reaction, 2 wt. % of the catalyst). These observations together with the GPC results reveal linear structure of the PLA macromolecules while the postpolycondensation process takes place at the end of the PLA precursor chains in the amorphous phase region[8].

## 4 CONCLUSIONS

This work was dedicated to investigation of the high molecular weight poly(lactic acid) (PLA) synthesis through multistep process including postpolycondensation reactions in solid state. Unlike other already published works in this field, presented work involves using of catalyst (stannous 2-ethylhexanoate) only in postpolycondensation step. The main attention was paid to determination of the catalyst concentration and time of the postpolycondensation reaction on the molecular weight of the resulting products by using gel permeation chromatography. It was correlated with the results from Fourier transform infrared spectroscopy and differential scanning calorimetry.

The results show that the role of the catalyst concentration is crucial to enhancement of molecular weight of the PLA during the solid state postpolycondensation process. While low concentration of the catalyst (up to 1 wt. %) do not provide sufficient results (enhancement up to 502 % after 24 hours), systems containing 2 wt. % of the catalyst showed noticeably higher molecular weight enhancement – 1655 % (from 5.5 to 91.0 kg/mol). Another important parameter is time of the postpolycondensation step. Obtained results reveal a possibility of an additional enhancement of PLA molecular weight for the postpolycondensation reaction times above 24 hours. However, finding of a time optimum must be further investigated.

## Acknowledgements

This research was financially supported by the Ministry of Education, Youth and Sports of the Czech Republic (project No. 2B08071 and ME09072) and Operational Program Research and Development for Innovations co-funded by the European Regional Development Fund (ERDF, project No. CZ.1.05/2.1.00/03.0111).

## 5 REFERENCES

[1] A. Gregorova, M. Hrabalova, R. Wimmer, J. Appl. Polym. Sci., 114 (**2010**) 5, 2616–2623

[2] V. Sedlarik, A. Vesel, P. Kucharczyk, P. Urbanek, Mater. Tehnol., 45 (**2011**) 3, 209–212

[3] I. Poljansek, M. Gricar, E. Zagar, M. Zigon, Macromolecular Symposia, 272 (**2008**), 75–80

[4] V. Sedlarik, N. Saha, J. Sedlarikova, P. Saha, Macromolecular Symposia, 272 (**2008**), 100–103

[5] M. Hrabalova, A. Gregorova, R. Wimmer, V. Sedlarik, M. Machovsky, N. Mundigler, J.Appl. Polym. Sci, 118 (**2010**) 3, 1534–1540

[6] S. Jacobsen, P. H. Degee, H. G. Fritz, P. H. Dubois, R. Jerome, Polym Eng Sci, 39 (**1999**), 1311–1319

[7] H. R. Kricheldorf, Chemosphere, 43 (**2001**), 49–54

[8] T. Maharana, B. Mohanty, Y. S. Negi, Prog. Polym. Sci., 34 (**2009**), 99–124

[9] R. Auras, B. Harte, S. Selke, Macromol. Biosci., 4 (**2004**), 835–864

[10] I. Poljansek, P. Kucharczyk, V. Sedlarik, V. Kasparkova, A. Salakova, J. Drbohlav, Mater. Tehnol., 45 (**2011**) 3, 261–264

[11] V. Sedlarik, P. Kucharczyk, V. Kasparkova, J. Drbohlav, A. Salakova, P. Saha, J. Appl. Polym. Sci., 116 (**2010**) 2, 1597–1602

[12] P. Kucharczyk, I. Poljansek, V. Sedlarik, V. Kasparkova, A. Salakova, J. Drbohlav, U. Cvelbar, P. Saha, J. Appl. Polym. Sci. DOI: 10.1002/app.34260

[13] K. M. D. Silvia, T. Tarverdi, R. Withnall, J. Silver, Plast. Rubber. Compos., 40 (**2011**) 1, 17–24

[14] J. R. Campanelli, D. G. Cooper, M. R. Kamal, J. Appl. Polym. Sci., 48 (**1993**), 443–451

[15] A. Vesel, M. Mozetic, A. Zalar, Vacuum, 82 (**2007**) 2, 248–251

[16] N. Krstulovic, I. Labazan, S. Milosevic, U. Cvelbar, A. Vesel, M. Mozetic, J. Phys. D: Appl. Phys., 39 (**2006**) 17, 3799–3804

[17] A. Vesel, Mater. Tehnol., 45 (**2011**) 2, 121–124

[18] W. X. Zhang, Y. Z. Wang, Chinese. J. Polym. Sci., 26 (**2008**) 4, 425–432

[19] H. Xu, M. Luo, M. Yu, C. Teng, S. Xie, J. Macromol. Sci. B, 45 (**2006**), 681–687

[20] F. Achmad, K. Yamade, S. Quan, T. Kokugan, Chem. Eng. J., 151 (**2009**), 342–350

[21] E. W. Fischer, H. J. Sterzer, G. Wegner, Colloid. Polym. Sci., 251, (**1973**), 980–990

UDK 533.9
Original scientific article/Izvirni znanstveni članek

ISSN 1580-2949
MTAEC9, 46(1)43(2012)

# PLASMA-ENHANCED CHEMICAL VAPOUR DEPOSITION OF OCTAFLUOROCYCLOBUTANE ONTO CARBONYL IRON PARTICLES

## PLAZEMSKO KEMIČNO NAPARJANJE OKTAFLUOROCIKLOBUTANA NA KARBONILNO ŽELEZO V PRAHU

**Michal Sedlacik[1,2], Vladimir Pavlinek[1,2], Marian Lehocky[1], Ita Junkar[3], Alenka Vesel[3]**

[1]Centre of Polymer Systems, University Institute, Tomas Bata University in Zlin, Nad Ovcirnou 3685, 760 01 Zlin, Czech Republic
[2]Polymer Centre, Faculty of Technology, Tomas Bata University in Zlin, namesti T. G. Masaryka 275, 762 72 Zlin, Czech Republic
[3]Department of Surface Engineering and Optoelectronics, Jozef Stefan Institute, Jamova 39, 1000 Ljubljana, Slovenia
lehocky@post.cz

*Prejem rokopisa – received: 2011-06-08; sprejem za objavo – accepted for publication: 2011-08-02*

Conformal films of fluoropolymer have been made onto carbonyl iron microparticles by plasma-enhanced chemical vapour deposition of octafluorocyclobutane in this study. RF plasma reactor with a frequency of 40 kHz and rotating barrel fixed between the two discharge electrodes arrangement was used to achieve a uniform surface modification of particles. The samples were treated for different times and various RF powers. Chemical changes in the surface composition after plasma modifications were, subsequently, determined using high-resolution X-ray photoelectron spectroscopy, while the surface texture was analyzed via scanning electron microscopy. The results revealed successful fluorination of carbonyl iron particles with a maximum of fluorine content of 2.9 %. The fluoropolymer film fabricated onto particles generally improves the corrosion protection and friction properties resulting in possible use of such magnetic particles in magnetorheological suspensions.

Keywords: carbonyl iron, functionalization, fluoropolymer, octafluorocyclobutane, modification, plasma, surface

Za namen tega dela je bila opravljeno plazemsko kemično naparevanje fluoropolimera na karbonilno železo v prahu. Enakomerno modifikacijo površine smo dosegli z uporabo RF plazemskega reaktorja s frekvenco 40kHz in z rotirajočim bobnom, ki je bil postavljen med razelektritveni elektrodi. Vzorci so bili obdelani pri različnih časih in pri različnih RF močeh. Spremembe kemijske sestave po obdelavi so bile določene z visokoločljivostno rentgensko fotoelektronsko spektroskopijo, morfološke spremembe površine pa smo določili iz slik vrstičnega elektronskega mikroskopa. Površina karbonilnega železovega prahu je bila uspešno flurinirana, saj smo na površini dosegli maksimalno 2.9 % fluora. Z nanosom fluoro polimernega filma na prašnate delce načeloma izboljšamo njihovo korozijsko odpornost in trenje ter jih naredimo primerne za uporabo v magnetnoreoloških suspenzijah.

Ključne besede: karbonilno železo, funkcionalizacija, fluoropolimer, oktafluorociklobutan, modifikacija, plazma, površina

## 1 INTRODUCTION

Magnetic particles have attracted increasing interest recently due to their novel applications. For example, magnetorheological (MR) fluids consisting of magnetic particles dispersed in carrier liquid can controllably change their rheological properties such as viscosity, yield stress and viscoelastic moduli according to the external magnetic field applied. These smart fluids can be used with benefit in applications utilizing adjustable control of the applied damping/force.[1] The corrosion, oxidation, and abrasive properties of iron and iron alloys frequently used as optimal magnetic agents in MR fluids are, however, obstacles for their wider commercial usage. To overcome this problem, modification of particle surface chemical composition has proven to be efficient.[2]

Recently, there is growing interest in using low-temperature plasma to modify the surface of various materials.[3–7] This interest has developed for two reasons. First, plasma can produce a unique surface structure and modification, and, second, the extent of modification can be easily controlled by treatment conditions.[7–14] Moreover, plasma treatment method is a non-polluting technique, which is not negligible for industrial fabrication, and only short reaction times are required.[15,16] Although there are several methods employed for film deposition onto iron, including sputtering, arc-plasma spray deposition, or various wet chemistry methods such as sol-gel deposition, the formed films are not uniform many times. Instead of the plasma reacting with and etching the substrate surface, plasma-enhanced chemical vapour deposition employs the conversion of gaseous monomer into reactive radicals, ions and neutral molecules and subsequent deposition of these precursors onto the substrate surface. Films formed in this way afterwards exhibit strong adhesion, low pinhole density and high surface uniformity.[17] Choice of proper plasma reactor type is another important factor for obtaining of conformal deposited film. Hence, fluidized bed or rotary plasma reactors with constant particles recirculation resulting in optimal fluid-solid contact and increased

heat transfer coefficient have to be used for three-dimensional materials such as powders.

As mentioned above, the corrosion and oxidation protection as well as friction properties have to be improved in order to use iron and its alloys in MR applications. For these purposes fluorocarbon plasma seems to be an efficient tool to improve the substrate hydrophobicity and frictional properties, since the produced Teflon-like surface film possess chemical inertness, low surface energy (non-wettable), excellent frictional properties, lower permeability, and relatively good thermal stability.[18–20] In addition, the relative amount of functional groups can be profitably controlled upon parameters adjustment during fluorocarbon plasma treatment.

The objective of this work is plasma-enhanced chemical vapour deposition of octafluorocyclobutane (OFCB) onto carbonyl iron (CI) particles using rotary plasma reactor. Effects on surface functionalization after variation of RF power and plasma treatment time were investigated by XPS, while surface morphology was determined from SEM images.

## 2 EXPERIMENTAL

### *2.1 Plasma modification*

The main material characteristics of CI particles (SL grade, BASF, Germany) are following: spherical shape of particles, non-modified surface, and content of $\alpha$–iron in a bulk > 99.5 %. Plasma treatment of CI particles was carried out with Diener Femto (Diener Electronic, USA) plasma reactor. The reactor, designed for powder treatment, is equipped with a 250 ml flask which is kept rotating during the treatment for a uniform modification, as schematically shown in **Figure 1**. The plasma is created inside the discharge chamber with an inductively coupled RF generator, operating at a frequency of 40 kHz. A controlled flow of OFCB gas (purity ≥ 99.998, Linde AG, Germany) diluted with argon gas (purity ≥ 99.998, Messer Industriegase GmbH, Germany) in the ratio of 1:1 was introduced inside the chamber. The resulting gas flow rate was 45 ccm and operating pressure of approx. 30 – 40 Pa. Treatment time (60 – 600 s) and RF power (33 – 100 W) were used as experimental variables. All samples were kept under the atmosphere of processing gas for next 2 minutes after the plasma was quenched.

### *2.2 Scanning electron microscopy*

Visual observation of fabricated films was carried out using a scanning electron microscopy (SEM, VEGA II LMU, Tescan Ltd., Czech Republic) operated at 30 kV with 30 kx magnification. Samples were coated with a thin layer of gold using a polaron sputtering apparatus before the observation.

### *2.3 XPS characterization*

In order to determine the surface chemical changes after the plasma treatments, XPS measurements (X-ray photoelectron spectroscopy, TFA XPS, Physical Electronics, USA) were used. To avoid dispersion of the sample during the pumping, investigated particles were compressed with a laboratory press at 250 kN to obtain the test pellets. The base pressure in the chamber was about $6 \times 10^{-8}$ Pa. The samples were excited with X-rays over a 400–μm spot area with a monochromatic Al $K_{\alpha 1,2}$ radiation at 1486.6 eV. Survey spectra were performed at two different spots on the surface of CI particles (pellet). Photoelectrons were detected by hemispherical analyzer positioned at the angle of 45° with respect to the sample surface. Survey-scan spectra were made at pass energy of 187.85 eV and an energy step was 0.4 eV. The concentration of individual elements was determined using MultiPak v7.3.1 software from Physical Electronics, which was supplied with the spectrometer.

## 3 RESULTS

A thin film suggesting a possible formation of fluoropolymer onto CI particles can be observed in **Figure 2**. Clearly from SEM images, OFCB plasma treatment does not change markedly surface morphology or roughness of modified samples. This is in good correlation with previously polymerized fluoropolymer

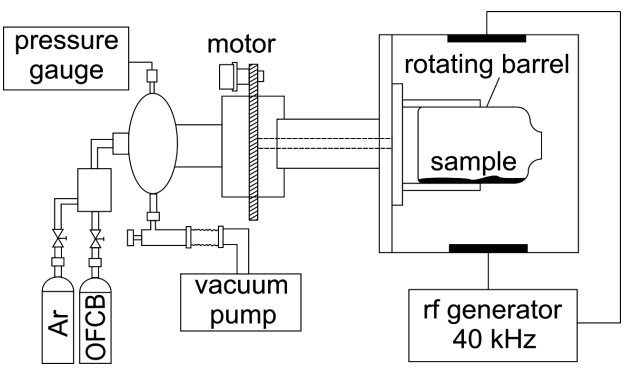


**Figure 1:** Rotary plasma reactor used for the treatment of CI particles
**Slika 1:** Rotirajoči plazemski reaktor za obdelavo CI prašnatih delcev

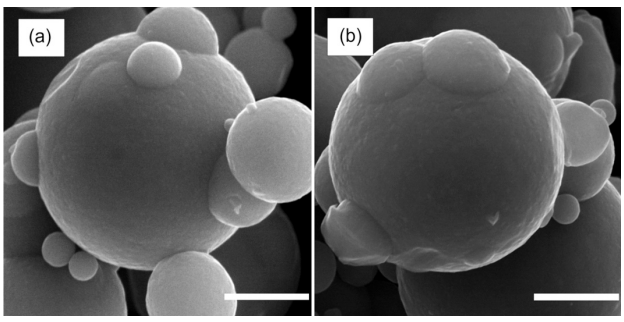


**Figure 2:** SEM images of mere CI particles (a) and plasma-treated (600 s, 100 W) CI particles (b); bar length 2 μm
**Slika 2:** SEM slika neobdelanih prašnatih delcev (a) in plazemsko obdelanih (600 s, 100 W) CI prašnatih delcev (b); dolžina merila 2 μm

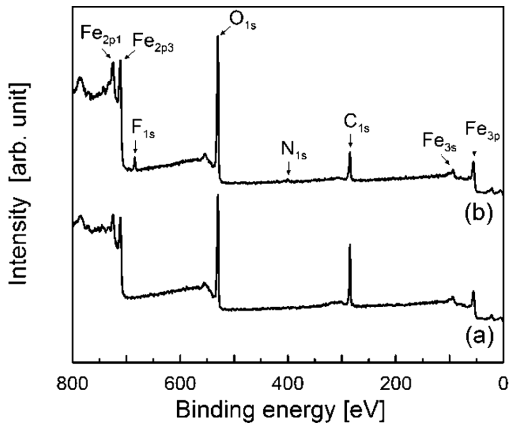


**Figure 3:** XPS survey spectra recorded on mere CI particles (a) and on plasma-treated (600 s, 100 W) CI particles (b)
**Slika 3:** Pregledni XPS-spekter neobdelanih CI prašnatih delcev (a) in plazemsko obdelanih (600 s, 100 W) CI prašnatih delcev (b)

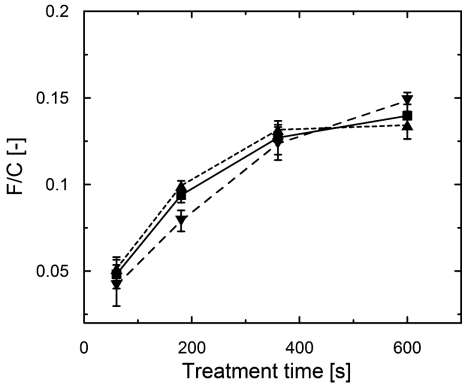


**Figure 4:** Dependence of the F/C atomic ratio versus the treatment time under an applied RF power of 33 W (■), 66 W (▼), and 100 W (▲)
**Slika 4:** Odvisnost atomskega deleža F/C glede na čas obdelave pri RF moči 33 W (■), 66 W (▼), in 100 W (▲)

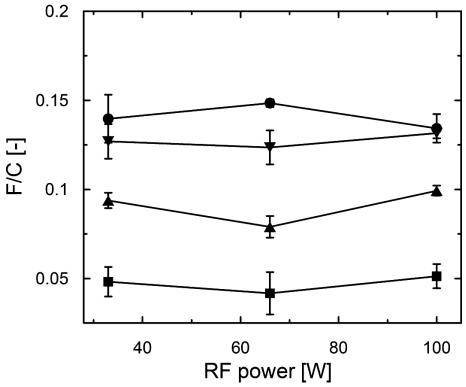


**Figure 5:** Dependence of the F/C atomic ratio versus the plasma power under 60 s (■), 180 s (▲), 360 s (▼), and 600 s (●) treatment time
**Slika 5:** Odvisnost atomskega deleža F/C glede na RF moč pri času obdelave 60 s (■), 180 s (▲), 360 s (▼) in 600 s (●)

films on various substrates in which extremely smooth interfaces and structures that were uniform through the thickness of the film have been demonstrated.[21]

**Figure 3** shows the XPS survey spectra of the CI particles recorded before and after the plasma treatment. The peaks attributed to $C_{1s}$, $O_{1s}$, and Fe orbitals are observed in both spectra. Nevertheless, two new peaks are observed in the XPS spectrum recorded after OFCB plasma treatment. A peak near 684.3 eV suggests the formation of covalent C–F bond and hence, effective grafting of fluorine on the CI surface while a weak peak near 400.7 eV attributed to nitrogenated species is probably due to the post-plasmatic reaction ongoing in the air.

The surface composition of untreated and treated particles is listed in **Table 1**. It is worth noting that standard deviation of atomic concentration of elements was below 10 % in all cases.

As can be seen in **Figure 4**, the efficiency of fluorine bonding is affected by treatment time. The F/C atomic ratio on the CI surface firstly increased with treatment time for all RF powers used and then reached more less equilibrium value.

Furthermore, the effect of the plasma power on the fluoropolymer formation was examined. The treatment power was varied from 33 W to 100 W under the same pressure. The obtained F/C atomic ratio dependence on RF power in various treatment times is shown in **Figure 5**. The F/C atomic ratio is almost independent on the RF power used for treatment times until 360 s. However, the highest fluorine bonding efficiency for 600 s treatment time is reached at 66 W plasma power.

## 4 DISCUSSION

From the XPS results shown in **Table 1**, it is obvious that certain amount of fluorine covalently-bonded to the CI particles surface is present after the OFCB plasma-

**Table 1:** Surface composition of CI particles at different treatment times and RF powers
**Tabela 1:** Kemijska sestava površine CI prašnatih delcev, obdelanih pri različnih časih in RF moči

| Power [W] | 0 | 33 | | | | 66 | | | | 100 | | | |
|---|---|---|---|---|---|---|---|---|---|---|---|---|---|
| Time [s] | 0 | 60 | 180 | 360 | 600 | 60 | 180 | 360 | 600 | 60 | 180 | 360 | 600 |
| C [%] | 42.3 | 26.1 | 15.2 | 22.7 | 17.4 | 15.1 | 20.2 | 17.9 | 15.2 | 19.8 | 15.1 | 15.9 | 21.9 |
| O [%] | 39.5 | 49.1 | 47.3 | 47.0 | 43.9 | 44.1 | 49.2 | 49.9 | 42.6 | 49.3 | 41.5 | 44.4 | 48.4 |
| N [%] | 0 | 1.3 | 0.7 | 1.6 | 1.6 | 0.7 | 0.5 | 1.3 | 1.5 | 0.9 | 0.7 | 0.5 | 1.2 |
| F [%] | 0 | 1.3 | 1.4 | 2.9 | 2.4 | 0.6 | 1.6 | 2.2 | 2.5 | 1.0 | 1.5 | 2.1 | 2.9 |
| Fe [%] | 18.2 | 22.2 | 35.5 | 25.1 | 34.7 | 39.5 | 28.5 | 28.8 | 38.2 | 29.0 | 41.3 | 37.0 | 26.6 |

enhanced chemical vapour deposition in a rotary plasma reactor. Fluorine atomic concentration on the surface of CI particles grows with the treatment time. However, the increase in fluorine content is getting slower at higher treatment times probably due to the saturation of surface reactive sites. The atomic concentration of bonded fluorine does not increase significantly with RF power used as could be expected. This is supposedly caused by the degradation of formed surface layer which takes place under severe conditions of plasma treatment. In other words, the etching phenomenon will occur and remove the surface atoms along with the functionalized groups at higher plasma powers. Above mentioned statements, which are furthermore in good correlations with dependencies shown in **Figure 4** and **Figure 5**, suggest that the parameters of OFCB plasma for optimal fluoropolymer film formation onto CI particles are lower power (33 or 66 W) and higher treatment time (360 or 600 s).

## 5 CONCLUSIONS

A successful plasma-enhanced chemical vapour deposition of OFCB as precursor and argon mixture was used to deposit ultrathin fluoropolymer films onto CI particles in a rotary plasma reactor. The fluorine atomic concentrations on the plasma treated CI particles surface increased with increasing treatment time until approximately 400 s while remained almost constant afterwards. The concentration of fluorine did not significantly increase with higher RF power and thus, lower plasma powers are preferred from economical point of view. Since plasma treatment is a non-polluting method with shorter treatment time compared with chemical modifications, this study provides a new way for the Teflon-like surface modification of CI particles to improve their corrosion, oxidation, and abrasive properties for MR applications.

### Acknowledgements

The authors wish to thank to the Ministry of Education, Youth and Sports of the Czech Republic (MSM7088352101) and the Czech Science Foundation (project 104/09/H080) for financial support.

This article was written with support of Operational Programme Research and Development for Innovations co-funded by the European Regional Development Fund (ERDF) and national budget of the Czech Republic, within the framework of the project Centre of Polymer Systems (reg. number: CZ.1.05/2.1.00/03.0111).

## 6 REFERENCES

[1] B. J. Park, F. F. Fang, H. J. Choi, Soft Matter, 6 (**2010**) 21, 5246
[2] M. A. Abshinova, N. E. Kazantseva, P. Saha, I. Sapurina, J. Kovarova, J. Stejskal, Polym. Degrad. Stabil., 93 (**2008**) 10, 1826
[3] M. Gorjanc, V. Bukovšek, M. Gorenšek, M. Mozetič, Tex. Res. J., 80 (**2010**) 20, 2204
[4] M. Lehocky, L. Lapcik, R. Dlabaja, L. Rachunek, J. Stoch, Czech. J. Phys., 54 (**2004**), C533
[5] U. Cvelbar, K. Ostrikov, M. Mozetič, Nanotechnology, 19 (**2008**) 40, 405605
[6] M. Mozetič, Vacuum, 71 (**2003**) 1–2, 237
[7] M. Lehocky, A. Mracek, Czech. J. Phys., 56 (**2006**), B1277
[8] M. Lehocky, P. F. F. Amaral, P. Stahel, M. A. Z. Coelho, A. M. Barros-Timmons, J. A. P. Coutinho, Surf. Eng., 24 (**2008**) 1, 23
[9] M. Mozetič, J. Phys. D-Appl. Phys., 44 (**2011**) 17, 174028
[10] T. Vrlinič, A. Vesel, U. Cvelbar, M. Krajnc, M. Mozetič, Surf. Interface Anal., 39 (**2007**) 6, 476
[11] M. Lehocky, P. F. F. Amaral, P. Stahel, M. A. Z. Coelho, A. M. Barros-Timmons, J. A. P. Coutinho, J. Chem. Technol. Biotechnol., 82 (**2007**) 4, 360
[12] M. Lehocky, P. F. F. Amaral, M. A. Z. Coelho, P. Stahel, A. M. Barros-Timmons, J. A. P. Coutinho, Czech. J. Phys., 56 (**2006**), B1256
[13] A. Doliška, A. Vesel, M. Kolar, K. Stana-Kleinschek, M. Mozetič, Surf. Interface Anal., Surf. Interface Anal., 44 (**2012**) 1, 56–61
[14] A. Vesel, M. Mozetič, S. Strnad, K. Stana-Kleinschek, N. Hauptman, Z. Peršin, Vacuum, 84 (**2010**) 1, 79
[15] M. Sowe, I. Novak, A. Vesel, I. Junkar, M. Lehocky, P. Saha, I. Chodak, Int. J. Polym. Anal. Charact., 14 (**2009**) 7, 641
[16] M. Lehocky, P. Stahel, M. Koutny, J. Cech, J. Institoris, A. Mracek, J. Mater. Process. Technol., 209 (**2009**) 6, 2871
[17] M. Wasilik, N. Chen: Deep reactive ion etch conditioning recipe, Proc. of the society of photo-optical instrumentation engineers (SPIE), San Jose, **2004**, 103–110
[18] S. H. Park, S. D. Kim, Korean J. Chem. Eng., 16 (**1999**) 6, 731
[19] D. Cheneler, J. Bowen, S. D. Evans, M. Gorzny, M. J. Adams, M. C. L. Ward, Polym. Degrad. Stabil., 96 (**2011**) 4, 561
[20] A. Vesel, M. Mozetič, A. Zalar, Surf. Interface Anal., 40 (**2008**) 3/4, 661
[21] H. Kim, M. D. Foster, H. Jiang, S. Tullis, T. J. Bunning, C. F. Majkrzak, Polymer, 45 (**2004**) 10, 3175

UDK 678.7
Original scientific article/Izvirni znanstveni članek

ISSN 1580-2949
MTAEC9, 46(1)47(2012)

# APPLICATION OF X-RAY PHOTOELECTRON SPECTROSCOPY FOR CHARACTERIZATION OF PET BIOPOLYMER

# UPORABA RENTGENSKE FOTOELEKTRONSKE SPEKTROSKOPIJE ZA KARAKTERIZACIJO PET BIOPOLIMERA

**Miran Mozetič**

Center of Excellence for Polymer Materials and Technologies, Tehnološki park 24, 1000 Ljubljana, Slovenia.
miran.mozetic@guest.arnes.si

*Prejem rokopisa – received: 2011-06-12; sprejem za objavo – accepted for publication: 2011-07-20*

X-ray photoelectron spectroscopy (XPS) is probably the most popular method for characterization of polymer surfaces. Although this technique is widely used, small details are often very important for proper evaluation of experimental results. Some details are addressed in this paper. First, the influence of surface roughness is examined and the results show substantial differences in high-resolution C1s spectra although the survey spectra remain fairly unaffected by the roughness. Second, the influence of the X-ray brilliance is studied for classical sources such as Mg $K_\alpha$ at 1253 eV, Al $K_\alpha$ at 1486 eV and Al $K_\alpha$ monochromized light. No substantial difference between the classical Mg and Al sources were found, while the high resolution spectra obtained using monochromatized light have a much better resolution. These details are very important in practical applications. Some examples including vascular grafts are shown in this paper.

Keywords: polymer, PET, surface characterization, XPS, roughness, vascular graft

Rentgenska fotoelektronska spektroskopija je bržkone najširše uporabljena metoda za karakterizacijo površin polimerov. Kljub široki uporabi pa se pogosto pripeti, da postanejo podrobnosti izredno pomembne za pravilno interpretacijo rezultatov. Nekatere tovrstne podrobnosti so obravnavane v tem prispevku. Pregledni spektri niso posebej občutljivi na hrapavost vzorcev, kar pa ne velja za visoko ločljive C1s spektre. Slednji so drugačni za gladko polimerno folijo, hrapavo folijo in umetno žilo, izdelano iz identično enakega materiala. Poleg hrapavosti lahko na videz C1s spektra vpliva tudi brilijantnost uporabljene svetlobe. V tem prispevku so bili uporabljeni trije različni izviri rentgenske svetlobe in sicer Mg $K_\alpha$ pri 1253 eV, Al $K_\alpha$ pri 1486 eV in monokromatizirana Al $K_\alpha$, pri čemer je bil za monokromatizacijo uporabljen silicijev kristal. Meritve so pokazale bistveno boljšo resolucijo visoko ločljivega C1s spektra z uporabo monokromatizirane svetlobe. Rezultati preiskav imajo neposredno praktično uporabnost, saj jasno nakazujejo omejitve Rentgenske fotoelektronske spektroskopije za karakterizacijo površin realnih vzorcev, ki so značilno hrapavi in površinsko funkcionalizirani, posebej še umetnih žil izdelanih iz polietilentereftalata.

Ključne besede: polimer, PET, karakterizacija površin, XPS, hrapavost, umetne žile

## 1 INTRODUCTION

Polymer materials are nowadays widely used in different branches of industry as well as in biology, pharmacy and medicine.[1–7] Examples of applications in biomedicine include a variety of containers for drugs as well as biological samples, simple instruments such as catheters, and very sophisticated body implants such as artificial blood vessels.[4,7] Polymer materials often express fairly good biocompatibility. In many cases, however, the biological response to polymer materials is not adequate. In such cases the surface properties of polymers should be modified. Modification stands for changing the surface morphology, composition and structure.[8–12] The surface properties depend on many parameters but the most important one is the presence of different surface functional groups. Polymers that are nowadays used for biomedical applications have fairly optimized surface properties – some of them are highly hydrophobic, some moderately hydrophilic, while the majority are in between these two limits. As mentioned earlier, such surface properties may be adequate for some applications, but in many other cases, more extreme surface properties are required. In such cases, the surface of biopolymers should be modified. A variety of methods for modification of the biopolymer surface properties have appeared including wet chemical treatments,[13] ion bombardment, exposure to intensive ultraviolet light sources, and application of gaseous discharges.[14–17] The latter seems to be predominant in the last decade. A reason for this is probably the fact that gaseous discharges combine effects that are achieved by other three groups of techniques mentioned above. Depending on specific requirements one can always choose a right discharge to create gaseous plasma with required characteristics. Most gases transformed to the state of plasma emit radiation in a wide range from infrared to ultraviolet, and some gases also emit in vacuum ultraviolet range.[18–20] On the other hand, the formation of specific functional groups on the surface of polymer materials during plasma treatment depends largely on the type of gas used to create plasma. In general, hydrophobization of polymer materials is achieved by application of fluorine rich gases with minimal admixture of oxidative gases.[21–25] On the other hand, hydrophilization is achieved using gases that form

highly polar functional groups on the surface of polymers.[26–34] Although air, nitrogen and sulphur oxide plasma can be used, best results are usually achieved using pure oxygen or a mixture of oxygen and a noble gas.[8] The newly formed functional groups depend also on the flux of plasma radicals onto the sample surface so it pays to measure basic plasma parameters,[35] especially density of neutral atoms formed from parent molecules by electron impact dissociation.[36–38]

Application of gaseous plasma for functionalization of polymers usually leads to improvement of the surface properties, but extreme results are always obtained only in the case of increased roughness of the material. The so called lotus effect which is well known from nature is actually a very good combination of surface hydrophobicity and microstructured surface.[39] This combination leads to extremely high contact angle of a water drop and thus to the so called self-cleaning effect.[40] Something similar holds for superhydrophilicity: it is a combined effect of a high surface energy and micro- or nanostructured texture that allows for the capillary effect. Such extreme conditions of the surface properties have found some important applications in biomedicine. Obviously, the nano- or microstructured polymer materials are of great importance in advanced biomedicine. Unfortunately, however, experimental techniques for surface characterization have been developed for characterization of perfectly flat materials. The most powerful methods for surface characterization of functionalized organic materials are X-ray photoelectron spectroscopy (XPS) and secondary ion mass spectroscopy (SIMS).[41–43] Application of such techniques to rough polymers represents a task that is not at all trivial. In this paper some practical considerations about characterization of such real materials by X-ray photoelectron spectroscopy (XPS) are addressed.

## 2 EXPERIMENTAL

Experiments were performed with a biopolymer that is often used for medical applications – polyethylenetheraphtalate (PET). The material is used for instance for body fluid containers, some types of catheters and some types of vascular grafts (artificial blood vessels). Three types of PET materials were used at our experiments: (*i*) a flat foil, (*ii*) a rough foil and (*iii*) a real vascular graft. The flat foil was purchased from Goodfellow. It was semi-crystalline PET foil with a thickness of 0.25 mm. A piece of the foil was treated with sand paper (grid 320) in order to increase the surface roughness. Both treated and untreated foils were cleaned in ultrasound bath with pure alcohol in order to remove any surface impurities.

X-ray photoelectron spectroscopy characterization was performed with our XPS device TFA XPS Physical Electronics. We used three different sources of X-rays: (i) Mg $K_\alpha$, (ii) Al $K_\alpha$, and (iii) Al $K_\alpha$, monochromatized. The first source gives fairly monochromatized light at the photon energy of 1253 eV. The FWHM is supposed to be 0.7 eV. The second source peaks at the photon energy of 1486 eV and has the FWHM of 0.85 eV. The second source was also used with a further monochromatization which was realized with a silicon crystal. The monochromatization allows for a better FWHM of 0.25 eV, but the monochromator itself represents a loss for X-rays.

The photoelectrons were detected with a hemispherical analyzer positioned at an angle of 45° with respect to the normal to the sample surface. Survey-scan spectra were obtained at a pass energy of 187.85 eV and 0.4 eV energy step. High-resolution spectra of C1s were made at a pass energy of 23.5 eV and 0.1 eV energy step. An additional electron gun was used for surface charge neutralization since the samples are insulators. The concentration of elements was determined by using MultiPak v7.3.1 software from Physical Electronics, which was supplied with the spectrometer.

## 3 RESULTS

All three types of PET samples were mounted in the XPS instrument just after the ultrasound cleaning. Survey spectra were taken with Al monochromatized light which we use as a default source of X-rays for polymer characterization. A typical survey spectrum is shown in **Figure 1**. As expected, only peaks corresponding to carbon and oxygen are found in the survey spectrum. Such spectra were found on all three samples and differences between different samples and between different spots on particular samples were hardly detected. The deviation in elemental composition as calculated from the survey spectrum shown in **Figure 1** was only about 1 at.%. It is important that the ratio between carbon and oxygen is very close to the theoretical value for PET material which is 71.4 at.% of carbon and 28.6 at.% of oxygen.

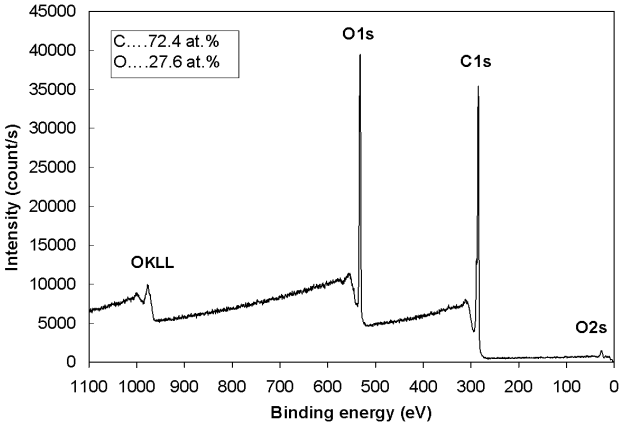


**Figure 1:** A typical XPS survey spectrum of a rough PET foil obtained by excitation with monochromatized X-rays

**Slika 1:** Značilni pregledni XPS-spekter hrapave PET folije, posnet z monokromatizirano rentgensko svetlobo

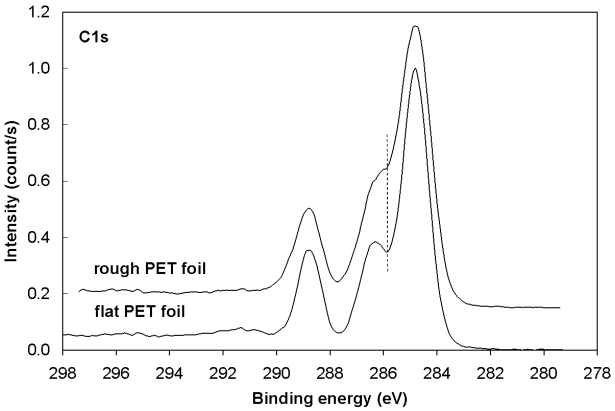


**Figure 2:** High resolution XPS spectra obtained for a flat PET foil (lower curve) and a rough foil (upper curve). Monochromatized X-rays were used for sample excitation.

**Slika 2:** Visokoločljivi XPS-spekter gladke folije PET (spodnja krivulja) in hrapave folije (zgornja krivulja), posnet z monokromatizirano rentgensko svetlobo.

Comparison between high-resolution C1s spectra obtained at a flat and a rough polymer foil is shown in **Figure 2**. It is clearly visible that a knee observed on the rough material at the binding energy of about 286 eV transforms to a well defined peak when the experiment is performed with a flat foil. Furthermore, the shape of the high-resolution C1s peak for the rough sample depends on the particular spot, while for flat samples we always obtain a spectrum as shown in **Figure 2**. In order to demonstrate the site dependence of the C1s spectrum for a rough surface, we performed characterization at different spots and selected results that differ extraordinary. Such a selection is shown in **Figure 3**. It is clearly visible that the knee which is at about 286 eV appears at different intensities. All spectra shown in **Figure 2 and 3** were taken with a monochromatized Al source.

In order to check the influence of the X-ray source on the quality of high-resolution C1s peaks we performed characterization of the same material with all three different sources. Typical results are presented in **Figure 4**.

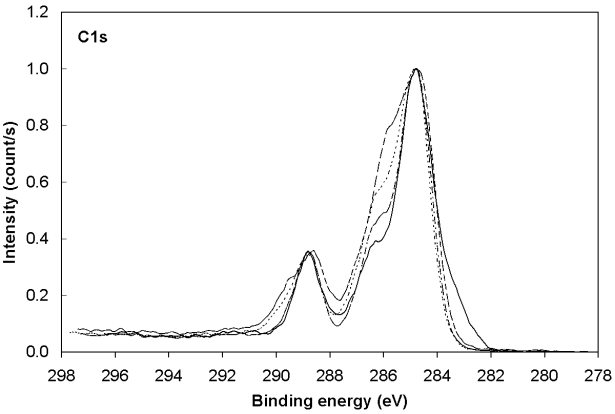


**Figure 3:** High resolution XPS spectra obtained at four different spots on the surface of a rough PET foil. Monochromatized X-rays were used for sample excitation.

**Slika 3:** Visokoločljivi XPS-spektri, posneti na štirih različnih področjih na površini hrapave folije PET. Za vzbujanje smo uporabili monokromatizirano rentgensko svetlobo.

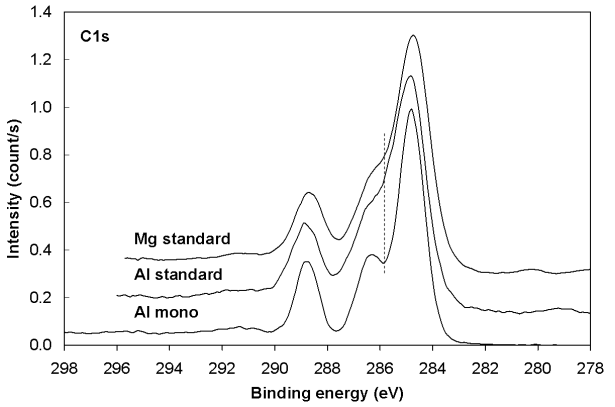


**Figure 4:** High resolution XPS spectra of a flat PET foil obtained using three different X-ray sources: monochromatized (lowest curve), standard Mg (middle) and standard Al (upper)

**Slika 4:** Visokoločljivi XPS-spektri, posneti na površini gladke folije PET s tremi različnimi rentgenskimi izvori: monokromatiziranim (spodnja krivulja), standardnim Mg (srednja krivulja) in standardnim Al izvorom (zgornja krivulja)

Finally, an experiment has been performed also using a real vascular graft. A comparison between a typical spectrum measured on a flat Al foil and a vascular graft is shown in **Figure 5**. In this case, as in most others, we used X-rays from a monochromatized source for sample excitation.

## 4 DISCUSSION

The high-resolution C1s spectra presented in **Figures 2-5** were all taken on exactly the same material (PET polymer) but one can observe rather big differences. Let as first address the influence of the surface roughness. The results obtained with a monochromatized light are shown in **Figures 2 and 3**. All spectra were normalized according to the height of the major peak which

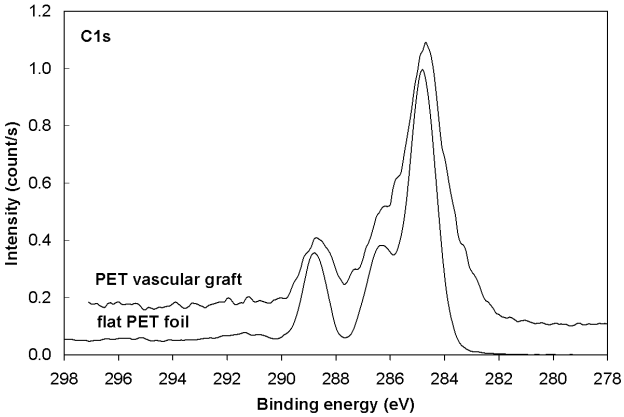


**Figure 5:** High resolution XPS spectra for a flat PET foil and a vascular graft made from PET polymer

**Slika 5:** Visokoločljivi XPS-spektri, posneti na površini gladke folije PET in na površini umetne žile iz polimera PET

corresponds to chemical bonds between carbon atoms or between carbon and hydrogen atoms. An important difference between a flat foil and the rough foil is observed in **Figure 2**. The most striking effect is the peak at the energy of about 286 eV which is fairly well seen from the spectrum obtained at the flat foil, while it transforms to a knee for the rough foil. More than obvious, the de-convolution of the spectrum obtained for the flat foils is a much simpler task than for the rough foil. Furthermore, the width of the major peak is larger for the case of the rough foil than for the flat foil. Finally, the minimum observed at the binding energy of about 287.5 eV is much better expressed for the flat foil. All these details are very important in proper explanation of the XPS results. Namely, many functional groups appear as peaks or just knees on the curve between 282 and 290 eV.[8,41] The left-most peak in **Figure 2** corresponds to the ester group. The middle peak (represented by a knee for the rough foil) corresponds to the ether group. In between there could be a carbonyl group. The height of the minimum between the left-most and the middle peak can be merrily due to a poor resolution of the spectrometer, but it can be also due to the presence of a functional group. Since our material is chemically very pure, we can exclude the presence of a functional group, so the behaviour of the curve for the rough foil is due to worsened resolution induced by surface roughness rather than presence of a carbonyl group.

The roughness effect on the high resolution XPS C1s spectrum is even much more pronounced in **Figure 3**. As mentioned earlier this Figure represents four measurements obtained at different spots on the surface of the same sample. De-convolution of the spectra presented in **Figure 3** is rather arbitrary. The middle peak could be attributed to different concentrations of ether group on the surface of the material. Such interpretation is definitely wrong since all spectra were taken for the same material which has been well cleaned prior to the XPS analyses. Similar considerations also apply for the left-most peak which corresponds to the ester group. Broadening of this peak is merely due to roughness and not appearance of new functional groups.

Spectra shown in **Figure 3** were all taken using monochromatized light. The effect of un-chromatized light is not shown in this paper for rough materials because even characterization by the rather brilliant light causes many artefacts. The effect of different light brilliance is therefore shown only for flat materials. **Figure 4** represents high-resolution C1s spectra obtained using all three different sources. The spectra are normalized to the height of the major peak. One can clearly observe that the effect of poor monochromatization of X-rays is similar to the effect of rough material. In both cases we can observe only a knee on the curve at the energy of about 286 eV. Also, the height of the well between the left most and the middle peak is increased in the similar way as in the case of the rough material characterized by monochromatized light. Namely, comparison of **Figures 3 and 4** show very little difference in the behaviour of the well.

The effect of surface roughness is even more pronounced for the case of vascular graft. The comparison between a spectrum obtained on the flat foil and a spectrum obtained on a vascular graft is presented in **Figure 5**. Here, the dominant peak becomes very broad due to extremely rough surface of knitted artificial blood vessel. It is even difficult to distinguish the knee corresponding to the ether group, although it is definitely present in the material. Also, the shape of the well between the left-most and the middle peak is difficult to interpret. Since we know well that material is pure PET, we can conclude that the peculiar shape is an artefact of the extremely high surface roughness. A person not knowing the exact chemical composition could have easily attributed the shape of the well to an existence of another functional group.

## 5 CONCLUSIONS

Experimental observations presented in this paper clearly indicate the importance of monochromatized light for characterization of PET biopolymer. While the survey spectrum is practically not influenced by the brilliance of the X-rays, the high resolution peaks are. Poor X-ray brilliance causes broadening of the spectral features and a loss of details that might be crucial for proper reading of high resolution spectra. The effect is particularly important for polymers where peak shifting due to different chemical bonding is relatively weak. The silicon-crystal monocromator obviously performs well although the FWHM is improved only by a factor of 2 as compared to an un-chromatized magnesium source. An even stronger broadening of peaks is observed for rough surfaces. High resolution C1s spectra measured for rough PET foil vary considerably from spot to spot so it pays to perform experiments on several spots and average them for better accuracy. Application of non-chromatized light for characterization of rough polymers is strongly discouraged – the distortion of spectra is often so strong that any result drawn from spectra de-convolution is questionable.

### Acknowledgement

The author acknowledges the financial support from the Ministry of Higher Education, Science and Technology of the Republic of Slovenia through the contract No. 3211-10-000057 (Center of Excellence Polymer Materials and Technologies).

## 6 REFERENCES

[1] A. Drenik, M. Mozetic, A. Vesel, U. Cvelbar, Journal of Physics: Conference Series, 207 (**2010**), 012009

[2] A. Asadinezhad, I. Novak, M. Lehocky, V. Sedlarik, A. Vesel, I. Junkar, P. Saha, I. Chodak, Plasma Processes Polym., 7 (**2010**) 6, 504–514
[3] A. Asadinezhad, I. Novak, M. Lehocky, V. Sedlarik, A. Vesel, P. Saha, I. Chodak. Colloids Surf. B Biointerfaces, 77 (**2010**) 2, 246–256
[4] B. Kasemo, Surf. Sci. 500 (**2002**), 656–677
[5] A. Vesel, M.Mozetic, S. Strnad, Vacuum, 85 (**2011**) 12, 1083–1086
[6] A. Asadinezhad, I. Novak, M. Lehocky, F. Bilek, A. Vesel, I. Junkar, P. Saha, A. Popelka, Molecules, 15 (**2010**) 2, 1007–1027
[7] D. Klee, H. Höcker, Adv. Polym. Sci. 149 (**2000**), 1–57
[8] A. Vesel, I. Junkar, U. Cvelbar, J. Kovac, M. Mozetic, Surf. Interface Anal., 40 (**2008**) 11, 1444–1453
[9] T. Belmonte, C. D. Pintassilgo, T. Czerwiec, G. Henrion, V. Hody, J. M. Thiebaut, J. Loureiro, Surf. Coat. Technol., 200 (**2005**) 1–4, 26–30
[10] T. Belmonte, T. Czerwiec, H. Michel, Surf. Coat. Technol. 142 (**2001**), 306–313
[11] N. Vourdas, D. Kontziampasis, G. Kokkoris, V. Constantoudis, A. Goodyear, A. Tserepi, M. Cooke, E. Gogolides, Nanotehnology, 21 (**2010**), 08530
[12] I. Junkar, U. Cvelbar, A. Vesel, N. Hauptman, M. Mozetic, Plasma Processes Polym., 6 (**2009**) 10, 667–675
[13] H. Fasl, J. Stana, D. Stropnik, S. Strnad, K. Stana-Kleinschek, V. Ribitsch, Macromolecules 11 (**2010**) 2, 377–381
[14] A. Doliska, A. Vesel, M. Kolar, K. Stana-Kleinschek, M. Mozetic, Surf. Interface Anal., 44 (**2012**) 1, 56–61
[15] M. Lehocky, A. Mracek, Czechoslovak J. Phys., 56 (**2006**) 7, B1277–B1282
[16] A. Vesel, M. Mozetic, A. Hladnik, J. Dolenc, J. Zule, S. Milosevic, N. Krstulovic, M. Klanjsek-Gunde, N. Hauptman, J. Phys. D: Appl. Phys., 40 (**2007**) 12, 3689–3696
[17] C.-M. Chan, T.-M. Ko, H. Hiraoka. Surf. Sci. Rep., 24 (**1996**), 1–54
[18] N. Krstulovic, U. Cvelbar, A. Vesel, S. Milosevic, M. Mozetic, Mater. Tehnol., 43 (**2009**) 5, 245–249
[19] R. Zaplotnik, M. Kolar, A. Doliska, K. Stana-Kleinschek, Mater. Tehnol., 45 (**2011**) 3, 195–199
[20] N. Krstulovic, I. Labazan, S. Milosevic, U. Cvelbar, A. Vesel, M. Mozetic, Mater. Tehnol., 38 (**2004**) 1, 51–54
[21] F. Poncin-Epaillard, G. Legeay, J.-C. Brosse, J. Appl. Polym. Sci. 44 (**1992**), 1513
[22] A. Vesel, Hydrophobization of polymer polystyrene in fluorine plasma, Mater. Tehnol., 45 (**2011**) 3, 217–220
[23] R. di Mundo, F. Palumbo, R. d'Agostino, Langmuir, 24 (**2008**), 5044–5051
[24] S. Marais, Y. Hirata, C. Cabot, S. Morin-Grognet, M. R. Garda, H. Atmani, F. Poncin-Epaillard, Surf. Coat. Technol. 201 (**2006**) 3–4, 868–879
[25] F. Poncin-Epaillard, D. Debarnot, Inf. Midem, 38 (**2008**), 252
[26] T. Vrlinic, A. Vesel, U. Cvelbar, M. Krajnc, M. Mozetic, Surf. Interface Anal., 39 (**2007**) 6, 476–481
[27] A. Vesel, M. Mozetic, A. Zalar, Vacuum, 82 (**2008**) 2, 248–251
[28] M. Sowe, I. Novak, A. Vesel, I. Junkar, M. Lehocky, P. Saha, I. Chodak, Int. J. Polym. Anal. Ch., 14 (**2009**) 7, 641–651
[29] M. Gorjanc, V. Bukosek, M. Gorensek, A. Vesel, Tex. Res. J., 80 (**2010**) 6, 557–567
[30] A. Vesel, M. Mozetic, S. Strnad, K. Stana-Kleinschek, N. Hauptman, Z. Persin, Vacuum, 84 (**2010**) 1, 79–82
[31] L.-A. O'Hare, S. Leadley, B. Parbhoo, Surf. Interface Anal., 33 (**2002**), 335–342
[32] A. Vesel, Surf. Coat. Technol., 205 (**2010**) 2, 490–497
[33] Z Kregar, M Bišćan, S Milošević, A Vesel, IEEE Trans. Plasma Sci. 39 (**2011**) 5, 1239–1246
[34] A. Vesel, K. Elersic, I. Junkar, B. Malic, Mater. Tehnol., 43 (**2009**) 6, 323–326
[35] N. Krstulovic, I. Labazan, S. Milosevic, U. Cvelbar, A. Vesel, M. Mozetic, J. Phys. D: Appl. Phys., 39 (**2006**) 17, 3799–3804
[36] G. Primc, R. Zaplotnik, A. Vesel, M. Mozetic, AIP Advances 1 (**2011**) 2, 022129-1-022129-11
[37] A. Vesel, A. Drenik, M. Mozetic, M. Balat-Pichelin, Vacuum, 84 (**2010**) 7, 969–974
[38] M. Balat-Pichelin, A. Vesel, Chem. Phys., 327 (**2006**) 1, 112–118
[39] Eui-Sung Yoon, Seung Ho Yang, Hosung Kong, Ki-Hwan Kim, Tribology Lett. 15 (**2003**) 2, 145–154
[40] B. Bhushan, Yong Chae Jung, K. Koch, Phil. Trans. R. Soc. A 367 (**2009**), 1631–1672
[41] A. Vesel, Inf. Midem, 38 (**2009**), 257–265
[42] T. Mohan, R. Kargl, A. Doliska, A. Vesel, S. Köstler, V. Ribitsch, K. Stana-Kleinschek, J. Colloid Interface Sci. 358 (**2011**) 2, 604–610
[43] J. Kovac, Mater. Tehnol. 45 (**2011**) 3, 187–193

UDK 678.7
Original scientific article/Izvirni znanstveni članek

ISSN 1580-2949
MTAEC9, 46(1)53(2012)

# CELL ADHESION ON HYDROPHOBIC POLYMER SURFACES

## ADHEZIJA CELIC NA HIDROFOBNIH POLIMERNIH POVRŠINAH

**Morana Jaganjac[1], Lidija Milković[1], Ana Cipak[1], Miran Mozetič[2], Nina Recek[2], Neven Žarković[1], Alenka Vesel[2]**

[1]Rudjer Boskovic Institute, Div. Molecular Medicine, Bijenicka 54, 10000 Zagreb, Croatia
[2]Jozef Stefan Institute, Plasma laboratory, Jamova 39, 1000 Ljubljana, Slovenia
morana.jaganjac@irb.hr

*Prejem rokopisa – received: 2011-06-02; sprejem za objavo – accepted for publication: 2011-07-22*

Adhesion of human osteosarcoma (HOS) cells on hydrophobic polymer surface was studied. Surface of polymer polystyrene (PS) was made hydrophobic by treatment in plasma created in tetrafluoromethane gas ($CF_4$). The PS samples were exposed for 30 s to $CF_4$ plasma created by RF generator powered at 200 W. This treatment time allowed for optimal polymer surface functionalization with fluorine functional groups. This caused an increase of surface hydrophobicity from initial 85° to about 110° as measured by water contact angle. The HOS cells were deposited on untreated and plasma treated samples and incubated for 1, 2 and 6 days. Both untreated and plasma treated samples were tested for biocompatibility by two different methods: optical micrographs were used to study the cell morphology and MTT test was used to study the cell viability. The results showed better adhesion of cells on plasma treated samples with more hydrophobic surface in comparison to the untreated sample. MTT test revealed about 1.6-times higher activity of cell enzymes after 6-day incubation for plasma treated sample. Optical micrographs have shown that both untreated and fluorine-plasma treated polymer surfaces are not optimal for cell proliferation, since cells need about 2 days to adapt to the surface. After this adaptation time cells start to proliferate on the polymer surface, especially, on that one treated in plasma.

Keywords: plasma surface modification, human osteosarcoma cells (HOS), biopolymers, hydrophobic surface, $CF_4$ plasma

Preučevali smo adhezijo rakastih (HOS) celic na hidrofobnih polimernih površinah. Hidrofobizacija površine polimera polistirena (PS) je potekala v $CF_4$ plazmi generirani z RF generatorjem moči 200 W. Vzorce polimera PS smo izpostavili plazmi za 30 s, kar je zadoščalo za optimalno funkcionalizacijo polimerne površine z nepolarnimi fluorovimi skupinami. To je povzročilo porast kontaktnega kota vodne kapljice iz 85° za neobdelan vzorec na 110° za plazemsko obdelan vzorec, kar je jasen dokaz, da se je hidrofobnost površine povečala. Biokompatibilnost neobdelanih in plazemsko obdelanih vzorcev smo spremljali z optičnim mikroskopom in MTT testom. Z optičnim mikroskopom smo preučevali morfologijo celic, medtem ko smo z MTT testom preučevali viabilnost celic. HOS celice smo deponirali na vzorce in jih inkubirali 1 dan, 2 dni in 6 dni. Iz rezultatov je razvidna boljša adhezija celic na plazemsko obdelanih bolj hidrofobnih površinah v primerjavi z neobdelano zmerno hidrofobno površino. Z MTT testom smo na plazemsko obdelani površini ugotovili 1,6-krat večjo aktivnost celičnih encimov po 6-dnevni inkubaciji v primerjavi z neobdelano. Posnetki z optičnim mikroskopom nakazujejo, da neobdelana in plazemsko obdelana površina nista najbolj optimalni za vezavo celic, saj celice potrebujejo precej časa (še posebej v primeru neobdelane površine), da se privadijo na okolje. Šele po tem času privajanja je opaziti proliferacijo celic po površini, ki je še posebej opazna na plazemsko obdelanem vzorcu.

Ključne besede: plazemska modifikacija površin, rakaste celice, biopolimeri, hidrofobna površina, $CF_4$ plazma

## 1 INTRODUCTION

Polymer materials are nowadays widely used in many different applications in medicine for various implants, tissue engineering, etc.[1–4] Chemical and physical properties of polymer surfaces are therefore very important since they have influence on interactions between the polymer material and a host environment which is normally composed of body fluids, proteins and various cells.[4,5] Therefore, often competitive adsorption appears. In some applications selective adhesion of cells is important. Adhesion and proliferation of cells on polymer surfaces can be controlled by preparing surfaces with particular characteristics.[7–12] This can be done by appropriate surface modification.[5,6] Polymer surfaces can be modified by different techniques. Among them plasma treatment is the most popular.[7–11] By plasma treatment we can introduce different chemical groups to the polymer surfaces and thus make surfaces either hydrophilic or hydrophobic; we can also change surface crystallinity, surface energy, roughness and morphology.[13–17] All these factors may play important (also synergistic) role in surface interactions. For making surface hydrophilic usually oxygen, nitrogen, ammonia, water or $CO_2$ plasma are used, while for making the surface hydrophobic the treatment is performed in a plasma created in halogens like $CF_4$. Hydrophilic surfaces are characterized by good wettability and good adhesion properties, while hydrophobic surfaces are known to be quite inert. Since the body liquids are normally composed of water, various proteins and cells synergistic interaction may appear so it is difficult to predict the exact interaction mechanism of hydrophilic/hydrophobic surfaces when exposed to biological system.[5,18]

In the present paper we were studying the adhesion of human osteosarcoma cells on polystyrene polymer which was treated in $CF_4$ plasma to make the surface

hydrophobic. Comparison of cell proliferation on plasma treated hydrophobic surface to the untreated one was performed by two different methods: optical micrographs were used to study the cell morphology and MTT test was used to study the cell viability.

## 2 EXPERIMENTAL

### *2.1 Preparation of HOS cells*

The human osteosarcoma cell line HOS was obtained from American Type Culture Collection (ATCC). Cells were grown in DMEM (Dulbecco's modified eagle's medium, Sigma, USA) supplemented with 10 % (v/v) foetal calf serum (FCS, Sigma, USA), 2 mM L-glutamine and penicillin/streptomycin (1 000 U/mL and 1000 µg/L respectively). Cells were maintained in an incubator (Heraeus, Germany) at 37 °C, with a humid air atmosphere containing 5 % $CO_2$. The cells were detached from semiconfluent cultures with a 0.25 % (w/v) trypsin solution for 5 minutes. Viable cells (upon trypan blue exclusion assay) were counted on a Bürker-Türk hemocytometer and used for experiments.

### *2.2 Plasma treatment*

Commercially available polystyrene (PS) foils supplied by Goodfellow Ltd were cut to discs with a diameter of 1 cm. The thickness of the foil was 0.25 mm. Before plasma treatment the samples were cleaned in ethanol in an ultrasound bath. No special sterilization of the samples was performed since plasma itself acts as a good method for surface sterilization.[19–21]

Samples were mounted in the glowing plasma of a radio-frequency (RF) discharge as shown in **Figure 1**. The RF generator operated at a power of 200 W and a frequency of 27.12 MHz. A discharge tube of a length 60 cm and a diameter of 4 cm is made of Pyrex glass. A rather uniform glow discharge is created within a RF coil which is 15 cm long. The impedance of the generator was optimized for such a configuration using a vacuum capacitor in parallel with the RF coil. The treatment was performed in tetrafluoromethane gas ($CF_4$) at a pressure of 75 Pa. The plasma treatment time was 30 s. According to our recent paper,[22] polystyrene foils become saturated with fluorine functional groups already in 10 s of treatment. Therefore, 30 s of treatment assured for optimal functionalization.

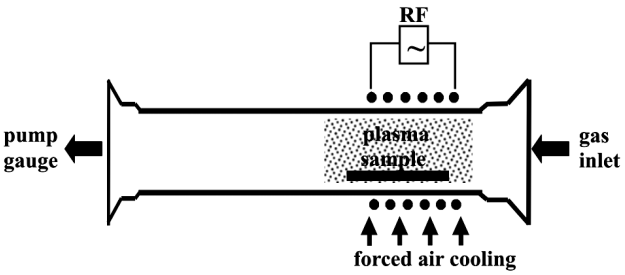


**Figure 1:** Optical microscopy image of polymer surface after 24 h of incubation for: (a) untreated sample and (b) plasma treated sample
**Slika 1:** Posnetek polimerne površine po 24-urni inkubaciji s celicami HOS: (a) neobdelan vzorec in (b) plazemsko obdelan vzorec

### *2.3 HOS cells viability*

Cells were seeded at $2 \times 10^4$ cells in 100 µl of medium on the upper side of polymers at density of 2.55 $\times 10^4$ cells/cm$^2$, and were left for 3 h to attach before covering the whole polymer discs with media.[23] Cells were plated in DMEM medium supplemented with 10 % FCS and left to grown on polymer discs in an incubator at 37 °C in a humidified atmosphere of 5 % $CO_2$. Triplicates of cultures for each time and treatment were prepared for adhesion and cell viability assay.

Cell adhesion was monitored daily and after 1$^{st}$, 2$^{nd}$ and 6$^{th}$ day of culture on the different polymer surfaces micrographs were taken. The MTT-related colorimetric assay (EZ4U; Biomedica, Austria) was used to determine cell growth and viability, according to the manufacturer's instructions and Jaganjac et al.[24] The method is based on the fact that living cells are capable of reducing less colored tetrazolium salts into intensely colored formazan derivatives. This reduction process requires functional mitochondria, which are inactivated within a few minutes after cell death.

Briefly, after 1$^{st}$ and 6$^{th}$ day of HOS cell culture on the different polymer surfaces the medium was removed and 1 ml of fresh Hanks' Balanced Salt Solution (HBSS) and 100 µl of the tetrazolium agent were added to each culture. After 2 h incubation, supernatants were transferred into 96-well plates and measured in a microplate reader (Easy-Reader 400 FW, SLT Lab Instruments GmbH, Austria) at 450/620 nm.

## 3 RESULTS AND DISCUSSION

Numerous samples were prepared by plasma treatment in $CF_4$ gas. As shown in our resent paper plasma treatment caused incorporation of about 56 at.% of fluorine to the surface of polystyrene which originally contains only carbon and hydrogen atoms.[22] Incorporation of nonpolar fluorine functional groups like CHF, CF, $CF_2$ and $CF_3$ caused increased surface hydrophobicity which was checked by water contact angle measurements.[22] The surface of untreated polystyrene is moderately hydrophobic with a contact angle of about 85°. After plasma treatment the surface hydrophobicity was increased giving a contact angle of about 110°.

Adhesion of HOS cells on plasma treated samples was monitored daily. After 1$^{st}$, 2$^{nd}$ and 6$^{th}$ day of cell culture incubation on the polymer surfaces optical micrographs were taken. Some representative images are shown in **Figures 2–4**. **Figure 2a** shows optical image of the untreated sample after 24 h incubation, while **Figure 2b** reveals an optical image of the plasma treated sample incubated for the same time. We can see that in both

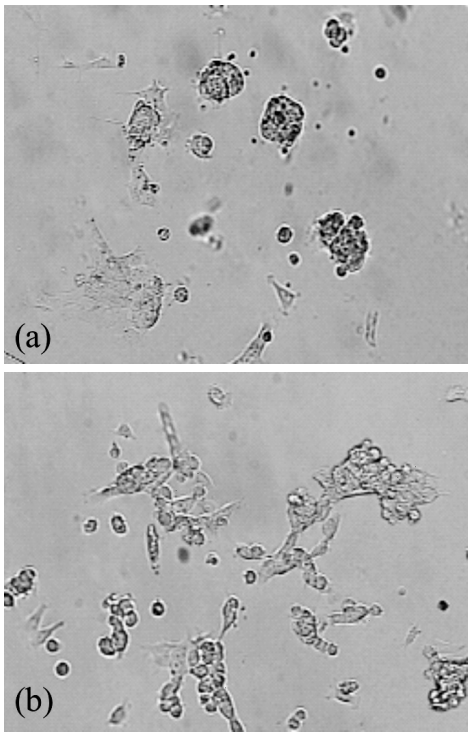


**Figure 2:** Optical microscopy image of polymer surface after 24 h of incubation with HOS cells for: (a) untreated sample and (b) plasma treated sample

**Slika 2:** Posnetek polimerne površine po 24-urni inkubaciji s celicami HOS: (a) neobdelan vzorec in (b) plazemsko obdelan vzorec

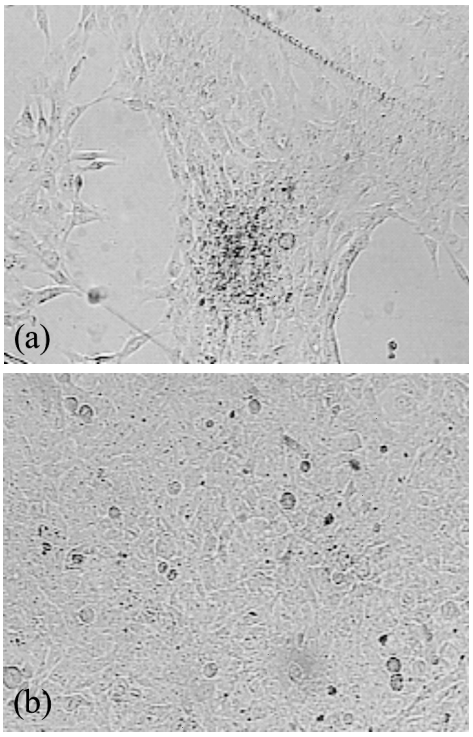


**Figure 4:** Optical microscopy image of polymer surface after 6 days of incubation with HOS cells for: (a) untreated sample and (b) plasma treated sample

**Slika 4:** Posnetek polimerne površine po 6-dnevni inkubaciji: (a) neobdelan vzorec in (b) plazemsko obdelan vzorec

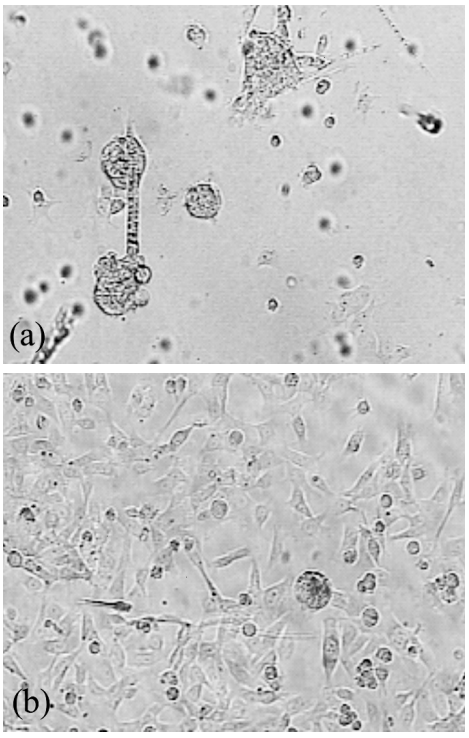


**Figure 3:** Optical microscopy image of polymer surface after 2 days of incubation with HOS cells for: (a) untreated sample and (b) plasma treated sample

**Slika 3:** Posnetek polimerne površine po dvodnevni inkubaciji s celicami HOS: (a) neobdelan vzorec in (b) plazemsko obdelan vzorec

cases the surface is not optimal for cell adhesion, since the cells tend to keep together and form agglomerates. The situation is better after 2 days of incubation as shown in **Figure 3b**, where we can observe that cells already have obtained elongated shape meaning that they have adapted to the plasma treated surface. Contrary, we can not observe this for untreated sample (**Figure 3a**) where situation is similar as after 1 day as already shown in **Figure 2a**. After 6 days of incubation (**Figure 4**) we can observe proliferation of HOS cells for both surfaces

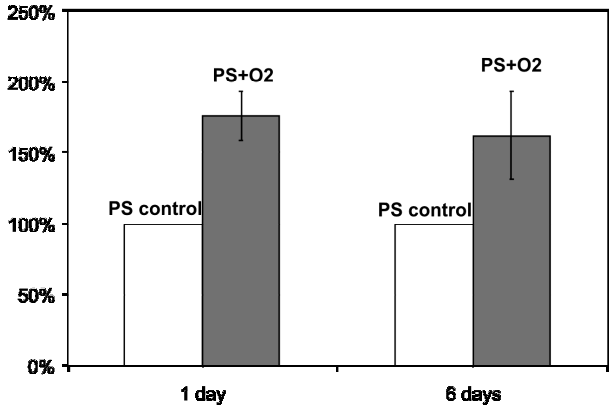


**Figure 5:** Results of MTT assay – comparison of untreated and plasma treated sample after 1 and 6 days of incubation with HOS cells

**Slika 5:** Rezultati MTT testa – primerjava neobdelanih in plazemsko obdelanih vzorcev po enodnevni in 6-dnevni inkubaciji s celicami HOS

untreated (**Figure 4a**) and treated one (**Figure 4b**). In the case of plasma treated surface (**Figure 4b**) the cells form dense structure on the surface. This is not observed for the case of untreated sample (**Figure 4a**) where we can still find empty places not covered by cells. These results clearly indicate that untreated surface is not optimal for cell adhesion, since the cells even after long incubation time did not completely adapt to the surface. In the case of plasma treated surface the cells managed to adapt to it after 2 days of incubation and then good proliferation is observed.

Qualitative results presented in **Figures 2–4** are confirmed by a quantitative technique – MTT assay. **Figure 5** summarizes the results of the cell enzyme activity which is an indicator of the cell viability. The histograms presented in **Figure 4** again indicate better proliferation of the HOS cells on plasma treated samples than on untreated ones. But within the experimental error no increase in the number of cells is observed with increasing incubation time meaning that the environment is not so optimal for cell division and multiplication although we can observe some rounded cells in Figure 4b which could be in process of division.

## 4 CONCLUSION

Polymer samples were treated in $CF_4$ plasma to make the surface hydrophobic. It is known that hydrophobic surfaces have water repealing character and worse adhesion properties. Therefore, effect of surface hydrophobicity on cell adhesion was studied. We have found that by making surface very hydrophobic we could not reduce adhesion and proliferation of HOS cells to the surface in comparison to the untreated moderately hydrophobic polymer. The cells only needed more time to adapt to the surface. The results clearly indicate that also untreated surface with moderate hydrophobicity is not optimal for cell adhesion, since the cells even after long incubation time did not completely adapt to the surface. In the case of plasma treated surface the cells managed to adapt to it after 2 days of incubation and after 6 days good proliferation is observed since the cells form dense structure on the polymer surface. Therefore, we can conclude that plasma has even little enhanced (and not prevent) proliferation of the cells on the sample treated in $CF_4$ plasma in comparison to the untreated one.

**Acknowledgement**

This project was partially supported by Slovenian Research Agency, and Slovenian-Croatian bilateral project BI-HR/10-11-020 "Improvement of adhesive properties of biomedical materials by plasma treatment".

## 5 REFERENCES

[1] B. Kasemo, Surf. Sci., 500 (**2002**), 656–677
[2] J. Jagur-Grodzinski, Polym. Advan. Technol., 17 (**2006**), 395–418
[3] T. Desmet, R. Morent, N. De Geyter, C. Leys, E. Schacht, P. Dubruel, Biomacromolecules, 10 (**2009**) 9, 2351–2378
[4] D. Klee, H. Höcker, Adv. Polym. Sci., 149 (**2000**), 1–57
[5] R. Vasita, K. Shanmugam, D. S. Katti, Curr. Top. Med. Chem., 8 (**2008**), 341–353
[6] Moon Suk Kim, Gilson Khang, Hai Bang Lee, Prog. Polym. Sci., 33 (**2008**), 138–164
[7] P. A. Ramires, L. Mirenghi, A. R. Romano, F. Palumbo, G. Nicolardi, J. Biomed. Mater. Res., 51 (**2000**) 3, 535–539
[8] F. R. Pu, R. L. Williams, T. K. Markkula, J. A. Hunt, Biomaterials, 23 (**2002**), 4705–4718
[9] C. M. Alves, Y. Yang, D. L. Carnes, J. L. Ong, V. L. Sylvia, D. D. Dean, C. M. Agrawal, R. L. Reis, Biomaterials, 28 (**2007**), 307–315
[10] D. P. Dowling, I. S. Miller, M. Ardhaoui, W. M. Gallagher, J. Biomater. Appl., 21 (**2010**), 1–21
[11] K. E. Geckeler, R. Wacker, F. Martini, A. Hack, W. K. Aicher, Cell. Physiol. Biochem., 13 (**2003**), 155–164
[12] Yu Na Shin, Byung Soo Kim, Hyun Hee Ahn, Jung Hwa Lee, Kyung Sook Kim, Ju Young Lee, Moon Suk Kim, Gilson Khang, Hai Bang Lee, Appl. Surf. Sci., 255 (**2008**), 293–296
[13] A. Vesel, Mater. Tehnol., 45 (**2011**) 2, 121–124
[14] I. Junkar, U. Cvelbar, A. Vesel, N. Hauptman, M. Mozetic, Plasma Processes Polym., 6 (**2009**) 10, 667–675
[15] A. Vesel, I. Junkar, U. Cvelbar, J. Kovac, M. Mozetic, Surf. Interface Anal., 40 (**2008**) 11, 1444–1453
[16] C.-M. Chan, T.-M. Ko, H. Hiraoka, Surf. Sci. Rep., 24 (**1996**), 1–54
[17] A. Vesel, K. Elersic, I. Junkar, B. Malic, Mater. Tehnol., 43 (**2009**) 6, 323–326
[18] K. Anselme, L. Ploux, A. Ponche, J. Adhes. Sci. Technol., 24 (**2010**), 831–852
[19] D. Vujosevic, Z. Vranica, A. Vesel, U. Cvelbar, M. Mozetic, A. Drenik, T. Mozetic, M. Klanjsek Gunde, N. Hauptman, Mater. Tehnol., 40 (**2006**) 6, 227–232
[20] Cvelbar U., Mozetic M., Hauptman N., Klanjsek-Gunde M., J. Appl. Phys., 106 (**2009**), 103303
[21] K. Elersic, I. Junkar, A. Spes, N. Hauptman, M. Klanjsek Gunde, A. Vesel, Mater. Tehnol., 44 (**2010**) 3, 153–156
[22] A. Vesel, Mater. Tehnol., 45 (**2011**) 3, 39–42
[23] L. Mrakovcic, R. Wildburger, M. Jaganjac, M. Cindric, A. Cipak, S. Borovic-Sunjic, G. Waeg, A.M. Milankovic, N. Zarkovic, Acta Biochim. Pol., 57 (**2010**), 173–178
[24] M. Jaganjac, T. Matijevic, M. Cindric, A. Cipak, L. Mrakovcic, W. Gubisch, N. Zarkovic, Acta Biochim. Pol., 57 (**2010**), 179–183

UDK 66.017
Original scientific article/Izvirni znanstveni članek

ISSN 1580-2949
MTAEC9, 46(1)57(2012)

# SYNTHESIS OF MICRO-COMPOSITE BEADS WITH MAGNETIC NANO-PARTICLES EMBEDDED IN POROUS $CaCO_3$ MATRIX

## SINTEZA MIKROKOMPOZITNIH KROGLIC Z MAGNETNIMI NANODELCI V POROZNI MATRIKI $CaCO_3$

**Alenka Vesel[1], Aljoša Košak[2], David Haložan[3], Kristina Eleršič[1]**

[1]Department F4, Jožef Stefan Institute, Jamova 39, 1000 Ljubljana, Slovenia
[2]University of Maribor, Faculty of mechanical engineering, Smetanova 17, 2000 Maribor, Slovenia
[3]Institute of Physical Biology, Toplarniška 19, 1000 Ljubljana, Slovenia
alenka.vesel@ijs.si

*Prejem rokopisa – received: 2011-05-20; sprejem za objavo – accepted for publication: 2011-07-22*

A method for synthesis of soft magnetic microbeads is presented. The microbeads are made from magnetic nanoparticles dispersed in $CaCO_3$ (calcium carbonate) matrix. The composite beads are almost perfectly spherical with a diameter of few micrometers. The majority of the composite beads consists of a porous $CaCO_3$ matrix. Magnetic nanoparticles with a size of about 10-15 nm are made of $Fe_2O_3$. They are captured inside the pores of $CaCO_3$ matrix during its formation. $CaCO_3$ matrix is formed by crystallization from saturated solution of sodium carbonate and calcium chloride. The composite beads are coated with a layer of functionalized polymer. The magnetic microbeads were characterized by SEM and XPS. Different functional groups were detected by XPS measurements including $SO_3^-$, $NH_3^+$, $NH_2$, $CO_3^{2-}$ and OH groups. The results indicate that the iron oxide particles are absent on the surface and that the polymer coating serves as a good biocompatible film.

Keywords: composite, surface characterization, XPS, functionalization, Fe nanoparticles, microbeads

V tem prispevku predstavljamo metodo za sintezo delcev, ki so sestavljeni iz kompozita magnetnih nanodelcev v matrici iz kalcijevega karbonata ($CaCO_3$). Velikost kompozitnih delcev, ki so popolnoma sferične oblike, je nekaj mikrometrov. Ključni del ogrodja kompozitnega delca sestavlja zelo porozna matrica $CaCO_3$. Magnetni nanodelci velikosti približno 10-15 nm so narejeni iz $Fe_2O_3$. Ti nanodelci se med tvorjenjem matrice $CaCO_3$ ujamejo v notranjost por. $CaCO_3$ matrica se tvori pri kristalizaciji nasičene raztopine natrijevega karbonata in kalcijevega klorida. Tako nastali kompozit je nato oplaščen še s plastjo funkcionaliziranega polimera. Sintetizirane magnetne kompozitne delce smo analizirali z metodama SEM in XPS. Kot je razvidno iz XPS meritev, je prišlo na površini do nastanka različnih funkcionalnih skupin kot so $SO_3^-$, $NH_3^+$, $NH_2$, $CO_3^{2-}$ in OH skupine. Rezultati dokazujejo, da na površini mikrodelcev ne najdemo nanodelcev, ki so skriti znotraj por, ter da lahko polimerna prevleka, ki prekriva mikrodelce, služi kot dobra biokompatibilna podlaga za nadaljnjo vezavo bioloških substanc.

Ključne besede: kompozit, površinska karakterizacija, XPS, funkcionalizacija, Fe nanodelci, mikrokroglice

## 1 INTRODUCTION

Superparamagnetic nanoparticles have found potential application in various diagnostic tests and assays as substrates or supports for immunollogically based reactions. They can be also used in therapeutic purposes for the transportation of active substances to specific targets.[1–4] Magnetic material for nanoparticles used in medicine is usually maghemit $\gamma$-$Fe_2O_3$ which is a non-toxic material.[5] Application of external magnetic field enables easy handling and distant manipulation with magnetic nanoparticles, or separation of nanoparticles from liquids. Magnetic nanoparticles must express their magnetic properties only in the presence of an external magnetic field but otherwise they must have no magnetic polarization which would otherwise cause their agglomeration. They must be well dispersed in a liquid medium. To fulfil these requirements they must be small enough (below approx. 15 nm) meaning that particles are single magnetic domains. On the other hand, in some applications they must also have sufficiently large specific surface, which provides enough binding sites. In such cases usually polymer metal composites are used.[6] Before application in diagnostic tests and assays the surface properties of magnetic nanoparticles or their composites must be improved by coating them with a layer of specific functionalized material to which specific molecules (e.g. proteins, antibodies) are linked. Usually they are first coated with a layer of polymer or silica and then functionalized with specific functional groups depending on particular application. Numerous methods for synthesis of metal oxide nanoparticles have been elaborated. Although advanced plasma treatments based on application of non-equilibrium processes enable synthesis of particles with interesting properties,[7–10] classical chemical methods are still popular since they often allow for uniform size distribution in quantities of industrial importance. These groups provide necessary binding sites for further covalent attachment of proteins (e.g. streptavidin) for capturing of molecules of interest.

In this paper we present a method for synthesis of magnetic composites consisting of $CaCO_3$ porous matrix with captured magnetic nanoparticles. The composite is coated with a layer of functionalized polymer. The

magnetic composites were characterized by SEM and XPS methods.

## 2 EXPERIMENTAL

### *2.1 Synthesis of magnetic nanoparticles*

The synthesis of superparamagnetic maghemite nanoparticles ($\gamma$-$Fe_2O_3$) has been carried out via a controlled chemical co-precipitation approach.[11–13] Prior to synthesis an aqueous mixture of ferric and ferrous salts and sodium hydroxide as an alkali source were prepared separately as stock solutions. In this method, the corresponding metal hydroxides were precipitated during the reaction between the alkaline precipitating reagent and the mixture of metal salts. The metal hydroxides were subsequently oxidized in air resulting in the formation of the $\gamma$-$Fe_2O_3$ spinel product.

Superparamagnetic $\gamma$-$Fe_2O_3$ nanoparticles obtained after the synthesis can not be directly dispersed in a liquid medium to obtain stable colloids. In this regard, it is necessary to chemically modify the particle surface in order to prevent the particles from aggregation and subsequent sedimentation. The surface of the prepared $\gamma$-$Fe_2O_3$ nanoparticles were stabilized electrostatically, and sterically with amino ($–NH_2$) and hydroxyl (-OH) alkyl groups.

Prepared samples were characterized using X-ray diffractometry (XRD) and transmission electron microscopy (TEM). Specific surface area of powders was determined by BET method (Brunauer, Emmett and Teller).[14] A specific magnetization of the prepared samples was also measured using a vibrating sample magnetometer (VSM). These results have been already published and can be found in Ref [12].

### *2.2 Synthesis of magnetic composite microbeads*

#### *2.2.1 Materials*

Polymer materials poly(sodium 4-styrenesulfonate) (PSS) and poly(alianin hydro chloride) (PAH), were received from Aldrich (Germany). Ethylene-diamine-tetraacetic acid trisodium salt (EDTA), calcium chloride ($CaCl_2$) and sodium carbonate ($Na_2CO_3$) were received from Sigma (Germany). HCl and NaOH were purchased from Riedel-de Haën and Sigma, respectively. Stabilized suspensions of iron oxide ($Fe_2O_3$) nanoparticles with average diameter 10 nm ± 2 nm and specific surface of 90 $m^2g^{-1}$ were prepared as described in a previous paragraph.

#### *2.2.2 Microparticles fabrication*

Polyelectrolyte microcapsules were self-assembled on narrow size $CaCO_3$ microparticles that were synthesized through recrystallization form 0.33 M $CaCl_2$ and $Na_2CO_3$ saturated solutions. The following chemical reaction occurred: $Na_2CO_3 + CaCl_2 \rightarrow CaCO_3 + 2NaCl$.

At room temperature the equal volumes of solutions were rapidly mixed and agitated for 30 s. Mixture was left for 15 min to form porous spherical-like microparticles. Synthesized microparticles were four times washed with water. Iron oxide nanoparticles were encapsulated in the porous microparticles by addition to one of saturated solutions on volume ratio 1,33 % of final solution to create magnetic $CaCO_3$ microparticles.

#### *2.2.3 Polyelectrolyte deposition*

The 1 $gL^{-1}$ polyelectrolyte solutions were prepared in 0.25 M NaCl. Magnetic $CaCO_3$ particles were suspended in PAH (polyallylaminehydrochloride) and PPS (polystyrenesulfonate) solutions, following the 15 min adsorption time during which the particles were continuously shaken. The pH value of polyelectrolyte solution was adjusted to 6.5. Following the adsorption procedure, the particles were rinsed using three centrifugal washings with 5 mM NaCl and subsequently re-suspended in different polyelectrolyte solutions. This sequential process was repeated, until a layer-by-layer polyelectrolyte film of eight bi-layers was assembled onto the magnetic microbeads. The resulting microcapsule suspension with encapsulated iron oxide nanoparticles was stored in water at 4 °C.

### *2.3 Characterization of composite particles with XPS*

Composite microbeads were also analyzed by XPS (X-ray Photoelectron Spectroscopy) to see their chemical composition. Samples were analyzed with an XPS instrument TFA XPS Physical Electronics. Since XPS analyzes are performed in vacuum, a drop of solution containing microbeads was put on Si slice and dried. Such sample was then placed in XPS chamber and excited with X-rays with a monochromatic Al $K_{\alpha 1,2}$ radiation at 1486.6 eV. The photoelectrons were detected with a hemispherical analyzer positioned at an angle of 45° with respect to the normal to the sample surface. Survey-scan spectra were made at a pass energy of 187.85 eV and 0.4 eV energy step. High-resolution spectra of C1s, N1s and S2p were made at a pass energy of 23.5 eV and 0.1 eV energy step The concentration of elements was determined by using MultiPak v7.3.1 software from Physical Electronics, which was supplied with the spectrometer.[15] The high-resolution spectra were fitted using the same software. The curves were fitted with symmetrical Gauss-Lorentz functions. A Shirley-type background subtraction was used. Both the relative peak positions and the relative peak widths (FWHM) were fixed in the curve fitting process.

## 3 RESULTS AND DISCUSSION

The schematic structure of magnetic composite microbeads which were prepared according to our procedure is shown in **Figure 1**. In **Figure 2** is shown the chemical structure of the polymers which were used for

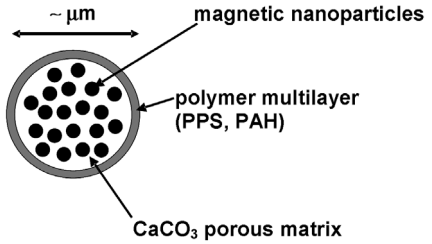


**Figure 1:** Schematic composition of magnetic microbeads
**Slika 1:** Shema sestave magnetnih mikrodelcev

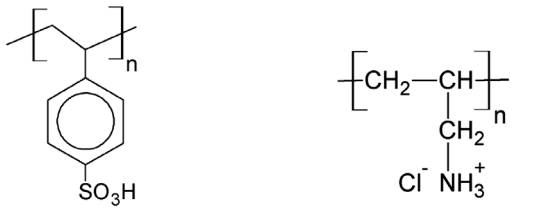


PSS (p-styrenesulfonate) PAH (p-allylamine hydrochloride)

**Figure 2:** Chemical structure of PPS and PAH polymer
**Slika 2:** Kemična struktura polimerov PPS in PAH

final coating the magnetic composite microbeads. We have used different polymers like PAH (polyallylaminehydrochloride) and PPS (polystyrenesulfonate) which were deposited in a multilayered structure. The whole polymer thickness is estimated to several nanometers. This will be discussed later in the text. SEM image of the magnetic composite microbeads is shown in **Figure 3**. We can see that composite microbeads are almost perfectly spherical. Their size is about 5 micrometers. The surface chemical composition of the magnetic composite microbeads was studied by XPS (X-ray photoelectron spectroscopy) in order to prove the presence of functionalized polymer coatings on the surface of magnetic composites. XPS is very powerful method for studying surface chemical composition of different materials especially organic samples[16–22] as well as other materials including micro and nanomaterials or powders like in our case.[23–25] In **Figure 4** is shown survey XPS spectrum of the composite microbeads. Concentration of

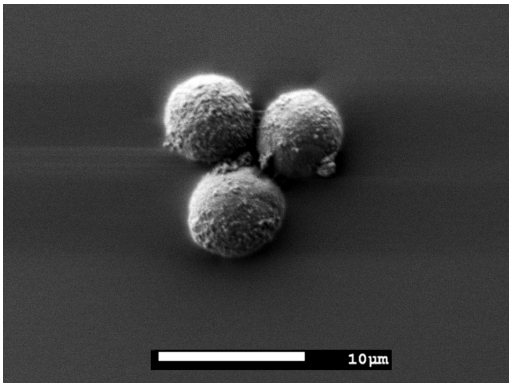


**Figure 3:** SEM image of the magnetic composite microbeads
**Slika 3:** Posnetek magnetnih mikrodelcev

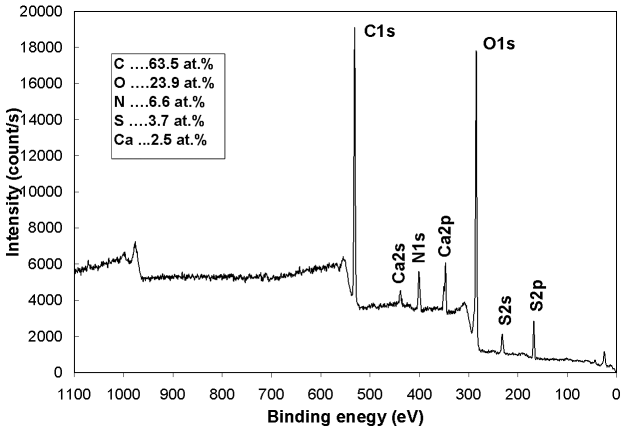


**Figure 4:** XPS survey spectrum of the magnetic composite microbeads
**Slika 4:** Pregledni XPS-spektri magnetnih mikrodelcev

the elements is shown as well. Elements like nitrogen, sulphur, carbon, and oxygen originates from the polymer shell. We can observe also calcium Ca from $CaCO_3$ matrix. Therefore, some of the oxygen and carbon are coming also from calcium matrix. We can not see any traces of iron meaning that iron oxide nanoparticles are hidden well inside the composite microbeads. A prove that composite microbeads really contain magnetic nanoparticles was mobility of these composite microbeads which was observed under the influence of external magnetic field.

Observation of calcium in the survey spectrum needs further discussion. Since a detection depth of XPS method is few nanometers only we can conclude that the polymer thickness must be of the same order. If it was thicker, we could not see calcium. By tilting the sample and changing the angle between electron analyzer and the sample's surface plane we can little vary the detection depth. But unfortunately, this works well only for perfectly flat samples. In our case the surface is rough and furthermore the samples are spherical. Therefore, we could not observe any difference in the surface composition during rotation of the sample.

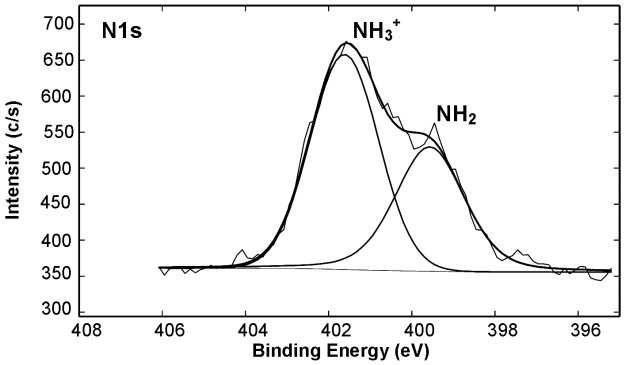


**Figure 5:** XPS high resolution spectrum of nitrogen measured at the surface of magnetic composite microbeads with polymer shell
**Slika 5:** Energijsko visoko ločljivi XPS-spektri dušika, izmerjeni na površini magnetnih mikrodelcev s polimerno prevleko

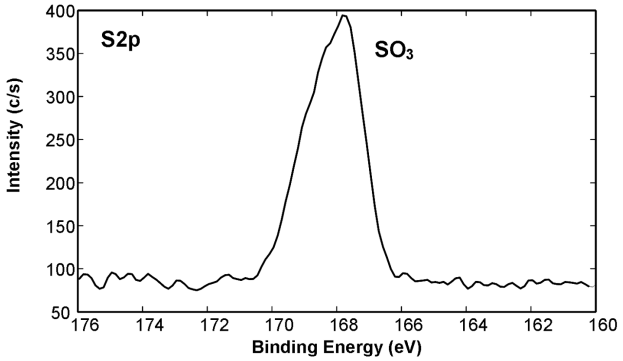


**Figure 6:** XPS high resolution spectrum of sulphur measured at the surface of magnetic composite microbeads with polymer shell
**Slika 6:** Energijsko visoko ločljivi XPS-spektri žvepla, izmerjeni na površini magnetnih mikrodelcev s polimerno prevleko

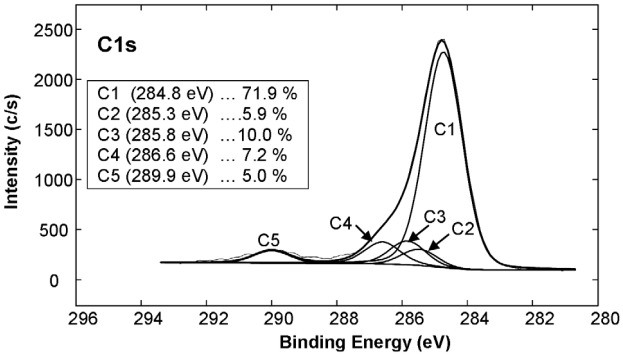


**Figure 7:** XPS high resolution spectrum of carbon measured at the surface of magnetic composite microbeads with polymer shell. Subpeak C1 is attributed to C-C bonding, C2 to C-S bonding, C3 to C-N bonding, C4 to C-O bonding and C5 to O=C-O bonding.
**Slika 7:** Energijsko visoko ločljivi XPS-spektri ogljika, izmerjeni na površini magnetnih mikrodelcev s polimerno prevleko. Spektri so bili razstavljeni na vrhove C1–C5, ki pomenijo različne vezi ogljikovih atomov: C1 pripada C-C vezavi ogljika, C2 pripada C-S vezavi, C3 pripada C-N vezavi, C4 pripada C-O vezavi ter C5 pripada vezavi ogljika v O=C-O skupini.

High resolution spectra of nitrogen N1s, sulphur S2p and carbon C1s which are shown in **Figures 5–7** can give further information about the surface functionalization. As shown in **Figure 5** nitrogen peak consists of two peaks located at the binding energy of about 399.8 eV and 401.7 eV. These two peaks correspond to $NH_2$ and $NH_3^+$ groups. $NH_3^+$ groups are expected for PAH polymer according to its chemical structure shown in Figure 2. During the formation of this polymer layer also $NH_2$ groups were formed. Sulphur peak is shown in **Figure 6**. It is located at a binding energy of about 168 eV and it is attributed to $SO_3$ groups originating from polymer PPS. Very interesting is a carbon peak shown in **Figure 7**. Carbon peak consists of many subpeaks indicating different binding of carbon atoms. The major peak marked as C1 is due to C-C (aliphatic) and –C=C (aromatic) bonds. Other small peaks are contributed to C-S bonds (C2), C-N bonds (C3), C-O bonds (C4) and carbonate bonding $CO_3^{2-}$ (C5). Bonds like C-S and C-N originate from PPS and PAH polymers respectively, while $CO_3^{2-}$ groups are from $CaCO_3$ matrix. These means, that a mixture of both polymers was successfully deposited on the outer surface of magnetic composite microbeads. These functional groups can enable further binding of specific molecules like proteins.

## 4 CONCLUSION

We have developed a method for synthesis of magnetic composite microbeads consisting of $CaCO_3$ matrix with magnetic nanoparticles and outer polymer shell. The composite magnetic microbeads were found to be almost perfectly spherical and their size was about few micrometers. The surface composition of the particles was analyzed by XPS. Elements like carbon, oxygen, nitrogen and sulphur were found on the surface. Calcium from $CaCO_3$ matrix was found as well meaning that the polymer shell has a thickness of about several nanometers. No iron was detected in XPS spectra. This means that magnetic nanoparticles are hidden well inside the $CaCO_3$ matrix. XPS measurements showed also formation of different functional groups like $SO_3^-$, $NH_3^+$, $NH_2$, $CO_3^{2-}$ and OH groups. Groups like $SO_3^-$ originate from PPS polymer, $NH_3^+$ and $NH_2$ are from PAH polymer and $CO_3^{2-}$ groups are from $CaCO_3$ matrix. We can conclude that a mixture of both polymers was successfully deposited onto the outer surface of magnetic composite microbeads. These functional groups can enable further binding of specific molecules like proteins used in biomedical application. Furthermore, polymer coating not just provides surface functional groups needed for good biocompatibility, but it also prevents aggregation of microbeads.

### Acknowledgement

The research was supported by Ministry of Higher Education, Science and Technology of the Republic of Slovenia (project L2-2047, Synthesis and functionalization of composite nanobeads for early diagnosis of neurodegenerative diseases).

## 5 REFERENCES

[1] V. P. Torchilin, Nanoparticulates as Drug Carriers, Imperial College Press, London, 2006
[2] M. Konerack, P. Kopcansky, M. Timko, C.N. Ramchand, J. Magn. Magn. Mater., 252 (**2002**), 409–411
[3] P. A. Gupta, C. T. Hung, Life Sci., 44 (**1989**), 175–186
[4] G. T. Hermanson, Bioconjugate Techniques, Academic Press, Amsterdam, 2008, 582
[5] U. Häfeli, W. Schüt, J. Teller, M. Zborowsky, Scientific and clinical application of magnetic carriers, Plenum Press, New York, 1997
[6] L. C. Santa Maria, M. A. S. Costa, F. A. M. Santos, S. H. Wang, M. R. Silva, Mat. Lett., 60 (**2006**), 270–273
[7] M. Mozetic, Mater.Tehnol. 44 (**2010**) 4, 165–171

[8] M. Mozetic, J. Phys. D Appl. Phys. 44 (**2011**) 17, 174028-1-174028-9
[9] I. Arcon, M. Mozetic, A. Kodre, Vacuum 80 (**2005**) 1–3, 178–183
[10] M. Mozetic, Vacuum (**2012**), doi:10.1016/j.vacuum. 2011.02.017
[11] S. Čampelj, D. Makovec, M. Bele, M. Drofenik, J. Jamnik, Mater. Tehnol., 41 (**2007**) 2, 103–107
[12] A. Kosak, D. Makovec, A. Znidarsic, M. Drofenik, Mater. Tehnol., 39 (**2005**) 1/2, 37–41
[13] D. Makovec, A. Kosak, A. Znidarsic, M. Drofenik, J. Magn. Magn. Mater., 289 (**2005**), 32–35
[14] S. Brunauer, P. H. Emmett, E. Teller, J. Am. Chem. Soc., 60 (**1938**), 309–319
[15] J. F. Moulder, W. F. Stickle, P. E. Sobol, K. D. Bomben, Ed: J. Chastain, R. C. King, Handbook of X-ray photoelectron spectroscopy, Physical Electronics: Minesota, 1995
[16] A. Vesel, M. Mozetic, S. Strnad, K. Stana-Kleinschek, N. Hauptman, Z. Persin, Vacuum, 84 (**2010**) 1, 79–82
[17] M. Gorjanc, V. Bukosek, M. Gorensek, M. Mozetic, Tex. Res. J., 80 (**2010**) 20, 2204–2213
[18] A. Vesel, M. Mozetic, A. Zalar, Vacuum, 82 (**2008**) 2, 248–251
[19] T. Vrlinic, D. Debarnot, M. Mozetic, A. Vesel, J. Kovac, A. Coudreuse, G. Legeay, F. Poncin-Epaillarda, J. Colloid. Interface Sci., 362 (**2011**) 2, 300–310
[20] A. Vesel, M. Mozetic, A. Zalar, Surf. Interface Anal., 40 (**2008**) 3–4, 661–663
[21] I. Junkar, U. Cvelbar, A. Vesel, N. Hauptman, M. Mozetic, Plasma Processes Polym., 6 (**2009**) 10, 667–675
[22] A. Vesel, M. Mozetic, A. Hladnik, J. Dolenc, J. Zule, S. Milosevic, N. Krstulovic, M. Klanjsek-Gunde, N. Hauptman, J. Phys. D: Appl. Phys., 40 (**2007**) 12, 3689–3696
[23] J. Kovac, P. Panjan, A. Zalar, Vacuum, 82 (**2007**) 2, 150–153
[24] G. Drazic, S. Novak, J. Kovac, Imaging Microsc., 8 (**2006**) 3, 36–37
[25] M. Remskar, J. Kovac, M. Virsek, M. Mrak, A. Jesih, A. Seabaugh, Adv. Funct. Mater., 17 (**2007**), 1974–1978

UDK 533.9:678.7
Original scientific article/Izvirni znanstveni članek

ISSN 1580-2949
MTAEC9, 46(1)63(2012)

# THE PLASMA POLYMERISATION PROCESS FOR THE DEPOSITION OF AMINO-CONTAINING FILM ON THE POLY(ETHYLENE TEREPHTHALATE) DRESSING-LAYER FOR SAFE WOUND-HEALING

## PLAZEMSKA DEPOZICIJA AMINO-FUNKCIONALIZIRANEGA FILMA NA POLIETILEN TEREFTALATNEM SLOJU OBLOGE ZA UČINKOVITO CELJENJE RAN

**Zdenka Peršin[1,2], Adolf Jesih[2,3], Karin Stana-Kleinschek[1,2]**

[1]University of Maribor, Faculty of Mechanical Engineering, Laboratory for Characterisation and Processing of Polymers, Smetanova 17, SI-2000 Maribor, Slovenia
[2]Centre of Excellence for Polymer Materials and Technologies, Tehnološki park 24, SI-1000 Ljubljana, Slovenia
[3]Jožef Stefan Institute, Jamova cesta 39, SI-1000 Ljubljana, Slovenia
zdenka.persin@uni-mb.si

*Prejem rokopisa – received: 2010-09-28; sprejem za objavo – accepted for publication: 2010-10-10*

This article presents a new approach for preparing antimicrobial layer as a part of multi-composite dressing for safe and efficient wound – healing within a moist environment. Plasma polymerisation using a mixture of argon, ammonia, and hexane gases was used for preparing a thin polymer film on the poly(ethylene terephthalate) (PET) surface. The plasma deposition efficiency, regarding the amount of nitrogen, was evaluated by the Kjeldahl method, whilst the absorption of C.I. Acid Orange 7 dye onto accessible amino groups was monitored within the UV/VIS spectral region. The quantitative amount of charged surface groups was determined by potencometric titration.
The results obtained using Kjeldahl method indicated the presence of a substantial amount of nitrogen within the deposited film. Furthermore, mono – azo acidic dye was absorbed onto the polymerised sample, pointing to the formation of an ionic bond between the sulphuric and amino groups. The plasma deposited PET samples resulted in inhibitions regarding all the pathogen microorganisms used, mostly those present in the infected wound.

Keywords: plasma polymerisation, argon, ammonia, hexane, poly(ethylene terephthalate), antimicrobial properties, wound dressing

Prispevek predstavlja nov pristop priprave protimikrobnega sloja, ki ga bo mogoče vključiti v obstoječe ali nove razvite obloge za učinkovito celjenje ran v vlažnem okolju. Postopek plazemske polimerizacije z uporabo mešanice plinov argona, amonijaka in heksana je bil uporabljen z namenom vpeljave funkcionalnih skupin na površino polietilen tereftalata (PET). Učinek nanosa oziroma vsebnost dušika se je ovrednotila s pomočjo konvencionalne Kjeldahl metode. Adsorpcija C.I. Acid Orange 7 barvila na dostopne aminske skupine funkcionaliziranega materiala se je spremljala s pomočjo UV/VIS spektroskopije. Kvantitativna količina funkcionalnih skupin z nabojem se je ovrednotila s potenciometrično titracijo.
Rezultati po Kjeldahl-u nakazujejo na prisotnost dušika v nastalem polimernem filmu na površini PET. Mono – azo barvilo se je uspešno adsorbiralo na površino polimeriziranega vzorca, kar nakazuje na nastanek ionske vezi med sulfonskimi in aminskimi skupinami. Plazemsko polimeriziran polietilen tereftalatni vzorec izkazuje učinkovito inhibicijo na vse testirane bakterijske kulture, ki so največkrat prisotne v okuženi rani.

Ključne besede: plazemska polimerizacija, argon, amonijak, heksan, polietilen tereftalat, protimikrobne lastnosti, obloga

## 1 INTRODUCTION

Dressing is designed to come into direct contact with a wound. Its properties should meet a number of requirements e.g. to abate blood – flow, to enhance the healing process, to absorb any fluids discharged from the wound, etc. Whilst the wound itself may be of particular cause for concern, the potential infections that could enter the body through the wound opening may be more serious[1].

One important aspect of a dressing usefulness is its ability to prevent infection. The development of such a dressing is thus based either on biologically – active polymers[2] or on the inclusion of potential antimicrobial compounds[3–5] within the dressings. Antimicrobial dressings can be made by binding drug onto the polymers[6–7] or chemically modifying the polymers[8–9] by introducing various functional groups such as amino[10–11], hydroxyl, carboxyl, aldehyde[2,4,12], and combinations of carboxyl and amino, epoxy, methoxy, thiol and sulphone.

There are a wide – variety of dressings possessing antiseptic chemical agents[10,13,14] that have been identified as acting destructively towards microbes, but only a few of them are safe for patients[15–16] and the environment. Their efficiency often decreases after incorporation into a dressing. In addition there is a well – known evidence for bacterial resistance to silver[17–23] that has a long history as an antimicrobial agent.

Plasma polymerization is known as an effective method for the modification of polymer surfaces[24–25] by generating a thin layer of polymerized material containing functional groups. Plasma polymerisation effect is mainly limited in regard to improving the adhesion,

mechanical, and optical properties[26] of those materials mainly developed for usage in agricultural, food and packaging industries, and protective clothing. The deposition of antimicrobial coating through plasma polymerization onto surfaces is mainly focused on improving polymer functional performance and properties[27–28], and the bacterial adhesion and biocompatibility of the biomedical implants[29–30]. Synthetic polymers (e.g. polyethylene terephthalate, polyamide, polypropylene, polyurethane, etc.) are generally applied for packaging and synthesis of textile fibres, whereas their application as medical polymers[31–33], especially as wound dressings, is less known and not exploited much, as yet[34].

Other possible methods for incorporation of nitrogen – rich functional groups into the surface films of polymer materials are functionalization by reactive nitrogen plasma and ion implantation of nitrogen ions[35–37]. The first one employs non – equilibrium plasma created either in pure nitrogen or a mixture of nitrogen and hydrogen or a mixture of nitrogen and a noble gas or ammonia. All these plasmas produce substantial quantities of reactive nitrogen particles[38–39]. Electrodeless discharges often create plasma with a huge density of neutral nitrogen atoms and negligible kinetic energy of nitrogen ions. Capacitively coupled high frequency discharges and simple DC discharges create plasma rich in ions that are accelerated in sheath to relatively high kinetic energies. The concentration of neutral atoms in such discharges is generally smaller than in electrodeless discharges. A best source of energetic ions is a simple ion gun or a more sophisticated ion implantation device. Ion guns create positively charged nitrogen ions with a kinetic energy of the order of 100 or 1000 eV, while implantation devices often operate at much higher kinetic energies[40]. The thickness of the modified film obviously depends on the type of plasma particles and kinetic energy of ions. The surface layer of polymer is enriched with nitrogen using electrodeless discharges. Discharges of reasonable high voltages would cause modification of surface films of the order of few nanometers. Thicker layers are modified using energetic ions either from ion guns or implantation devices.

Baring this in mind, plasma polymerization, using a mixture of argon, ammonia, and hexane gases, was introduced in order to gain antimicrobial activity on the poly(ethylene terephthalate) (PET) surface. A plasma deposited PET surface was characterized by the conventional Kjeldahl method, UV/VIS adsorption studies and potenciometric titrations. The antimicrobial activities of the non-treated and plasma polymerised samples were determined by the AATCC 100-1999 standard test.

In this way modified PET material would be designed to come into direct contact with a wound as a first layer within a multi-layered medical dressing possessing effecting inhibition strategy directed towards skin microorganisms.

## 2 EXPERIMENTAL PART

### *2.1 Materials*

Poly(ethylene terephthalate) (PET) was studied in its mesh form, as produced by BETI d.o.o., Slovenia. The sample was made of 100 % polyester, with a specific surface mass of 75 g/m$^2$, and atlas weaving.

### *2.2 Treatment procedures*

Plasma polymerization was carried out in a stainless steel reactor. Stainless steel reactor was an in house constructed modified GEC reference cell[41] of 200 mm i.d. and 284 mm in height. The plasma in the reactor was inductively coupled through a silica window by a five-turn planar coil of 3 mm diameter[42] with a maximum power of 30 W, and at a frequency of 13.5 MHz. During polymerisation the pressure in the reactor was fixed at 0.4 mbar. The sample was placed in a reactor chamber and evacuated to $10^{-3}$ Pa. When the pressure in the plasma reactor fell below 0.001 mbar, argon gas with a flow rate of 8.0 mL/min (standard conditions, T=0 °C, 1.01 bar) was introduced into the system using a mass flow controller. The material was first treated with argon plasma in order to ensure better adhesion of the plasma polymer to the substrate material. The plasma was ignited with an electric spark and after three minutes, hexane (0.65 mL/min) and ammonia (74.5 % $NH_3$ in hexane; 0.5 to 6.0 mL/min) were introduced as working gases. The polymerisation procedure lasted 2 h and then the sample was stored in argon atmosphere. Details of the apparatus and treatment procedure are given elsewhere[43].

### *2.3 Methods*

#### *2.3.1 Kjeldahl method*

The quantitative amount of nitrogen (%) present in the samples was determined using the conventional Kjeldahl analysis[44]. About 0.5 g of the sample was digested with $H_2S0_4$ and a catalyst containing 2.8% $TiO_2$, 3.0% $CuS0_4$ $5H_2O$, and 94.2 % $K_2SO_4$. The residue was treated with NaOH to liberate $NH_3$ which was subsequently absorbed in boric acid and titrated with HCl. The total of bound – nitrogen (TN) was determined, in such way that the bound nitrogen was oxidized and thermally – decomposed into $NO_2$, which was then detected using an electrochemical detector (ChD). The nitrogen oxides underwent oxidation at the anode, causing a change in the current between the electrodes. This change was proportional to the concentrations of nitrogen oxides. All samples were analysed in at least triplicate to ensure reproducibility and to exclude statistical errors.

#### *2.3.2 UV/VIS spectroscopy*

The absorption of C.I. Acid Orange 7 (AO7) dye onto the accessible amino groups was monitored using

UV/VIS spectroscopy. Adsorption experiments were carried out at 20 °C, in magnetically – stirred thermostated cylindrical glass vessels, under batch conditions. 2 mL of AO7 dye solution (1.75 g/L) was added to 250 mL of aqueous solution. The pH of the solution was adjusted to 3.66 using Acetic acid. An absorbance value at 482 nm was used to monitor the adsorption process, and the colour was measured according to Lambert–Beer's Law[45] using a UV-Visible Spectrophotometer Cary 50 Conc. The initial absorbance ($A_o$) of the solution (without a sample) was measured at the beginning, whilst when adding the sample (0.25 g), the absorbance ($A_t$) was automatically measured as a function of time. The data was collected every 30 s within the first hour, then every hour within 24 h until equilibrium was established. All the experiments were carried out in triplicate. The dye concentration on the sample in equilibrium was calculated as:

$$\frac{c_t}{c_{eq}} = \frac{A_0 - A_t}{A_0 - A_{eq}} \quad (1)$$

where $A_o$ is the initial absorbance, $A_t$ is absorbance in time $t$, $A_{eq}$ is absorbance in equilibrium, $c_t$ is concentration in time $t$, $c_{eq}$ is concentration in equilibrium.

*2.3.3 Potenciometric titration*

Potenciometric titration was used to define quantitative amount of charged groups present in the sample. Potenciometric titration is an electrochemical titration based on determining the volume of the reagent (titrant) that is stehiometrically equal to the amount of measured substance. The pH potentiometric titration of the sample suspension was carried out with a Mettler Toledo T70 two-burette instrument, within an inert atmosphere ($N_2$ bubbling). The burettes were filled with 0.1 M HCl and 0.1 M KOH. All solutions were prepared in Mili-Q water with low carbonate content (< $10^{-5}$ M). This was achieved by boiling and cooling in nitrogen atmosphere. The suspension was titrated in a back and forth manner between the initial pH = 2.8 to the pH = 11. The titration experiments were carried out at 0.01 M ionic strength, set to its appropriate value with KCl. The titrant was added dynamically within a step interval of [0.001 – 0.25] mL. The equilibrium criteria was obtained by d$E$/d$t$ = 0.1/150 s. 150 s was the minimum time to reach equilibrium conditions between the two additions of the titrant, and the maximum time was set at 7200 s. The pH value was measured with a Mettler Toledo DG-117 – combined glass electrode. All the experiments were carried out in triplicate. Blank HCl-KOH titration was carried out under the same conditions as above.

*2.3.4 Antimicrobial activity*

The general method described in 'AATCC Test Method 100 – 1999, Antibacterial Finishes on Textile Materials: Assessment of'[46] with modifications, was the basis for the protocol used when measuring the qualitative and quantitative antibacterial tendencies of the investigated materials. The three challenging bacterial species were used throughout: *Staphylococcus aureus*, *Escherichia coli*, and *Enterococcus faecalis*. Before each assay, the test bacteria were incubated in either a trypticase soy broth (TSB, BBL® No. 11768 trypticase soy broth) or on trypticase soy agar slants (TSA, BBL® No. 11768 trypticase soy broth, and 2.0% agar) at 37 ± 2 °C for 1 – 3 days, before being used to inoculate the broth's (TSB) cultures for testing. The inoculated broth cultures were incubated at 37 ± 2 °C and stored at 5 ± 1 °C. Standardized density of bacteria ((1 – 2) × $10^5$ CFU/mL) was used for the challenge inoculation. For each sample replicate, 1.0 ± 0.1 mL of inoculum was dispersed over the samples, inoculated at 37 ± 2 °C for 24 h, before being assayed for bacterial population density, or were immediately assayed for bacterial population density as the zero – time population density. The bacterial population densities were determined by first extracting the bacteria from the sample by adding 100 mL of diluent to each jar, and then shaking the jars on a table top shaker for 1 min. Then the aliquots were removed and plated directly into petri dishes or further diluted, before being plated. The percentage reduction of bacteria by the samples was determined as:

$$R = 100\ (B–A)/B \quad (2)$$

where $R$ is the reduction (%), $A$ is the number of bacteria recovered from the inoculated test specimen swatches in the jar, incubated over the desired contact period (24 h), and $B$ is the number of bacteria recovered from inoculated test specimen swatches in the jar immediately after inoculation ("zero" contact time).

No antibiotics were used and incubation was at 37 ± 2 °C for at least 24 h before counting the plates.

## 3 RESULTS

In **Table 1**, the results for the amount of nitrogen per mass of sample (Ni) are shown.

**Table 1:** Amount of nitrogen per mass (Ni) of non-treated and plasma polymerised samples
**Tabela 1:** Vsebnost dušika glede na maso (Ni) neobdelanega in plazma polimeriziranega vzorca

| Sample | Volume of sample (mL) | Mass of sample (g) | Ni (mmol/kg) |
|---|---|---|---|
| Non-treated | 250 | 0.5133 | 15.48 |
| Plasma polymerised | 250 | 0.5174 | 38.62 |

The Total Nitrogen results indicated a significant increase in the nitrogen present in the deposited film on the PET samples. These results were supported by the infra – red spectroscopy results, determined previously; for details see Z. Persin et al.[47]. The spectra showed an appearance of peaks within 3500 – 3300 $cm^{-1}$, or at around 1600 $cm^{-1}$, 1100 $cm^{-1}$, 900 $cm^{-1}$, and 700 $cm^{-1}$.

These peaks are characteristic for R-$NH_2$ functional groups.

The concentrations of the adsorbed C.I. Acid Orange 7 dye on the samples, depending on the treatment are presented in **Table 2**.

**Table 2:** Concentrations of the adsorbed C.I. Acid Orange 7 dye on the non-treated and plasma polymerised samples
**Tabela 2:** Koncentracija barvila C.I. Acid Orange 7 na neobdelanih in plazemsko polimeriziranih vzorcih

| Sample | Concentration of AO7 dye on the sample (mmol/kg) | Concentration of AO7 dye on the sample (g/g) |
|---|---|---|
| Non-treated | 0.00368 | 1.3 E-06 |
| Plasma polymerised | 0.16607 | 5.8 E-05 |

A very low concentration of AO7 dye was adsorbed on the non-treated sample, whilst the dye concentration on plasma – polymerised sample was significantly higher.

**Table 3** present the amount of charged groups in the non-treated and plasma-polymerised poly(ethylene terephthalate) samples.

**Table 3:** Amount of charged groups in the non – treated and plasma polymerised poly(ethylene terephthalate) samples
**Tabela 3:** Količina funkcionalnih skupin z nabojem v neobdelanem in plazemsko polimeriziranem polietilen tereftalatnem materialu

| Sample treatment | Amount of charged groups (mmol/kg) | |
|---|---|---|
| | Positively | Negatively |
| Non-treated | 12.7 | – |
| Plasma polymerised | 19.4 | – |

Both PET samples, regardless of the treatment used, exhibited no negative charge, whilst the non-treated PET sample showed approximately 13 mmol/kg of positive charge. The PET mesh coated with a plasma-polymerized film revealed 19.4 mmol/kg of positive charge. Compared to the non-treated sample, the treated sample showed an increase of positive charge for 6.4 mmol/kg.

The results for antimicrobial activity by non-treated and plasma polymerised PET samples are presented in **Table 4**. The results represent a reduction (*R*) of bacteria that are likely to be present in an infected wound.

**Table 4:** Reduction R (%) of the bacteria, mostly present in the infected wound, for non-treated and plasma polymerised sample
**Tabela 4:** Stopnja redukcije R (%) neobdelanega in plazemsko polimeriziranega materiala na bakterije, ki so najpogosteje prisotne v okuženi rani

| Sample | Reduction *R* (%) on bacterial culture | | |
|---|---|---|---|
| | *Staphylococcus aureus* (gram positive) | *Escherichia coli* (gram negative) | *Enterococcus faecalis* (gram positive) |
| Non-treated | 75 % | No reduction | No reduction |
| Plasma polymerised | 100 % | 99.96 % | 93.7 % |

The results for the non-treated samples, as shown in **Table 4**, indicate no reduction for *Escherichia coli* and *Enterococcus faecalis*, but a significant reduction for 75% for *Staphylococcus aureus.* The plasma polymerised PET samples indicated higher antimicrobial activity. The deposited film containing amino groups resulted in inhibition on all the used pathogen microorganisms. These results are valid within the limits of the experimental error.

## 4 DISCUSSION

A polymer film containing nitrogen functional groups arose on the material surface after applied plasma polymerisation. The efficiency of plasma deposition resulted in a 150 % increase of total nitrogen content as revealed from measured IR – spectra.

UV/VIS spectrophotometric results indicate increased concentrations of AO7 dye on the plasma polymerised samples. The groups introduced by plasma polymerisation present accessible locations for the efficient binding of mono – azo acidic dye molecules. The ionic bond between dye sulphate groups ($SO_3^-$) and amino ($NH_3^+$) groups introduced by plasma polymerisation occur in a stehiometric ratio of 1 to 1.

Results obtained by potenciometric titration indicate by non-treated sample a presence of a positive charge groups. This surprisingly existence of positive charge might be explained due to dyes and other chemicals used during the manufacturing process of the PET sample in a form of a mesh. The PET sample coated with a film deposited by plasma polymerization shows a higher amount of positive charge, which could be attributed to the introduction of amino groups by plasma polymerisation treatment. On contrary, no negative charge by non – treated sample as well by plasma polymerised samples was observed. The obtained results could be explained due to fact that titration is a technique used for determining the $H^+$ ions resulting due to present functional groups that are able to dissociate (e.g. weak acid, amino groups). Since basic PET molecule do not possess weak acid functional groups, while plasma treated sample possess amino groups, the obtained results are reasonable and explain the discrepancy regarding high negative surface charge groups obtained in the same material by other authors[48–49].

When compared with the non-treated sample, only a 75 % reduction was evidenced on *S. aureus*. This result was rather unpredictable, although the percentage does not account for antimicrobial activity; the noticeable antimicrobial challenge delivering a higher value[50]. In addition, it could indicate that the inhibition of the specific bacteria is not only due to the presence of amino groups, but could also be due to the changed (i.e. improved) hydrophilic properties of the tested material[51]. In addition, bacteria exist over a wide range of shapes, ranging from spheres to rods and spirals, which differ in dimensions. *S. aureus* is a round – shaped cocci bacterium with a diameter of 0.5 – 1.0 μm[52], compared to the

rod – shaped *E. coli* that is 0.5 – 1.0 μm wide and 1 – 4 μm long[53]. In this agreement, the bacteria molecule having smaller diameter could more easily penetrate into the porous sample, resulting in apparent antimicrobial activity.

A PET material coated with a layer deposited by plasma polymerisation turned out to be antimicrobial. Such a property is expressed for all the tested bacteria. Within the limits of experimental error a 100 % reduction was observed for *Staphylococcus aureus*, which is one of the more important pathogens, causing illnesses from minor skin infections to life – threatening diseases. Its incidences are from skin, soft tissue, respiratory, bone, joint, and endovascular wound infections. *S. aureus* is nowadays one of the five most common causes of nosocomial infections, often causing postsurgical wound infections. A 93.7 % reduction was obtained for the second gram – positive bacteria used. *E. faecal*[54] is listed as the first to the third leading cause of nosocomial infections. Most of these infections occur after surgery on the abdomen or a puncturing trauma, but can also be linked to the increased use of catheters, which are considered compromising devises. It is also responsible for urinary tract infections, bacterimia, endocarditis, meningitis, and can be found in wound infections along with many other bacteria[54]. A noteworthy reduction (99.96 %) was also evident for gram – negative bacteria from a species type of the genus Escherichia. The *E. coli* bacteria is known for spreading from one person to another, as well as being able to spread from an infected person hands to other people or to objects[55].

## 5 CONCLUSION

The plasma polymerization process proved to be a successful tool for polymer surface functionalization. Using the proposed preparation procedure, a universal layer could be prepared and incorporated into newly – prepared and also existing multilayer composites. Based on the inertness and acquired antimicrobial activity of such a layer, it could even be used for dressings having direct contact with the wound. The latter enables the use of such dressings, even for patients suffering from hypersensitive reactions.

### Acknowledgement

This work was supported by the Ministry of Higher Education, Science and Technology of the Republic of Slovenia [Grant number 3211-10-000057].

## 6 REFERENCES

[1] T. Mustoe, American Journal of Surgery, 187 (**2004**) 5A, 65S–70S
[2] I. A. Chekmareva, Bulletin of Experimental Biology and Medicine, 133 (**2002**), 226–30
[3] A. R. Lee, W. H. Huang, Journal of Pharmacy and Pharmacology, 47 (**1995**) 6, 503–9
[4] J. Hart, D. Silcock, S Gunnigle, International Journal of Biochemistry & Cell Biology, 34 (**2002**), 1557–70
[5] A. E. C. C. Pecharroma´n, E.A. J. S. S. Moya, Journal of Materials Science, 41 (**2006**), 5208–5212
[6] C. Watanakunakorn, C. Glotzbecker, Antimicrobial Agents and Chemotherapy, 11 (**1977**) 1, 88–91
[7] M. R Wessels, Streptococcal and enterococcal infections, in Harrison's principles of internal medicine, 14th edition, (Isselbacher, K. J., Braunwald, E., Wilson, J. D., Martin, J. B., Fauci, A. S., Kasper, D. L., eds), McGraw-Hill, Inc (Health Professions Division), 1998, 890–891
[8] T. N. Yudanova, I. V. Reshetov, Pharmaceutical-Chemistry-Journal, 40 (**2006**), 24–31
[9] L. G. Ovington, Clinics in Dermatology, 25 (**2007**), 33–8
[10] P. Gilbert, L. E. Moore, Journal of Applied Microbiology, 99 (**2005**) 4, 703–15
[11] L. Zemljic Fras, S. Strnad, O. Sauperl, Textile Research Journal, 79/3 (**2009**), 219–226
[12] K. Jansson, A. Haegerstrand, G. Kratz, Scandinavian Journal of Plastic and Reconstructive Surgery and Hand Surgery, 35 (**2001**), 369–75
[13] J. B. Wright, K. Lam, D. Hansen, R. E. Burrell, American Journal of Infection Control, 27 (**1999**) 4, 344–50
[14] H. Q. Yin, R. Langford, R. E. Burrell, Journal of Burn Care & Rehabilitation, 20 (**1999**) 3, 195–200
[15] J. F. Fraser, L. Cuttle, M. Kempf, R. M. Kimble, ANZ Journal of Surgery, 74 (**2004**) 3, 139–42
[16] S. L. Percival, P. G. Bowler, D. Russell, Journal of Hospital Infection, 60 (**2005**) 1, 1–7
[17] G. L. McHugh, R. C. Moellering, C. C. Hopkins, M. N. Swartz, Lancet, 1(7901) (**1975**), 235–40
[18] R. P. Wenzel, K. J. Hunting, C. A. Osterman, M. A. Sande, American Journal of Epidemiology, 104 (**1976**) 2, 170–80
[19] W. E. Gayle, C. G. Mayhall, V. A. Lamb, E. Apollo, B. W. Haynes, Journal of Trauma-Injury Infection and Critical Care, 18 (**1978**) 5, 317–23
[20] K. Bridges, A. Kidson, E. J. Lowbury, M. D. Wilkins, British Medical Journal, 1 (**1979**) 6161, 446-9
[21] X. Z. Li, H. Nikaido, K. E. Williams, Journal of Bacteriology, 179 (**1997**) 19, 6127–32
[22] H. J. Klasen, Burns, 26 (**2000**) 2, 131–8
[23] N. McCallum, B. Berger-Bächi, M. M. Senn, International Journal of Medical Microbiology, 300 (**2010**) 2–3, 118–129
[24] H. Yasuda, Journal of Polymer Science Macromolecular Reviews, 16 (**1981**), 199–293
[25] H. Yasuda, Journal of Membrane Science, 18 (**1984**), 273–284
[26] E. M. Bachari, S. Ben Amora, G. Baud, M. Jacquet, Materials Science and Engineering B-Solid State Materials for Advanced Technology, 79 (**2001**) 2, 165–174
[27] K. H. Hong, N. Liu, G. Sun, European Polymer Journal, 45 (**2009**) 8, 2443–2449
[28] R. Davis, A. El-Shafei, P. Hauser, Surface & Coatings Technology, 205/20 (**2011**) 15, 4791–4797
[29] J. Wanga, N. Huang, P. Yang, Y. X. Leng, H. Sun, Z. Y. Liu, P. K. Chu, Biomaterials, 25/16 (**2004**), 3163–3170
[30] S. Lerouge, A. Major, P. L. Girault-Lauriault, M. A. Raymond, P. Laplante, G. Soulez, F. Mwale, M. R. Wertheimer, M. J. Hébert, Biomaterials, 28/6 (**2007**), 1209–1217
[31] W. Zhang, J. Jia, Y. Zhang, Q. Yan, E. Z. Kurmaev, A. Moewes, J. Zhao, P. K. Chu, Applied Surface Science, 253/22 (**2007**), 8981–8985
[32] T. P. Martin, S. E. Kooi, S. H. Chang, K. L. Sedransk, K. K. Gleason, Biomaterials, 28/6 (**2007**), 909–915
[33] J. Wang, J. Li, L. Ren, A. Zhao, P. Li, Y. Leng, H. Sun, N. Huang, Surface & Coatings Technology, 201/15 (**2007**), 6893–6896

[34] D. Hegemann, M. Mokbul Hossain, D. J. Balazs, Progress in Organic Coatings, 58 (**2007**), 237–240
[35] A. Vesel, I. Junkar, U. Cvelbar, J. Kovac, M. Mozetic, Surf. Interface Anal., 40/11 (**2008**), 1444–1453
[36] A. Vesel, M. Mozetic, S. Strnad, Vacuum, 85/12 (**2011**), 1083–1086
[37] A. Vesel, M. Mozetic, A. Zalar, Surf. Interface Anal., 40 (**2008**) 3–4, 661–663
[38] M. Mozetic, U. Cvelbar, A. Vesel, A. Ricard, D. Babic, I. Poberaj, J. Appl. Phys., 97 (**2005**) 10, 103308-1–103308-7
[39] F. Gaboriau, U. Cvelbar, M. Mozetič, A. Erradi, B. Roufflet, J. Phys. D Appl. Phys., 42 (**2009**) 5, 055204-1–055205-5
[40] J. Jagielski, G. Gawlik, A. Zalar, M. Mozetič, Inf. MIDEM, 29 (**1999**) 2, 61–67
[11] P. J. Hargis Jr., K. E. Greenberg, P. A. Miller, J. B. Gerardo, J. R. Torzynski, M. E. Riley, G. A. Hebner, J. R. Roberts, J. K. Olthoff, J. R. Whetstone, R. J. Van Brunt, M. A. Sobolewski, H. M. Anderson, M. P. Splichal, J. L. Mock, P. Bletzinger, A. Garscadden, R. A. Gottscho, G. Selwyn, M. Dalvie, J. E. Heidenreich, J. W. Butterbaugh, M. L. Brake, M. L. Passow, J. Pender, A. Lujan, M. E. Elta, D. B. Graves, H. H. Sawin, M. J. Kushner, J. T. Verdeyen, R. Horwath, T. R. Turner, Rev. Sci. Instrum., 65 (**1994**), 140–154
[42] P. A. Miller, G. A. Hebner, K. E. Greenberg, P. D. Pochan, B. P. Aragon, Res. Natl. Inst. Stand. Technol., 100 (**1995**), 427–439
[43] P. Klampfer, T. Skapin, B. Kralj, D. Žigon, A. Jesih, Acta Chimica Slovenica, 50 (**2003**), 29–41
[44] K. Vaideki, S. Jayakumar, R. Rajendran, G. Thilagavathi, Applied Surface Science, 254 (**2008**), 2472–2478
[45] P Atkins in J. de Paula, Atkins' Physical Chemistry, 7th Edition, Oxford University press Inc., New York 2002, 483–497
[46] Anonymous, 1999 Anonymous, 'AATCC Test Method 100-1999, Antibacterial finishes on textile materials: Assessment of' AATCC Technical Manual 75 (2000), Technical Manual of the American Association of Textile Chemists and Colorists 1999, AATCC, Triangle Park, NC 1999, 147–149
[47] Z. Peršin, K. Stana-Kleinschek, A. Jesih, U. Maver, 4th International Conference on Advanced Plasma Technologies (iCAPT-IV) with Workshop on Plasma Synthesis and Applications of Nanomaterials & 112th IUVSTA Executive Council Meeting, September 9th [i. e.] 11th – September 13th 2011, Strunjan, Slovenia, Conference proceedings. Ljubljana: Slovenian Society for Vacuum Technique: = DVTS – Društvo za vakuumsko tehniko Slovenije, (2011), 127–130
[48] T. Indest, S. Strnad, K. S. Kleinschek, V. Ribitsch, L. Fras, Colloids and Surfaces A: Physicochemical and Engineering Aspects, 275 (**2006**) 1–3, 17–26
[49] J. Wang, N. Huang, P. Yang, Y. X. Leng, H. Sun, Z. Y. Liu, P. K. Chu, Biomaterials, 25 (**2004**) 16, 3163–3170
[50] L. Fras-Zemljic, V. Kokol, D. Cakara, DOI: 10.1177/0040517511404600
[51] L. Fras Zemljic, O. Sauperl, I. But, A. Zabret, M. Lusicky, DOI: 10.1177/0040517510397572
[52] U. Cvelbar, M. Mozetič, N. Hauptman, M. Klanjšek Gunde. J. Appl. Phys., 106 (**2009**) 10, 103303-1–103303-5
[53] K. Elersic, I. Junkar, A. Spes, N. Hauptman, M. Klanjsek Gunde, A. Vesel, Mater. Tehnol., 44 (**2010**) 3, 153–156
[54] K. J. Ryan, C. G. Ray, Sherris Medical Microbiology (4th ed.), McGraw Hill, 2004, 294–5
[55] K. Todar, "Pathogenic E. coli", Online Textbook of bacteriology, University of Wisconsin–Madison Department of Bacteriology, Retrieved 2007, 11–30

UDK 533.9
Original scientific article/Izvirni znanstveni članek

ISSN 1580-2949
MTAEC9, 46(1)69(2012)

# EFFECTS OF PLASMA TREATMENT ON WATER SORPTION IN VISCOSE FIBRES

## UČINKI PLAZEMSKE OBDELAVE NA SORPCIJO VODE V VISKOZNIH VLAKNIH

**Miha Devetak[1], Nejc Skoporc[2], Martin Rigler[2], Zdenka Peršin[1,3], Irena Drevenšek-Olenik[2,4], Martin Čopič[2,4], Karin Stana-Kleinschek[1,3]**

[1]Co PoliMaT, Tehnološki park 24, SI-1000 Ljubljana, Slovenia
[2]Faculty of Mathematics and Physics, University of Ljubljana, Jadranska 19, SI-1000 Ljubljana, Slovenia
[3]Faculty of Mechanical Engineering, University of Maribor, Smetanova 17, SI-2000 Maribor, Slovenia
[4]Department of Complex Matter, Jožef Stefan Institute, Jamova Cesta 39, SI-1000 Ljubljana, Slovenia
miha.devetak@polimat.si

*Prejem rokopisa – received: 2011-09-30; sprejem za objavo – accepted for publication: 2011-10-14*

We investigated water sorption in viscose nonwoven fibres manufactured by Tosama d.d. with the surface density of 175 g/m$^2$. A comparison between untreated fibres and by oxygen plasma treated fibres was made using optical polarization microscopy. Plasma treatment was done for 10 minutes at pressure of 75 Pa at current of 250 mA at the power of 500 W. Swelling was characterized by measurements of fibre diameter. Modifications of intensity of the polarized light transmitted through the fibre were measured as a function of time of exposure to water. Characteristic swelling and intensity modification times were resolved for untreated and oxygen plasma treated fibres. The swelling time of oxygen plasma in comparison to untreated plasma is reduced by the factor of 0.54 and intensity change time by the factor of 0.4. From the characteristic swelling and intensity change times it was concluded that oxygen plasma treatment of viscose increases the speed of water sorption.

Keywords: plasma treatment, viscose, swelling, optical polarization microscopy

Proučevali smo sorpcijo vode pri vlaknih v viskozni kopreni, ki jo proizvaja podjetje Tosama d.d., s površinsko gostoto 175 g/m$^2$. Primerjali smo neobdelana in s kisikovo plazmo obdelana vlakna z uporabo optično-polarizacijske mikroskopije. Plazemska obdelava je trajala 10 minut pri tlaku 75 Pa, toku 250 mA in pri moči 500 W. Nabrekanje viskoznih vlaken smo opazovali preko sprememb premera vlakna. Z optično polarizacijsko mikroskopijo smo merili spremembe intenzitete polarizirane svetlobe, ki potuje skozi vlakno med močenjem. Iz meritev na neobdelanih in s plazmo obdelanih vlaknih smo ocenili karakteristične čase nabrekanj vlaken in spremembe intenzitete polarizirane svetlobe, ki potuje skozi vlakna. Pri s plazmo obdelanih vlaknih se časi nabrekanja zmanjšajo za faktor 0.54 in čas spremembe intenzitete za 0.4. Iz meritev smo zaključili, da obdelava s kisikovo plazmo pohitri proces sorpcije vode.

Ključne besede: plazemska obdelava, viskoza, nabrekanje, optična polarizacijska mikroskopija

## 1 INTRODUCTION

The importance of viscose fibres in medical, sanitary, textile and construction industry is vastly increasing. Viscose fibres are often chemically treated to improve their wettability. Especially the surface layers of fibre structure have to be modified to achieve higher uptakes of liquids.[1] Chemical treatment of fibres to alter their physical properties can be ecologically questionable and expensive. An environmental friendly alternative to chemical treatment is plasma treatment of viscose veils.[2] Viscose nonwoven exposed to oxygen plasma exhibit modified surface layers in comparison to untreated viscose nonwoven fibres.[3–7] The same applies to numerous other textiles as well as organic materials. [8–13] Surface and internal structure modifications are reflected in altered physical and sorptive properties of material that are very important for production of napkins, tampons, tissues, waddings and other sanitary materials. Viscose contains high level of crystalline structure and some amorphous regions, which are responsible for the accessibility of water binding groups.[14] To increase the performance of viscose fibres a variety of chemical compounds is used to introduce new functional groups or compounds to the fibres.[15]

Current fibre treatment analysis focuses mainly on measurements of properties like water retention, water contact angle, braking force and elongation[3]. We focused mainly on changes of optical properties, which can be related to fibre treatment.[16–21] Optical polarization microscopy (OPM) is a contrast enhancing technique that improves the quality of the images of birefringent materials.[22,23] OPM uses the concept of two polarizers oriented at right angles with respect to each other, commonly termed as crossed polarization. The most notable application of OPM is to examine birefringent or doubly refractive specimens. To determine quantitative aspects of the observed specimen with birefringent properties, the optical axis of the sample should be rotated at the angle of 45° with respect to the analyser to achieve maximum brightness. The surrounding isotropic material remains dark, providing basis for the analysis of birefringent material only.[24]

Our aim was to analyse the light transmission changes trough fibre and swelling using highly sensitive recording camera.

## 2 EXPERIMENTAL METHODS

The material used was a Tosama d.d. viscose nonwoven fibre with the average nonwoven sample surface density of 175 g/m$^2$.[3,4] The fibres were stored in a sealed environment.

### *2.1 Oxygen plasma treatment*

Viscose non-woven samples were mounted into the discharge chamber of a plasma system. The chamber is pumped with a two stage rotary pump with a pumping speed of 60 m$^3$/h. The chamber was pumped down to the ultimate pressure which was about 10 Pa. Weakly ionized plasma was created in the discharge chamber by an inductively coupled radiofrequency (RF) discharge.[25–27] The RF generator operates at a frequency of 27.12 MHz and nominal power up to 5000 W. The power absorbed by plasma is adjustable by a matching unit. At these particular experimental conditions the absorbed power was about 500 W. The plasma parameters were estimated by electrical and catalytic probes.[28–32] When oxygen is applied as the working gas and the pressure in the system is 75 Pa, the electron temperature is about 3 eV, the density of charged particles (predominantly $O_2^+$) is about $1 \times 10^{15}$ m$^{-3}$ and the dissociation fraction of oxygen molecules is about 10%. Samples were kept in plasma for 10 min. The nonwoven sample was then sealed and stored in plastic containers at room temperature until used in experiments. An untreated viscose nonwoven was also sealed and stored under the same condition until used in experiments.

### *2.2 Optical polarization microscopy imaging and analysis*

Optical polarization imaging was done with a Nikon Polarizing Microscope Optiphot2-pol. Viscose fibres were fixed between object and cover microscopy glass to enable stable focusing of a specific part of the fibre or the entire fibre depending on the magnification. The glass plates were glued by epoxy two component glue leaving small holes for water injection. For long term measurements these holes were sealed with a silicon lubricant to prevent water leakage and evaporation. High resolution video recordings of the time evolution of wetting process were captured by the high resolution video camera (PixeLINK Monochrome Machine Vision Camera) that enables recording 8 frames per second. The recordings were made in two regimes: cross polarizer-analyser configuration and parallel polarizer-analyser arrangement. The fibre axis was oriented at 45° with respect to the polarizer direction to get the maximal intensity output even during cross-polarization measurements. When the fibre was put in contact with water, the intensity of the transmitted light changed, which was ideal for quantitative analysis of kinetics of the water sorption process. The recorded high resolution movies were decomposed into frames, followed by frame to frame analysis of the transmitted intensity values of a selected region of the fibre. To enable statistical analysis several fibres were analysed and for each fibre several regions were investigated to avoid any anomalies that can occur due to the morphological inhomogeneity in some fibre parts. Frame by frame intensity analysis was made by using Matlab software environment. The exponential growth function was used in fitting procedures to obtain characteristic time of the wetting process. Swelling changes were determined by usage of ImageJ programme.

## 3 RESULTS

In **Figure 1** an example of the time evolution of the swelling process of an untreated viscose fibre is presented from 8 selected frames. Fibre diameter was determined and a relative radius was plotted versus time the fibre was exposed to water. **Figure 2** shows time evolution curves of the relative radius values for the treated and untreated viscose fibres.

**Figure 3** shows the wetting process of a viscose fibre. The selection squares indicate the image area where the normalized intensity of transmitted light was calculated from.

Frame by frame intensity values provide information on kinetics of the sorption process. In **Figure 4** the normalized intensity versus wetting time is presented for untreated and plasma treated viscose fibres.

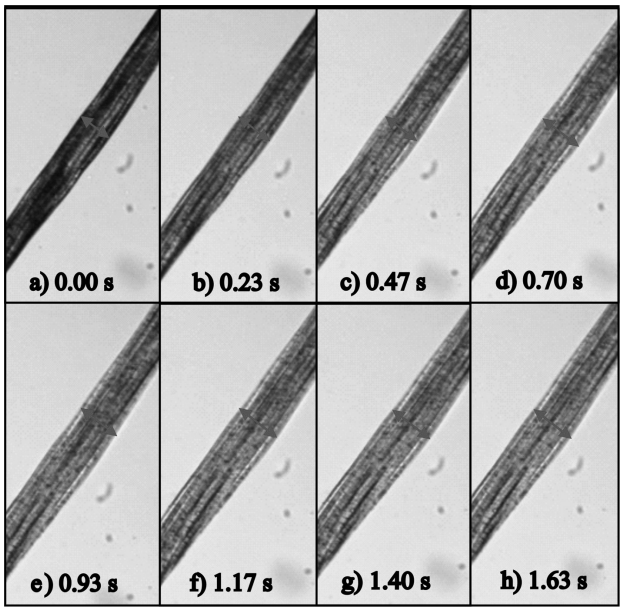


**Figure 1**: Observation of the wetting process under parallel polarizers. The dependence of fibre diameter versus time, when the untreated fibre is exposed to water. The image sequences a)–h) display the swelling of the fibre after introducing water at t = 0.00 s.

**Slika 1**: Premer viskoznega vlakna v odvisnosti od časa, ko je vlakno izpostavljeno vodi. Zaporedje slik a)–h) prikazuje nabrekanje vlakna z začetkom močenja ob t = 0.00 s.

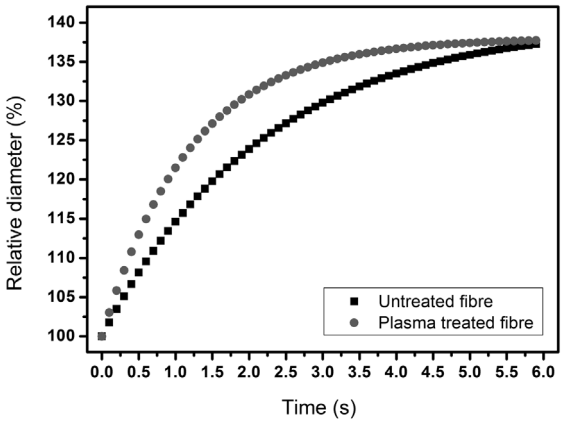


**Figure 2**: The relative diameter of viscose fibre versus the time, when water was introduced to the fibre for untreated and plasma treated viscose fibres

**Slika 2**: Relativni premer viskoznega vlakna v odvisnosti od časa, ko je vlakno izpostavljeno vodi za neobdelana in s plazmo obdelana vlakna

To obtain characteristic swelling times for treated and untreated viscose fibres a fitting function of exponential saturation was used:

$$R(t) = R_0 + \Delta R(1 - e^{-t/\tau_R}) \quad (1)$$

where the $R(t)$ represents the relative radius at time $t$, $R_0$ = 100 % is the relative radius of a dry fibre, the $\Delta R$ represents the relative changes of radius before and after the wetting process takes place and the $\tau_R$ represents the time in which the fibre becomes swollen.

To obtain characteristic intensity changing times for treated and untreated viscose fibres a fitting function of exponential saturation was used:

$$I(t) = \Delta I(1 - e^{-t/\tau_I}) \quad (2)$$

where the $I(t)$ represents the normalized intensity at time $t$, the $\Delta I$ represents the normalized changes of intensity before and after the wetting process takes place and the $\tau_I$ represents the time in which the intensity changes.

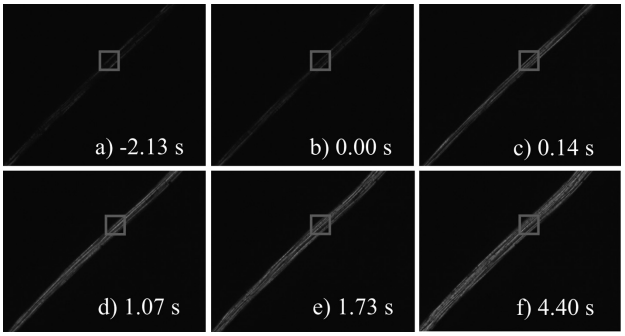


**Figure 3**: Image sequence a)–f) attained in cross-polarized. At time 0.00 s the water was introduced to the fibre. The squares represent the areas for normalized intensity calculation of the light transmitted through the fibre.

**Slika 3**: Zaporedje slike viskoznega vlakna a)–f). Polarizator in analizator sta bila prekrižana. Ob času 0.00 s je vlakno bilo izpostavljeno vodi. Okviri na slikah predstavljajo površino, ki je bila izbrana za izračun normalizirane intenzitete svetlobe, ki je potovala skozi vlakno.

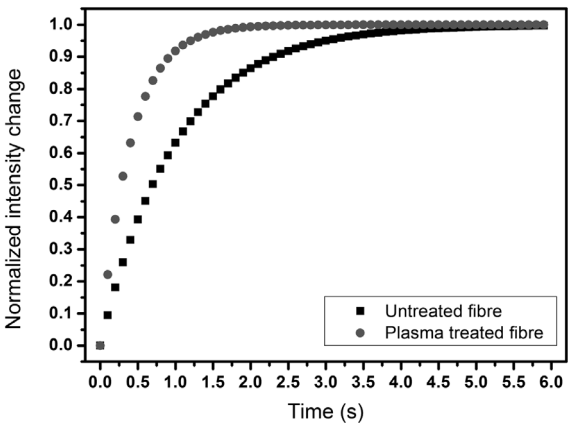


**Figure 4**: The normalized intensity of the polarized light that was passing through the viscose fibre versus the time, when the water was introduced to the fibre for untreated and plasma treated fibres.

**Slika 4**: Normalizirana intenziteta polarizirane svetlobe, ki je potovala skozi viskozno vlakno v odvisnosti od časa, ko je bilo vlakno izpostavljeno vodi. Slika prikazuje normalizirano intenziteto za neobdelana in s plazmo obdelana vlakna.

In **Table 1** the average values of $\tau_R$ and $\tau_I$ are displayed. They were calculated from data obtained in analysis from graphs, such as in **Figure 2** and **Figure 4**.

**Table 1**: Characteristic response times for untreated and plasma regenerated viscose fibres when exposed to water

**Tabela 1**: Karakteristični odzivni časi za neobdelana in s plazmo obdelana vlakna, ko jih začne močiti voda

| Fibre treatment | Untreated | Plasma |
|---|---|---|
| $\tau_R$ (s) | 2.2 ± 0.8 | 1.2 ± 0.2 |
| $\tau_I$ (s) | 1.0 ± 0.3 | 0.4 ± 0.1 |

## 4 DISCUSSIONS

The viscose fibre consists of micro fibrils. The water sorption is dependent on the accessibility of amorphous regions to the water, and the water accessibility to the space between the micro fibrils.[18] The content of carboxyl group increases with plasma treatment which increases the wettability of the fibre.[33] Fibre morphology due to the sub-fibre structure makes the fibres optical properties more complex.[23] The intensity of the light transmitted trough the fibre in crossed-polarized regime changes during wetting, since water sorption changes fibre's optical properties. Experimentally obtained characteristic intensity change times indicate the velocity of internal structure change while the water is introduced to the fibre. The swelling of the fibre is also an indicator for water sorption.[18] As water is absorbed, the water bound into cell wall exerts a swelling pressure, resulting in increase of the volume of the material.[34] The difference between swelling times and intensity change times indicate that we have to differentiate between internal changes of optical properties in the fibre and swelling during water sorption. Namely the sorption process

results in several modifications of fibre mechanical and optical properties.[18] Oxygen plasma treatment modifies the fibre's surface, making it more susceptible to faster water sorption.[33] The changes of properties of modified viscose fibres with chemical treatment like bleaching and slack mercerization can be compared with plasma treatment modifications.[35] Comparable increase of hydrophilicity in comparison to chemical treatment was achieved by plasma modifications of viscose non-woven fibres. Measurements of contact angle, surface energy and polar interactions were performed in previous research to compare plasma treatment effects with different chemical treatment for sorption of water and other fluids.[35] Water retention and improvement of some of the physical properties after oxygen plasma treatment was also studied.[3] On the basis of the experiments described in previous research in addition to this this article it can be stated that oxygen plasma treatment is a viable alternative to chemical treatment of fibres to increase the kinetics of water sorption.[3,18,33,35]

## 5 CONCLUSIONS

Oxygen plasma treatment of viscose fibres increases the kinetics of water sorption, making it a promising candidate for substitution of chemical treatment. The swelling time of oxygen plasma in comparison to untreated plasma is reduced by the factor of 0.54 and intensity change time by the factor of 0.4. Findings, obtained with the optical polarization microscopy approach, agree with the other research done on comparison between chemical and plasma treatment of viscose fibres, making plasma treatment an alternative procedure of viscose nonwoven modification in sanitary and medical applications, which require faster water sorption kinetics.

### Acknowledgements

This work was supported by the Ministry of Higher Education, Science and Technology of the Republic of Slovenia, Grant number 3211-10-000057, (Centre of Excellence Polymer materials and Technology).

## 6 REFERENCES

[1] U. Vrabič, A. Jesih, D. G. Svetec, Physical and Absorptive Changes in Plasma Treated Viscose Fibres, Fibres and Textiles in Easter Europe, 15 (**2007**) 5–6, 64–65

[2] G. Primc, R. Zaplotnik, A. Vesel, M. Mozetič, Microwave discharge as a remote source of neutral oxygen atoms, AIP Advances, 1 (**2011**) 2, 022129

[3] K. Stana-Kelinschek, Z. Peršin, T. Maver, Modification of non-woven cellulose form medical applications using non-equilibrium gaseous plasma, Mater. Tehnol., 45 (**2011**) 3, 253–257

[4] A. Vesel, M. Mozetič, S. Strnad, Z. Peršin, K. Stana-Kleinschek, N. Hauptman, Plasma modification of viscose fibre, Vacuum, 84 (**2010**), 79–82

[5] M. Gorjanc, V Bukošek, M. Gorenšek, A. Vesel The influence of water vapor plasma treatmenton specific properties of bleached and mercerized cotton fabric. Tex. Res. J., 80 (**2010**) 6, 557–567

[6] A. Vesel, M. Mozetič, A. Hladnik, J. Dolenc, J. Zule, S. Miloševic, N. Krstulovic, M. Klanjšek Gunde, N. Hauptman. Modification of ink-jet paper by oxygen-plasma treatment. J. Phys. D: Appl. Phys., 40 (**2007**), 3689–2696

[7] M. Gorjan, V. Bukošek, M. Gorenšek, M. Mozetic. CF4 plasma and silver functionalized cotton.Tex. Res. J., 80 (**2010**) 20, 2204–2213

[8] A. Vesel, Modification of polystyrene with a highly reactive cold oxygen plasma. Surf. Coat. Technol., 205 (**2010**) 2, 490–497

[9] T. Vrlinic, A. Vesel, U. Cvelbar, M. Krajnc, M. Mozetic. Rapid surface functionalization of poly(ethersulphone) foils using a highly reactive oxygen-plasma tretament. Surf. Interface Anal., 39 (**2007**) 6, 476–481

[10] A. Vesel, I. Junkar, U. Cvelbar, J. Kovac, M. Mozetic. Surface modification of polyester by oxygen-and nitrogen-plasma treatment. Surf. Interface Anal., 40 (**2008**) 11, 1444–1453

[11] I. Junkar, U. Cvelbar, A. Vesel, N. Hauptman, M. Mozetic. The role of crystallinity on polymer interaction with oxygen plasma. Plasma Processes Polym., 6 (**2009**) 10, 667–675

[12] A. Vesel, K. Elersic, I. Junkar, B. Malic, Modification of a polyethylene naphthalate polymer using an oxygen plasma treatment, Mater. Tehnol., 43 (**2009**) 6, 323–326

[13] A. Vesel, XPS study of surface modification of different polymer materials by oxygen plasma treatment, Inf. MIDEM, 38 (**2008**) 4, 257–265

[14] D. Ciolacu, F. Ciolacu, V. I. Popa, Amorphous Cellulose – structure and characterization, Cellulose Chemistry and Techniology, 45 (**2011**) 1–2, 13–21

[15] J. V. Edwards, G. Buschle-Diller S. C. Goheen, Modified Fibers with Medical and Specialty Applications, **2006**, Springer, 240p

[16] I. M. Fouda, A. H. Oraby, E. A. Seisa, Some Parameters Characteristics of Thermally Treated Viscose Fibres, Journal of Applied Polymer Science, 118 (**2010**), 1306–1312

[17] C. Alvarez-Lorenzo, J. L. Gomez-Ampza, R. Martinez.Pacheco, C. Souto, A. Concheiro, Interactions between hydroxypropylcelluloses and vapour/liquid water, European Journal of Pharmaceutics and Biopharmaceutics, 50 (**2000**), 307–318

[18] Y. Xie, C. A. S. Hill, Z. Jalaludin, D. Sun, The water vapour sorption behaviour of three celluloses: analysis using parallel exponential kinetics and interpretation using the Kelvin-Voight viscoelastic model, Cellulose, 18 (**2011**), 517–530

[19] I. M. Fouda, E. A. Seisa, Optomechanical properties of the morphology of viscose fibers due to the Cold-Drawing process, Journal of Applied Polymer Science, 110 (**2008**), 872–879

[20] I. M. Fouda, E. A. Seisa, Birefringence and orientation parameters of cold-drawn viscose fibers, Journal of Applied Polymer Science, 106 (**2007**), 1768–1776

[21] Y. Yang, A. Kloczkowski, J.E. Mark, B. Erman, I Bahar, Experimental studies of elastomeric and optical properties and strain induced liquid-crystalline phase transitions, in deformed (hydroxypropyl) cellulose networks in the swollen state, Macromolecules, 28 (**1995**), 4927

[22] S. Ross, R. Newton, Y. M. Zhou, J. Haffegee, M. W. Ho, J. P. Bolton, D. Knight, Quantitative image analysis of birefringent biological material, Journal of Microscopy 187 (**1997**), 62–67

[23] R. Oldenbourg, A new view on polarization microscopy, Nature 381 (**1996**), 811–812

[24] R. Weaver, Rediscovering Polarized Light Microscopy, American Laboratory 35 (**2003**), 55–61

[25] R. Zaplotnik, A. Vesel, M. Mozetic. Transition from E to H mode in inductively coupled oxygen plasma : hysteresis and the behaviour of oxygen atom density. Europhys. Lett., 95 (**2011**) 5, 55001-1–55001-5

[26] R. Zaplotnik, A. Vesel, Radiofrequency induced plasma in large-scale plasma reactor, Mater. Tehnol., 45 (**2011**) 3, 227–231

[27] A. Drenik, U. Cvelbar, A. Vesel, M. Mozetic. Weakly ionized oxygen plasma. Inf. MIDEM, 35 (**2005**), 85–91

[28] M. Balat-Pichelin, A. Vesel, Neutral oxygen atom density in the MESOX air plasma solar furnace facility. Chem. Phys., 327 (**2006**), 112–118

[29] M. Mozetic, A. Vesel, A. Drenik, I. Poberaj, D. Babic, Catalytic probes for measuring H distribution in remote parts of hydrogen plasma reactors. J. Nucl. Mater., 363–365 (**2007**), 1457–1460

[30] A. Vesel, M. Mozetic, A. Drenik, M. Balat-Pichelin, Dissociation of $CO_2$ molecules in microwave plasma. Chem. Phys., 382 (**2011**) 1/3, 127–131

[31] G. Primc, R. Zaplotnik, A. Vesel, M. Mozetic, Microwave discharge as a remote source of neutral oxygen atoms. AIP advances, 1 (**2011**) 2, 022129-1–022129-11

[32] A. Drenik, A. Tomeljak, M. Mozetic, A.Vesel, D. Babic, M. Balat-Pichelin, Behaviour of neutral hydrogen atom density in the presence of a sample holder in a plasma reactor. Vacuum, 1 (**2009**), 90–93

[33] R. M. A. Malek, I. Holme, The effects of plasma treatment on some properties of cotton, Iranian Polymer Journal, 12 (**2003**) 4, 271–280

[34] H. L. Boss, A. M. Donald, In situ ESEM study of the deformation of elementary flax fibres, J. Matter Sci. 34 (**1999**), 3029–3034

[35] Z. Peršin, P. Steinus, K. Stana-Kleinschek, Estimation of the Surface Energy of Chemically and Oxygen Plasma-Treated Regenerated Cellulosic Fabrics using various Calculation Models, Tex. Res. J., 81 (**2011**) 16, 1673–1685

UDK 533.9:66.017
Original scientific article/Izvirni znanstveni članek

ISSN 1580-2949
MTAEC9, 46(1)75(2012)

# BINDING SILVER NANO-PARTICLES ONTO VISCOSE NON-WOVEN USING DIFFERENT COMMERCIAL SOL-GEL PROCEDURES

## VEZAVA SREBROVIH NANO-DELCEV NA VISKOZNO KOPRENO Z RAZLIČNIMI KOMERCIALNIMI SOL-GELI

**Tanja Pivec[1,2], Zdenka Peršin[2,3], Silvo Hribernik[3], Tina Maver[2,3], Mitja Kolar[2,4], Karin Stana-Kleinschek[2,3]**

[1]Predilnica Litija d.o.o., Kidričeva 1, SI-1270 Litija, Slovenia
[2]Center of Excellent PoliMat, Tehnološki park 24, SI-1000 Ljubljana, Slovenia
[3]Faculty of Mechanical Engineering, University of Maribor, Smetanova 17, SI-2000 Maribor, Slovenia
[4]Faculty of Chemistry and Chemical Engineering, University of Maribor, Smetanova 17, SI-2000 Maribor, Slovenia
karin.stana@uni-mb.si

*Prejem rokopisa – received: 2011-09-30; sprejem za objavo – accepted for publication: 2011-10-07*

The paper presents possible solution of Ag binding using commercial sol-gel systems which enable its low release into a wound, providing a good antimicrobial effect on those bacterial cultures that are most likely present in the wound. The influence of different sol-gel systems on the hydrophilic properties of carrier materials and the level of released silver has been studied. The results showed that sol-gel as binding-systems could provide proper hydrophilic properties of material, whilst binding silver strongly enough providing at the same time excellent antimicrobial activity of the treated viscose meterials.

Keywords: silver nano-particles, sol-gel, viscose non-woven, silver release, hydrophilicity, antimicrobial properties

V prispevku je predstavljana ena izmed možnih rešitev za uporabo srebra z majhnim sproščanjem v rano, pri čemer se je dosegel dober protimikrobni učinek na bakterijske kulture, ki se v rani najpogosteje pojavljajo. Uporabili smo komercialne sol-gel sisteme s katerimi smo inkorporirali srebrove nano-delce na viskozo. Spremljali smo vpliv različnih sol-gelov na hidrofilne lastnosti nosilnega materiala in raven sproščenega srebra. Rezultati so pokazali, da lahko uporaba sol-gel sistema zagotovi dobre hidrofilne lastnosti in obenem dovolj močno veže srebro, ki daje odlične protimikrobne lastnosti obdelanemu materialu.

Ključne besede: srebrovi nanodelci, sol-gel, viskozna koprena, sproščanje srebra, hidrofilnost, protimikrobne lastnosti

## 1 INTRODUCTION

The skin is an extremely effective biological barrier but if breached by trauma, the body becomes highly susceptible to microbial attack. Certainly, wound infection presents one of the major problems and can evolve into different serious medical complications. Treatment with silver-content wound dressings is becoming an increasingly popular strategy for eliminating the growth of opportunistic wound pathogens during the healing process. Silver has been known as a very effective natural antibiotic and for centuries has been in use for the treatment of burns and serious wounds. The antimicrobial property of silver is related to the amount of silver and the rate of silver released. Silver in its metallic state is inert but it reacts with the moisture in the skin and the fluid of the wound and becomes ionized. The ionized silver is highly reactive, as it binds to tissue proteins and causes structural changes in the bacterial cell wall and nuclear membrane (nucleolemma orkaryotheca), leading to cell distortion and death. Silver also binds to bacterial DNA (deoxyribonucleic acid) and RNA (ribonucleic acid) by denaturin, and inhibits bacterial replication. Recently, due to the emergence of antibiotic-resistant bacteria and limitations on the use of antibiotics, clinicians have started to implement silver into wound dressings containing varying levels of silver[1–4]. Ag NPs (silver nano-particles) have emerged as an important class of nano-materials over a wide range of industrial and medical applications, but nevertheless they present a potential risk to human health. In vitro studies have reported that Ag NPs produce toxicity targeted at a variety of organs including the lungs, liver, brain, vascular system and reproductive organs. Ag NPs have induced the expressive level of those genes involved in cell cycle progression and apoptosis. The possible mechanisms of Ag NPs toxicity include the induction of ROS (reactive oxygen species), oxidative stress, DNA damage and apoptosis[5–8]. Therefore, silver release is very important for antimicrobial activity, but only in a controlled manner, due to toxicity.

The sol-gel process is one of the possible methods for incorporating Ag NPs onto cellulose matrices as viscose, and for the attainment of controlled Ag release. The sol-gel technique is a suitable method for incorporating homogeneously bioactive compounds, biomolecules and even whole living cells, into metal oxide matrices[9–13]. In comparison with organic matrices, inorganic sol-gel matrices provide higher mechanical, thermal, chemical and photochemical stability and are toxicologically and biologically inert, i.e., they are not a food source for microorganisms[13–15].

In presented study insignificant Ag release from treated samples in a controlled manner was attained, using commercial sol-gel systems for the incorporation of Ag NPs on viscose non-woven, which is sufficient for providing good antimicrobial activity, as well as a proper hydrophilicity of viscose non-woven.

## 2 EXPERIMENTAL

### *2.1 Preparation*

#### *2.1.1 Materials*

A 100 % viscose non-woven (Kemex, The Netherlands) with a mass of 175 g/m$^2$ was used during the experiments. Ag NPs were incorporated onto viscose using different sol-gel procedures. Silver nano-particles in AgCl form, iSys Ag (CHT, Germany) were used as an antimicrobial agent in combination with iSys MTX or iSys LTX (CHT, Germany) being organic-inorganic binders. Kollasol CDO (CHT, Germany) was used as a wetting agent.

#### *2.1.2 Viscose non-woven treatment*

Firstly, the solutions of binder and silver nano-particles were prepared. The composition of the solution is shown in **Table 1**.

**Table 1:** The composition of the treatment solutions
**Tabela 1:** Sestava obdelovalne raztopine

| sample | 5 g/L iSys Ag | 5 g/L iSys MTX | 5 g/L iSys LTX | 0,7 g/L Kollasol |
|---|---|---|---|---|
| S1 | ✓ | ✓ | | |
| S2 | ✓ | | ✓ | |
| S3 | ✓ | | ✓ | ✓ |

10 g of viscose non-woven was impregnated in 300 mL of solution for 1 h at room temperature. After treatment, the viscose was wrung-out with a foulard (Werner Mathis Ag, Switzerland), dried in an oven in a stretched state at 80 °C, and also condensed for 1 min at 150 °C (Werner Mathis Ag, Switzerland).

### *2.2 Methods*

#### *2.2.1 Inductively-coupled plasma using mass spectroscopy (ICP/MS)*

The concentrations of Ag on the viscose samples were determined by inductively-coupled plasma using mass spectroscopy (ICP/MS).

7 mL of $HNO_3$ (s.p.) and 1 mL of $H_2O_2$ (s.p.) were added to 100 mg of sample. The microwave system Milestone Ethos® touch control with a segmented rotor for high pressures (HPR – 1000/10S) was used for digestion of the samples. The sample digestion was performed over two steps: step 1 – sample was heated to 200 °C (1000 W) for 10 min, step 2 – the temperature was kept stable at 200 °C (1000 W) for 10 min. After digestion the sample was diluted to 50 mL with 1% $HNO_3$. Further dilutions were automatically performed with 1% $HNO_3$ to adjust the measuring ranges (10 / 50 / 100 µg/L) of the Ag solutions.

A Perkin Elmer® Sciex Elan DRC-e was used for ICP/MS analysis. The instrumental and acquisition parameters were: RF power 1125 W, lens voltage 12,75 V, argon gas flow: nebulizer 0,95 L/min, auxiliary 1,20 L/min, plasma 15 L/min, dwell time 50 ms and number of sweeps 20. Three replicates of the samples were measured using the peak-hopping measuring mode (one point per peak) at an integration time of 1000 ms. The reference element (Rh) at a concentration of 10 µg/L was used as internal standard.

#### *2.2.2 Atomic absorption spectroscopy (AAS)*

Ag concentration in milli-Q solution after the Ag release from viscose samples was determined using atomic absorption spectroscopy (Perkin-Elmer AAnalyst 600). An atomic absorption spectrometer equipped with an air-acetylene burner and silver hollow cathode lamp operating at 5 mA was used for determining silver without background correction. The operating conditions were as follows: wavelength: 328.1 nm, band pass: 0.7 nm, flow rate of acetylene: 2.5 L/min, and thr flow-rate of air: 8 L/min.

A stock standard solution of silver (500 mg/L) was prepared by dissolving the appropriate amount of silver nitrate ($AgNO_3$) in water with 1 % (v/v) $HNO_3$. The working standard solutions were prepared by dilution.

#### *2.2.3 In vitro silver release*

In vitro release studies were performed using static diffusion cells, according to Franz[16]. The receptor compartment had a mean volume of 7,5 mL, filled with milli-Q water, and its temperature was maintained at 37 °C by stirring of termostated water surrounding the cell.

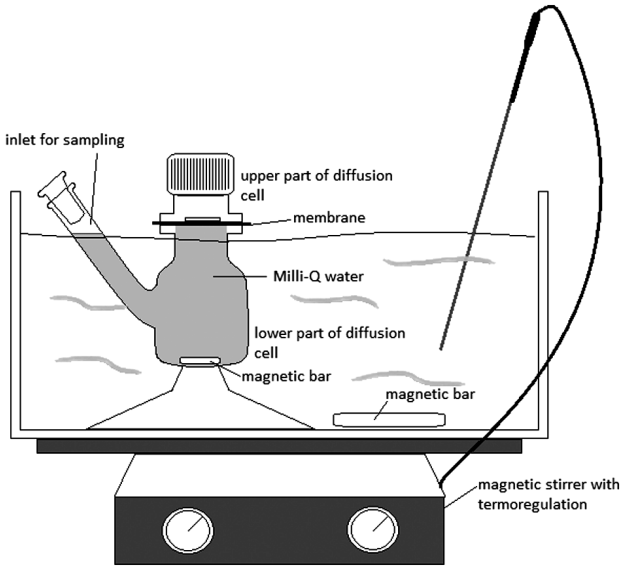


**Figure 1:** Thermoregulated system of Franz diffusion cell
**Slika 1:** Termoregulacijski sistem s Frazevo difuzijsko celico

This temperature value was chosen in order to reproduce the human temperature under normal conditions. The Ag release was determined after 24 h. The thermoregulation system of the Franz diffusion cell, is presented in **Figure 1**.

*2.2.4 Tensiometry*

The hydrophilic/hydrophobic character was studied by contact angle measurements between the polymer material samples and water. The Powder contact angle method was used as developed for determining the wetting properties of porous materials. The samples were cut into 2 × 5 cm rectangular pieces and suspended in a special sample holder of a Krüss K12 processor Tensiometer. Immediately before measurement, the container with the liquid (n-heptane; water) was raised until the sample edge touched the liquid surface.

The change in samples' mass *(m)*, as a function of time *(t)* during the water adsorption phase, was monitored. The initial slope of the function $m^2 = f(t)$ is known as the capillary velocity, from which the contact angle between the solid (polymer sample) and the water was calculated using a modified Washburn equation[17]:

$$\cos\theta = \frac{m^2}{t} \cdot \frac{\eta}{\rho^2 \cdot \gamma \cdot c} \quad (1)$$

where $\theta$ is the contact angle between the solid and liquid phases, $m^2/t$ is the capillary velocity, $\eta$ is the liquid viscosity, $\rho$ is the liquid density, $\gamma$ is the surface tension of the liquid, and $c$ is a material constant.

For more detailed description of this experimental method, see Persin et al.[18] and Fras Zemljic et al.[19,20].

*2.2.5 Reduction of bacteria*

The antimicrobial effect of viscose non-woven loaded with AgNPs on gram-negative bacteria *Escherichia coli* and *Pseudomonas aeruginosa* and on gram-positive bacteria *Staphylococcus aureus* and *Enterococcus faecalis* was investigated by modified AATCC 100-1999 standard method. These bacteria were chosen as being the most frequently isolated micro-organisms from skin wounds in humans[21–23].

Circular swatches (4,8 cm in diameter) of viscose samples were put into a 70 mL container and inoculated with 1.0 mL of inoculums containing 1–2 · $10^5$ colony forming units of bacteria. After incubation at 37 °C for 24 h, the bacteria were eluted from the swathes by shaking in 50 mL of sterilized water for 1 min. 0,1 mL of these suspensions (2 · $10^2$ cfu) and diluted suspensions with physiological solution (2 · $10^1$ cfu) were plated on trypticase soy agar (TSA) and incubated at 37 °C for 24 h. Afterwards the number of bacteria was counted and the reduction of bacteria, *R*, was calculated as follows:

$$R = \frac{B - A}{b} \times 100\ (\%) \quad (2)$$

where *A* is the number of bacteria recovered from the inoculated swatch of the viscose sample in the plastic container incubated over the desired contact period (24 h) and *B* is the number of bacteria recovered from the inoculated swatch of the viscose sample in the container immediately after inoculation (at "0" contact time).

## 3 RESULTS

The amount of silver on the viscose samples and amount of silver in the milli-Q solutions after Ag release from the samples, are shown in **Figure 2**.

Although the amount of silver in the treated solutions was the same for all samples, the concentrations of Ag on the treated fibres differed. The highest measured concentration of silver was detected for sample S3.

Independent of the binding procedure (using different sol-gel systems) the amount of released silver was very low. All the measured concentrations were at or below the detection limit (LOD) of AAS.

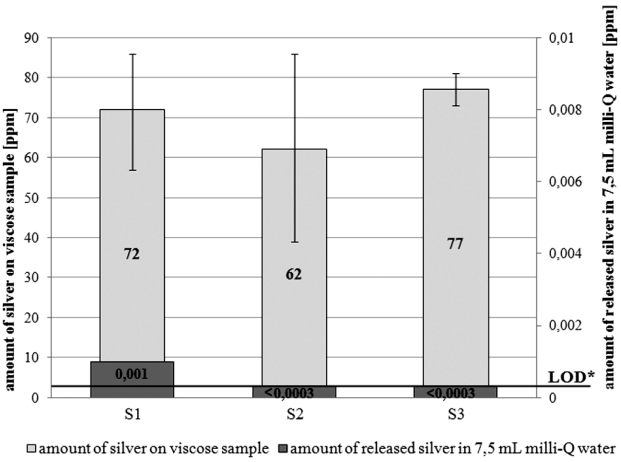


*LOD: less than 0,05 mg /L (or 0,0003 ppm Ag in 7,5 mL of the milli-Q solution)

**Figure 2:** The amount of silver on the viscose samples, and amount of silver in the milli-Q solutions after Ag release from the samples

**Slika 2:** Vsebnost srebra na viskozni kopreni in vsebnost srebra v milli-Q raztopini po sproščanju srebra iz vzorcev

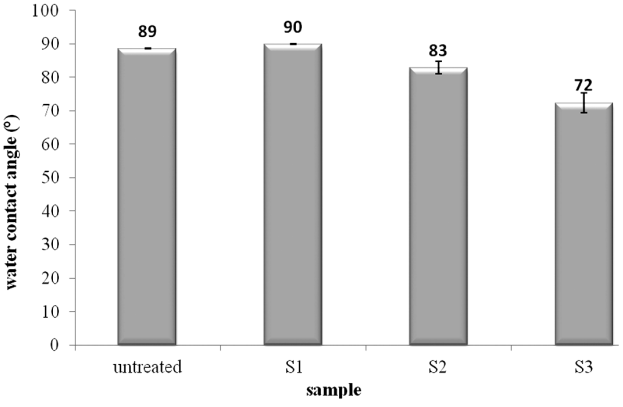


**Figure 3:** Water contact angle

**Slika 3:** Stični kot med vodo in vzorcem

The water contact angles for the untreated sample and with the silver treated samples, are shown in **Figure 3**.

The contact angle of sample S1 was higher than that of the untreated one. An improvement in the hydrophilic properties can be observed for both the other samples. The contact angle for sample S3 decreased by 19 %.

The results of antimicrobial activity for the untreated and with silver-treated viscose samples, are presented in **Table 2**.

**Table 2:** Reduction, *R*, of bacteria determinate according to the AATCC 100-1999 standard method

**Tabela 2:** Redukcija, *R*, bakterij, določena po AATCC100 – 1999 standardni metodi

| sample | Reduction, *R* (%) | | | |
|---|---|---|---|---|
| | *Staphylococcus aureus* (G+) | *Escherichia coli* (G-) | *Pseudomonas aeruginosa* (G-) | *Enterococcus faecalis* (G+) |
| **untreated** | No reduction | No reduction | No reduction | 77 |
| **S1** | 100 | 100 | 98,8 | 100 |
| **S2** | 100 | 100 | 100 | 100 |
| **S3** | In regard to the concentration of silver on this sample, the same antimicrobial activity as for other samples can be predicted. | | | |

As expected, no reduction of the bacteria *S. aureus*, *E. Coli* and *P. aeruginosa* was found for the untreated viscose sample. The reduction of *E. faecalis* was 77 %. All the silver-treated samples showed excellent antimicrobial activity. Sample S3 was not tested. In regard to the concentration of silver on this sample, the same antimicrobial activity as for other samples can be predicted.

## 4 DISCUSSION

Existing studies of the binding of silver to fibrous materials[12–14] using a sol-gel procedure show that the selection of this method is a good solution for the development of materials intended for the treatment of open wounds. Sol-gel systems vary significantly in their chemical composition. Differently chemically modified sol-gels therefore act differently and can thermally and chemically change or improve the material to which they were bound. Thus, a sol-gel system that will provide the desired properties can be chosen with regard to the intended purpose of the material. For example, in order to achieve hydrophilicity of a material intended for wound dressings for faster wound healing, sol-gel precursors that are completely hydrolysed can be chosen. Sol-gels containing derivates with long alkyl chains, phenol rings or fluorine[13] work the opposite way (are hydrophobic). Commercial products that give textile materials such properties are already available on the market.

In our research commercial sol-gel systems produced by CHT (Germany) were used. Our aim was to observe how differently chemically modified sol-gel systems affect the quantity of the adsorbed silver on the material, and its release from the material. Dispersion of AgCl nanoparticles (iSys Ag) was used as the source of silver nanoparticles in all samples. The following binding agents were used for binding Ag particles: iSys MTX, a sol-gel system with a hydrophobic character, in the S1 sample, and iSys LTX, a sol-gel system with a hydrophilic character, in the S2 and S3 samples. Kollasol CDO, described by the producer as a hydrophilic silicone surface-active substance mixed with higher alcohols, was also added to the S3 sample.

The selection of the sol-gel has a different influence on the silver adsorption on viscose and, consequently, the amount of Ag on the material, as is evident from **Figure 2**. Discrepancies in the measured concentrations of silver on viscose are, of course, also possible because of measurement errors, but an increase in adsorption of AgCl nanoparticles is expected when using a more hydrophilic sol-gel system. It is clear that the addition of a surfactant (Kollasol CDO) to a hydrophilic cross-linking agent, iSys LTX, in the treatment of the S3 sample increased the concentration of the bound Ag by 6.5 %. The measurement results of silver released also show better adsorption of AgCl nanoparticles when using a hydrophilic sol-gel system. The hydrophilic sol-gel system in combination with a surfactant affects the formation of a three-dimensional network that is created from $SiO_4$ tetrahedrons[24,25] and captures the AgCl nanoparticles in its structure, as well as causes a slight release of silver from viscose (S2 and S3 samples).

It is known that AAS in ICP/MS methods enable the detection of Ag without high measuring error, what is not the case in presented results. The explanation for this we can find in the low solubility of the commercial viscose non-woven due to the commercial coatings residues (on the basic of different polysaccharides). The commercial viscose samples were not soluble good enough in $HNO_3$. We founded out that the use of the $H_2SO_4$ and $HNO_3$ mixture give us a clear solution of dissolved commercial viscose, nevertheless the AAS detected Ag was below 1 ppm. Another used dissolution procedure (dissolving of the commercial viscose non-woven in microwave under the high pressure in the solution of $HNO_3$ and $H_2O_2$) leads to a clear viscose solution, but again the measuring error of ICP/MS detected Ag have been too high. Contrary to described viscose dissolution and connected Ag detection problems, our preliminary studies showed that the pure viscose (without surface coating) could be dissolved very well in the heated $HNO_3$, contrary to commercial viscose non-woven used in this study. The AAS detected Ag, of well dissolved viscose, without measuring error could be obtained.

The hydrophilic/hydrophobic properties of the samples were determined by measuring the contact angles between water and differently treated viscose non-

wovens. The results shown in **Figure 3** confirm that the use of iSys MTX in the S1 sample leads to an increase in the hydrophobic character compared to the untreated sample, while the use of the cross-linking agent iSys LTX increases the hydrophilic properties of cellulose non-wovens by 8 %. These properties are further improved by 19 % with the addition of the wetting agent Kollasol CDO to iSys LTX in the S3 sample. The hydrophilic properties of fibrous materials can also be provided by other methods as the non-equilibrium gaseous plasma treatment that represents a quick technique which could be performed after silver deposition using sol-gel procedure[26–30]. Finally, these must be taken into account in our future development of materials which could be used in wound dressing.

According to the literature, antimicrobial activity of silver is related to its concentration and its release rate[1]; therefore, the antimicrobial activity of our samples on the bacteria most commonly found in wounds[21–23] was also examined. It was established that silver concentrations ranging from 62 ppm to 77 ppm are sufficient to give a viscose non-woven excellent antimicrobial properties, regardless of the strength of its adsorption to viscose and its release, contrary to the literature reports which show that even the application of modern reliable techniques for destruction of bacteria like *S. aureus* and *E. coli* shows limited sterilization efficiencies[31–35]. Furthermore, M. Gorjanc et al. studied similar effects on textiles and never found 100 % bacteria reduction[26]. Contrary to this report S. Strnad at al. found out that even pure viscose shows antimicrobial activity on some microorganisms[36], but the appearance is not completely explained. It can be seen that it is very difficult to compare different antimicrobial material activities reported in the literature. The main reason for that are testing procedures used in different studies and reported in the literature (testing procedures as ASTM E2149-01, AATCC 100-1999 which are not direct comparable…) as well as the differences in studied and modified materials which differ in their supra-molecular structure and chemistry.

Franz diffusion cells in combination with AAS were used to monitor the release of Ag from viscose non-woven. We believe the use of Franz cells serves as a good representation of realistic conditions inside a wound and therefore an excellent method for monitoring the release of other drugs[40]. We also believe that the AAS method is a good choice to determine the concentration of the silver released. Although silver concentrations that can acceptably enter the body have not been determined in the literature, we believe that detection limit of AAS is so low that those viscose non-woven samples with a released silver concentration below the detection limit can be seen as potential wound dressings for open wound treatment.

## 5 CONCLUSION

In our research, the greatest attention was paid to the study of the influence of differently chemically modified sol-gel systems on the adsorption of AgCl nanoparticles to viscose non-woven and the release of Ag from viscose non-woven. It was established that, when compared to a hydrophobic sol-gel system, a combination of a hydrophilic sol-gel system and a surfactant improves the hydrophilic properties of the carrier material (19%), increases the concentration of bound Ag (6.5%) and reduces the release of Ag from the non-woven to a concentration detectable below the AAS detection limit. With regard to the excellent antimicrobial properties of treated materials, it can be concluded that the selection of the right sol-gel system combination, which ensures the best hydrophilic properties of the materials and the strongest binding of silver to it, can be seen as a good starting point in the preparation of safe wound dressings with positive effects on the wound healing process.

### Acknowledgments

The authors acknowledge the financial support from the Ministry of Higher Education, Science and Technology of the Republic of Slovenia through contract No. 3211-10-000057 (Center of Excellence Polymer Materials and Technologies).

The authors are also grateful to CHT (Germany) for providing all chemicals and sol-gel systems.

## 6 REFERENCES

[1] M. Rai, A.Yadav, A. Gade, Silver nanoparticles as a new generation of antimicrobials, Biotechnology Advances, 27 (**2009**), 76–83

[2] S. Gaisford, A. E. Beezer, A. H. Bishop, M. Walker, D. Parsons, An in vitro method for the quantitative determination of the antimicrobial efficacy of silver-containing wound dressings, International Jurnal of Pharmaceutics, 366 (**2009**), 111–116

[3] D. Troitzsch, U. Borutzky, U. Junghannß, Detection of antimicrobial efficacy in silver-coated medical devices, Hygiene & Medizin, 34 (**2009**) 3, 80–85

[4] R. Babu, J. Zhang, E. J. Beckman, M. Virji, W. A. Pasculle, A. Wells, Antimicrobial activities of silver used as a polymerization catalyst for a wound-healing matrix, Biomaterials, 27 (**2006**), 4304–4314

[5] M. Ahamed, M. S. AlSalhi, M. K. J. Siddiqui, Silver nanoparticle applications and human health, Clinica Chimica Acta, 411 (**2010**), 1841–1848

[6] X. Chen, H. J. Schluesener, Nanosilver: A nanoproduct in medical application, Toxicology Letters, 176 (**2008**), 1–12

[7] S. Hackenberg, A. Scherzed, M. Kessler, S. Hummel, A. Technau, K. Froelich, C. Ginzkey, C. Koehler, R.Hagen, N. Kleinsasser, Silver nanoparticles: Evaluation of DNA damage, toxicity and functional impairment in human mesenchymal stem cells, Toxicology Letters, 201 (**2011**), 27–33

[8] F. F. Larese, F. D'Agostin, M. Crosera, G. Adami, N. Renzi, M. Bovenzi, G. Maina, Human skin penetration of silver nanoparticles through intact and damaged skin, Toxicology, 255 (**2009**), 33–37

[9] B. Mahlting, H. Haufe, H. Böttcher, Functionalisation of textiles by inorganic sol-gel coatings, Journal of materials chemistry, 15 (**2005**), 4385–4398

[10] H. Haufe, A. Thron, D. Fiedler, B. Mahltig, H. Böttcher, Biocidal nanosol coatings, Surface Coatings International, 88 (**2005**) 6, 55–60
[11] B. Tomšič, B. Simonič, B. Orel, L. Černe, P. F. Tavčar, M. Zorko, I. Jerman, A. Vilčnik, J. Kovač, Sol-gel coating of cellulose fibres with antimicrobial and repellent properties, Journal of Sol-Gel Science and Technology, 47 (**2008**), 44–57
[12] B. Mahltig, D. Fiedler, H. Böttcher, Antimicrobial Sol–Gel Coatings, Journal of Sol-Gel Science and Technology, 32 (**2004**), 219–222
[13] B. Mahlting, F. Audenaert, H. Böttcher, Hydrophobic silica sol coating on textile –the influence of solvent and sol concentration, Journal of Sol-Gel Science and Technology, 34 (**2005**), 103–109
[14] N. Veronovski, S. Hribernik, M. Sfiligoj-Smole, Funkcionalizacija tekstilij z nano $TiO_2$ in $SiO_2$, Tekstilec, 51 (**2008**), 300–318
[15] C. Gutierrez-Wing, R. Perez-Hernandez, G. Mondragon-Galicia, G. Villa-Sanchez, M. E. Fernandez-Garcia, J. Arenas-Alatorre, D. Mendoza-Anaya, Synthesis of silica–silver wires by a sol–gel technique, Solid State Sciences, 11 (**2009**), 1722–1729
[16] T. J. Franz, On the relevance of in vitro data, Journal of Investigative Dermatology, 93 (**1975**), 633–640
[17] H. J. Jakobasch, K. Grundke, E. Mäder, K. H. Freitag, U. Panzer, Application of the surface free energy concept in polymer processing, in K. L. Mittal (ed): Contact angle, wettability & adhesion, 2003, 921–936
[18] Z. Peršin, K. Stana-Kleinschek, M. Sfiligoj-Smole, T. Kreže, Determining the surface free energy of cellulose materials with the powder contact angle method, Textile Research Journal, 74 (**2004**), 55–62
[19] L. Fras-Zemljič, Z. Peršin, P. Stenius, K. Stana-Kleinschek, Carboxyl groups in pre-treated regenerated cellulose fibres, Cellulose, 15 (**2008**), 681–690
[20] L. Fras-Zemljič, Z. Peršin, P. Stenius, Improvement of chitosan adsorption onto cellulosic fabrics by plasma treatment, Biomacromolecules, 10 (**2009**), 1181–1187
[21] Q. H. Kiani, M. Amir, M. A. Ghazanfar, M. Iqbal, Microbiology of wound infections among hospitalised patients following the 2005 Pakistan earthquake, Journal of Hospital Infection, 73 (**2009**), 71–78
[22] C. Basualdo, V. Sgroy, M. S. Finola, J. M. Marioli, Comparison of the antibacterial activity of honey from different provenance against bacteria usually isolated from skin wounds, Veterinary Microbiology, 124 (**2007**), 375–381
[23] M. A. A. O'Neill, G. J. Vine, A. E. Beezer, A. H. Bishop, J. Hadgraft, C. Labetoulle, M. Walker, P. G. Bowler, Antimicrobial properties of silver-containing wound dressings: a microcalorimetric study, International Journal of Pharmaceutics, 263 (**2003**), 61–68
[24] B. Himmel, H. Biirger, Th. Gerber, A. Olbertz, Structural characterization of $SiO_2$ aerogels, Journal of Non-Crystalline Solids, 185 (**1995**), 56–66
[25] Y. A. Shchipunov, Sol–gel-derived biomaterials of silica and carrageenans, Journal of Colloid and Interface Science, 268 (**2003**) 1, 68–76
[26] M. Gorjanc, V. Bukošek, M. Gorenšek, A. Vesel, The influence of water vapor plasma treatment on specific properties of bleached and mercerized cotton fabric, Textiles Research Journal, 80 (**2010**) 6, 557–567
[27] A. Vesel, Modification of polystyrene with a highly reactive cold oxygen plasma, Surface and Coatings Technology, 205 (**2010**) 2, 490–497
[28] A. Vesel, I. Junkar, U. Cvelbar, J. Kovac, M. Mozetic, Surface modification of polyester by oxygen-and nitrogen-plasma treatment, Surface and Interface Analysis, 40 (**2008**) 11, 1444–1453
[29] I. Junkar, U. Cvelbar, A. Vesel, N. Hauptman, M. Mozetič, The role of crystallinity on polymer interaction with oxygen plasma, Plasma Processes and Polymers, 6 (**2009**) 10, 667–675
[30] A. Vesel, M. Mozetič, A. Hladnik, J. Dolenc, J. Zule, S. Miloševic, N. Krstulovic, M. Klanjšek Gunde, N. Hauptman, Modification of ink-jet paper by oxygen-plasma treatment, Journal of Physics D: Applied Physics, 40 (**2007**), 3689–2696
[31] U. Cvelbar, M. Mozetič, N. Hauptman, M. Klanjšek Gunde, Degradation of Staphylococcus aureus bacteria by neutral oxygen atoms, Journal of Applied Physics., 106 (**2009**) 10, 103303-1–103303-5
[32] M. Mozetič, Z. Vratnica, Destruction of Bacillus stearothermophilus bacteria by weakly ionized low pressure cold oxygen plasma, Vacuum, 12 (**2011**), 1080–1082
[33] M. Mozetič, Surface modification of materials using an extremely non-equilibrium oxygen plasma, Mater. Tehnol., 44 (**2010**) 4, 165–171
[34] A. Asadinezhad, I. Novák, M. Lehocký, F. Bílek, A. Vesel, I. Junkar, Ita, P. Sáha, A. Popelka, Polysaccharides coatings on medical-grade PVC : a probe into surface characteristics and the extent of bacterial adhesion, Molecules, 15 (**2010**) 2, 1007–1027
[35] A. Asadinezhad, I. Novák, M. Lehocký, V. Sedlarik, A. Vesel, P. Sáha, I. Chodák, An in vitro bacterial adhesion assessment of surface-modified medical-grade PVC, Colloids and Surfaces B: Biointerfaces, 77 (**2010**) 2, 246–256
[36] S. Strnad, O. Šauperl, L. Fras-Zemljič, Cellulose Fibres Functionalised by Chitosan: Characterization and Application, V: ELNASHAR, Magdy M. (ed.). Biopolymers, Rijeka: Sciyo, cop. (**2010**), 181–200
[37] T. Maver, Z. Peršin, K. Herzič, D. Smrke, K. Stana-Kleinschek, Novel wound dressings for controlled release of NSAID. V: International Conference on Fibrous Products in Medical and Health Care, FiberMed11, Tampere Hall, Finland. Fibrous products in medical and health care: papers and poster abstracts. Tampere: University of Technology, 2011

UDK 678.7
Original scientific article/Izvirni znanstveni članek

ISSN 1580-2949
MTAEC9, 46(1)81(2012)

# HEPARIN ADSORPTION ONTO MODEL POLY(ETHYLENE TEREPHTALATE) (PET) SURFACES MONITORED BY QCM-D

## SPREMLJANJE ADSORPCIJE HEPARINA NA MODELNE POLIETILENTEREFTALATNE (PET) POVRŠINE S POMOČJO KREMENOVE MIKROTEHTNICE

**Aleš Doliška[1,2], Simona Strnad[2], Karin Stana-Kleinschek[1,2]**

[1]Center of excellence for polymer materials and technologies (PoliMaT), Tehnološki park 24, SI-1000 Ljubljana, Slovenia
[2]University of Maribor, Faculty of Mechanical Engineering, Laboratory for Characterization and Processing of Polymers, Smetanova 17, SI-2000 Maribor, Slovenia
ales.doliska@uni-mb.si

*Prejem rokopisa – received: 2011-09-30; sprejem za objavo – accepted for publication: 2011-10-06*

The adsorption of anticoagulant heparin onto model poly(ethylene terephtalate) (PET) film was monitored using a quartz crystal microbalance with a dissipation unit (QCM-D). Synthetic vascular grafts are usually made from PET, a material with appropriate mechanical properties but moderate haemocompatibility. Therefore anticoagulant heparin is usually used to improve haemocompatibility of PET surfaces. Heparin possesses a high negative charge and as such does not adsorb directly onto hydrophobic PET, which is also negatively charged. To increase heparin adsorption different cationic polymers were investigated as spacers and the highest adsorption was achieved using polyethyleneimine (PEI) as an anchoring agent. The heparin was adsorbed from water solution as well as from phosphate buffer saline (PBS). Heparin dissolved in PBS adsorb better onto PET than heparin from water solution. The results were characterized using Sauerbrey equation and Voigt based viscoelastic model. We found out that heparin adsorbed onto PET formed a thin and rigid film and that Sauerbrey equation is appropriate for characterization of heparin adsorption onto PET.

Keywords: poly(ethyleneterephtalate), PET, heparin, QCM-D, haemocompatibility

Adsorpcijo antikoagulanta heparina na modelni film polietilentereftalata (PET) smo merili s pomočjo kremenove mikrotehtnice s spremljanjem dušenja nihanja (QCM-D). PET, ki se uporablja za izdelavo sintetičnih žilnih vsadkov, ima sicer primerne mehanske lastnosti, vendar slabšo hemokompatibilnost. Heparin, ki izboljša hemokompatibilnost površine polimera v stiku s krvjo, ima močno negativen naboj, zato je njegova adsorpcija na hidrofobni in zato prav tako bolj negativen PET, zanemarljiva. Zato je bilo za uspešno adsorpcijo potrebno uporabiti vmesni vezivni sloj kationskega polimera. Preverili smo učinke več različnih kationskih polimerov in ugotovili, da se heparin najbolje adsorbira na sloj polietilenimina (PEI). Heparin smo adsorbirali iz vodne raztopine in iz fiziološke raztopine (PBS). Heparin se je iz raztopine PBS znatno bolje adsorbiral. Meritve smo ovrednotili z uporabo Sauerbreyeve enačbe in Voigtovega viskoelastičnega modela in ugotovili, da heparin na površini PET tvori čvrst film.

Ključne besede: polietilentereftalat, PET, heparin, QCM-D, hemokompatibilnost

## 1 INTRODUCTION

There are around 500 surgical treatments using vascular prosthetic material per 1 million residents per year in Western countries, and the number is increasing every year.[1] Woven or knitted vascular grafts are mainly made from polyester (poly(ethylene terephthalate) or PET) filaments of tubular shape. When foreign material is exposed to blood, the blood proteins adsorb on the surface, which triggers the activation of an intrinsic clotting system, the activation of platelets, thrombolysis, and the activation of a complementary system.[2]

Surface properties that influence blood interactions at polymer interfaces are described by surface morphology and roughness, surface chemistry and charge and, as such, by surface- free energy. Therefore, improved knowledge about chemical and physical surface characteristics can lead to improved material haemocompatibility. Intensive investigations are in progress[3–10] to define and develop polymeric materials with appropriate haemocompatibility.

It is a generally accepted theory that hydrophilic environment at the blood polymer interface is beneficial for reducing platelet adhesion and thrombus formation.[5,7,11] Several techniques have been proved to improve surface hydrophilicity and, in this way the haemocompatibility of materials.[12–14] Many techniques are based on application of highly non-equilibrium gaseous plasma.[15–24] Very high surface free energy can be obtained using such a plasma created in different gases including oxygen[25–29], nitrogen[30,31], air[32,33] and carbon dioxide.[34,35] Optimal treatments are often achieved using plasma with a very high degree of dissociation. Such plasma is usually created in high-frequency electrodeless discharges.[36,37] In such discharges the dissociation fraction exceeding 10% is often achieved although the kinetic temperature of neutral gas remains close to room temperature.[37]

Other commonly used techniques for obtaining better hemocompatible properties are surface modifications by grafting with hydrophilic materials or bioactive agents. Currently the commercially available PET vascular

grafts are coated with heparin for improving their antithrombotic properties. However, it has been proved that heparin coating on an inner graft surface remains stable only for 4 weeks after implantation, and during that time it is gradually released from the graft surface.[38,39] This effect can lead to certain adverse effects, such as abnormal bleeding of treated patients.

In this research detailed analysis of heparin adsorption and interaction with model PET surfaces using a quartz crystal microbalance with a dissipation unit (QCM-D) was performed in order to define the most appropriate system and conditions for more efficient heparin binding.

## 2 EXPERIMENTAL

Quartz crystal microbalance with a dissipation unit (QCM-D) was used for adsorption studies of heparin onto model PET surfaces. QCM-D is one of few techniques that give direct information on the adsorption process in situ. It is based on the change in resonance frequency of a thin AT-cut piezoelectric quartz crystal disc. The crystal frequency change is in correlation to the adsorbed mass following the Sauerbrey relationship (Eq. 1), which is only valid for rigid, evenly distributed thin adsorbed layers.

$$m = \frac{C \cdot \Delta f}{n} \tag{1}$$

Where $C$ is the mass sensitivity constant (17.7 ng Hz$^{-1}$ cm$^{-2}$ for a 5 MHz quartz crystal), $n$ is the overtone number (1, 3, 5, 7, 9, 11, 13), $\Delta m$ is the change in mass and $\Delta f$ is the frequency change.

To obtain more accurate mass change and structural properties during adsorption, energy dissipation should be taken into account. Dissipation occurs when periodically switching the AC voltage on and off over the crystal and the energy from the oscillating crystal dissipates from the system. Dissipation is proportional to film elasticity and viscosity and is defined as:

$$D = \frac{E_{\text{lost}}}{2\pi E_{\text{stored}}} \tag{2}$$

Where $E_{\text{lost}}$ is the energy lost during one oscillating cycle, and $E_{\text{stored}}$ is the total energy stored in the oscillator.

The applied apparatus (QSense, Sweden) was supplied with QTools software, which includes as well the Voigt viscoelastic model. The application of this model was included in our study, and the results were compared to Sauerbrey relation. Voigt viscoelastic model takes into consideration also the dissipation change and is, as such, more suitable for the evaluation of soft adhering layers, for which the Sauerbrey equation is not valid anymore. The instrument measures frequency and dissipation at several overtones, and this enables modelling in QTools using the mentioned Voigt viscoelastic model (**Figure 1**), where $\Delta f$ and $\Delta D$ are calculated according to Voinova et al. (Equations 3,4).

$$f \approx \frac{1}{2\pi\rho_0 h_0}\left\{\frac{\eta_l}{\delta_l} + h_f \rho_f \omega - 2h_f\left(\frac{\eta_l}{\delta_l}\right)^2 \frac{\eta_f \omega^2}{\mu_f^2 + \eta_f^2 \omega^2}\right\} \tag{3}$$

$$D \approx \frac{1}{\pi f \rho_0 h_0}\left\{\frac{\eta_l}{\delta_l} + 2h_f\left(\frac{\eta_l}{\delta_l}\right)^2 \frac{\eta_f \omega}{\mu_f^2 + \eta_f^2 \omega^2}\right\} \tag{4}$$

Where $\rho_0$ and $h_0$ are the density and thickness of the crystal, $\eta_l$ is viscosity of the bulk fluid, $\delta_l$ is the viscous penetration depth of the shear wave in the bulk liquid, $\rho_l$ is the density of the liquid and $\omega$ is the angular frequency of the oscillation. The adsorbed layer is the function of density ($\rho_f$), thickness ($h_f$), elastic shear modulus ($\mu_f$) and shear viscosity ($\eta_f$).

The experimental values of $\Delta f$ and $\Delta D$ of several overtones were fitted and Simplex algorithm was used to find the minimum in the sum of the squares of the scaled errors between the experimental and modelled $\Delta f$ and $\Delta D$ values.[40] This model has been successfully used in many publications, however it is assumed that the coated quartz crystal was purely elastic and the bulk solution is Newtonian and purely viscous.

From adsorbed masses (ng/cm$^2$) is also possible to obtain the thickness (Equation 5) of the adsorbed layer, however in this case the effective density of adsorbed layer $\rho_{\text{ef}}$ should be estimated.

$$h_f = \frac{10^7\left(\frac{nm}{cm}\right)\Delta m\left(\frac{ng}{cm^2}\right)}{10^9\left(\frac{ng}{g}\right)\cdot\rho_{ef}\left(\frac{g}{cm^3}\right)} \tag{5}$$

In our study the quartz crystals covered with a thin gold film (QSX 301, QSense, Sweden) were used as substrates for model PET surface preparation. The model PET surfaces were prepared by a "spin coating" technique from a 1 wt % PET solution in 1,1,2,2-tetrachloroethane. Detailed procedure is described elsewhere.

Since heparin possesses a highly negative charge at pH of around 7.0[41] and the PET is negatively charged as well[42,43], the repulsion forces between them are too high and heparin did not adsorb onto the surface (not shown here). Therefore, different cationic polymers were studied as anchoring layers in order to achieve sufficient

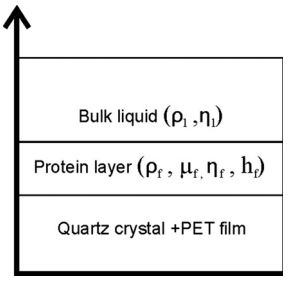


**Figure 1:** The Voigt based visoelastic film model
**Slika 1:** Voigtov model viskoelastičnega filma

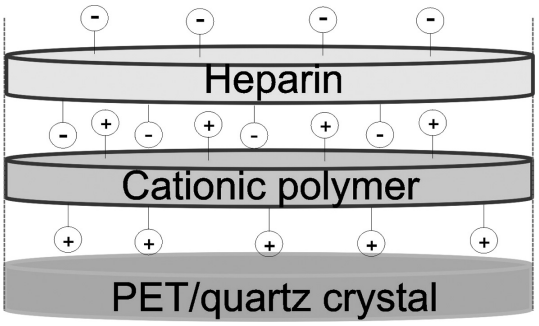


**Figure 2:** Schematic presentation of layer-by-layer polymer film formation onto quartz crystal coated with model PET surface

**Slika 2:** Shematski prikaz formiranja sloj-na-sloj polimernega filma na kremenovem kristalu z modelno PET površino

adsorption and binding of heparin. After rinsing of the model PET film with MilliQ water for 20 min at 0.25 mL/min, the cationic polymers (0.02 wt %, dissolved in MilliQ water) were adsorbed on PET surfaces with solution flow rate 0.1 mL/min. Thereafter the solution of heparin in MilliQ water and phosphate buffer saline (PBS) at 200 mg/L was used with the same flow rate (0.1 mL/min) to form layer by layer film as shown in **Figure 2**.

## 3 RESULTS AND DISCUSSION

In the **Figure 3** typical diagrams of frequency change during the heparin adsorption are represented for PET films previously coated with different cationic polymers (PEI – Poly(ethylene imine), PAH – poly(allylamine hydrochloride), pDADMAC – Poly(diallyl dimethyl ammonium chloride), and polylysine). The anchoring polymer and heparin additions as well as rinsing steps

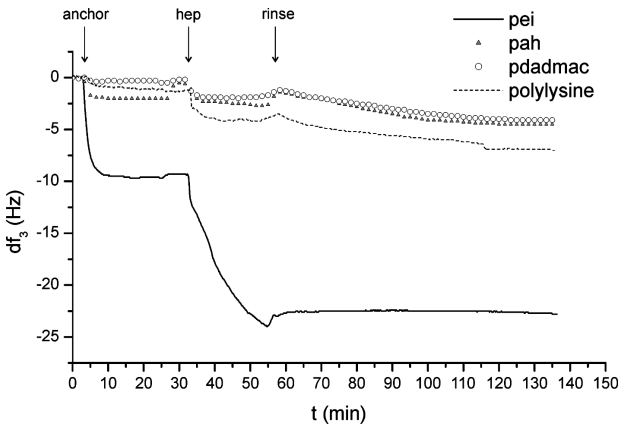


**Figure 3:** Frequency change (at 3rd overtone) during the adsorption of heparin (hep) from the water solution onto the model PET surfaces coated with different cationic polymers (PEI – Poly(ethylene imine), PAH – poly(allylamine hydrochloride), pDADMAC – Poly(diallyl dimethyl ammonium chloride), and polylysine)

**Slika 3:** Sprememba frekvence tretjega nadtona med adsorpcijo heparina (hep) v vodni razopini na modelne PET površine predhodno obdelane z različnimi kationskimi polimeri (PEI – Poly(ethylene imine), PAH – poly(allylamine hydrochloride), pDADMAC – Poly(diallyl dimethyl ammonium chloride), and polylysine)

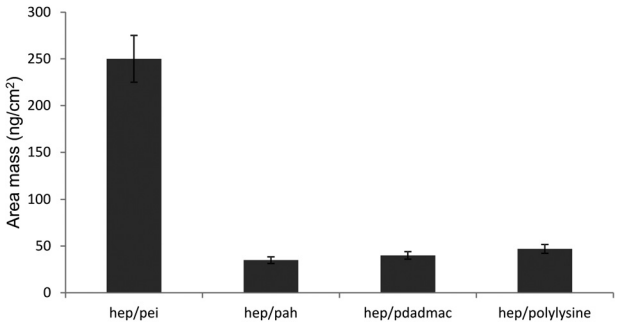


**Figure 4:** Area mass of adsorbed heparin calculated using the Sauerbrey equation from frequency change at 3rd overtone for PET films covered by different cationic polymers (PEI, PAH, pDADMAC, polylysine)

**Slika 4:** Površinska masa adsorbiranega heparina, določena s pomočjo Sauerbreyeve enačbe, pri spremembi frekvence tretjega nadtona za PET film, prekrit z različnimi kationskimi polimeri (PEI, PAH, pDADMAC, polylysine)

are marked with arrows. It can clearly be seen from the diagram that the largest frequency change was achieved in the case of PEI followed by heparin adsorption.

In **Figure 4** area masses of adsorbed heparin calculated using the Sauerbrey equation (1) from frequency change at 3rd overtone are represented for the PET films with adsorbed different anchoring agents. In the case of PEI application as an anchoring layer, the area mass of adsorbed heparin was approximately 5-times higher in comparison with other anchoring agents (**Figure 4**).

In the **Figures 5 and 6** the frequency and dissipation changes at 3rd overtone during the adsorption of heparin dissolved in MilliQ water (hep/w) and heparin dissolved in phosphate buffer saline PBS (hep/pbs) are represented. From the figures it can clearly be seen that the decreases in frequencies are significantly higher in the case of adsorption from buffer solution in comparison to the adsorption from pure water. From the extreme minimum of the frequency during the heparin adsorption from water solution it can be assumed that the

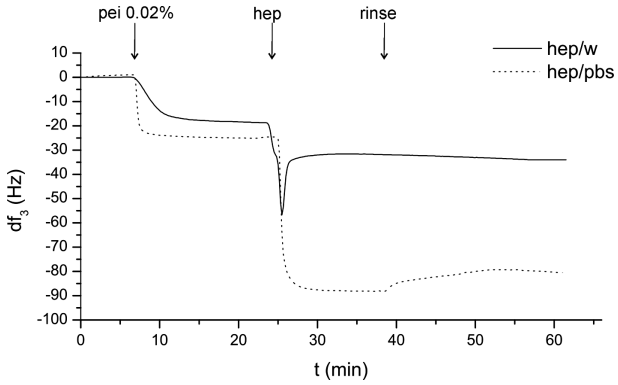


**Figure 5:** Frequency change (at 3rd overtone) during the adsorption of heparin, dissolved in MilliQ water (w) and in phosphate buffer saline (PBS) onto the polyethyleneimine (PEI) layer on the PET film

**Slika 5:** Sprememba frekvence tretjega nadtona med adsorpcijo heparina, raztopljenega v MilliQ vodi (w) in v fosfatnem pufru (PBS) na sloj polietilenimina (PEI) na PET filmu

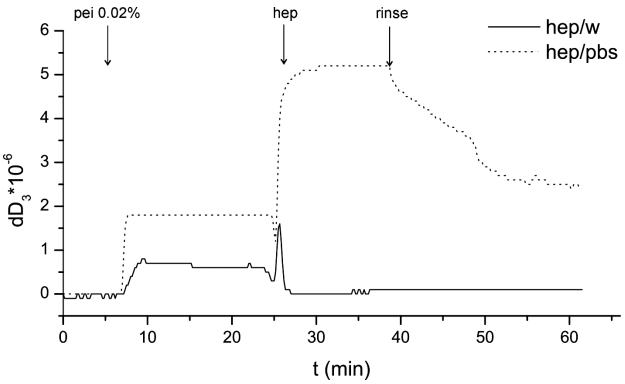


**Figure 6:** Dissipation change (at 3rd overtone) during the adsorption of heparin, dissolved in MilliQ water (w) and in phosphate buffer saline (PBS) onto the polyethyleneimine (PEI) layer on the PET film
**Slika 6:** Sprememba disipacije tretjega nadtona med adsorpcijo heparina, raztopljenega v MilliQ vodi (w) in v fosfatnem pufru (PBS) na sloj polietilenimina (PEI) na PET filmu

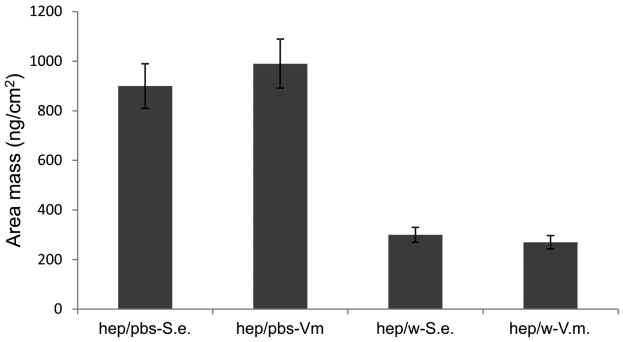


**Figure 7:** Area mass of heparin adsorbed from water solution (hep/w) and adsorbed from PBS (hep/pbs), calculated using the Sauerbrey equation (S.e.) or Voigt based viscoelastic model (V.m.)
**Slika 7:** Površinska masa adsorbiranega heparina, raztopljenega v vodi (hep/w) in v PBS (hep/pbs), določena s pomočjo Sauerbreyeve enačbe (S.e.) in s pomočjo Voigtovega viskoelastičnega modela (V.m.)

migration/desorption of heparin molecules at the beginning is rather intensive. After that the adsorbed layer is relatively thin and firm (**Figure 6**).

In water solution, which is slightly acidic (pH=5.7), most of the functional groups of heparin molecules are deprotonated and the molecule is negatively charged. This is the reason the molecules are in more or less unfolded conformation. As such they relatively quickly cover the positive charges on the PET/PEI surface. Ionic strength of buffer solution is high and deprotonated functional groups of heparin are occupied by counter ions from the buffer. Therefore, heparin molecules in such a solution obtain a more folded conformation and much higher amounts of such molecules are needed to cover positive PET/PEI surface (**Figure 7**).

From the **Figure 7** it is obvious that different models (Suerbrey eq. and Voight model) had no influence on the calculated mass area in the case of adsorption from water solution. It can be assumed that the adsorbed layers in these cases are more or less firm. The evaluations using these two models, however, gave different results in the case of adsorption from the buffer solution, which indicates formation of much softer adhering layers, for which Suerbrey equation is not valid anymore.

Assuming that density of adsorbed layer of heparin is around 1 g/cm$^2$ one can easily get the thickness of the adsorbed heparin, just dividing the estimated area mass with $10^2$ (according to Eq. 5). That means that layer thickness of heparin on PET surface is around 2.5 nm in case of water solution and the heparin layer thickness is almost 10 nm when heparin in PBS was used.

## 4 CONCLUSION

In order to find out most appropriate system for heparin binding in the present research heparin adsorption onto PET model surfaces was investigated using QCM-D. Several cationic polymers were analysed as an anchoring layer for better heparin binding onto PET surfaces.

The results showed that quartz crystal microbalance was a suitable tool for the analysis of the adsorption of heparin onto PET surfaces. Furthermore, from the QCM measurements, important data about adsorbed polymer masses and adsorbed film thicknesses onto surfaces can be achieved using the Sauerbrey equation and Voigt viscoelastic model.

Poly(ethyleneimine) (PEI) showed best results as an anchoring layer, thus in that case the area mass of adsorbed heparin was approximately 5-times higher as for other anchoring agents.

The adsorbed layers of heparin were much thicker and adsorbed amounts much higher in the case of heparin adsorption from PBS solution in comparison to the adsorption from pure water solution. Folded conformation of heparin molecules in the solution with high ionic strength form thicker and softer adsorbed layer on the PET/PEI surfaces.

## Acknowledgement

The authors acknowledge the financial support from the Ministry of Higher Education, Science and Technology of the Republic of Slovenia through contract No. 3211-10-000057 (Center of Excellence Polymer Materials and Technologies).

## 5 REFERENCES

[1] T. Indest, Study of polethylene terephtalate surface tretment with polysaccharides for medical application, University of Maribor, PhD Thesis, Maribor 2007, 143

[2] B. D. Ratner, A. S. Hoffman, F. J. Schoen, J. E. Lemons, Biomaterials Science: An introduction to materials in medicine, Academic press, 1996

[3] P. Zilla, D. Bezuidenhout, P. Human, Biomaterials, 28 (**2007**), 5009–5027

[4] M. Chaouat, C. Le Visage, A. Autissier, F. Chaubet, D. Letourneur, Biomaterials, 27 (**2006**) 32, 5546–5553

[5] I. Junkar, A. Vesel, U. Cvelbar, M. Mozetic, S. Strnad, Vacuum, 84 (**2009**) 1, 83–85
[6] I. Junkar, U. Cvelbar, A. Vesel, N. Hauptman, M. Mozetič, Plasma Processes Polym., 6 (**2009**) 10, 667–675
[7] A. Vesel, I. Junkar, U. Cvelbar, J. Kovac, M. Mozetic, Surf. Int. Anal., 40 (**2008**) 11, 1444–1453
[8] M. Gericke, A. Doliška, J. Stana, T. Liebert, T. Heinze, K. Stana-Kleinschek, Macromolecular Bioscience, 11 (**2011**) 4, 549–556
[9] H. Fasl, J. Stana, D. Stropnik, S. Strnad, K. Stana-Kleinschek, V. Ribitsch, Biomacromolecules., 11 (**2010**), 377–381
[10] T. Indest, J. Laine, L. S. Johansson, K. Stana-Kleinschek, S. Strnad, R. Dworczak, V. Ribitsch, Biomacromolecules, 10 (**2009**) 3, 630–637
[11] I. Junkar, Plasma treatment of polymers for biomedical applications, Jožef Stefan International Postgraduate School, PhD Thesis, Ljubljana 2010, 131
[12] A. Doliška, A. Vesel, M. Kolar, K. Stana-Kleinschek, M. Mozetič, Surf. Int. Anal., 44 (**2012**) 1, 56–61
[13] A. Doliška, M. Kolar, Mater. Tehnol., 45 (**2011**) 3, 275–279
[14] R. Zaplotnik, A. Doliška, M. Kolar, K. Stana-Kleinschek, Mater. Tehnol., 45 (**2011**) 3, 199–203
[15] M. Mozetič, Mater. Tehnol., 44 (**2010**) 4, 165–171
[16] K. Eleršič, I. Junkar, A. Špes, N. Hauptman, M. Klanjšek Gunde, A. Vesel, Mater. Tehnol., 44 (**2010**) 3, 153–156
[17] A. Vesel, M. Mozetic, S. Strnad, Vacuum, 85 (**2011**) 12, 1083–1086
[18] A. Asadinezhad, I. Novak, M. Lehocky, V. Sedlarik, A. Vesel, I. Junkar, P. Saha, I. Chodak, Plasma Processes Polym., 7 (**2010**) 6, 504–514
[19] A. Vesel, M. Mozetič, P. Panjan, N. Hauptman, M. Klanjsek-Gunde, M. Balat-Pichelin, Surf. Coat. Technol., 204 (**2010**) 9–10, 1503–1508
[20] K. Eleršič, I. Junkar, M. Modic, R. Zaplotnik, A. Vesel, U. Cvelbar, Mater. Tehnol., 45 (**2011**) 3, 233–239
[21] A. Vesel, M. Mozetic, A. Drenik, N. Hauptman, M. Balat-Pichelin, Appl. Surf. Sci., 255 (**2008**) 5, Part 1, 1759–1765
[22] R. Kulčar, M. Friškovec, N. Hauptman, A. Vesel, M. K. Gunde, Dyes Pigm., 86 (**2010**) 3, 271–277
[23] A. Vesel, M. Mozetic, A. Drenik, S. Milosevic, N. Krstulovic, M. Balat-Pichelin, I. Poberaj, D. Babic, Plasma Chem. Plasma P., 26 (**2006**) 6, 577–584
[24] A. Drenik, A. Vesel, M. Mozetič, J. Nucl. Mater., 386-388 (**2009**), 893–895
[25] A. Vesel, A. Drenik, M. Mozetic, M. Balat-Pichelin, Vacuum, 84 (**2010**) 7, 969–974
[26] M. Mozetic, A. Vesel, U. Cvelbar, A. Ricard, Plasma Chem. Plasma P., 26 (**2006**) 2, 103–117
[27] G. Primc, R. Zaplotnik, A. Vesel, M. Mozetic, AIP Advances, 1 (**2011**) 2, 022129
[28] A. Drenik, U. Cvelbar, A. Vesel, M. Mozetic, Inf. MIDEM, 35 (**2005**), 85–91
[29] A. Drenik, U. Cvelbar, A. Vesel, M. Mozetic, Strojarstvo, 48 (**2006**) 1/2, 17–22
[30] A. Vesel, M. Mozetic, M. Balat-Pichelin, Inf. MIDEM, 41 (**2011**) 1, 18–21
[31] M. Mozetic, U. Cvelbar, A. Vesel, A. Ricard, D. Babic, I. Poberaj, J. Appl. Phys., 97 (**2005**) 10, 103308
[32] M. Balat-Pichelin, A. Vesel, Chem. Phys., 327 (**2006**) 1, 112–118
[33] A. Asadinezhad, I. Novák, M. Lehocký, V. Sedlarík, A. Vesel, I. Junkar, P. Sáha, I. Chodák, Colloids Surf. B Biointerfaces, 77 (**2010**) 2, 246–256
[34] A. Vesel, M. Mozetic, A. Drenik, M. Balat-Pichelin, Chem. Phys., 382 (**2011**) 1–3, 127–131
[35] A. Vesel, Mater. Tehnol., 45 (**2011**) 2, 121–124
[36] R. Zaplotnik, A. Vesel, Mater. Tehnol., 45 (**2011**) 3, 227–231
[37] R. Zaplotnik, A. Vesel, M. Mozetič, Europhys. Lett., 95 (**2011**) 5, 55001
[38] P. a. S. Mourao, Current Pharmaceutical Design, 10 (**2004**) 9, 967–981
[39] P. Vongchan, W. Sajomsang, D. Subyen, P. Kongtawelert, Carbohydrate Research, 337 (**2002**) 13, 1239–1242
[40] M. V. Voinova, M. Rodahl, M. Jonson, B. Kasemo, Physica Scripta, 59 (**1999**) 5, 391–396
[41] D. L. Nelson, M. M. Cox, Lehninger principles of biochemistry, W.H. Freeman, New York, 2004
[42] T. Indest, S. Strnad, K. S. Kleinschek, V. Ribitsch, L. Fras, Colloids and Surfaces A: Physicochemical and Engineering Aspects, 275 (**2006**) 1–3, 17–26
[43] J. Wang, N. Huang, P. Yang, Y. X. Leng, H. Sun, Z. Y. Liu, P. K. Chu, Biomaterials, 25 (**2004**) 16, 3163–3170

UDK 678.7
Original scientific article/Izvirni znanstveni članek

ISSN 1580-2949
MTAEC9, 46(1)87(2012)

# UV POLYMERIZATION OF POLY (N-ISOPROPYLACRYLAMIDE) HYDROGEL

## UV POLIMERIZACIJA POLI (N-ISOPROPILAKRILAMIDNEGA) HIDROGELA

**Manja Kurečič[1,2], Majda Sfiligoj-Smole[1,2], Karin Stana-Kleinschek[1,2]**

[1]Center of excellence for polymer materials and technologies (PoliMaT), Tehnološki park 24, SI-1000 Ljubljana, Slovenia
[2]University of Maribor, Faculty of Mechanical Engineering, Laboratory for Characterization and Processing of Polymers, Smetanova 17, SI-2000 Maribor, Slovenia
manja.kurecic@uni-mb.si

*Prejem rokopisa – received: 2011-09-30; sprejem za objavo – accepted for publication: 2011-11-07*

This contribution is focused on the determination of polymerization and crosslinking mechanism of poly (N-isopropylacralymide) hydrogel and its swelling properties. Hydrogels were synthesized by environmental friendly UV polymerization method, from monomer N-isopropylacrylamide (NIPAM) and crosslinker N,N´-methylenebisacrylamide (BIS) of different concentrations. UV polymerization was performed in an UV chamber using UVA light with the wave length 350 nm. Surface morphology and pore structure analysis was carried out using SEM microscopy. The polymerization and crosslinking mechanism was determined by Fourier Transform Infrared spectroscopy (FT-IR). It was confirmed that crosslinker concentration influences the hydrogel structure and swelling properties. By increasing the crosllinker concentration the hydrogel structure changes from homogen to heterogen and the equilibrium degree of swelling decreases.

Keywords: poly (N-isopropylacrylamide) hydrogel, UV polymerization, FTIR, polymerization mechanism, swelling properties, SEM

V prispevku je predstavljen mehanizem polimerizacije in zamreženja poli(N-isopropilakrilamidnega) hidrogela in njegova sposobnost nabrekanja. Hidrogele smo sintetizirali z okolju prijazno metodo UV polimerizacije iz monomera N-isopropilakrilamida (NIPAM) in zamreževalca N,N´-metilenebisakrilamida (BIS) različnih koncentracij. UV polimerizacija je potekala v UV komori z UVA svetlobo valovne dolžine 350 nm. Površinsko morfologijo in strukturo por smo spremljali s SEM mikroskopijo. Mehanizem polimerizacije in zamreženja smo določili na podlagi posnetih spektrov s Fourier Transform Infrardečo spektroskopijo (FT-IR). Ugotovili smo, da koncentracija zamreževalca vpliva na strukturo hidrogela in njegovo sposobnost nabrekanja. Z večanjem koncentracije zamreževalca pride do spremembe v strukturi hidrogela iz homogene v heterogeno, kar vpliva na zmanjšanje sposobnosti nabrekanja.

Ključne besede: poli (N-isopropilakrilamide) hidrogel, UV polimerizacija, FTIR, mehanizem polimerizacije, nabrekanje, SEM

## 1 INTRODUCTION

Hydrogels are three-dimensional hydrophilic polymer networks. Their most characteristic property is swelling in aqueous solutions[1]. Hydrogels can be used for several applications including superabsorption in diapers and for contact-lenses, just to mention two well-established applications[2–6]. Recently, they have gained considerable attention also within the environmental field especially for wastewater treatments (dye and heavy metal adsorption)[7].

Hydrogels are crosslinked during polymerization via condensation polymerization or free radical polymerization (thermal polymerization, radiation polymerization, photopolymerization or plasma polymerization)[8–12]. Photopolymerization, in addition to its environmental-friendly aspect, offers a number of advantages, such as ambient temperature operations, location and time-control of the polymerization process and minimal heat production, in comparison with other techniques[13]. Photopolymerization can be induced by ultraviolet (100–400 nm), visible (400–700 nm) or infrared (780–20000 nm) radiation. Light quanta are absorbed by molecules via electronic excitation[14]. During photopolymerization process, photoiniciators are generally used having high absorption capacities at specific wavelengths of light thus enabling them to produce radically initiated species[15].

Our work is focused on the preparation of nanocomposite hydrogels for water purification. This contribution represents preliminary studies that were performed for better understanding of synthesis mechanism of UV polymerized poly (N-isopropylacrylamide) hydrogel, which is essential for formation of nanocomposite hydrogel with defined properties.

## 2 EXPERIMENTAL

For the polymerization of poly (N-isopropylacrylamide) hydrogels we used N-isopropylacrylamide (NIPAM) as monomer, N,N-methylenebisacrylamide (BIS) as crosslinker and Irgacure 2959 as photoiniciator. All chemicals were purchased form Sigma-Aldrich and their chemical structures are presented in **Figure 1**.

PNIPAM hydrogels were synthesized in aqueous solutions containing 1% of NIPAM monomer in the presence of different concentrations of N,N-methylenebisacrylamide (0 – 5 wt%). NIPAM and BIS were kept

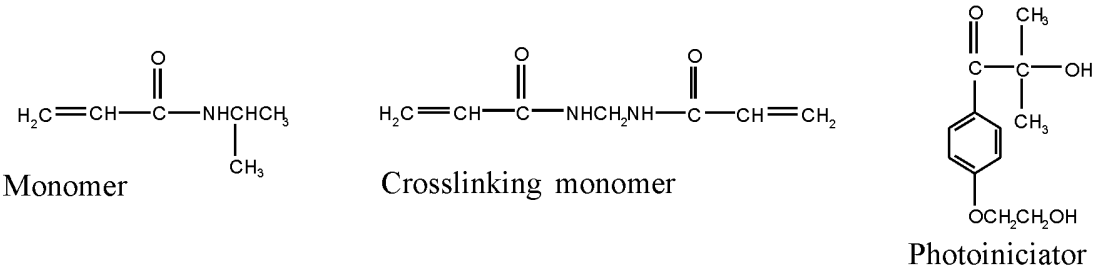


**Figure 1:** Chemical structure of monomer, crosslinker and photoiniciator
**Slika 1:** Kemijska struktura monomera, zamreževalca in fotoiniciatorja

under constant stirring for 1 hour at room temperature. After this period, Irgacure 2959 photoiniciator was added and the solution was kept under the same conditions for additional 30 minutes. Prepared solutions were pored in glass Petri dishes, bubbled with nitrogen for 5 minutes and covered. Petri dishes were placed on the sample holder in the middle of a UV chamber (Luzchem). Polymerization was carried out in UV chamber using 6 UVA lamps (centered at 350 nm) placed on top of the chamber with the distance to the sample 15 cm. Time of polymerization was 2 hours. After polymerization the hydrogels were washed with deionized water for 4 days (daily exchange of water). After washing, the hydrogels were dried at 40°C until a constant mass was reached.

For determination of an equilibrium degree of swelling (EDS) and equilibrium water content (EWC), we used pre-weighted hydrogel samples and immersed them into deionized water. Samples were removed from water every hour, wiped with filter paper in order to remove surface water, weighted and placed back into the water for further swelling. The equilibrium was reached when no mass difference was determined. EDS and EWC were calculated using these equations[16]:

$$EDS(\%) = \frac{W_s - W_d}{W_d} \cdot 100 \quad (1)$$

$$EWC(\%) = \frac{W_s - W_d}{W_s} \cdot 100 \quad (2)$$

where $W_s$ and $W_d$ are the masses of the gel in swollen and dried states, respectively.

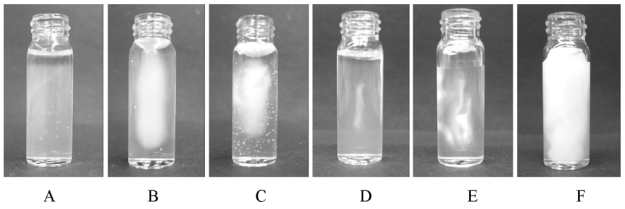


**Figure 2:** Polymerized hydrogels with different crosslinker concentrations (A:0 wt%, B:0.25 wt%, C:0.5 wt%, D: 1 wt%, E:2.5 wt%, F:5 wt% BIS regarding the monomer content)
**Slika 2:** Polimerizirani hidrogeli z različnimi koncentracijami zamreževalca (A:0 u.t.%, B:0,25 u.t.%, C:0,5 u.t.%, D: 1 u.t.%, E:2,5 u.t.%, F:5 u.t.% BIS glede na delež monomera)

The structural properties of the hydrogels were examined using the Perkin-Elmer Spectrum One FT-IR spectrophotometer. Hidrogel disks were cut into small pieces and dried at 40°C until a constant mass was reached. Spectra were recorded by placing a dried gel piece over the attenuated total reflectance crystal. Recording conditions were: 16 scans and an estimated resolution of 4 $cm^{-1}$.

The surface morphology of the hydrogels was studied using the scanning electron microscope FE-SEM-ZEISS Gemini Supra 35 VP. The samples were equilibrated in distilled water at room temperature and freez-dried (Lyotrap freez-drier) for 2 days prior to SEM analyses.

## 3 RESULTS AND DISCUSSIONS

Polymerized hydrogels with crosslinker concentrations less than 1 wt% regarding the monomer content form sticky gels that decay during the washing or subsequent swelling. At the cross-linker concentration of 1 wt% and above regarding the monomer content, polymerized hydrogels retained their structure also during the washing and swelling process. We assume that the ratio monomer/crosslinker under 100:1 is too small for the material to polymerize completely and form a firm and resistible hydrogel. In **Figure 2** it is demonstrated that hydrogel with crosslinker concentration of

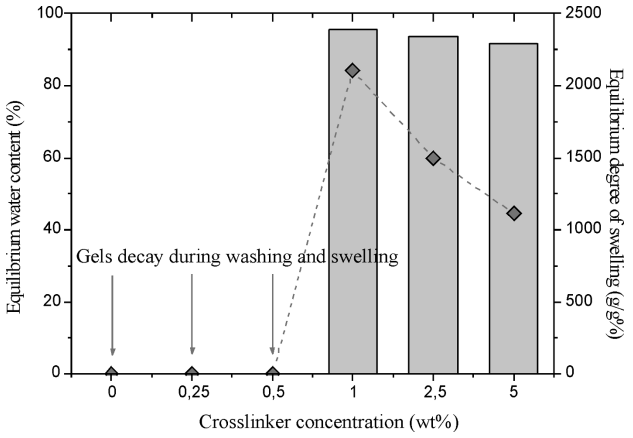


**Figure 3:** Equilibrium water content and equilibrium degree of swelling vs. crosslinker concentration
**Slika 3:** Delež vode v hidrogelu in stopnja nabrekanja v ravnotežju v odvisnosti od deleža zamreževalca v hidrogelu

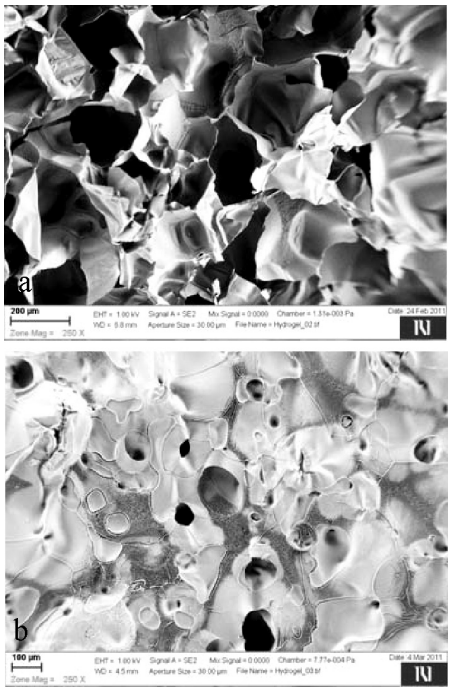


**Figure 4:** SEM micrographs of cross-section (A) and surface (B) of hydrogel with crosslinker concentration 1 wt% regarding the monomer content

**Slika 4:** SEM posnetki prereza (A) in površine (B) hidrogela s koncentracijo zamreževalca 1 u.t.% glede na delež monomera

1 wt% is transparent, which indicates that the crosslinking structure is homogeneous. Increased concentration of crosslinker causes formation of opaque segments, which indicate a formation of heterogen hydrogel structure (**Figure 2**).

When hydrogel is exposed to water, water molecules diffuse into hydrogel structure and consequently hydrogel swells. Hydrogel ability to swell or uptake water is one of the key characteristics. Therefore, the optimal monomer/crosslinker concentration ratio was determined in regard to the degree of swelling. **Figure 3** represents the equilibrium degree of swelling and equilibrium water content for polymerized hydrogels with different concentrations of crosslinker.

It was established that when increasing the crosslinker concentration above 1 wt% the amount of water in equilibrium and consequently the degree of swelling starts to decrease. This decrease can be related to the formation of hydrogel heterogene structure. With the increasement of crosslinker concentration we create a denser hydrogel structure which affects the water uptake. Water uptake represents the migration of water molecules into preformed gapes between polymer chains[17]. Denser hydrogel structure diminish the accesability of water molecules to hydrophilic parts of polymer molecules, therefore less water can penetrate into the hydrogel structure.

**Figure 4** shows SEM micrographs of a cross-section and a surface of hydrogel with crosslinker concentration of 1 wt% regarding the monomer content. Samples were lyophilized after the equilibrium swelling has been reached at room temperature in order to preserve natural hydrogel structure in swollen state. Hydrogel cross-section (**Figure 4a**) shows very porous structure with several pores and wide pore size distribution. The pore structure has a sponge-like shape with spherical opens and interconnected cells. This porous microstructure is essential for a large active surface of hydrogel and assures the capillary effect of water uptake. **Figure 4b** shows a hydrogel surface. It is noticeable that hydrogel surface is covered with a surface layer with few smaller pores. Hydrogel surface differs from its interior probably due to the difference in effect of UV light. On the surface the UV intensity is higher in comparison to the interior and therefore it causes higher crosllinking efficiency and density on the surface. Therefore a core/shell structure is suggested for the polymerized hydrogels.

Unfortunately, however, neither the UV radiation intensity nor the penetration depth of the photons with the wavelength of 350 nm is known, so we can not give any quantitative estimation. Differences in SEM images between the surface of a porous sample and the bulk could be easily attributed to the artefact of the cutting technique. Namely, porous materials are inhomogeneous and thus difficult to cut and/or polish. The proper method for monitoring distribution of grains and/or

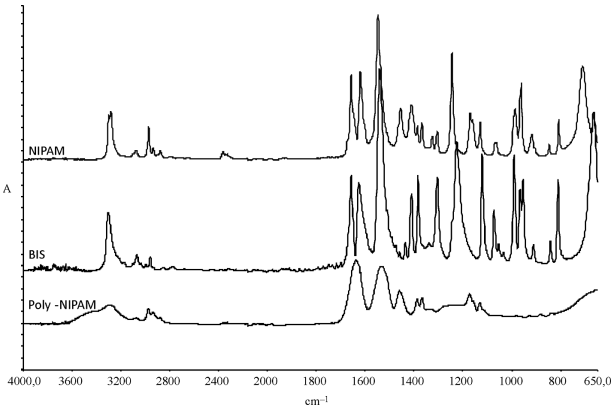


**Figure 5:** FTIR spectra of monomer (NIPAM), crosslinker (BIS) and synthesized hydrogel (poli-NIPAM – 1 wt% of BIS)

**Slika 5:** FTIR spektri monomera (NIPAM), zamreževalca (BIS) in polimernega hidrogela (poli-NIPAM –1 u.t.% BIS)

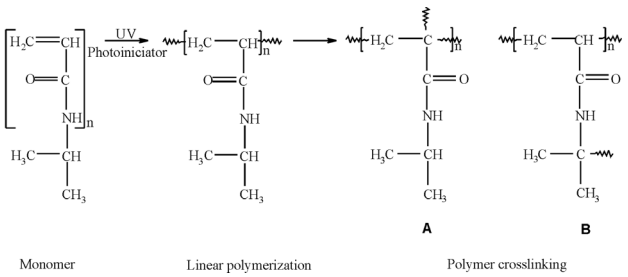


**Figure 6:** Mechanism of UV polymerization of poly (N-isopropylacrylamide) hydrogel

**Slika 6:** Mehanizem UV polimerizacije poli (N-isopropilakrilamidnega) hidrogela

pores inside a porous material is based on selective removal of the upper layers of materials. A common used method applies highly non-equilibrium gaseous plasma treatment. Gaseous particles interact with the surface material but not with the bulk. If proper parameters are taken, the material can be slowly removed without influencing the structure or composition below the surface. Such a method has been used for investigation of the structure of variety of composite materials[18–25]. Unfortunately, however, this technology was not available at our experiments.

FTIR spektra of monomer, cross-linker and polymerized NIPAM hydrogel (poly-NIPAM) are presented in **Figure 5**. The FT-IR spectra of the monomer and crosslinker show typical absorption peaks that are summarized in **Table 1**. In comparison to FT-IR spectrum of poly (N-isopropylacrylamide) hydrogel several changes can be observed. First difference is observed in the spectrum from 3600–3100 $cm^{-1}$. In this part of the spectrum of monomer the absorption peak characteristic for N-H vibrations is located at 2970 $cm^{-1}$, while in spectrum of hydrogel this peak is much broader due to the overlapping with an absorption peak which is characteristic for O-H vibrations of water molecules. This change is attributed to the interactions of polymer molecules with neighbouring water molecules. Generally, the state of water in the polymer hydrogel can be divided into free water, freezing bound water and non-freezing bound water. Free water is the water which does not take part in hydrogen bonding with polymer molecules. Freezing bound water (intermediate water) is water which interacts weakly with polymer molecules. Non-freezing water (bound water) are the water molecules which are bound to polymer molecules through hydrogen bonds[26–29]. Therefore the water that is presented in the FTIR spectrum of poly (NIPAM) hydrogel represents non-freezing bound water that remains in hydrogel structure also after extensive drying. The absorption peak at 1640 $cm^{-1}$ is assigned to C=O stretching vibrations in C=O····$H_2O$ and C=O····H-N hydrogen bonding with neighbouring water molecules.

**Tabel 1:** Characteristic absorption peaks in FTIR spectrum of monomer and crosslinker[11,30,31]

**Tabela 1:** Značilni absorbcijski vrhovi FTIR spectra monomera in zamreževalca[11,30,31]

| Absorption peaks ($cm^{-1}$) | Assignment |
|---|---|
| 3280 | N-H stretching of secondary amide |
| 2970 | Asymmetric and antisymmetric stretching of C-H bond |
| 2876 | |
| 1656 | C=O stretching of amide I bond |
| 1620 | |
| 1540 | N-H stretching of amide II bond |
| 1387 | Antisymmetric deformation of isopropyl –$C(CH_3)_2$ group |
| 1367 | |

Due to the polymerization and crosslinking process of hydrogels, significant differences in absorption maxima of FTIR spectra were observed. Absorption peak at 2970 $cm^{-1}$ in the hydrogel spectrum, that is characteristic for =C-H vibrations, is higher in comparison to the same peak of the monomer spectrum, which indicates that a double bond of NIPAM is initiated by the photoinitiator radicals, resulting in the point of polymerization (**Figure 6** – linear polymerization). Absorption peaks at 1387 and 1367 $cm^{-1}$, characteristic for vibrations of isopropyl group, are lower in comparison to monomer spectra, what indicates that the isopropyl groups represent the crosslinking points. Crosslinking is formed on the tert-C atom of the side isopropyl group and tert-C atom of the main chain isopropyl group (**Figure 6** – polymer crosslinking). According to FTIR measurements proposed mechanism of UV polymerisation of poly (N-isopropylacrylamide) hydrogel is shown in **Figure 6**.

## 4 CONCLUSIONS

In the present study poly (N-isopropylacrylamide) hydrogels were UV polymerized. The method presented in this paper represents an environmental friendly alternative to conventional polymerization techniques. By the procedure elaborated here both the polymerization and crosslinking processes occur. Stabile hydrogels were obtained, which are water insoluble but swell considerably in water. The optimal concentration of crosslinker in polymerization process of poly (NIPAM) hydrogel was found to be at about 1 wt% regarding the monomer content, where polymerized hydrogels form a rather homogeneous structure with the swelling degree of 2100% and the equilibrium water content of 95,5 %. An increase in crosslinker concentration influences the crosslinking point density in the hydrogel and, consequently, it becomes more heterogeneous. A heterogeneous structure is undesirable since it creates a fragile hydrogel causing a decrease of the swelling capacity.

### Acknowledgement

The authors acknowledge the financial support from the Ministry of Higher Education, Science and Technology of the Republic of Slovenia through contract No. 3211-10-000057 (Center of Excellence Polymer Materials and Technologies).

## 5 REFERENCES

[1] Osada Yoshihito, Kajiwara Kanji. Gels Handbook, Volume 1. London: Academic press, 2001

[2] Haraguchi Kazutoshi, Macromol. Symp., 256 (**2007**), 120–130

[3] Haraguchi Kazutoshi, Curr. Opin. Solid. St. M., 11 (**2007**), 47–54

[4] K. T. Nguyen, J. L. West, Biomaterials, 23 (**2002**), 4307–4314

[5] K. Haraguchi, Macromol. Symp., 256 (**2007**), 120–130

[6] Y. Bulut, G. Akcay, D. Elma, I.E. Serhatli, J. Hazard. Mater., 171 (**2009**), 717–723
[7] Y. Liu, W. Wang, A. Wang, Desalination, 295 (**2010**), 258–264
[8] Nguyen Kytai Truong, West L. Jennifer, Biomaterials, 23 (**2002**), 4307–4314
[9] M. G. Neumann, C. C. Schmitt, F. Catalina, B. E. Goi, doi:10.1016/j.polymertesting.2006.09.012
[10] D. He, H. Susanto, M. Ulbricht, Prog. Polym. Sci., 34 (**2009**), 62–98
[11] P.A. Tamirisa, J. Koskinen, D.W. Hess, Thin Solid Films, 515 (**2006**), 2618–2624
[12] Ortega, E. Bucio, G. Burillo, Polym. Bull., 58 (**2007**), 565–573
[13] He Hongyan, Li Ling, Lee L. James, Polymer, 47 (**2006**), 1612–1619
[14] Dongming, Susanto Heru, Ulbricht Mathias, Prog. Polym. Sci., 34 (**2009**), 62–98
[15] Wang Dong. An, Elisseeff H. Jennifer. Photopolymerization. V: Encyclopedia of biomaterial and biomedical engineering. USA: Dekker, 2004, 1212–1225
[16] L. Janovak, J. Varga, L. Kemeny, I. Dekany. Appl. Caly. Sci., 43 (**2009**), 260–270
[17] V. Can, S. Absurrahmanoglu, O. Okay, Polymer, 48 (**2007**), 5016–5023
[18] R. Kulcar, M. Friskovec, N. Hauptman, A. Vesel, M. Klanjsek-Gunde, Dyes Pigm., 86 (**2010**) 3, 271–277
[19] A. Vesel, M. Mozetic, P. Panjan, N. Hauptman, M. Klanjsek-Gunde, M. Balat-Pichelin, Surf. Coat. Technol., 204 (**2010**) 9/10, 1503–1508
[20] M. Klanjšek Gunde, M. Kunaver, M. Mozetič, P. Pelicon, J. Simčič, M. Budnar, M. Bele, Surf. Coat. Int. B, Coat. Trans., 85 (**2002**) 2, 115–121
[21] M. Kunaver, M. Klanjšek Gunde, M. Mozetič, A. Hrovat. Dyes Pigm., 57 (**2003**) 3, 235–243
[22] I. Junkar, U. Cvelbar, A. Vesel, N. Hauptman, M. Mozetic, Plasma Processes Polym., 6 (**2009**) 10, 667–675
[23] M. Kunaver, M. Mozetič, M. Klanjšek Gunde, Thin Solid Films, 459 (**2004**) 1/2, 115–117
[24] M. Klanjšek Gunde, M. Kunaver, M. Mozetič, A. Hrovat, Powder Technol., 148 (**2004**) 1, 64–66
[25] M. Kunaver, M. Klanjšek Gunde, M. Mozetič, M. Kunaver, A. Hrovat, Surf. Coat. Int. B, Coat. Trans., 86 (**2003**) 3, 175–179
[26] S. J. Kim, S. J. Park, S. I. Kim, Reactive and functional polymers, 55 (**2003**), 53–59
[27] Ping Z. H., Nguyen Q. T., Chen S. M., Zhou J. Q., Ding Y. D., Polymer, 42 (**2001**), 8461–8467
[28] S. Sunm J. Hu, H. Tang, P. Wu, J. Phys. Chem. 114 (**2010**), 9761–9770
[29] Z. H. Ping, Q. T. Nguyen, S. M. Chen, J. Q. Zhou, Y. D. Ding, Polymer 42 (**2001**), 8461–8467
[30] R. da Silva, M. G. de Oliveira, Polymer 48 (**2007**), 4114–4122
[31] Y. Bao, J. Ma, N. Li, Carbohy Polym, 84 (**2011**), 76–82